Establishment of Subgrade Undercut Criteria and Performance of Alternative Stabilization Measures

By
Roy H. Borden, Ph.D., P.E
Ben M. Cote
M. A. Gabr, Ph.D., P.E.
Young Jin Park
Sang Chul Pyo
Brent R. Robinson. P.E.

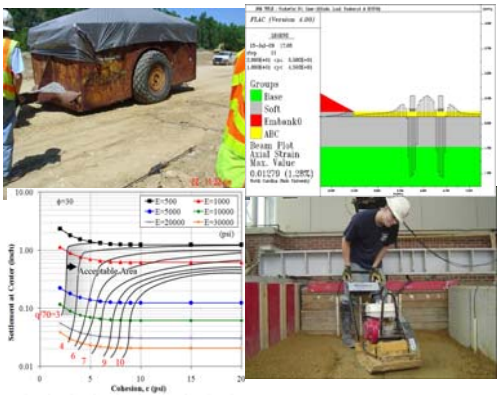

Department of Civil, Construction, and Environmental Engineering
North Carolina State University

In Cooperation with
The North Carolina Department of Transportation

North Carolina State University

Raleigh, North Carolina
August 25, 2010

Technical Report Documentation Page

1. Report No. FHWA/NC/2008-07	2. Government Accession No.	3. Recipient's Catalog No. …
4. Title and Subtitle **Establishment of Subgrade Undercut Criteria and Performance of Alternative Stabilization Measures**		5. Report Date *August 25, 2010* 6. Performing Organization Code …
7. Author(s) Roy H. Borden, Ph.D., P.E, Ben M. Cote, M. A. Gabr, Ph.D., P.E., Young Jin Park, Sang Chul Pyo, and Brent R. Robinson. P.E.		8. Performing Organization Report No. …
9. Performing Organization Name and Address Department of Civil, Construction, and Environmental Engineering North Carolina State University, Raleigh, North Carolina 27695-7908		10. Work Unit No. (TRAIS) … 11. Contract or Grant No. …
12. Sponsoring Agency Name and Address North Carolina Department of Transportation Research and Analysis Group 1 South Wilmington Street Raleigh, North Carolina 27601		13. Type of Report and Period Covered Final Report *8/2007 – 12/2009* 14. Sponsoring Agency Code 2008-07
Supplementary Notes:		

16. Abstract

The main objectives of the research work were to develop a systematic approach for determining whether or not undercut is necessary, and to investigate the adequacy of stabilization measures as implemented in conjunction with the undercut approach. The research work encompassed small and large scale laboratory testing, limited field testing using DCP, and numerical analyses and modeling. The following milestones were achieved based on the work performed in this project:

i. Establishment of undercut design criteria based on the magnitude of strength and modulus of the subgrade soils. The undercut criteria were based on meeting a deformation limit state of 1 inch for both pumping and rutting, but with the additional requirement that bearing resistance of subgrade is at least twice the applied tire pressure to minimize the potential for rutting.

ii. Development of a procedure for the use of DCP to provide input data for undercut criteria on the basis of modulus and strength. The proposed procedures are based on the analysis of the DCP data using wave mechanics and offer the advantage of using the DCP data to discern the need for undercut with depth (by applying the proposed undercut criteria incrementally) at the various phases of design and construction.

iii. Development of guidelines for specifying a stabilization measure to achieve adequate subgrade support. Five stabilization measures were investigated through the performance of 22 large scale laboratory tests. These included the use of select fill, aggregate base course (ABC), geogrids with ABC, geotextiles with ABC, and lime stabilization. The performance of each stabilization measure was investigated in the laboratory and through numerical analyses.

iv. Demonstrating the applicability of the proposed measures in several field configurations. Four field cases were idealized from actual project sections. The field cases were numerically modeled with the stabilization measures, and observations were made regarding subgrade response under static, proof roll, and cyclic loading.

v. Performance of a comparative cost analysis to illustrate the relative cost of each stabilization measure in relation to measured performance (surface deformation). The cost analyses were performed with results presented in a normalized form in an attempt to account for variables such as strength of the stabilization measure and subgrade deformation.

17. Key Words Aggregate, Cone, Criteria, Excavation, Experimental, Fill, Geosynthetics, Lime, Load, Model, Numerical, Soils, Stabilization, Undercut	18. Distribution Statement

19. Security Classif. (of this report) Unclassified	20. Security Classif. (of this page) Unclassified	21. No. of Pages 304	22. Price

Form DOT F 1700.7 (8-72) **Reproduction of completed page authorized**

DISCLAIMER

The contents of this report reflect the views of the authors, who are responsible for the fact and accuracy of the data presented herein. The contents do not necessarily reflect the official views or policies of the North Carolina Department of Transportation. This report does not constitute a standard, specification or regulation.

ACKNOWLEDGEMENTS

The authors would like to thank the members of the NCDOT Geotechnical, Materials, and Construction divisions who worked on this project. The time, expertise and guidance of NCDOT engineers were invaluable to this project. Special thanks are due to the members of the steering committee:

Njoroge W. Wainaina, P.E.
Kyung J. Kim, Ph.D., P.E.
John L. Pilipchuk, P.E., L.G.
Chris Kreider, P.E.
Dean Argenbright, L.G.
J. Dean Hardiste, P.E.
Robert E. Capehart, P.E.
Scott Hidden, P.E

Mrinmay Biswas, Ph.D., P.E.
Ernest Morrison, P.E.

Mehdi Haeri
Chun Kun Su

.

TABLE OF CONTENTS

Page No.

LIST OF TABLES xii

LIST OF FIGURES xv

EXECUTIVE SUMMARY xx

CHAPTER 1: INTRODUCTION 1

Problem Statement 2
Undercutting in Unstable Soils 3
Chemical Stabilization 6
Geosynthetics in Subgrade Stabilization 6

Objectives 6

Scope of Work 7
Phase I: Laboratory-Scale Testing Program 8
Phase II: Pilot-Scale Testing Program 8
Phase III: Numerical Modeling 9

Report Layout 10

CHAPTER 2: LITERATURE REVIEW 11

Geosynthetic Reinforcement of Paved and Unpaved Road Sections 11
Paved Roads: Unbound Layers and Subgrade 11

Large Scale Cyclic-Plate Load Testing 14
Summary—Large Scale Cyclic Plate Load Testing 25

The Dynamic Cone Penetrometer (DCP) 25
Development 25
Factors Affecting Results 26
DCP Correlations to Material Properties 27
DCP Correlations to California Bearing Ratio (CBR) 27
Empirical Correlations between DCP and Young's Elastic Modulus (E) 28
CBR and Resilient Modulus (M_R) Correlations 29
Use of Combined Equations to Predict Resilient Modulus (M_R) from DCP 29
Empirical Correlations between DCP and Resilient Modulus (M_R) 29

DCP for Compaction Evaluation 31

Chemical Stabilization 31
Improvement of soil properties by incorporation of lime or cement 32
Durability of stabilized soil 33

Numerical Analysis 34
Criteria for establishing required magnitude of undercut 38

Summary 42

CHAPTER 3: Test Materials Characterization 43

Subgrade soils 43
California bearing ratio testing 46
Resilient modulus testing 46
Selection of M_R value 49
Consolidated undrained triaxial testing 51
Unconfined compressive strength testing 52
Permeability testing 53

Aggregate Base Course (ABC) 53

Select fill 55
California bearing ratio testing 56
Resilient modulus testing 56
Consolidated undrained triaxial testing 57

Lime treated subgrade 57
Standard proctor compaction testing 57
Unconfined compressive strength testing 58
Resilient modulus testing 60

Summary 62

Chapter 4: Prototype Experimental Design via Field Measurements and Numerical Models 65

DCP Field Measurements 65
Bladen County 65
High Point, NC 68
Wake County, NC 68

Wave Equation Analysis of the DCP 71
Hammer Model 71

Pile Model 72
Soil Model 72
Shear strength estimation using wave equation 73
Resilient modulus using the wave equation 75
Summary 79

Prototype Test Design: Load Pulse Magnitude and Duration: Field Measurements 79
Site Description 79
Loading vehicles 79
Instrumentation 81
Results 81
Proof roll tests 81
Pan Scraper 83
Analysis 88
Rise to Rise vs. Peak to Peak 88
Pulse Duration 88
Pulse Magnitude 90

Prototype Test Design: Sample Size 90

Prototype Test Design Summary 93

Summary 93

Chapter 5: Prototype Testing and Quality Control 94

Instrumentation 95
Earth Pressure Cells 96
Surface Displacement 96
Data Acquisition 97
Surface Profile Measurements 97

Test Section Construction 98
Soil Preparation 98
Chemical Stabilizer Addition 99
Compaction 100
Geosynthetic Installation 102

Quality Control Testing 103
Nuclear Moisture-Density Gauge 103
Sand Cone 103
Rubber Balloon 105
Dynamic Cone Penetrometer (DCP) 105
Lime Stabilized Subgrade (LSS) Quality Control 106

Loading Sequence 107
Static Loading 107
Cyclic Loading 107
Proof-Roll Loading 107
Section Demolition 108

Large Scale Testing 108
Applied Loading 108

Measured Layer Thicknesses 111
Instrumentation Locations 112

CHAPTER 6: PROTOTYPE TEST QUALITY CONTROL 115

Moisture Content and Unit Weight 115

Dynamic Cone Penetrometer (DCP) 121
Aggregate Base Course (ABC) and Select Fill 122

Lime Stabilized Subgrade (LSS) 126

Section Reuse 128

Subgrade Remolding 130

ABC Gradations 132

Summary 134

CHAPTER 7: TESTING RESULTS 135

Static Load-Deformation Response 135

Bearing Capacity Tests 138
Static Analysis 139
Proof-Roll Loading 141
Cyclic Loading 145
14" Select Fill/3" ABC with Geotextile A (11) 146
Displacement Contours 150
Cumulative Displacements 151

CHAPTER 8: COMPARATIVE STABILIZATION PERFORMANCE 153

Comparison by Stabilization Type 153
Unreinforced Granular Layer Tests 153

Reinforcement Geotextile A Tests 157
Separation Geotextile B Tests 163
Geogrid A and Geogrid B Tests 167
Lime Stabilized Subgrade (LSS) Tests 171

Comparisons by Stabilization Depth 174
12 inch Undercut Stabilization Tests 174
18 inch Undercut Stabilization Tests 176
Deep Undercut Tests 179

Comparison to Results in Literature 181
Unreinforced Granular Layer Tests 181
Geosynthetic-Reinforced Tests 182

Equivalent Stabilization Comparison Methodology 184
Equivalence Comparison during Initial Cycles 186

Equivalence Comparison: Post-Repair Cycles 189

CHAPTER 9: NUMERICAL MODEL: INPUT PARAMETERS AND CALIBRATION 192

Material Properties 192
Index Properties 192
Shear Strength Parameters 193
Index Properties and Empirical Correlations 194

Stiffness Factors 194
Initial and Secant Modulus Values of Subgrade Soil 197
Inverse Analysis for the Stiffness of the Subgrade Soil Layer 198
Interface Properties 199
Hardening Effect 200

Loading Conditions 201

Model Configurations 202
Preliminary Analysis: Determination of Elements for Modeling Geosynthetic Material 203
Results of Static Load Correlations 205
Proof Rolling Case 207
Cyclic Loading Case 208

CHAPTER 10: UNDERCUT CRITERIA 211

Numerical Modeling 211

Model Description 212
Axisymmetric Model 212
Constitutive Soil Model 213
Material Properties 213

Simulation Modes 214
Simulated Field Loading 214
Simulation Cases 215
Proof Roller Loading 215
Flexibility of Loading 216

Results of Numerical Simulations 217
Bearing Capacity Analysis 217
Strength and Stability 219

Axisymmetric Loading Condition 220
Bearing Capacity 220
Design Criteria Based on Maximum Shear Strain 222
Undercut Criteria: Axisymmetric Condition 223
Undercut Design Criteria: Proof Roller Loading 224

Plane Strain Condition 225
Bearing Capacity 226
Undercut Criteria: Static Loading 227
Undercut Criteria: Pulse Loading 228
Bearing Capacity by Limit Equilibrium 230

Application of Undercut Criteria 231
Laboratory Testing 231
Application to Field Data 233

Summary 234

CHAPTER 11: SIMULATION OF FIELD CASES 235

Study Cases 235

Stabilization Measures 239

Input Material Properties 240

Equivalent Loading Condition 242

Results of Numerical Simulation 243
Bearing Capacities 243
Deformation Response: Proof Roller Loading 247

Deformation Response: Cyclic Loading 248

Aspects of Response 251

Summary 255

CHAPTER 12: COST ANALYSIS 257

Performance-Cost Analysis: Average Unit Costs 257

Stabilization Method Cost Calculation 258

Notes on Performance-Cost Analysis 261

CHAPTER 13: SUMMARY AND CONCLUSIONS 264

REFERENCES 272

APPENDICIES 284

LIST OF TABLES

Table 1. Test Configurations for Undercutting and Stabilization Measures 9
Table 2. B-values from Chua (1988) DCP to E Correlation..... 29
Table 3. Average Percent Change of Engineering Properties for Clay Soil (Christensen, 1969)..... 32
Table 4. Previous Research Using Numerical Programs..... 35
Table 5. Existing Analytical and Numerical Solutions for Inhomogeneous Isotropic Media Due to a Circular Load (After Wang et al., 2006)..... 37
Table 6 Soil Index Properties..... 44
Table 7. Corrected Soaked CBR Values..... 46
Table 8. Corrected Unsoaked CBR Values..... 47
Table 9. Load Sequence for Resilient Modulus Test (AASHTO T-307) 49
Table 10. Mohr-Coulomb Strength Parameters from CU Tests (June 2008) 51
Table 11. Comparison of Mohr-Coulomb Strength Parameters: Tests 2 and 4..... 51
Table 12. Comparison of Undrained Shear Strength (Su): Tests 2 and 4..... 51
Table 13. UCS Test Results..... 52
Table 14. Permeability Test Results 53
Table 15. ABC Index Properties..... 54
Table 16. Select Fill Index Properties..... 55
Table 17. Select fill Unsoaked CBR Test Results 56
Table 18. Select Fill Mohr-Coulomb Strength Parameters From CU Tests..... 57
Table 19. UCS Test Results For Lime Treated Subgrade Soils..... 59
Table 20. UCS Test Result For Test Pit Lime Treated Subgrade Soil 59
Table 21. Soil Index Properties..... 63
Table 22. Corrected Unsoaked CBR Values at Test Pit Condition 63
Table 23. Mohr-Coulomb strength Parameters from CU Tests at Test Pit Condition..... 63
Table 24. UCS Test Results on Coastal Plain Soil 4 63
Table 25. Resilient Modulus Test Results 64
Table 26. DCP Measurements and CBR Correlations..... 68
Table 27. Summary of DCP Efficiency Measurement Results..... 72
Table 28. Proofroll compiled data 86
Table 29. Pan scraper compiled data (rise to rise speeds calculated but not shown due to space constrain)
Table 30. Assumed Material Properties for Flac Prototype Models..... 91
Table 31. Depth to Vertical Stress Equal to 10% of the Applied Stress for Subgrade Depths of 3, 4, 5 and 10 ft. 92
Table 32. Summary of Constructed Test Sections..... 109
Table 33. Applied Loading Outline 110
Table 34. Intended versus Measured Stabilization Layer Depths..... 112
Table 35. Test Section Designations Reflecting Measured Layer Thicknesses 113
Table 36. Average Subgrade Dry Unit Weight and Water Content from Uncorrected and Corrected Nuclear Gauge Measurements..... 116
Table 37. Average Subgrade Dry Unit Weight and Water Content from Corrected Nuclear Gauge Measurements Using Average K-Value of -17.2 117

Table 38. Average Subgrade Dry Unit Weight and Water Content from Sand Cone and Balloon Density Tests 118
Table 39. Average Coastal Plain Subgrade DCPI 122
Table 40. Uncorrected Nuclear Gauge Dry Unit Weight and Water Content of ABC Layers 123
Table 41. Uncorrected Nuclear Gauge Dry Unit Weight and Water Content of Select Fill Layers 123
Table 43. Balloon Dry Unit Weight and Water Content of Select Fill 124
Table 44. Average Oven-Water Content of LSS Before and After Mellowing 126
Table 45. Average Percent Passing of LSS After Mellowing Compared to NCDOT Specifications 126
Table 46. Corrected Nuclear Gauge Dry Unit Weight and Water Content of LSS 127
Table 47. Sand Cone and Balloon Dry Unit Weight and Water Content of LSS 127
Table 48. Test Pit Versus Laboratory 7-day UCS for LSS 127
Table 49. LSS Average DCPI 128
Table 50. Corrected Nuclear Gauge Dry Unit Weight and Water Content Values for Tests with Reused Test Section 128
Table 51. Sand Cone and Balloon Dry Unit Weight and Water Content Values Loading for Tests with Reused Test Section 129
Table 52. DCPI for Tests with Reused Test Section 129
Table 53. Coastal Plain Subgrade Mohr-Coulomb Strength Parameters from CU Triaxial Testing performed by Pyo (2009) 131
Table 54. Static Load Test Plate Displacements (inches) 136
Table 55. Cumulative Displacements (inches) Bearing Capacity Tests 138
Table 56. Estimated Initial Subgrade Moduli (psi/in) 140
Table 57. Layered Elastic Analysis of Static Test Results: 40 psi using Fox (1948) Graph 142
Table 58. Proof-Roll Test Displacement Data (inches) 143
Table 59. Proof-Roll Test: Displacement Sorted by Permanent Displacement (inches) 144
Table 60. Load Plate Displacement During Cyclic 1 Loading (inches) 146
Table 61. Load Plate Displacement During Cyclic 2 Loading (inches) 147
Table 62. Maximum Test Pit Boundary Stresses (psi) at Log Cycles for Cyclic 1 149
Table 63. Cumulative Plate Displacements to Observed Tension Cracks 152
Table 64. Tests Sorted by Cyclic 1 Displacement between 0 and 200 Cycles 186
Table 65. Tests Sorted by Cyclic 1 Displacement between 200 and 1,000 Cycles 187
Table 66. Tests Sorted by Cyclic 1 Displacement between 1,000 and 10,000 Cycles ... 188
Table 67. Tests Sorted by Cyclic 2 Displacement between 0 and 200 Cycles 189
Table 68. Tests Sorted by Cyclic 2 Displacement between 200 and 1,000 Cycles 190
Table 69. Tests Sorted by Cyclic 2 Displacement between 1,000 and 10,000 Cycles ... 191
Table 70. Index Properties of Prototype Test Soils 192
Table 71. Typical Effective Angle of Internal Friction and At-Rest Earth Pressure Coefficients for Unbound Granular and Subgrade Material (NCHRP 2004) 193
Table 72. Results of Triaxial Test for Piedmont Residual Soil (NCDOT) 193
Table 73. Results of Triaxial Tests for Coastal Plain Soil 193
Table 74. Basic Statistics of Results of Triaxial Tests 195
Table 75. Elastic Moduli and Poisson's Ratio Values Used in Previous Research 195

Table 76. Elastic Moduli for Different Materials (Huang, 2004) 196
Table 77. Poisson's Ratio for Different Materials (Huang, 2004)..... 196
Table 78. Range of Elastic Moduli Values Used in Backcalculation 198
Table 79. Determination of Elastic Modului Values for Subgrade Soil Layer..... 199
Table 80. Stiffness and Strength Parameters Used in the Analysis 200
Table 81. Material Properties for Modeling Geosynthetic and Interface Materials 203
Table 82. Parameters of the Regression Curves by Power Functions 210
Table 83. Predicted Settlement and Estimation by Measured Values 210
Table 84. Material Properties Used in the Design Criteria Analysis..... 214
Table 85. Number of Cases According to Strength Parameters 215
Table 86. Classification of Numerical Simulations for Design Criteria..... 219
Table 87. Minimum Cohesion Threshold Values (assuming bearing capacity ratio = 2) 220
Table 88. Estimation of Ultimate Bearing Capacity by Terzaghi and Vesic Methods (c = 15 psi) 230
Table 89. Results of CU Triaxial Testing for Mixed Coastal Plain Subgrade Soil 232
Table 90. DCPI Values and Correlated Parameters: Demonstration of Undercut Criteria Using Field Data..... 233
Table 91. Typical Sections of Field Cases..... 235
Table 92. Computed Stabilization Factors for onditions Modeled in Case 1 240
Table 93. Computed Stabilization Factors for Conditions Modeled in Case 1 254
Table 94. Unit Costs from NCDOT 2008 Statewide Project Bid Averages..... 257
Table 95. Geosynthetic Unit Costs Provided by Manufacturers..... 257
Table 96. Stabilization Method Cost per Square Yard for Cyclic 1 258
Table 97. Sorted Cyclic 1 Performance-Cost between 0 and 200 Cycles 259
Table 98. Sorted Cyclic 1 Performance-Cost between 200 and 1,000 Cycles 259
Table 99. Sorted Cyclic 1 Performance-Cost between 1,000 and 10,000 Cycles 260
Table 100. Performance-Cost between 0 and 200 Cycles Considering Subgrade Stiffness 262
Table 101. Performance-Cost between 200 and 1,000 Cycles Considering Subgrade Stiffness 262
Table 102. Performance-Cost between 1,000 and 10,000 Cycles Considering Subgrade Stiffness 263

LIST OF FIGURES

Figure 1. Various Scenarios of Undercutting for Roadway Construction in Cut and Fill Situations 4
Figure 2. Three-Layer Elastic System (Huang, 1971) 38
Figure 3. Effect of Thickness on Deflection-Curvature Ratio (Huang, 1971) 39
Figure 4. Scheme of the Laboratory Stand: (1) Rear Cart; (2) Front Cart; (3), (5), (7) Hydraulic Cylinders; (4) Rigid Frame; (6) Rigid Cylinder; (8) Gear Belts (Maciejewski and Jarzebowski, 2004) 39
Figure 5. Structure of the Soil Layer During the Towed Cylinder Test (Maciejewski and Jarzebowski, 2004) 40
Figure 6. Depth and Mean Distance Between Cracks Versus Weight of the Cylinder (Maciejewski and Jarzebowski, 2004) 40
Figure 7. Relationship Between Penetration Depth and Strength Parameters for Rolling Wheel With Qv=67 Kn, D=1.52 M, B=0.46m, and γ=18 Kn/M3 (1mm=0.0394 inch and 1 kPa=20.89 Kpa) 41
Figure 8. Grain Size Distribution Curves of Various Soils Considered for Large Scale Testing 45
Figure 9. Moisture-Density Standard Compaction Test Results 45
Figure 10. Unsoaked CBR Test Results 48
Figure 11. MR Test Results on Coastal Plain Soil 4 50
Figure 12. Change in Undrained Shear Strength Between Test 2 and Test 4 at Three Different Confining Pressures 52
Figure 13. Correlation of Undrained Shear Strength from UCS With CBR 53
Figure 14. ABC Gradation Curves 54
Figure 15. ABC Modified Proctor Compaction Test Results 54
Figure 16. Select Fill Gradation Curve 55
Figure 17. Select Fill Moisture Content and Dry Unit Weight Relationships 55
Figure 18. Select Fill Resilient Modulus Test Results 56
Figure 19. Lime Stabilized Soil Standard Proctor Compaction Test Results 58
Figure 20. Lime Effect on UCS with Change in Lime Dosage and Curing Period 59
Figure 21. MR Values for 3% Lime Treated Subgrade 61
Figure 22. MR Values for 5% Lime Treated Subgrade 61
Figure 23. Comparison of Mr Values for Three Different Soil Conditions 62
Figure 24. Bladen County DCP Results, Proof Roll Fail from Station 19+00 To 28+00 (Kreider, 2009) 66
Figure 25. Excerpted Data and Incremental DCPI From Selected Data Sets Shown in Figure 24. 67
Figure 26. DCPI Plot for Passed Proof Roll Locations, NC 98 Bypass 69
Figure 27. DCPI Plot for Failed Proofroll Locations, NC 98 Bypass 70
Figure 28. Measured Efficiency Distribution 72
Figure 29. Correlation Between CBR and Su, from Multiple Sources 74
Figure 30. DCPI Vs. Undrained Shear Strength from GRLWEAP Analysis 75
Figure 31. Detail from Moduli of 0 To 200 Mpa. 76
Figure 32. Mohammad Et Al. (2007) Mr to DCPI Correlation. 77
Figure 33. Resilient Modulus yo DCPI Data from George and Uddin (2000) 77

Figure 34. Comparison of Measured To GRLWEAP Predicted DCPI Vs. Mr. 78
Figure 35. Proofroll Trailer (Courtesy M. Valiquette, NCDOT)..... 80
Figure 36. Caterpillar 631 Scraper (Courtesy M. Valiquette, NCDOT)..... 80
Figure 37. Proof Roll Trailer over Soft Subgrade, Fourth Pass. 82
Figure 38. Proof Roll Trailer over Stiff Subgrade, Third Pass. 82
Figure 39. Pan Grader over Soft Subgrade, Fourth Pass. 83
Figure 40. Pan Grader over Soft Subgrade, Fourth Pass (Detail. Note Time Scale). 84
Figure 41. Pan Grader over Stiff Subgrade, Fourth Pass 84
Figure 42. Pan Grader over Stiff Subgrade, Fourth Pass (Detail. Note Time Scale)..... 85
Figure 43. Comparing Rise to Rise and Peak To Peak Methods for Determining Time In Speed Calculations. 88
Figure 44. Relationship Between Pulse Duration and Vehicle Speed 89
Figure 45. Relationship Between Pulse Duration and Vehicle Speed, Pan Scraper Only89
Figure 46. Barksdale (1971) Load Pulse Duration Comparison with Data (Huang, 1993) 90
Figure 47. Pulse Magnitude Versus Speed 91
Figure 48. FLAC Results, 4 Foot Deep Subgrade Section 92
Figure 49. Completed Test Section Showing Test Pit, Load Actuator, and Reaction Frame 95
Figure 50. Typical Load Plate and Pad Configuration 95
Figure 51. Installed Earth Pressure Cells (Epcs) 96
Figure 52. Typical Surface Displacement Instrumentation Setup 97
Figure 53. Typical Surface Profile Measurement 98
Figure 54. Soil Preparation with Front-Tine Tiller 99
Figure 55. Spreading of Hydrated Lime on Coastal Plain Subgrade 99
Figure 56. Initial Soil Compaction Using Vibratory Plate Compactor..... 101
Figure 57. Additional Soil Compaction Using Jack-Hammer 101
Figure 58. Additional Compaction on LSS Using Jumping-Jack Rammer 101
Figure 59. Installed Geogrid B Before Granular Layer Placement 102
Figure 60. Installed Geotextile A Before Granular Layer Placement..... 102
Figure 61. Grain Size Distribution Curves Of Sands Used In Sand Cone Testing..... 104
Figure 62. Typical Sand Cone Test Setup 104
Figure 63. Typical Rubber Balloon Test Setup 105
Figure 64. Typical Dynamic Cone Penetrometer (DCP) Test 106
Figure 65. Instrumentation Cross Section for Test 1 (Not To Scale) 114
Figure 66. Sand Cone and Balloon Versus Uncorrected Nuclear Gauge Dry Unit Weight for Coastal Plain Subgrade 119
Figure 67. Oven Versus Uncorrected Nuclear Gauge Water Content for Coastal Plain Subgrade 120
Figure 68. Corrected Nuclear Gauge Versus Oven Water Content for Coastal Plain Subgrade 120
Figure 69. Corrected Nuclear Gauge Versus Sand Cone and Balloon Dry Unit Weight for Coastal Plain Subgrade 121
Figure 70. Uncorrected Nuclear Gauge Versus Oven Water Content 125
Figure 71. Uncorrected Nuclear Gauge Vs. Balloon Dry Unit Weight :ABC and Select Fill 125

Figure 72. Corrected Nuclear Gauge Dry Unit Weight and Water Content Versus Test Number 130
Figure 73. Coastal Plain Subgrade DCPI Versus Test Number 130
Figure 74. Coastal Plain Subgrade Undrained Shear Strength (Su) for Various Confining Pressures From CU Triaxial Testing Performed by Pyo (2009) 131
Figure 75. ABC Gradations for Tests 2 Through 6 133
Figure 76. ABC Gradations for Tests 14 Through 21 133
Figure 77 Static Load Test Surface Displacement for 16” ABC With Geogrid B (4) Test Section 137
Figure 78 Static Load Test Vertical Stress Increase Distribution for 16” ABC With Geogrid B (4) Test Section 137
Figure 79. Initial (Red), Incremental (Blue), and Unloading (Green) Subgrade Reaction Modulus (K, Psi/In) Calculation 139
Figure 80. Static Test Data At 40 Psi Plotted On Fox (1948) Graph 141
Figure 81. Proof-Roll Displacement for 19” ABC With Geotextile A (6) Section 144
Figure 82. Surface Displacement Per Log Cycles for 13” ABC With Geotextile B (14) Cyclic 1 Test 148
Figure 83. Vertical Stress Increase Per Log Cycles for 13” ABC With Geotextile B (14) Cyclic 1 Test 148
Figure 84. 19” ABC With Geotextile A (6) ABC Surface Displacement Contour Plan (Inches) 150
Figure 85. Cumulative Permanent Displacements From Static and Proof-Roll Loads for 19” ABC With Geotextile A (6) Test Prior To Cyclic 1 151
Figure 86. Tension Crack Formation During Cyclic 1 Of 17" Select Fill/3" ABC With Geotextile A (8) Test 152
Figure 87. Displacement Curves for Unreinforced Granular Layer Test 154
Figure 88. Intrusion Of ABC Into Coastal Plain Subgrade Surface - Post 14" ABC (5) Test 155
Figure 89. Displacement Curves for Tests Reinforced With Reinforcement Geotextile A 158
Figure 90. Punching Failure During 14" Select Fill/3" ABC With Geotextile A (11) Test 159
Figure 91. Displacement Curves for Unreinforced and Reinforcement Geotextile A ABC Tests 162
Figure 92. Fabric Stained By Pumped Subgrade Fines - Post 19" ABC With Geotextile A (6) Test 163
Figure 93. Displacement Curves for Tests Reinforced With Separation Geotextile B .. 164
Figure 94. Fabric Stained By Subgrade Fines - Post 13" ABC With Geotextile B (14) Test 165
Figure 95. Displacement Curves for Unreinforced and Separation Geotextile B ABC Tests 166
Figure 96. Displacement Curves for Unreinforced and Geogrid Reinforced ABC Tests 169
Figure 97. Layer Mixing (Geogrid Removed) - Post 16" ABC With Geogrid B (4) Test 170
Figure 98. Permanent Deformation - Post 11" ABC With Geogrid A (Test 17) 171

Figure 99. Displacement Curves for LSS Tests 173
Figure 100. Displacement Curves for 12 Inch Stabilization Tests 175
Figure 101. Displacement Curves for 18 Inch Stabilization Tests 177
Figure 102. Displacement Curves for Deep Stabilization Tests 180
Figure 103. 14" ABC (5) Displacement Curve Compared To Literature Test Results .. 181
Figure 104. Geotextile Tests Compared To Literature Test Results 183
Figure 105. Geogrid Tests Compared To Literature Test Results 183
Figure 106. Incremental Displacement Calculation Example for 18" ABC (15) Test ... 185
Figure 107. Extrapolated Displacements From 17" Select Fill/3" ABC With Geotextile A (8) Tests 185
Figure 108. Friction Angle From Index Properties 194
Figure 109. Range Of Elastic Modulus Values Obtained From the Literature 197
Figure 110. Determination Of Initial Elastic Modulus Values From Hyperbolic Curves 197
Figure 111. Rate Of Displacement for Various Elastic Modulus Values 199
Figure 112. Stress-Strain Curves Of Typical Triaxial Tests 200
Figure 113. Strain Hardening Curves for Subgrade and Select Fill Materials 201
Figure 114. Stress-Strain Relationship With Illustration Of Strain Hardening for Aggregate Base Course (After Cunningham, 2009) 201
Figure 115. Static Load Sequences 202
Figure 116. One Cycle Of Dynamic Loading 202
Figure 117. Three Different Models 203
Figure 118. Simulated Models With Various Thicknesses 204
Figure 119. Comparison Of Three Different Modeling Methods 204
Figure 120. Pressure and Displacement Plots for Large-Scale Tests 206
Figure 121. Displacement Results Of the Proof Roller Cases 207
Figure 122. Settlement Development Under Cyclic Loading for All Tests 208
Figure 123. Computed Error for Cyclic Loads 209
Figure 124. Log-Log Plots and Regression Curves Of the Power Function 209
Figure 125. Finite Difference Model and Three-Dimensional Shape for Simulated Model 212
Figure 126. Mechanical Characteristics Of Axisymmetric Condition 213
Figure 127. Stress-Strain Relationship Of Elastic-Perfectly Plastic Model 213
Figure 128. Loading Function and Displacement Response 215
Figure 129. Proof Roller and Dimensions Applied On Subgrade Soil 216
Figure 130. Deformed Wheel Configuration and Flexibility Factor for Different Strengths 217
Figure 131. Bearing Capacity Based On Prediction Of Prandtl's Wedge Theory Versus Deformation Approach 218
Figure 132. Typical Bearing Capacity Plots for Cohesive Soils 218
Figure 133. Bearing Capacity Plots for E = 5,000 Psi Cases 221
Figure 134. Capacity Ratios According To Elastic Modulus Values 221
Figure 135. Design Criteria Chart Based On Maximum Shear Strain At Boundary Of Loading Plate 222
Figure 136. Design Criteria Charts for Axisymmetric Load Condition 223
Figure 137. Design Charts for Proof Roller Loading 224

Figure 138. Design Charts for Permanent Settlement Of Proof Rolling Test 225
Figure 139. Bearing Capacity Plots for E = 5,000 Psi Cases..... 226
Figure 140. Capacity Factors According To Elastic Modulus..... 227
Figure 141. Design Criteria Charts for the Plane Strain Load Condition..... 228
Figure 142. Design Charts for Proof Roller Loading for the Plane Strain Condition 229
Figure 143. Maximum and Permanent Settlement Curves for Proof Roller Loading 229
Figure 144. Comparison Of Maximum and Permanent Displacement for Axisymmetric and Plane Strain Conditions 230
Figure 145. Comparison Of Bearing Capacity Using General Approaches 231
Figure 146. Application Of Undercut Criteria for the Subgrade Soil and Stabilization Measures Used In Large-Scale Testing..... 232
Figure 147. Samples Located In Design Chart 233
Figure 148. Project Section and Corresponding Idealization for Numerical Model: 236
Figure 149. Dimensions, Construction Sequences, and Numerical Mesh: Case 1 236
Figure 150. Dimensions, Construction Sequences, and Numerical Mesh: Case 2 237
Figure 151. Modeled Sections for Case 3..... 238
Figure 152. Numerical Mesh for Case 4 Section..... 239
Figure 153. Simulated Models According To Construction Sequence..... 240
Figure 154. Modeling Of Stabilization Options for Case 1..... 241
Figure 155. Ratio Of Mobilized Pressures Assuming Axisymmetric Versus Plane Strain Conditions At A Uniform Displacement..... 242
Figure 156. Bearing Capacity Analysis 243
Figure 157. Displacement and Mobilized Pressure Curves..... 244
Figure 158. Pressure Versus Displacement Plots 245
Figure 159. Settlements for Each Stabilization Method for All Field Conditions..... 246
Figure 160. Effectiveness Of the Stabilization Methods 246
Figure 161. Settlement With Time At the Center Of Proof Roller Loading Pulse..... 247
Figure 162. Permanent Settlements for Proof Roller Loading 248
Figure 163. Maximum Displacements for Proof Roller Loading..... 248
Figure 164. Displacement Plots for Field Conditions Under Cyclic Loading..... 249
Figure 165. Maximum Settlement Of Each Case According To Stabilization Method . 250
Figure 166. Effectiveness Of Stabilization Method By Estimating the Ratio Of Settlement Magnitudes 250
Figure 167. Vertical Displacement Contours and Vectors: Case 1 251
Figure 168. Strain Distribution Of Geotextile (HP570) Stabilized Cases 252
Figure 169. Y-Direction Displacement Profiles for Each Stabilization Method for Case 1 253
Figure 170. Stress Increase With Depth for Various Stabilization Measures (Case 1): Loading Imposed By the Fourth Lift and 60 Psi Surface Pressure 254
Figure 171. Relationship Of Stabilization Factor With Settlement: Case 1 255
Figure 172. Performance-Cost Visualization Graph..... 260

EXECUTIVE SUMMARY

Work in this report is focused on the development of systematic criteria for discerning the need for undercutting and stabilization of soft subgrade, and the comparative performance of various stabilization measures. The North Carolina Department of Transportation (NCDOT) typically identifies sections for undercut based on the strength and plasticity of *in situ* soils during the design phase, or when proof roll testing shows excessive rutting and/or pumping. Similarly, NCDOT experience with the dynamic cone penetrometer (DCP) for identifying soft soils has shown that when testing yielded a DCP index of approximately 38 mm/blow (1.5 inches/blow), or greater, undercut will likely be required. The main objectives of the research were to develop a systematic approach for determining whether or not undercut is needed, and to investigate the adequacy of stabilization measures typically employed if undercut was deemed necessary. To that end, work in this research project provided the following:

i. Establishment of undercut design criteria based on the magnitude of strength and modulus of the subgrade soils. The undercut criteria were based on meeting a deformation limit state of 1 inch for both pumping and rutting, but with the additional requirement that bearing resistance of subgrade is at least twice the applied tire pressure to minimize the potential for rutting. The proposed criteria are validated through data from the large scale laboratory testing as well as data from field testing.

ii. Development of a procedure for the use of DCP to provide input data for undercut criteria on the basis of modulus and strength. The proposed procedures are based on the analysis of the DCP data using wave mechanics and has the advantage of discerning the need for undercut with depth (by applying the proposed undercut criteria incrementally) at the various phases of design and construction.

iii. Development of guidelines for specifying a stabilization measure to achieve adequate subgrade support. Five stabilization measures are investigated through the performance of 22 large scale laboratory tests. These included the use of select fill, aggregate base course (ABC), geogrids with ABC, geotextiles with ABC, and lime stabilization. The performance of each stabilization measure is investigated in the laboratory and through numerical analyses.

iv. Demonstrating the applicability of the proposed measures in field configuration including cut and fill situations. Four field cases are idealized from actual project sections and are numerically modeled with the stabilization measures. Case 1 represents at-grade road widening of an existing roadway by adding a fill section. Case 2 represents the construction of a new alignment in a fill situation. Thickness of fill is typically less than six feet. Case 3 represents a new alignment in a cut situation. In areas where the subgrade fails proof rolling, typically 3 ft of undercut has been implemented. Case 4 represents projects in which a highway median is widened. Observations are made regarding subgrade response under static, proof roll, and cyclic loading.

Performance of a comparative cost analysis to illustrate the relative cost of each stabilization measure in relation to measured performance (surface deformation). The cost analyses are performed with results presented in a normalized form in an attempt to account for variables such as strength of the stabilization measure and subgrade. The relative economics of the stabilization methods were calculated using the measured displacement from the large scale tests and the bid averages collated by the NCDOT.

CHAPTER 1: INTRODUCTION

The construction of roadways often requires traversing areas that contain materials that are unsuitable for the subgrade soils that lie beneath the pavement. These materials can be expansive, highly plastic, soft, wet, and/or weak. The exact nature of potential construction problems depends on whether or not the natural grade is to be excavated or if an embankment is to be constructed. The supporting soils may be susceptible to excessive consolidation, shrinking and/or swelling with changes in moisture conditions, or heave-induced volume changes due to the excavation of overlying soils, i.e., a cut section. Accordingly, the following four questions, for which timely answers are crucial, usually arise when soil-related construction issues must be addressed:

1. Is undercutting necessary for the construction of the roadway, and, if so, has it been predicted or taken into account in the design phase of the project?
2. To what depth should the undercut be performed?
3. Is implementation of the undercut sufficient, or should it be supplemented (or replaced) with other approaches, such as chemical stabilization or geosynthetic reinforcement?
4. What are the changes in the properties of the subgrade over the short term (during construction) that occur as a result of undercutting and implementing any proposed supplemental measures that may be quantified for the benefit of the pavement design?

At present, the need for undercutting generally is determined by subjectively observing the proof rolling process. If the proof roller causes subgrade pumping or excessive rutting, then an undercut usually is recommended. Generally, undercutting is performed until “good” soils are encountered. Typically, 3 to 6 ft of the soft subgrade is undercut and replaced with backfill materials (per NCDOT engineers). At times, the NCDOT endeavors to reduce the depth of an undercut (termed by the NCDOT as a “shallow undercut") by incorporating fabric and/or aggregate base course (ABC) stone as reinforcement. Keeping in mind this desire to reduce the amount of undercutting or even eliminating the need for undercutting, if appropriate to do so, the NCDOT Geotechnical Engineering Unit has identified this research to accomplish the following tasks:

i. Review the current NCDOT practice of: (a) specifying undercutting in the design and (b) determining the amount of undercutting to be performed during construction.
ii. Establish the factors that determine the need for undercutting in soft subgrade and in situations with high groundwater conditions. These factors should be based on the target stiffness and strength properties of the subgrade layers. Identification of such factors can be assisted by the use of *in situ* testing techniques.
iii. Implement the dynamic numerical modeling of short-term (during construction) condition to investigate the factors that affect the need for and extent of the undercut. Use the modeling results to identify the key parameters that help determine the depth of the undercut, the stress distribution in the layered system, and the potential for subgrade instability under repeated traffic loading.

iv. Develop guidelines for alternative and/or supplemental approaches to undercutting, including the use of geosynthetics and chemical stabilization to limit volume changes and improve subgrade properties and workability, and possibly alter/control moisture content, if deemed advantageous. Note that the emphasis here is not research into chemical stabilization or geosynthetics reinforcement, but rather, determining the allowable reduction in the depth of the undercut and the equivalent cost factors when these stabilization measures are utilized.

Addressing these issues is necessary to avoid cost overruns in construction projects where undercutting is implemented. In addition, establishing undercut guidelines will ensure the adequate performance of construction haul roads as well as completed roadway pavements.

Problem Statement

In many cases, the NCDOT uses the undercut approach as a means to facilitate construction in areas with unstable soils. At present, the NCDOT is seeking to establish criteria to systematically define situations in which undercutting should be implemented, and develop guidelines for estimating the associated key design parameters in such situations. Although proof rolling is one approach for determining the need for undercutting, it is unclear how much "pumping" of the field soils occurs before undercutting is deemed necessary. According to NCDOT engineers, proof rolling is performed with a 50 T load. In some cases, if undercutting is not implemented and the compacted fill later fails during proof rolling, then the fill must be removed and undercutting is necessary after all. This repair is expensive.

However, even when undercutting is deemed necessary, no systematic and quantifiable criteria are available to determine the required depth of the undercut and whether the subgrade properties are adequate to support the construction traffic loads (short term) and the final pavement section (long term). NCDOT engineers have indicated that, on occasions, the Dynamic Cone Penetrometer (DCP) has been used; however, a minimum penetration-resistance criterion has yet to be established.

It is reasonable to suggest that the establishment of systematic criteria for specifying situations in which subgrade soils should be undercut, and specifying the corresponding depth and required properties of the soil at the base of the cut, would help minimize unexpected cost overruns and construction schedule delays. This is especially true in situations where the subgrade is incapable of supporting construction traffic and the decision to undercut is based on scant data once construction has already started. The unavailability of published undercut guidelines has also led to inconsistent practices throughout North Carolina. According to NCDOT engineers, it is possible that soils with potentially good properties, but which happen to be too wet, are undercut and replaced, when instead, reworking and drying the materials to an appropriate moisture level may have been a viable alternative. In addition, the use of undercutting as the sole stabilization

measure in some instances may not be sufficient. Alternative and supplemental approaches, such as chemical stabilization or geosynthetic reinforcement, may actually provide a more cost-effective stabilization measure than undercutting. However, such alternatives to undercutting, as they apply to North Carolina soils, have not been evaluated systematically in conjunction with undercut implementation. Accordingly, it is beneficial to explore the cost equivalence for each of the candidate stabilization measures to assist in the implementation decision.

Undercutting in Unstable Soils

As outlined by Wiggins et al. (1978), the lack of appropriate improvement measures for unstable soils leads to billions of dollars in damage each year. As populations increase and urban areas expand, it is unavoidable that pavement subgrades, highway embankments, and foundations are placed in areas with poor soil conditions. Examples of such unstable soils can be found within the Triassic basins of North Carolina, and generally in coastal plain and piedmonet geologic regions. The stability of highway structures on unstable soils is time-dependent and of serious concern, first during construction on the soft soils, and then on a long-term basis when these structures may experience significant movement and plastic deformation that compromise their intended function.

According to NCDOT engineers, undercutting is employed usually when the existing ground in a fill section or subgrade soils in a cut section (on occasions also subgrade soils in a fill section) are judged by the Roadway Inspector (RI) to have poor engineering qualities. Figure 1 shows a number of cases of the need to evaluate subgrade suitability.

Case 1 represents the at-grade road widening of an existing roadway by adding a fill section. After clearing and grubbing, the RI determines the possible presence of shallow groundwater (4 ft or less) and soft subgrade conditions, and whether soil improvement is needed. This decision is made based on proof rolling and/or visual inspection (possibly by digging a test pit and observing its soil) as well as experience. If high groundwater is the cause of the soft subgrade, the use of subsurface drainage measures may be sufficient to stabilize the subgrade by reducing its moisture content. If groundwater is not a factor, the questionable materials (typically 3 ft or less in depth) are excavated and replaced with select fill. For unsuitable materials that are deeper than 3 ft, geosynthetics are sometimes used in conjunction with some measure of undercut. Empowering the RI with a systematic tool for making a sound decision whether or not to undercut and for determining the depth of the undercut would be advantageous in this case.

Case 2 represents the construction of a new alignment in a fill situation. In this case, the area is cleared but not necessarily grubbed (i.e., the root mat is left in place). The decision to undercut typically is made prior to construction, and the amount of undercut is indicated on the construction plans. In the case of poor soils, the undercut can be as deep as 6 feet. A high groundwater table condition, if present, needs to be addressed during the implementation of the “excavate and replace” process (once construction is completed,

groundwater is not a factor with the addition of 6 ft of fill). In addition to the need to determine the depth of the undercut with the proper backfill replacement, another concern in this case is heavy and repetitive hauling, as it causes deterioration of the fill section's subgrade stability.

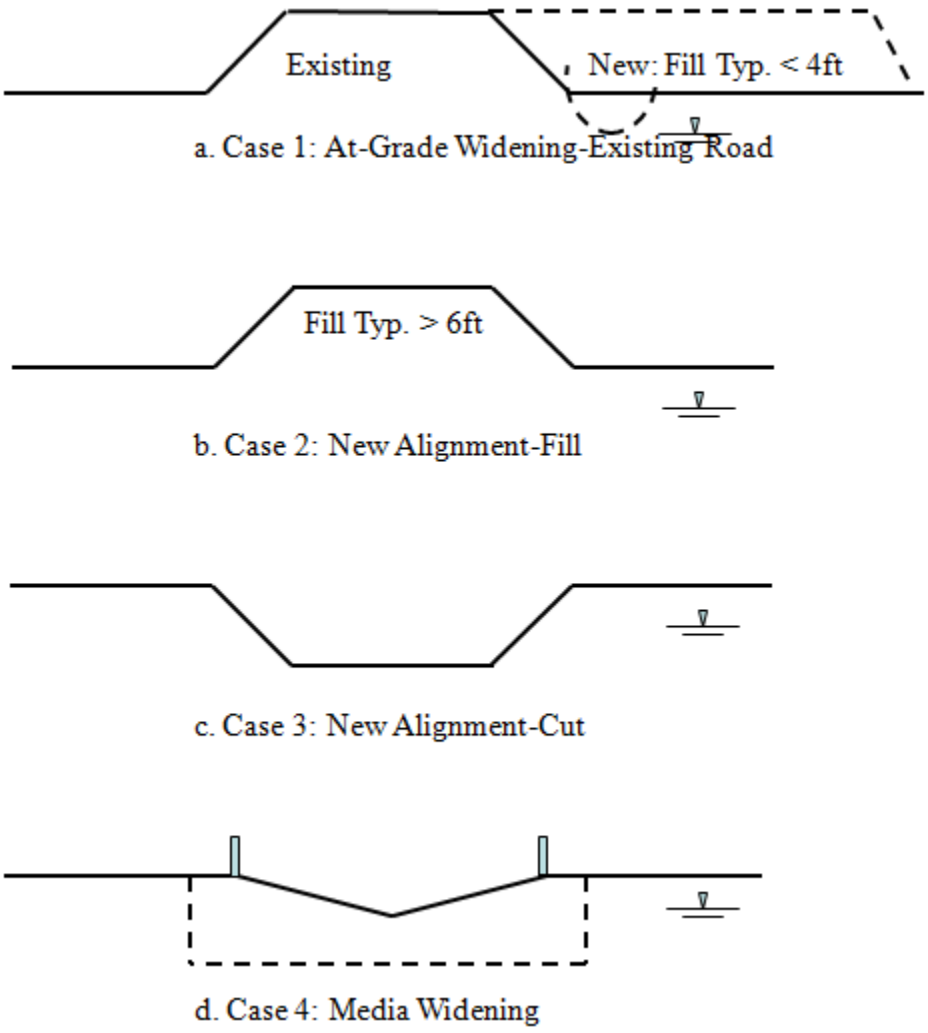

Figure 1. Various Scenarios of Undercutting for Roadway Construction in Cut and Fill Situations

Case 3 represents a new alignment in a cut situation, which is a typical scenario in the Piedmont physiographic locations. With the presence of a high groundwater table, the depth of the undercut is affected by the level of moisture, which can fluctuate with seasonal groundwater elevation changes. Depending on the value of the *in situ* moisture content ($w_{in\ situ}$) as compared to the optimum moisture content (w_{opt}), chemical stabilization is implemented. If the $w_{in\ situ}$ is within 3% of the $w_{opt,}$ cement is used, and if it is within 6%, lime is used. In the Piedmont area, however, soils classified by AASHTO as A-4 and A-5 tend to be micaceous in nature and do not dry easily to fall near the w_{opt}.

In addition, haul traffic causes deterioration of the subgrade. In areas where the subgrade has failed proof rolling, typically 3 ft of undercut has been implemented with the addition of select backfill reinforced with geosynthetics. Recently, the NCDOT also considered 1.5 ft of undercut with the use of geosynthetic reinforcement and an ABC as the backfill.

Case 4 represents projects in which a highway median is widened; these projects are among the most challenging and high visibility projects to construct, because the existing road often needs to remain in operation while construction proceeds. In this case, access and hauling are key concerns. The construction is staged to one side of the roadway while hauling takes place on the other side, which concentrates the repetitive construction traffic and causes subgrade deterioration. The depth of the undercut should be limited in this case so that shoring can be avoided. High groundwater and surface water conditions should be addressed so that the construction area remains free of ponding water. The preferred method for stabilization in these cases is a shallow undercut (less than 1.5 ft) with reinforcement geosynthetics.

At present, when poor subgrade soils are encountered, four approaches are taken, individually or in combination. These approaches are to: i) excavate and replace with adequate backfill (referred to here as *undercut*); ii) install chemical stabilization, which is usually performed by mixing the top 6 to 8 inches of soil with cement or lime, and generally implemented in the central and western parts of the State; iii) employ reinforcement geosynthetics in cases where the depth of the undercut is limited by, for example, the presence of subsurface utilities in order to attenuate applied traffic loads and therefore reduce the required depth of the excavation; and, iv) install subsurface drainage using vertical or horizontal drainage elements.

For the four case studies, when undercutting is recommended, the objective of the research described in this study is not only to reduce the depth of excavation, if possible, and therefore expedite the construction process, but also to implement the most cost-effective means of stabilization.

To summarize, the main challenges for the successful and economical stabilization of poor subgrades using undercutting are:

- Determining the situations in which undercutting is needed based on quantifiable criteria presented in terms of the strength and stiffness of the subgrade soils.
- Determining the depth of the undercut required in cases where no other additional means of stabilization are to be used. The depth of the undercut should be established based on the required short-term and long-term strength and deformation criteria. The short-term (during contruction) objective is to maintain a stable subgrade during the time the subgrade is subjected to repeated construction equipment traffic. The long-term (design life) objective is to provide the strength and modulus properties for the design of the pavement layers after construction is completed.

- Establishing guidelines to provide information regarding the benefits of supplemental and/or additional stabilization measures for undercutting. These additional measures include geosynthetics reinforcement, chemical stabilization, and/or subsurface drainage.

Chemical Stabilization

It is emphasized here that the investigation into chemical stabilization that is presented in this report is limited and focuses on the economic equivalence of using chemical stabilization in modifying poor subgrades compared to undercutting. In general, information in the literature about the chemical stabilization of soft soils can be grouped into three categories: improvement of the stabilized soil's properties, durability of the stabilized soil, and exploring non-traditional stabilizers and recycled materials.

Over the past two decades, an extensive body of research has been published on subgrade stabilization using cementitious materials. However, the main emphasis of these efforts has been the performance of the stabilized subgrade once the material has cured under near ideal conditions. Major challenges using this method arise due to the required curing times, which consequently result in traffic delays and less than optimum utilization of construction resources. In addition, there are circumstances under which the use of chemical stabilization is not effective. These situations include lack of sufficient clay content for the proposed use of lime, high organic content, unsuitable soil gradation, and low soil pH values. In these cases, the use of geosynthetics as a stabilization mechanism may be warranted.

Geosynthetics in Subgrade Stabilization

Geosynthetic materials are being used increasingly as a means for ground improvements in applications such as embankments on soft soils and for roadway systems. In pavement systems, geosynthetics have been used mainly for layer separation and drainage, with subgrade reinforcement applications emerging over the past few years. Geosynthetic reinforcements typically are placed at the interface between the subgrade layer and the aggregate base course. Through interface shear resistance, the reinforcement material confines the granular layer and attenuates induced stresses in the subgrade below.

Objectives

This research program was envisioned to encompass four phases that incorporate small-scale laboratory testing, pilot-scale laboratory testing for simulating field conditions, and numerical modeling. The research data have been used for the development, validation, and verification of guidelines and criteria for discerning the need for undercutting under poor soil conditions, the required depth of the undercut, and associated stabilization measures to achieve adequate subgrade support for short-term (during construction) and

long-term roadway construction objectives. Specifically, the objectives of the research are to:

i. Establish factors that determine the need for undercutting and to document the NCDOT's practice in addressing such situations and in establishing quantitative criteria to assist and inform the decision of whether or not to undercut. Such criteria are developed in terms of the subgrade strength and modulus, and moisture content and strength properties under repeated loading.
ii. Explore simple *in situ* testing techniques to provide data for the establishment of the undercut criteria on the basis of dynamic stiffness and strength. In parallel, develop proof-rolling guidelines for establishing the need for undercutting.
iii. Develop guidelines for specifying the depth of the undercut and the quality of the replacement material to achieve adequate subgrade support for short-term (during construction) and long-term (design life) objectives.
iv. Establish implementation schemes for alternative or supplemental approaches to undercutting, including the use of geosynthetics and chemical stabilization to limit volume change, alter/control moisture content, and improve soil properties and workability.
v. Perform a comparative cost analysis to illustrate the relative cost of each measure so that an informed decision regarding subgrade stabilization can be made.

Scope of Work

The scope of this research includes the development of criteria to define the need for undercutting, the depth of the undercut, and the quality of the backfill material such that cost and performance are optimized. In addition, chemical stabilization and geosynthetics reinforcement, in combination with several thicknesses of the ABC were studied to provide comparative criteria for the enhancement of various poor subgrade soils encountered in North Carolina with, or in lieu of, undercut and replacement with select fill. The criteria are presented along with the associated relative costs of each alternative.

This research is envisioned to encompass four phases. Phase I consists of laboratory testing of a soil typically encountered in an undercut situation in North Carolina, and includes the engineering properties and resilient modulus degradation with accumulated strain under repeated loading. Phase II includes pilot-scale testing to develop a systematic approach to use *in situ* methods for discerning the need for undercutting, and to provide data to assist in estimating the depth of the undercut. Data from Phase II were used to evaluate improvements in subgrade properties with the implementation of chemical and geosynthetics stabilization techniques and to aid in the development of equivalency factors. Phase III comprises the numerical modeling of the subgrade sections to investigate the sensitivity of modulus degradation to the accumulated levels of deformation and plastic strain under traffic loading. Data obtained from Phases I and II were used to develop input for the numerical modeling. The results of Phases I, II and III are contained in this report.

Finally, Phase IV, not yet undertaken, will encompass field instrumentation and monitoring of test sectons to collect data on the performance of implemented undercut areas, using both conventional fill as well as geosynthetic-reinforced aggregate layers and lime-stabilized subgrade approaches. These data will be used eventually for the validation and verification of the short-term and long-term criteria that are presented in this report

Phase I: Laboratory-Scale Testing Program

The focus of the laboratory-scale testing program is to estimate the baseline physical and engineering properties, which include the resilient modulus values of subgrade soils typically encountered in undercut situations in North Carolina. Test soils were obtained from two sites at which NCDOT expect undercutting to be performed (or from the vicinity of sites where undercutting has been performed in the past).

Conventional geotechnical testing was conducted in accordance with ASTM standards to define the test soils' physical and engineering properties. These properties include grain size, specific gravity, relative density, Atterberg limits, compaction, and shear strength, as appropriate to each soil type. Resilient modulus tests were conducted to develop a correlation with index properties and were conducted using AASHTO T 307 "Standard Method of Test for Determining the Resilient Modulus of Soils and Aggregate Materials". The degradation of the modulus with repeated loading was characterized at different moisture contents, because one of the reasons for unexpected undercutting is the seasonal fluctuation of groundwater levels.

Phase II: Pilot-Scale Testing Program

The pilot-scale experiments were conducted in a test pit 6 ft wide x 9 ft long x 7 ft deep in the Constructed Facilities Laboratory (CFL) at North Carolina State University (NCSU). The experimental program includes two stages:

i. Conducting the DCP test to characterize the subgrade modulus and establish correlations with the resilient modulus.
ii. Characterizing the subgrade behavior and responses (including the deformation profile) under repeated loading as a function of various undercut depths and geosynthetic reinforcement and chemical stabilization measures.

Cyclic plate load tests were used to estimate the capacity and stiffness of the various subgrades tested. The cyclic load tests were performed on a 1 ft circular plate subjected to simulated traffic loading from a servo-hydraulic MTS system. This system consists of a loading frame, a hydraulic actuator, and a servo-control unit connected to both a data acquisition system and a hydraulic control valve. Details of the test set-up, including instrumentation, are presented in Chapter 5. A total of 22 plate load tests, as detailed in Table 1, were conducted for this phase of the investigation. Ten tests were performed using geosynthetic reinforcement, with two geotextile types (one separation and one

reinforcement) and two geogrids typically used in soft soils stabilization. Two of the reinforcement tests were repeated for quality assurance. The undercut depth varied between 6 inches and 3 feet. Four tests were performed using lime stabilization, with the stabilized layer being 8 inches thick.

Table 1. Test Configurations for Undercutting and Stabilization Measures

Planned Depth of Undercut	No Backfill	ABC	Select Fill	Geogrid		Geotextile*		Chemical Stabilization
0	1	-	-	Stone	A-2	Stone	A-2	4 tests: stabilized thickness 8 inches + 3 inches ABC
6	-	1						
12	-	1		1		2R 1S	1R	
18	-	3		1		1R 1S	1R	
24							1S	
36			2					

*R = Reinforcement, S = Separation

Phase III: Numerical Modeling

Given the four scenarios described in the Background section and their construction sequences, the subgrade conditions and traffic loading were modeled to answer the following questions:

i. Once the depth of the undercut is specified, what is the rate of degradation of the subgrade modulus with repeated construction traffic loading, and what are the input values for the pavement layer design after construction is complete?
ii. What is the distribution of the stresses within the pavement and subgrade layers given the variability in modulus magnitudes, including the case of a shallow stiff layer underlying a soft subgrade that is 4 to 6 feet deep (i.e., the range of the undercut depth)?
iii. How do seasonal fluctuations of the groundwater conditions affect the plastic deformation of the subgrade under construction and traffic loading?
iv. Will repeated traffic loading cause bearing capacity failure of the subgrade under high groundwater conditions?
v. What is the sensitivity of the estimated deformation and of the accumulated level of plastic strain to the level of stabilization measures that are implemented?

The modeling effort utilizes the two-dimensional numerical analysis computer program FLAC2D (which is also used by the NCDOT). The base case of the model simulates undercutting with subsequent backfill and loading in cut-and-fill roadway construction situations. The model analysis follows the sequence of construction in the field. Key parameters to be analyzed include: depth of the undercut, the subsurface layers of soft over stiff soils, a variety of subgrade strength and modulus values, the extent of alternative measures, that is, either geosynthetic reinforcement or chemical stabilization, and the impact

of seasonal fluctuations of the groundwater conditions on the deformation of the subgrade under construction and traffic loading.

Report Layout

The Scope of Work (described above) was performed from September 2007 to October 2009. This report is organized as follows:

- Chapter 2 reviews appropriate studies from the literature.
- Chapter 3 presents the laboratory characterization of the mechanical properties of the materials used in the subsequent test pit experiments.
- Chapter 4 presents the experimental design for the test program and the determination of significant field parameters.
- Chapter 5 describes the prototype-scale experimental set-up, including the test pit, sample formation procedures, and loading and instrumentation systems.
- Chapter 6 presents documentation of the quality control program undertaken throughout the prototype-scale testing.
- Chapter 7 presents the results of the prototype-scale testing in terms of measured subgrade stresses and displacements as a function of cycles of load application.
- Chapter 8 presents a performance comparison of the various subgrade stabilization measures and configurations explored in the prototype-scale tests.
- Chapter 9 describes the numerical modeling techniques and model calibration.
- Chapter 10 describes the development and application of the undercut criteria.
- Chapter 11 explores by numerical analysis several of the most frequently encountered cut-and-fill field configurations.
- Chapter 12 presents a cost analysis of the various stabilization measures investigated.
- Chapter 13 presents a summary of the research, draws conclusions from the results, and suggests directions for the field implementation project and future research.

CHAPTER 2: LITERATURE REVIEW

A survey of the literature was undertaken to review the state of practice and recent findings for the scope of this report. This review summarizes large scale cyclic plate load testing programs performed in the past, descriptions of and correlations using the dynamic cone penetrometer (DCP), stabilization of subgrades using geosynthetic or lime, and approaches to numerical analysis.

Geosynthetic Reinforcement of Paved and Unpaved Road Sections

Gabr et al. (2006) looked at the state of practice of geosynthetics usage in paved and unpaved road sections. Some of those findings are summarized here. Reinforcement of roadway subgrade can be broken into methods for paved roads and unpaved roads.

Paved Roads: Unbound Layers and Subgrade

There are a number of national guidelines and manuals that have been proposed for geosynthetic use in paved roads. AASHTO PP 46-01 (AASHTO 2001) provides guidelines for base course reinforcement by geosynthetics by recommending the designer to follow the procedures specified in Holtz et al. (1998) or the procedures from the GMA White Paper II (Berg et al., 2000).

Holtz et al. (1998) proposed design methods for temporary or permanent roadways. In temporary roadway design (i.e. construction access roads, etc.), the engineer may assume the geosynthetic improves the drainage and keeps the subbase separated from the weaker native subgrade soil. This improvement is modeled using an increased bearing capacity factor, which reduces the required calculated thickness of the roadway and provides benefits in terms of material and labor savings. The increased bearing capacity implicitly assumes that the rut depth be large enough to mobilize this additional bearing capacity.

In permanent applications, the above method can be used to reduce the thickness of any stabilizing layers, but it is assumed the reinforcement will not improve the bearing capacity of the structural layers. As such, no reduction in the design base course thickness is allowed. However, economies may be realized by reducing the aggregate required for stabilization and construction.

The U.S. Army Corps of Engineers (Tingle and Webster, 2003) specifies a method of design for subgrade and unpaved road reinforcement similar to that described in Holtz et al. (1998). The bulk of these recommendations are based on the effect of geotextile separation and filtration on subgrade strength by Steward et al. (1977), although the design methodology has been expanded to include geogrids based on engineering judgment.

Berg et al. (2000) proposed a method for design of base course and subbase reinforcement based on the results of a number of field studies from literature. Base course reinforcement is quantified using three different factors: Base Course Reduction (BCR) to reduce the thickness of base courses, Traffic Benefit Ratio (TBR) to extend the life of the pavement and Layer Coefficient Ratio (LCR), which is used in some methods to match reinforced to unreinforced cross section performance by modifying the base course portion of the AASHTO structural number equation. Each factor depends on the type of reinforcement, aggregate, and design cross section for which it was calculated. Currently, however, the design approach has no mechanistic basis and the method suggests obtaining one of these ratios on the basis of lab tests that have been correlated to a field section for a particular reinforcement.

For subgrade restraint in permanent paved roads, Berg et al. (2000) recommend procedures outlined by other researchers to estimate subgrade thicknesses required to support construction activities. In these cases, the geosynthetic layer may act in one or more of the following functions: separation, filtration or reinforcement. Nine different possible design methods are listed, including the method described by Holtz et al. (1998). Seven of the remaining eight methods are for specific products calibrated by the product's manufacturer.

Berg et al. (2000) also discuss the separation and stabilization function of geotextiles in temporary and permanent roads. The geotextile acts to maintain distinct layers of base course and subbase materials. This prevents mixing, and at a minimum helps to ensure the designed layer thicknesses are maintained throughout the pavement's (unreinforced) design life. In many cases, the stabilization function is often primary for roadways with CBR greater than two or three.

Recent research on design methods for unbound layers includes both subgrade reinforcement and base or subbase reinforcement. The European practice described by Watn *et al.* (2005) mainly focused on the subgrade stabilization aspects, where geotextiles, geogrids and geocomposites are used to increase the bearing capacity of very soft soils. The thrust of the application is that the use of these geosynthetics reduces the pressure on the soft subgrade, and also tends to reduce deformation due to traffic or construction loading. Watn et al. (2005) observe the benefit of geosynthetic reinforcement tends to increase as the quality of the subgrade decreases or as the number of traffic loadings increase.

Perkins *et al.* (2005a) also noted geosynthetics usage in the subbase to reduce deterioration and fatigue cracking due to dynamic loading. Perkins et al. (2005b) stressed the importance of geosynthetics in subgrade reinforcement. This usage appears to be in practice in at least some USFS roadways, as discussed by Vischer (2003). In this case, geogrid reinforcement with a geotextile separator was used to rehabilitate a paved road over a soft subgrade. Al-Qadi and Appea (2003) also reported on an eight year study investigating the effects of geogrid and geotextile reinforcement placed between the base course and subgrade. They investigated three different base course thicknesses, and

realized a measurable increase in service life and pavement quality only on the thinnest, 100-mm thick, base course.

For permanent unpaved roadways, current practice tends to treat reinforcement of unpaved roads as a separate topic from subgrade reinforcement for paved roads. This comes from the lower traffic volume and acceptance of larger ruts that can develop in unpaved road applications. For nationally used guidelines, the work of Holtz et al. (1998) described previously treats permanent unpaved roads like permanent paved roads—stabilizing layers may be reinforced and reduced in thickness, but structural layers are assumed to be unaffected. Berg et al. (2000) does not explicitly cover unpaved roads, but the same principles outlined in that report could also be applied.

Permanent unpaved road design has appeared often in literature. Early work by Giroud and Noiray (1981) and Steward *et al.* (1977) proposed design methods that required deep and large rutting magnitudes to mobilize a tensioned membrane effect in the geotextile layer. Recently, Giroud and Han (2004a and 2004b) proposed a new empirical design model for geogrid reinforced unpaved roads, based in part on lab model tests that were reported by Gabr (2001). This model accounts for aggregate base course deterioration as the number of traffic loading cycles increase, and, while developed for a rut depth of 75 mm (3 inches), allows for the input of different rut depth values, and is calibrated for a geogrid's aperture stability modulus (ASM). In their closure to the paper, Giroud and Han (2006), defended the use of ASM, comparing traffic benefit ratios of reinforced unpaved roads measured by Watts et al. (2004) to 5% secant moduli for the geogrids used. Based on those measurements, it was noted that there was no correlation, that the average strains mobilized in the geogrids ranged from 0.1 to 1.2% and that ASM is a better indicator to use in this case.

Tingle and Webster (2003) back-calculated bearing capacity factors using results from four test sections subjected to simulated traffic loading, observing rut depths up to three inches. Finite element analyses of unpaved road sections were performed by Perkins et al. (2005b) and Leng and Gabr (2002) and attempted to explain the contribution of geosynthetics to increasing the service life of the unpaved section. Leng and Gabr (2005) also presented a design model that estimates the benefits realized in an unpaved section with inclusion of reinforcement. The model includes effect of level of mobilization of subgrade bearing capacity as a function of rutting as well as the relative aggregate base course to subgrade modulus ratio.

There are barriers to implementing these design methods on a wider scale. The methodologies presented by FHWA and GMA still recommend a laboratory calibration study for the geosynthetic to be used and the expected soils to be encountered, which is a significant barrier to implementation in the design phase. As another example, the recent methods proposed by Giroud and Han (2004a and 2004b) are largely uncalibrated. In their closure (2006) the authors mention that more than 20 paved road designs have since been implemented using their methods. Such a database needs to be considerably increased, with long term monitoring and model verification for wide acceptance of the proposed approach.

The numerical finite element studies reported in literature may be a first step toward a more mechanistically based design model. These methods, however, are unlikely to make their way into common practice unless (i) the interface between user and finite element model are more stream lined and user friendly, (ii) interface and material models are accepted and (iii) the results are well correlated to measured behavior. So far, the finite element studies have provided design charts that are dependent on the type of reinforcement modeled and the initial boundary conditions assumed. These numerical studies must be considered in light of measured laboratory and field data.

Large Scale Cyclic-Plate Load Testing

Dozens of studies have reported the response of cyclically-loaded full and small scale test sections with and without geosynthetic reinforcement or subgrade stabilization. This review summarizes findings of large scale cyclic-plate load tests similar to the testing performed for this study. In essence, the experiments consist of either unreinforced or geosynthetic-reinforced aggregate base course (ABC) over soft subgrade. The cross section is then cyclically loaded in a large test pit or box. Deflections and stresses are often measured through various instrumentation arrangements to determine the composite section's resistance to rut development.

Bender and Barenberg (1978) performed early tests on subgrade reinforced with geotextiles. Both large scale (three-dimensional) and small scale (two-dimensional) tests were performed on reinforced (MIRAFI-140 and -280) and unreinforced roadway sections with a clay subgrade having a CBR between 0.6 and 2.5, and moisture content between 20.5 and 26.6%. The aggregate layer above it consisted of crushed limestone.

Bender and Barenberg (1978)'s large scale (three-dimensional) test consisted of static and repeated-loading in a section of circular test track with a 9-foot inner diameter and 25-foot outer diameter (for a width of 8 feet), and depth of 5 feet. For the static tests, plate diameters used were 12, 18, 24, and 30 inches, and applied a stress on the subgrade of 2 and 5 psi in different test trials. Depth of the aggregate layer varied from 0 to 15 inches in three-inch increments. Repeated load tests, up to 1000 cycles, were performed on same aggregate layer thicknesses and plate diameters. Although the loading frequency was not specified, the vertical loads applied to the surface varied from 500 to 6000 pounds. All reinforced tests used either one or two layers of MIRAFI-140 geotextile. Because the applied stresses were 2 to 5 psi, there was no noticeable difference between the reinforced and unreinforced sections, and permanent surface deformations ranged from only 0.05 to 0.15 inches. The authors noted that in field situations, heavy vehicles would apply much higher stresses and that a higher number of load applications would also be necessary to simulate field behavior.

Their small-scale (two-dimensional) tests consisted of both static and repeated-loadings. The small test-pit was 4.25 ft long by 0.5 ft wide by 1.5 ft deep, and loaded through a steel plate 4 inches wide by 6 inches long. Subgrade depths were 3, 6, and 9 inches, and

subgrade stress ranged from 4 to 20 psi. Here, single layers of both MIRAFI-140 and MIRAFI-280 fabric were tested as reinforcement. The small scale (two dimensional) tests, with thinner aggregate layers showed that the geosynthetic slowed the rate of permanent surface rutting, and seemed to stabilize at very high stress/strength ratios while the unreinforced sections did not.

Based on the small scale results, Bender and Barenberg (1978) matched Boussinesq stress distribution calculations with measured soil parameters from testing, and developed a design procedure using allowable subgrade stresses of reinforced and unreinforced sections as 3.3 and 6 times the subgrade shear strength, respectively. The applied stress can then be calculated using a value K, which is a percent of the effective applied contact pressure from wheel loads. Using Boussinesq graphical distributions of vertical stress, the designer can determine the depth of aggregate to use to adequately reduce the subgrade stress.

Lai and Robnett (1981), using Typar 3401 geotextile, conducted large (8 ft) and small (3ft) diameter tests on both unreinforced and reinforced road sections. A subgrade (USCS of CL) with low shear strength was used. Lai and Robnett (1982) show a subgrade CBR of 0.9, with a subgrade depth of 30 inches below 15 inches of ABC in the large pit instrumented with pressure cells at various depths. The small scale pit used four additional geotextiles and different depths of ABC (11.5, 18, and 25.4 cm). Surface deformations for both pits were measured manually by pausing load application at various numbers of cycles.

The cross-sections were loaded through a 12-inch and 6-inch plate for the large and small scale pits, respectively. Both cases had a maximum applied pressure of 70 psi using two loading patterns. Pattern A, which was only used in the small pit, represented “slow speed transit of a heavily loaded vehicle” by load rise and decay to zero over a three second period, followed by a three second lapse between cycles. Pattern B, used in both large and small pits, simulated higher speeds through a 0.2 second load pulse and a 2.8 second rest time. The tests were conducted to 20,000 cycles or 1.5 inches or surface deflection, whichever was achieved first.

The results of surface deformation on the large pit showed that the reinforced section slowed rut development by one-seventh, and the deformation rate for both reinforced and unreinforced sections was linear throughout the loading cycles. However, the number of cycles that both large pit sections took to fail (defined as a rut depth of 13mm/1.5 in) was fairly low (about 50 for unreinforced and 550 for reinforced sections).

Only in the small scale test on Typar 3401 with 25.4cm (10 in) of ABC above the fabric was about 11000 cycles with 4.5cm of rutting in the reinforced section achieved. For all small scale tests, the reinforced sections performed better than the unreinforced section of equal ABC thickness. The authors note a clear trend between initial rate of rut deformation and initial geotextile modulus (obtained from geosynthetic testing). Four of the five fabrics tested showed a clear trend between initial geotextile modulus and load repetitions to rut depth.

Bauer and Abd El Halim (1987) analyzed the benefits of geogrid reinforcement at the base-subgrade interface. The test-box used was 6 ft x 15 ft x 3.3 ft deep. The subgrade was fairly uniform medium size sand" to a height of 3 ft and the aggregate base course (ABC) consisted of a well-graded crushed limestone, which varied in thickness from 3 to 12 inches, depending on the test series. The geogrid used was a Tensar AR1, which was instrumented with 18 strain gauges. The profiles were loaded through a 12-in diameter steel plate. The actuator applied a load of 40 kN (9000 lbs) at a frequency of 3 Hz. An LVDT and load cell within the actuator recorded data during loading. Several LVDTs were placed at the surface at different radial distances from the center of the applied load, but these distances were not specified. All test sections were not run to a specified number of cycles. Instead, loading ceased at failure, which was assumed to have occurred when surface deformation reached 1.1 in.

According to the test results for road sections with 3 in of ABC, the reinforcing resulted in 40% less surface deformation, and 50% more load repetitions to failure. The authors also noted a less "steep" surface depression in the reinforced sections, which are attributed to the ability of the geogrid to redistribute the applied stresses over a greater area. However, there were a limited number of tests listed (2, one reinforced and one unreinforced).

Douglas and Valsangkar (1992) conducted research on large-scale models of unreinforced and geosynthetic-reinforced logging roads in New Brunswick and contend that road stiffness is more important than rut development, since ruts can be eliminated with regular maintenance and road deflections hamper rolling of vehicle wheels (and subsequently reduce fuel efficiency). Large-scale sections were constructed in a test pit 10 ft x 13 ft x 6.5 ft deep. Subgrade consisted of soft peat (CBR<1) approximately 4 ft deep beneath 6 inches of granular base (either pit run or crushed stone gravel). Although peat was used for its uniformity and ease of mixing, the authors note the difficulty of compacting base material on such a soft subgrade. The peat was also at very high water contents (300-500%).

A total of six sections were tested with reinforced sections using either a nonwoven geotextile or a Tensar geogrid. Three sections consisted of just peat subgrade without reinforcement or a granular base layer. A fourth section consisted of 6 inches of loose pit run gravel with geotextile at the layer interface, and the last two sections with 6 inches of compacted crushed rock with geogrid at mid-base height.

The sections were loaded to 30,000 cycles at 0.5 Hz through a 12 inch diameter steel plate. The sinusoidal pulses were 1000 to 25 lbs for the model pavement sections, and 450 to 25 lbs for just the peat subgrades. Displacements and loadings were measured by the actuator's internal LVDT and load cell, respectively. Continuous measurements were not made, however, and only taken at certain cycles (1-10, 30, 100, 300, 1000, 3000, 10000, and 30000).

The authors note that the actuator was not able to reach min or max load due to the "relatively rapid load applications". They do not, though, give the actual loads that were applied to the sections. Instead, the authors give findings in terms of section stiffness, perhaps because the loads, even though small, may not have been able to be developed on the soft subgrades or due to inadequate hydraulic fluid flow from the pump supplying the actuator.

Ping and Yang (1998) performed large and small (repetitive-load triaxial) tests for the Florida DOT on five typical Florida subgrade soils to compare estimates of the soil resilient modulus (M_r). These granular sands were tested at three different moistures: optimum, drained and dried, and soaked. The tested material was at the surface and 24 inches thick, which was placed over 24 inches of A-3 subgrade. This subgrade was over 12 inches of builders sand, and 12 inches of river gravel (for an overall depth of 6 feet). The CBR of the granular sands tested were very high and ranged from 30.4 to 86.4.

The moisture contents were created by raising and lowering the water level in the pit through underlying drainage galleries. For optimum, this meant the water level was approximately 12 inches below the tested subgrade. For dry, the water level was 24 inches below the material, which was allowed to drain for seven days before testing. Soaked samples were run with water levels about 0.5 inches below the top of the tested subgrade.

The test pit itself was 7.9 feet wide by 24 feet long. The load actuator and reaction frame were mounted on rollers, which allowed the testers to move the 12-inch diameter loading plate to run multiple tests on a single section. The authors ran 9 tests per section in a three by three grid pattern. Three tests at each of the moisture contents were conducted on each soil.

Before cyclic loading, an initial 500-lb static load was applied. After obtaining maximum deflection, the load was increased to 2000 lbs in 500-lb increments. The static load was removed, and after the section rebounded, the process was repeated two more times. Cyclic loading consisted of 10,000 cycles of 137.8 kPa (20 psi) vertical stress applied for 0.1 seconds with a 0.9 second rest period.

Although instrumentation schemes were not discussed in the article, the schematic diagram of the test setup shows a load cell placed below the loading device, and LVDTs placed on the loading plate.

The resilient modulus of the large scale tests were calculated using Burmister's theory of a two-layered elastic system. The equivalent single layer elastic modulus can be calculated using equation 1.

$$\mathbf{Mr = (\pi pa / \Delta_r)^* (1-\nu^2)} \qquad \mathbf{(1)}$$

where p is the applied plate pressure, a is the plate radius, Δ_r equals the resilient deflection, and ν is the Poisson's ratio of the soil. The authors assumed 0.35 as a Poisson's ratio for a granular subgrade, and assumed the two-layered system consisted of the tested subgrade and the A-3 subgrade beneath it.

Laboratory repeated-load triaxial tests were conducted according to AASHTO T292-91(I). Samples were 4 inches in diameter by 8 inches tall and prepared in a steel split-mold. Two replicated samples of each test were prepared, as well. Internal instrumentation consisted of four vertically-oriented LVDTs, two placed at mid-height, and two at the top of the sample. Loadings occurred at the same 0.1 second load period followed by 0.9 seconds of rest. Resilient modulus was taken as the deviatoric stress divided by the recoverable (resilient) strain. Regression equations to calculate resilient modulus in terms of minor principal stress and bulk stress were also produced.

According to the triaxial test results, the resilient modulus remains constant (or increases slightly) for increasing deviatoric stress at constant cell pressure. For one of the silty/clayey sands tested, the resilient modulus decreases with increasing deviatoric stress at constant cell pressure. In both the lab and large scale tests, the increased moisture content decreased the resilient modulus.

The resilient modulus values from the laboratory tests, though, vary depending on the measurement location of deformation. The resilient modulus resulting from the LVDTs at sample mid-height are consistently greater (by 22 to 97 MPa) than those calculated with deflection data from the top of the sample. While deviatoric stress obviously dissipates with height, this was not measured, so any difference in calculated resilient modulus would be due to differences in resilient strain. Hence, resilient strain at the top of the sample is smaller than that measured at mid-height. The resilient modulus values for the test-pit assume that it is equivalent for the entire layer, and only depended on moisture content. The authors compare test-pit and laboratory results by first calculating the resilient deformation of the test-pit using the triaxial resilient modulus. This calculated resilient deformation is then compared to the measured resilient deformation.

In the test pit, the resilient modulus is assumed to be constant along a horizontal plane, and vertical variation is approximated by dividing the tested subgrade into several layers (each layer with a constant resilient modulus). These moduli can be calculated using the horizontal stresses in each layer. Both horizontal and vertical stresses, though, are assumed using Boussinesq theory calculations and were not measured by instrumentation. Horizontal stress from the soil weight is assumed from a K_o of 0.5 and from the applied load with an assumed Poisson's ratio of 0.35. Both resilient moduli and deflections are estimated using this theory.

For all of the soaked tests and some of the optimum tests, the measured test pit deformations are much greater (nearly two times) than the calculated deformation using resilient moduli obtained from the mid-height LVDT deflections in triaxial tests (with Poisson's ratio equal to 0.5). The authors partially attribute this to the non-uniform distribution of pressure beneath the loading plate, although quantified data does not support this statement.

In a table comparing measured to calculated deformations, it is apparent that there is no single Poisson's ratio (0.35 or 0.5) or measurement point (top or mid-height) that

produces better estimates. The differences, though, are relatively small, and typically only 0.1 to 0.2mm This is because the measured deformations are of the test-pit are relatively small (0.066 to 0.5mm for all tests) due to the high-CBR soils. The authors also did not present CBRs for the different moisture contents, and only for optimum, so that the actual CBRs may be much lower than reported.

Gabr *et al.* (1998) and **Gabr and Hart (2000)** performed a series of 14 static plate load tests on geogrid-reinforced sand in a steel box. These studies found that the measured stresses were generally predicted by the Westergaard method, and that as the depth to the reinforcement layer increased, the equivalent elastic modulus of the system decreased.

Perkins (1999) conducted unreinforced and geosynthetic-reinforced (geogrid and geotextile) large-scale tests of paved road sections for the Montana DOT. The test pit was 6.3 x 6.3 x 5 ft deep and comprised of 3.3 ft of soft clay subgrade with CBR of 1.5 and water content of 45%. The subgrade was overlain by 11.8 or 14.8 inches of crushed aggregate base course with classification GW, and a surface course of 3 in of hot mix asphalt (HMA).

A total of eight sections, with differing reinforcement and base thicknesses, were tested. The author reported that the sections were constructed to strict quality control standards to eliminate the effects of differing soil conditions on test results. One duplicate test section was constructed, and measurements from instruments at symmetric locations were compared. Densities were measured by both nuclear density gauge and sand cone method, and CBR values were confirmed by DCP. Moisture content and density of individual layers was often adjusted through adding moisture or reconstructing sections entirely.

The system was loaded through a 12 in diameter steel plate over a 0.16 inch thick rubber pad. Loads were approximately 9000 lbs for an applied pressure of 80 psi at a frequency of 0.67 Hz. The test sections were heavily monitored with over 90 instruments. A load cell and eight surface LVDTs monitored applied load and surface deformations, respectively. Stress and strain cells were placed throughout the base and subgrade layers, and strain gauges were attached to the geosynthetic to measure deformation behavior of the reinforcement. Although the tests were performed indoors, temperature probes and time domain reflectometers for estimating water content were also installed.

Reinforcement consisted of two biaxial geogrids (Tensar BX 1100 and BX 1200) and one geotextile (Amoco 2006). Additional geosynthetic testing was performed to confirm mechanical and soil interaction properties of the reinforcing used. The results show that all reinforcing provided better surface deformation behavior than the unreinforced sections, and that the geogrids proved better at reinforcing than the geotextile. All test sections significantly improved the initial rate of rutting to 0.2 inches (110 load cycles for unreinforced versus 3,500-5,700 load cycles for various reinforced sections). The stiffer geogrid and placing the geogrid closer to the surface (4 inches from HMA compared to the interface of the base/subgrade) both performed better in comparison to similar test sections.

In comparing different base thicknesses, more improvement from reinforcement was seen for the 15-inch than the 12-inch base section. According to the author, this implies that further rutting is needed to mobilize the reinforcement in the thicker base section, and that these reinforcing effects may diminish over some threshold value as the base thickness increases. Also, all reinforced sections with 12 inches of base performed better than the unreinforced 15 inch base section.

Soil and geosynthetic strain measurements confirmed that the reinforcing was able to minimize the lateral movement of the base material. For all reinforced sections, the lateral strain was greatest directly beneath the loaded area. The dynamic strain on the reinforcement was relatively constant for each load cycle, indicating that the dynamic load on the reinforcement was also relatively constant. The instrumentation also showed that the reinforcement reduced the subgrade stress not only directly beneath the loading area, but at various radial distances, as well. The geogrid reduced these stresses more so than did the geotextile.

Additionally, the geotextile reinforced test sections both behaved similarly to the unreinforced sections at low number of load cycles. The reinforced sections only began to exhibit improvement after 6 or 7mm of rutting. This is in contrast to the geogrid sections, which showed improvement from the start of loading. Upon exhuming, the authors noted a "dimpling pattern" in the geotextile from the larger aggregate stones penetrating into the subgrade. The authors believe that this explains the initial poor behavior of the geotextile sections. Gradually, the aggregate moved downward and laterally to tension the geotextile to produced a "pseudo-interlocking" effect.

Tingle and Jersey (2005) conducted laboratory research to determine the benefits of geotextile and geogrid reinforcement in unpaved roads. Large-scale tests were performed in a steel box with dimensions 6 ft x 6 ft x 4.5 ft deep. A hydraulic actuator applied a 9000 lb load to a 12 inch diameter steel plate. A 0.25 inch thick rubber pad was used beneath the plate to minimize stress concentrations at the edges of the plate. The loading was designed to simulate a one-half ESAL, and was applied through a 0.1-second load duration followed by a 0.9-second rest period.

The subgrade within the box consisted of high-plasticity clay (CH) with a design California Bearing Ratio (CBR) of 1. Above the subgrade was a layer of crushed limestone to act as an Aggregate Base Course (ABC). Geosynthetics were used between the ABC and subgrade layers, and consisted of a needle-punched polypropylene geotextile, a biaxial punched and drawn polypropylene geogrid, or a combination of both. Six different tests were performed, each of which varied the thickness of ABC and reinforcement type used.

To collect data from the tests, earth pressure cells (EPCs) were placed at various depths beneath the center of the loading plate to measure vertical stress. One EPC was laterally offset to measure horizontal stress near the bottom of the pit. Linear variable differential transducers (LVDTs) were placed at 7, 18, and 30 inches horizontally away from the

center of the plate to measure surface deflections. There was also an internal LVDT in the load actuator, and another 4 inches from the center of the plate to monitor plate bending. All instrumentation was fed to a data acquisition system that obtained 500 readings per second. Additionally, a dynamic cone penetrometer (DCP) was used to evaluate the CBR of the subgrade.

The dynamic deformation profiles of the various sections as measured from the surface LVDTs. The least deflection was encountered in a 20 inch thick unreinforced ABC section. Three sections with reinforcement deflected more than the section without reinforcement and equal ABC depth (14 inches of ABC). Two sections consisted of combinations of geogrid over geotextile. A geogrid reinforced section, could not be loaded to 10,000 cycles because of significant surface deflections.

Interestingly, the USACE previously suggested using at least 14 inches of material above geogrid to properly utilize its tensile properties (Tingle and Webster, 2003). Because of the significant deflections in the tested geogrid reinforced section, the authors suggest changing this number to 16 inches.

Overall, the EPC data showed the increase in vertical stress for all test sections with increasing ESALs. As expected, the stresses in the geogrid reinforced section were highest in this test series, while the thick unreinforced section stresses were the lowest. Tingle and Jersey (2005) also recorded variable CBR values between some tests, so increased subgrade strength may explain some discrepancies.

Kim *et al.* (2006) simulated reinforced and unreinforced working construction platforms over soft subgrades. Both "breaker run" and Grade 2 crushed stones were tested, with breaker run stone having more large particles and more widely graded than Grade 2 stone (with classifications of GW for breaker run and SW for Grade 2 gravel). Overall, four different geosynthetics were tested (a biaxial geogrid, a slit-film woven geotextile, a nonwoven needle-punched geotextile, and a drainage geocomposite consisting of geonet and nonwoven heat bonded geotextile). Pullout tests performed on each of the four materials indicated that the geogrid was the least extensible, and the nonwoven geotextile was the most extensible of the options.

Tests were conducted in a 10 ft cubic test pit. The tested profile was 8.2 ft of dense uniform sand beneath 1.5 ft of a simulated soft subgrade comprised of expanded polystyrene (EPS) geofoam. The foam was found to have properties similar to typical soft Wisconsin subgrades and used for replication purposes. A thin layer of base material (1 inch) was placed between the EPS and geosynthetic. Two different thicknesses (12 and 18 inches) of base material were used and run unreinforced and reinforced. The profiles were loaded with a 9.8-in diameter plate with an applied pressure of 102 psi. One-thousand cycles were applied for a 0.1-second load period followed by 0.9-seconds of rest.

Instrumentation consisted of surface LVDTs placed at the loading plate, and radial distances 12, 18, and 26 inches from the center of load application. Replicate measurements were made on the opposite side. LVDTs attached to steel wires and strain gauges measured geosynthetic movement and were run through tubing at 5, 10, 15, and 20 inch radial distances.

For the reinforced test sections, deformations essentially ceased after approximately 200 load cycles. As one would expect, the 18-inch base test sections performed better (~40-50%) than the thinner 12-inch base sections. The authors measured essentially the same deflections at the center and edge of the loading plate. The deflection basins were small and essentially diminished 16 inches away from the center of the plate.

The comparison of unreinforced and reinforced test sections showed that the 12-inch thick geogrid-reinforced test section performed as well as the 18 inch unreinforced section. For all tests, the reinforced test sections performed better than the unreinforced. For both layer thicknesses, the geogrid- and woven geotextile-reinforced sections performed best (least permanent deflection). The authors found that the interaction modulus from pullout tests is inversely proportional to permanent deflection.

Strain measurements indicate that most geosynthetic deformation occurred near the edge of the loading plate. The strain is more affected by thickness of the base layer for the geogrid than the geotextiles, indicating that strain mobilization is critical to utilize geogrid reinforcing effects. The authors noted a greater areal distribution of strain in the less extensible geosynthetics (geogrid and woven geotextile) compared to the distribution in the non-woven geotextile and drainage geocomposite.

The authors conclude by making recommendations to the Wisconsin DOT for target deflections and base thicknesses based on linear interpolation of the results for the two thicknesses tested. However, the obvious discrepancy is that geofoam rather than real soft subgrade was tested. The geosynthetics were placed in the base course, but are more typically placed on the subgrade/base interface. This was obviously infeasible with the geofoam subgrade used in this study.

Christopher and Lacina (2008) performed large-scale tests to simulate geosynthetic-stabilized roadways over soft Piedmont residual soils. The test box used was 6.6 by 6.6 by 5 ft deep and loaded with a 12 inch diameter (1 inch thick) steel plate underlain by a 0.25 inch thick rubber pad. The loading function increased the load from 0 to 9000 lbs over 0.3 seconds, held 9000 lbs load for 0.2 seconds, decrease back to 0 kN over 0.3 seconds, and finally a rest time of 0.5 seconds (for a frequency of 0.67 Hz). This loading function was based on the abilities of the data acquisition system. The instrumentation included two LVDTs on the load plate, four LVDTs at spanned distances on the test surface, pore-pressure transducers within the subgrade, and strain gauges mounted to the geosynthetics.

The subgrade used was Piedmont silt prepared to a CBR of 1% at 35% water content, and placed in the test box to a depth of 3.3 ft. Geosynthetics placed on the subgrade consisted

of seven different types (three woven geotextiles of different strengths, one slit film woven geotextile, a woven biaxial geogrid, a punched biaxial geogrid, and a composite reinforced nonwoven geotextile). Aggregate base course (ABC) was placed on the geosynthetics (or subgrade when unreinforced) to a depth of 12 inches and compacted to optimum conditions. One set of replicate tests were performed for quality control purposes.

Two additional tests, one unreinforced and one reinforced with a geotextile were performed at higher subgrade strength (CBR of 2%) with 6 inches of ABC. The test sections were loaded to 10,000 cycles or 3 inches of permanent deformation, whichever occurred first. The deformation bowl was then refilled with ABC to its original level and reloaded. All of the reinforced tests sections displaced less than the unreinforced sections. The geogrid reinforced sections displaced more than the geotextiles, which was attributed to the contamination and mixing of the layers before interlocking could occur. The woven geotextiles with higher stiffness provided better rutting resistance, but the weakest of all the woven geotextiles performed the worst out of all the geosynthetics and failed at a very low number of load cycles (121). Of all of the geosynthetics tested, the geocomposite performed the best. The pore-water pressure measurements indicated increases in pore-water pressure during loading, and the data showed that the geogrids were unable to aid in pore-water pressure dissipation. The geotextiles with better filtration and drainage traits performed better than those with low permeability and permittivity.

Tingle and Jersey (2009) constructed eight full-scale test sections to analyze the benefits of geosynthetic inclusion at the layer interface. The test pit used was 18 ft wide, 235 ft long and 2.5 ft deep. All eight tests were constructed next to one another in the long direction. The bottom of the pit was lined with a silty-clay subgrade with CBR of 10%. Above it, a high-plasticity clay (CH) with CBR of 4% and depth of 24 inches was overlain by 6 inches of either crushed limestone (GW), crushed aggregate (GW), or “clay gravel” (GP-GC), a locally used term. Reinforced test sections had a polypropylene needle-punched geotextile, a polypropylene geogrid, or a combination of both at the subgrade-aggregate base interface.

The test sections were loaded with a dual-wheel tandem axle truck that traversed back and forth over the test sections in the long direction. The gross vehicle weight was approximately 19.8 metric tons with a 50 psi individual tire pressure. The truck drove forward and then backed over the test sections over the same wheel path, representing two load cycles. The sections were loaded to either 10,000 cycles or failure at 3 inches of rutting. System responses were measured by earth pressure cells buried within the subgrade along the wheel paths two inches below the layer interface, single-depth deflectometers (SSDs) measuring subgrade surface deflection through tubes buried in the aggregate layer, time domain reflectometry (TDR) moisture and temperature probes, vibrating wire pore pressure transducers, and foil strain gages attached to the geosynthetics. A falling weight deflectometer (FWD) was also utilized to measure surface deflection basins.

Results showed that geosynthetic inclusion increased the number of passes to equal rut depth for all equivalent sections. The test sections with highest number of load cycles to a given surface deformation were those with clay gravel as a granular layer. This was attributed to the high shear strength of the dry cemented clay particles. Tingle and Jersey (2009) noted that infiltration of moisture into such a granular layer would weaken it significantly, especially in field conditions. A comparison to the other aggregate types on unreinforced test sections showed that the clay gravel displaced less than the crushed limestone and the crushed aggregate displaced more.

Overall, the geosynthetic inclusion showed the least amount of improvement for the clay gravel sections, both of which performed extremely well. The geosynthetics showed the most improvement for the crushed aggregate and crushed limestone, with geogrid provided better rut resistance than geotextile for the crushed limestone. The test section with geocomposite (geogrid and geotextile) reinforcement showed the most overall improvement, and the geogrid reinforced sections with crushed limestone and clay gravel had similar displacement profiles.

Tingle and Jersey (2009) found that pore-pressure data did not yield significant results. This may have been caused by slow load application from the passing truck which allowed for significant pore-water pressure dissipation. Strain gage data showed that geogrid strain magnitude was much less than the geotextile. All strain was localized along the wheel path area and was highest in the longitudinal direction.

For all tests, there was a significant stiffening over a low number of passes followed by plateau of deformation, attributed to a densification of the upper aggregate layers followed by a mobilization of the geosynthetic reinforcement (when included). Tingle and Jersey (2009) noted that this trend explains the geosynthetic manufacturers' apprehension of using surface deflection to measure reinforcement benefits after minimal traffic passes, and that some deformation is required to mobilize the stiffening effects of geosynthetics.

Cuelho and Perkins (2009) performed a field test consisting of 12 test sections, 10 of which were reinforced with geosynthetics. A 13 ft wide by 640 ft long by 3.3 ft deep test pit was lined with plastic and filled with a low CBR (~1.7) subgrade material and topped with aggregate base course, whose 20 inch thickness was determined using FHWA design methodology. The aggregate was placed from the side, so that only compaction traffic would be allowed on the test section. Pre- and post-testing DCP measurements, as well as manual surveys were performed on the sections, while geosynthetic strains and pore water pressure measurements were also recorded.

In general, Cuelho and Perkins (2009) observed the welded, woven and strongest integrally formed geogrids withstood the highest number of passes of the loading vehicle, while geotextile and a weaker integrally formed geogrid showed significant rutting at a smaller number of truck passes. Generally speaking lower strength geosynthetics withstood fewer ruts than the higher strength textiles.

Summary—Large Scale Cyclic Plate Load Testing

Overall, geosynthetic reinforcement has shown to deter rut development in cyclically loaded test sections. The magnitude of this benefit is dependent on the compatibility of the geosynthetic with the soil layers, the strength of the geosynthetic itself, and the stiffness of the underlying subgrade.

Interestingly, many papers do not report soil resilient modulus values or its relevance to section behavior. Only one article (Ping and Yang, 1995), who did not test geosynthetic reinforcing, mentioned this soil property. Of the articles reported above, Perkins (1999) is the most thorough laboratory study found to date while Tingle and Jersey (2009) and Cuelho and Perkins (2009) appear to start a more recent trend toward moving from the lab to instrumented, unpaved field sections.

From the chronology of the studies presented, one can see that great advances in large-scale cyclic plate load testing have been made over the past quarter century. Previous authors have shown that the following issues must be properly addressed:

- Use of appropriate loading pressures and rates
- Proper quality control and preparation of subgrade soils
- Compatibility of geosynthetic reinforcing with aggregate and subgrade soils, including preliminary design of aggregate layer depths
- Proper measurement of surface deformations, subsurface stresses, and geosynthetic strain
- Discussion of possible boundary effects
- Adequate discussion of reinforcing mechanisms and soil behavior during cyclic loading

The Dynamic Cone Penetrometer (DCP)

As alluded to in some studies above, the Dynamic Cone Penetrometer (DCP) is used to measure an index value as a proxy for other soil parameters. A DCP test is performed by dropping a weight along a rod of specified height onto an anvil to drive a cone into the underlying soil. Although typically performed by hand, automation of the DCP has occurred in recent years to ensure consistent drop height. All readings for the DCP are given as length per blow (typically as mm/blow), and is referred to as the DCP Index (DCPI) or Penetration Rate (PR).The DCP is essentially a miniature-hybrid of the Cone Penetrometer (CPT) and the Standard Penetration Test (SPT). While it is conical like the CPT, it is dynamically-driven like the SPT.

Development

The DCP was originally invented by A.J. Scala (1956). The original model comprised of a 9.1-kg (20 lb) drop hammer with a fall distance of 508mm (20 inches). The hammer

slid along a 5/8-inch diameter rod, which ended with a 30-degree (from horizontal) cone tip. The original purpose was to obtain field estimates of California Bearing Ratio (CBR) of subgrade soils.

Another version of the DCP was created by Van Vuuren (1969) in an attempt to solve several field issues with conducting DCP tests. The drop hammer was modified to 10 kg (22 lbs) with a drop height of 383.5mm (18.1 inches). While the cone tip remained 30 degrees, the shaft diameter was changed to 16mm (0.63 inches).

The basic configuration was later revisited by Kleyn and Savage (1982). The newer model used a hammer weight of 8 kg (17.6 lbs) with a drop height of 576mm (22.6 inches). After studying different cone angles, a 60-degree cone was finally utilized. This is the standard configuration used today, and was the model adopted by ASTM under the standard ASTM D6951-03, *Standard Test Method for Use of the Dynamic Cone Penetrometer in Shallow Pavement Applications.*

Although the DCP is not a static test, it is often valuable to first analyze dynamic systems in such a manner. Static cone penetration analysis in granular materials has been analyzed by Meier and Baladi (1988) using theoretical analysis and some laboratory verification. The authors assume that the soil fails in shear as the cone is advanced. An applied normal stress (σ), which creates a spherical cavity, can be expressed as:

$$\sigma = 3 (q + C \cot\varphi) * (1+\sin\varphi / 1-\sin\varphi)*[G/(C+q \tan\varphi)]m – C \cot\varphi \qquad (2)$$

Where q=hydrostatic or mean stress, G = soil shear modulus, C = soil cohesion, and $m=[4\sin\varphi / 3(1+\sin\varphi)]$.

Dynamic cone penetration analysis has been modeled by considering the cone as a soil-penetrating projectile. Chua (1988), using the one-dimensional projectile penetration theory presented in Yankelevsky and Adin (1980), noted that the DCP is substantially slower than a typical “projectile”. In the theory, the soil is modeled as a series of disks, which expand radially and experience plastic shock under dynamic penetration. Chua uses this model by making the disk the same height as the penetrating cone. Ultimately, the model was used as a theoretical predictor of soil elastic modulus (E), which will be discussed in following sections.

Factors Affecting Results

Livneh (2000) and Livneh *et al* (1995) analyzed how vertical confinement of the surrounding soil influenced DCPI. Livneh et al (1995) concluded that vertical confinement occurred in granular soils and not in cohesive soils. The authors also noted that for proper results, field DCP tests on soils covered with Hot Mix Asphalt (HMA) should first have a hole drilled (significantly larger than the cone diameter) through the asphalt before conducting the test. Aside from the possibility of damaging the cone tip, the HMA confines the soil around the penetration area and prevents soil heave upon penetration, thus increasing the apparent soil resistance (decreasing DCPI).

Livneh et al. (1995) also showed that when the DCP is not performed perfectly vertical, and the soil makes contact with the rod. In turn, this decreases the DCPI values obtained by providing skin-friction resistance to penetration.

DCP Correlations to Material Properties

The DCP has been correlated to several soil material properties. The relationships are both empirically and theoretically derived. Differences in empirical models will exist from laboratory and field testing, and the soil type tested. Fundamental differences in soil failure mechanisms during different tests prevent better correlation, as well. This is most notable between the resilient modulus, which does not induce soil failure, and DCP test, which fails soil in shear.

DCP Correlations to California Bearing Ratio (CBR)

The original intention of Scala (1956) in the development of the DCP was to obtain a relation to CBR. The two tests are fundamentally similar, albeit with different sized penetrometers. A multitude of different empirically-based (laboratory and field) relations between CBR and DCP have been developed over the past 30 years. These are conveniently presented in the Table below from Gabr *et al* (2000), which also includes an equation developed by Coonse (1999) for Piedmont Residual Soils:

Researcher (1)	Correlation equation (2)	Number of data points *N* (3)	Field or laboratory based study (4)	Material tested (5)	Year of work (6)
Livneh	log(CBR) = 2.56 − 1.16 log(DCP)	76	Laboratory	Granular and cohesive	1991
Livneh et al. (1992)	log(CBR) = 2.45 − 1.12 log(DCP)	135	Field and laboratory	Granular and cohesive	c.1993
Harison (1987)	log(CBR) = 2.55 − 1.14 log(DCP)	72	Laboratory	Granular and cohesive	1987
Smith and Pratt	log(CBR) = 2.56 − 1.16 log(DCP)	Unknown	Field	Unknown	1983
Kleyn (1975)	log(CBR) = 2.62 − 1.27 log(DCP)	2,000	Laboratory	Unknown	1975
NCDOT (*Pavement* 1998)	log(CBR) = 2.60 − 1.07 log(DCP)	Unknown	Adaptation field, and laboratory	ABC and cohesive	c.1998
Norwegian Road Research (Ese et al. 1995)	log(CBR) = 2.44 − 1.07 log(DCP)	79	Field and laboratory	ABC	1995
Coonse (1999)	log(CBR) = 2.53 − 1.14 log(DCP)	15	Laboratory	Piedmont residual soil	1999

The relationships all have the same log-log relationship form, with differences in coefficients a result of materials tested, and field versus laboratory testing. The log-log relationship is therefore linear and was first noted by Kleyn (1975). This eliminates the influence of other soil properties such as moisture content and dry density.

Gabr *et al* (2000) studied the DCP and CBR relationships for aggregate base course (ABC) layers. Field and laboratory testing was performed, and differences between the values were most likely from the boundary effect differences in the underlying layers. The following equation was produced to determine in-situ CBR of the ABC from laboratory data with $R^2 = 0.82$:

$$\textbf{Log (CBR) = 1.55 – 0.55*Log (DCPI)} \quad \textbf{(3)}$$

A correction factor of 30% was applied to the laboratory model to develop a field testing equation:

$$\textbf{Log (CBR) = 1.4 – 0.55*Log (DCPI)} \quad \textbf{(4)}$$

Empirical Correlations between DCP and Young's Elastic Modulus (E)

Chen *et al* (2005) developed an equation relating DCPI and Falling Weight Deflectometer (FWD) test back-calculated moduli with an R^2 =0.855:

$$\textbf{E (ksi) = 78.05*DCPI}^{\textbf{-0.6645}} \quad \textbf{or} \quad \textbf{E (MPa) = 537.76*DCPI}^{\textbf{-0.6645}} \quad \textbf{(5)}$$

Chai and Roslie (1998) presented results from DCP field tests performed in Malaysia. These results were used to determine the in-situ elastic modulus using the equation:

$$\textbf{E (MN/m}^{\textbf{2}}\textbf{) = 17.6*(269/DCP)}^{\textbf{0.64}} \quad \textbf{(6)}$$

In this formula, the DCP is taken as the number of blows for 300mm of penetration, versus the standard DCPI, which is the distance (in mm) per blow. All other references to DCPI are in mm/blow unless otherwise noted.

The authors also used CBR-DCP relationships to back-calculate the elastic modulus using the equation:

$$\textbf{E (MN/m}^{\textbf{2}}\textbf{) = 2224*(DCP)}^{\textbf{-0.996}} \quad \textbf{(7)}$$

In a comparison of in-situ test methods, Abu-Farsakh et al (2004) compared the DCP, Static Plate Load Test (SPL), Lightweight FWD (LFWD), and Geogage tests in laboratory and field situations. The authors concluded that the DCP is more replicable and reliable than the Geogage and LFWD for in-situ testing. The authors developed the following equation relating back-calculated LFWD elastic modulus to DCPI (R^2 = 0.91):

$$\textbf{ln (E) (MPa) = 2.35 + 5.21 / ln (DCPI)} \quad \textbf{(8)}$$

All tests were done on Louisiana subgrade soils. The authors also developed the following two equations relating the elastic modulus from the SPL to DCP. The equations use E_i as the initial modulus and E_R as the reloading modulus (with R^2 = 0.94 and 0.95, respectively):

$$\textbf{E}_{\textbf{i}}\textbf{ (ksi) = [2526.7 / (DCPI}^{\textbf{2.05}}\textbf{ + 62.53)] -0.828} \quad \textbf{(9)}$$

$$\textbf{E}_{\textbf{R}}\textbf{ (ksi) = [745.873 / (DCPI}^{\textbf{1.57}}\textbf{ – 14.8)] – 0.506} \quad \textbf{(10)}$$

As discussed previously, Chua (1988) performed a theoretical analysis of the DCP to develop a relation to Young's modulus (E). The author developed the following equation to predict elastic modulus (E) from DCPI as a function of the principal stress differences at failure (2τ):

$$\textbf{Log (E) = B – 0.4 Log (DCPI)} \qquad \textbf{(11)}$$

The value of B is dependent on 2τ, and is outlined in Table 2 below:

Table 2. B-values from Chua (1988) DCP to E Correlation

Soil Type	2τ	B
Plastic Clay	25	2.22
Clayey Soil	50	2.44
Silty Soil	75	2.53
Sandy Soil	150	2.63

It should be noted that the relationship is only valid for DCPI between 10 and 60 mm/blow.

CBR and Resilient Modulus (M_R) Correlations

The 1993 AASHTO *Guide for Design of Pavement Structures* adopted a relationship developed by Heukelom and Klomp (1962):

$$\textbf{M}_\textbf{R}\textbf{ (lb/in}^2\textbf{) = 1500*CBR} \quad \text{or} \quad \textbf{M}_\textbf{R}\textbf{ (MPa) = 10.34*CBR} \qquad \textbf{(12)}$$

The above equation, though, is more accurate for soils with CBR $\leq$ 10. A more widely-accepted relationship was developed by Powell *et al* (1984):

$$\textbf{M}_\textbf{R}\textbf{ (lb/in}^2\textbf{) = 2550*CBR}^{\textbf{0.64}} \quad \text{or} \quad \textbf{M}_\textbf{R}\textbf{ (MPa) = 17.58*CBR}^{\textbf{0.64}} \qquad \textbf{(13)}$$

Use of Combined Equations to Predict Resilient Modulus (M_R) from DCP

Combining equations such as 2.11 and 2.12 relating CBR to M_R have been combined with any one of the DCP-CBR relationships (e.g. equation 2.3) to obtain resilient modulus estimates from DCPI directly. This was done by Chen *et al* (2005), who combined Powell *et al* (1984) with Livneh *et al* (1992) and obtained good correlation for DCPI over 10mm/blow. The combined equations used are as follows:

$$\textbf{M}_\textbf{R}\textbf{ (ksi) = 96.468*DCPI}^{\textbf{-0.7168}}\textbf{ or M}_\textbf{R}\textbf{ (MPa) = 664.67*DCPI}^{\textbf{-0.7168}} \qquad \textbf{(14)}$$

The authors did not compare their equation substitutions with field measurements. Interestingly, attempts to use Powell *et al* (1984) with CBR-DCP relationships for Piedmont Residual soils (such as the one from Coonse, 1999) have not been published.

Empirical Correlations between DCP and Resilient Modulus (M_R)

Jianzhou *et al* (1999) noted that when equation combinations are used, scattered results are often obtained for the same road section. This is a result of equation sensitivity to changing DCPI values. In an attempt to provide a more accurate model, the authors

performed a study for the Kansas DOT by comparing DCP tests to FWD back-calculated moduli. The study resulted in the following relationship with an $R^2 = 0.42$:

$$\mathbf{M_R\ (MPa) = 338*DCPI^{-0.39}} \quad \textbf{(15)}$$

Herath *et al* (2005) performed a study on Louisiana subgrade soils to relate resilient modulus and DCPI. The testing comprised of laboratory triaxial resilient modulus tests on remolded soil samples, and a combination of laboratory and field DCP testing. Importantly, the authors included soil index properties in one of their relations to improve the robustness of the models:

Direct Model:

$$\mathbf{M_r\ (MPa) = 16.28 + 928.24 / DCPI} \quad (R^2 = 0.82) \quad \textbf{(16)}$$

Soil Property Model:

$$\mathbf{M_r\ (MPa) = 520.62\ (\ 1 / (DCPI^{0.7362})) + 0.40\ (\gamma_d / w\%) + 0.44}\boldsymbol{PI}$$

$(R^2 = 0.85)$ **(17)**

Where γ_d = kN/m^3

Rahim and George (2002) performed laboratory triaxial resilient modulus tests on undisturbed tube samples of subgrade soils in Mississippi. Simultaneous field FWD and DCP testing near tube sample locations were performed to correlate the laboratory and field back-calculated modulus values with DCPI. Again, basic soil properties were included to improve robustness. Two models were formed for fine and coarse grained soils:

Fine-Grained soils:

$$\mathbf{M_r\ (MPa) = a_0*(DCPI)^{a1}*[\ \gamma_d^{a2} + (LL / w\%)^{a3}]} \quad (R^2 = 0.71) \quad \textbf{(18)}$$

Coarse-Grained soils:

$$\mathbf{M_r\ (MPa) = b_0*[DCPI / \log (c_u)]^{b1} * (\gamma_d^{b2} + w\%^{b3})} \quad (R^2 = 0.72) \quad \textbf{(19)}$$

Where DCPI = mm/blow, γ_d = kN/m^3, and other parameters are as follows:

Soil Type	Coefficient	Value	Soil Type	Coefficient	Value
Fine Grain	a_0	27.86	Coarse Grain	b_0	90.68
	a_1	-0.114		b_1	-0.305
	a_2	7.82		b_2	-0.935
	a_3	1.925		b_3	0.674

The authors noted the difficulty in obtaining undisturbed samples, and obtained a smaller R^2 than Herath *et al* (2005), who performed triaxial tests on remolded samples.

Hassan (1996) performed DCP tests on molded laboratory samples, and laboratory resilient modulus testing of Oklahoma subgrade soils to relate resilient modulus to DCPI. The author developed an equation to predict resilient modulus from DCPI at optimum moisture content with $R^2 = 0.37$:

$$\mathbf{M_r\ (psi) = 7013.065 - 2040.783*ln(DCPI)} \quad \mathbf{(20)}$$

DCP for Compaction Evaluation

There have been a number of studies to evaluate the use of the DCP as a compaction control or evaluation device. Gabr *et al* (2001) used the DCP in laboratory testing on soils at various moisture contents to establish relationships between DCPI and soil moisture-density properties. The soil types tested were Piedmont residual soils. The authors noted the affects of different size molds on laboratory DCPI results. The smaller (6-in) mold yielded DCPI readings that were 80-85% that of the DCPI obtained in the larger (10-in) diameter mold. The authors developed the following equation relating Liquidity index (LI) to soil DCPI with $R^2 = 0.86$:

$$\mathbf{LI\ (\%) = 0.65\ Log\ (DCPI) - B} \quad \mathbf{(21)}$$

where B ranges from 1.15 (10-in mold) to 1.2 (6-in mold). By substituting the equation for LI into the empirical equation, the authors developed an equation to estimate the in-situ water content (*w%*) using the DCPI, Plastic Limit (PL) and Plasticity Index (PI):

$$\mathbf{w\% = PL + [(0.65\ *Log(DCPI) - 1.2)*PI]} \quad \mathbf{(22)}$$

The authors note that because shear strength of partially saturated cohesive soils is controlled by negative pore pressure, then saturation is a representation of the negative pore pressure state. The authors also developed the following equation to estimate the degree of saturation (S%) of in-place soils with $R^2 = 0.82$:

$$\mathbf{S\% = 1 - e^{(C*DCPI)}} \quad \mathbf{(23)}$$

where C ranges from -0.07 (10-in mold) to -0.065 (6-in mold). This was combined to estimate the in-situ dry density (γ_d) using the following equation (with G_s = specific gravity, and γ_w = unit weight of water :

$$\mathbf{\gamma_d = [\gamma_w*(1-e^{-0.065*DCPI})] / [w\% + (1- e^{-0.065*DCPI})/G_s]} \quad \mathbf{(24)}$$

Wu and Sargand (2007) performed an evaluation of using the DCP for construction evaluation for the Ohio DOT. DCPI field data were gathered over two years on both treated and untreated subgrades. The authors used DCP-CBR relationships, the AASHTO resilient modulus-CBR relationship, and other relationships to determine layer coefficients and structural number (SN). These equations were used to provide the Ohio DOT with a design methodology using the DCP to measure soil stiffness. The authors also found that DCPI values correlate well with vertical stress and loading. Final recommendations of 8mm/blow for base layers (both treated and untreated), and 7mm/blow for HMA-covered bases were given as cutoff points for acceptance.

Chemical Stabilization

Chemical stabilization has been widely utilized for road construction since it provides fast, efficient, reliable improvement to weak subgrades. In general, chemical stabilizers

rich in calcium are added to weak subgrade soils and these chemicals react with soil minerals forming compounds that in turn improve soil properties. Two of the most common chemicals are lime and cement. The past research on chemical stabilization on soft subgrade soils can be grouped into three categories: improvement of soil properties, durability of the stabilized soils, and non-traditional stabilizers and recycled materials.

Improvement of soil properties by incorporation of lime or cement

Numerous research studies have been conducted on the effect of lime and cement on the engineering properties of subgrade soils. Christensen (1969) investigated the effect of lime and cement on PI, shrinkage, and compressive strength of 11 subgrade clay soils modified with 3 and 5 percent Portland cement and lime. Table 1 summarizes the resulting improvement of soil properties. A small amount of dosage reduced the plasticity index and increased shrinkage limit and unconfined compressive strength significantly.

Table 3. Average Percent Change of Engineering Properties for Clay Soil (Christensen, 1969)

Stabilizer	Plasticity Index	Shrinkage Limit	7-Day UCS	28-Day UCS
3% Cement	-52%	122%	468%	605%
3% Lime	-55%	123%	183%	348%
5% Cement	-64%	158%	775%	993%
5% Lime	-64%	151%	266%	481%

Thompson (1969) performed CBR tests to investigate the effect of lime stabilization on fine-grained soil. The value of CBR, with lime-stabilized and uncured samples, was at least three times greater than that of natural soil. Furthermore, samples that were cured for 48 hours at 48.9 C exhibited values of CBR which were greater than 100%.

In-situ CBR testing under 3 to 17 years-old pavement in several states carried out by Aufmuth (1970), showed that the average CBR value of lime stabilized subgrade was 65% but that of untreated subgrade was 10%.

Neubauer and Thompson (1972) investigated the immediate effect of lime stabilization on the resilient modulus of soil. Soil stabilized with 4 to 6% lime (without curing) exhibited 3 to 10 times moduli of natural soil. Little et al. (1995) established a correlation between the resilient modulus and unconfined compressive strength for lime stabilization soil. For example, an unconfined compressive strength of 700 kPa corresponded to the M_R of 250 MPa. Biczysko (1996) and Evans (1998) verified the effect of cementation on lime stabilized soil using backcalculated M_R from field falling weight deflectometer (FWD) and dynamic cone penetration testing. The typical value of M_R reported was in range of 210 to 3,500 MPa as a result of lime treatment. Little (1999) stated that M_R or stiffness increase by 1000% or more with lime stabilization during long-term period.

Petry and Wohlgemuth (1988) investigated increasing dosage effect on the strength of lime and cement stabilized soil and concluded that the strength of stabilized soil

increased with lime dosage to an optimum and then remained constant, but it increased with cement dosage in almost all dosage cases.

One of the methods for determining appropriate lime content for road construction was established by Little et al. (1995). A general outline of the procedure is as follows:

1. The lime percentage is determined to satisfy initial soil-lime reaction and provide enough residual lime to drive pozzolanic reaction. A pH of at least 10 for the soil-lime mixture is induced by the appropriate amount of added lime.
2. Specimens of the soil-lime mixture are compacted at optimum moist content to maximum dry density and cured for 48 hours at 49°C before testing.
3. Unconfined compression tests are conducted and the strength of soil-lime mixture is compared with natural soil. If the strength of the soil-lime mixture is at least 350 kPa, the mixture is suitable for structural layer application
4. Subsequent sets of specimens with different lime percentages are compacted, cured and tested (following Steps 2 and 3). Unconfined compression tests are conducted.
5. From the results of unconfined compression tests, the design lime percentage above which further increases do not produce significant additional strength is determined.
6. For field construction, the lime content is increased 0.5 to 1.0 percent to supplement construction losses, uneven distribution, etc.

Durability of stabilized soil

Soil stabilized with lime and cement should maintain desired engineering properties during service life. Research on factors affecting long-term durability of stabilized soil has been performed for a few decades. Cyclic wetting-drying or freezing-thawing processes can degrade the strength properties of chemically stabilized soils. Generally, volume increase caused by freezing and thawing reduces strength properties of soils. Dempsey and Thompson (1968) reported that the strength of typical lime stabilized soil decreased by 100 kPa during a freeze-thaw cycle. Kennedy et al. (1987) and Petry and Wohlgemuth (1988) reported that lime exhibited better resistance to wetting-drying cycles than did cement.

McAllister and Petry (1991) performed extensive leaching tests on lime stabilized soil. They had chosen lime dosage based on two cases: lime modification optimum (LMO) value determined by Eades and Grim pH test (1966) and lime stabilization optimum (LSO) determined by maximum unconfined compressive strength. The lime dosage was 3 to 4 % for LMO and 7 to 8 % for LSO. Soil treated at or less than LMO exhibited deterioration of engineering properties such as PI, shrinkage limit, and compressive strength.

Mitchell (1986) studied deterioration of lime stabilized subgrade induced by sulfate attack. It was concluded that, where subgrade soils contain sulfates, lime and cement

should be avoided as stabilizers as subsequent expansion and cracking may result in deterioration of the stabilized soil.

Oklahoma State (1980) investigated the long-term performance of chemical stabilized soil. In 1938, a 7-mile test area constituted of expansive clay soils was selected and stabilized with cement. Cement contents added to soils varied from 4 to 16 %. The original high value of PI from 18 to 51 decreased to between 7 and 18 with cement stabilization. After 45 years, samples from the cement stabilized soil was retested and showed further decrease in the PI between nonplastic and 13. Shrinkage limit reduced slightly but still retained a value sufficient for soil improvement. These results show that the cement stabilized soil preserved its improved engineering properties over a very long time (Roberts, 1986).

Numerical Analysis

Numerical analysis is a technique to calculate the mechanical behavior of roadway components with the required material properties and constitutive models. Contrary to design methodologies based on empirical relationships, numerical methods have the advantage of being able to incorporate various loading configurations, environmental conditions, and complicated nonlinear models (Masad and Scarpas, 2007).

With the development of numerical methods, many researchers in the pavement field have applied numerical techniques to simulate pavement systems consisting of flexible pavements, aggregate base, and subgrade soil layers. Some researchers have developed models under axisymmetric and cyclic loading conditions, and some have used commercial programs such as ABAQUS and FLAC to simulate field conditions. This portion of the literature review focuses on the previous numerical approaches and their simulation of roadway cross sections.

Schwartz (2002) categorized the numerical methods for determining the stresses, strains, and deformations in flexible pavement systems as follows:

1. Analytical method (e.g., Burmister solution)
2. Multilayer Elastic Theory
    a. Rate-Independent (e.g., BISAR, CHEVRON)
    b. Viscoelastic (e.g., VESYS)
3. Finite Difference Method (e.g., FLAC)
4. Finite Element (FE) Method
    a. General purpose
    b. Pavement-specific (e.g., ILLI-SLAB, ILLI-PAVE, and MICH-PAVE)
5. Boundary Element (BE) Methods (e.g., BEASY)
6. Hybrid Methods

Schwartz (2002) considered three aspects to determine an appropriate pavement structural response model: 1) material nonlinearity for simulating viscoelastic materials

for the AC (Asphalt Concrete) layer, 2) analysis dimensionality for rigorously analyzing in-situ composite pavement and loading conditions, and 3) computational practicality for performing a complicated 3-Dimensional Finite Element model. Representative programs to simulate the mechanical behavior of pavement systems are presented in Table 4.

Table 4. Previous Research Using Numerical Programs

Program	Analysis Method	Source(s)
JULEA	2D Axisymmetric Multi-Layer Elastic (MLE)	Ayres (1997)
ILLI-SLAB	2D linear Finite Element analysis 2.5D Nonlinear Finite Element	Schwartz (2002)
ILLI-PAVE	2D Nonlinear Axisymmetric Finite Element	Chen et al. (1995)
ABAQUS	2D and 3D Finite Element (Commercial Program)	Hammons (1998) Hibbitt (1998) Schwartz (2002) Cho et al. (1996) Yen & Lee (2007)
EVERFE	3D Linear Finite Element with Layer Separation and Contact Element for Rigid Pavement	Davids (1998)
FLAC	2D & 3D Finite Difference (Commercial Program)	Wallace & Sapkota (1994) Haque (1998) Chen et al. (2000) Sun et al. (2006)
NIKE3D	3D Nonlinear Finite Element for Airport Pavement	Brill et al. (1997) Brill & Parsons (2001)
GEOSYS	3D Nonlinear Finite Element	Ioannides & Donnelly (1988)
FEAP	3D Finite Element Program	Blab & Harvey (2002)
INSAP	3D Finite Element Program	Erkens (2002)
SYSTUS	3D Finite Element Program (Commercial)	Leonard et al. (2002)
EverFE	3D Finite Element for Rigid Pavement	Davids (2001)
MARC	3D Finite Element Program (Commercial)	Dong et al. (2001)

For flexible pavement systems, it can be considered that an in-situ pavement is placed in various mechanical and environmental conditions. So, many researchers have tried to simulate the behavior of pavement system by their own constitutive model. Recently, Desai (2007) suggested a disturbed state concept (DSC): DSC provides a modeling approach that includes various responses such as elastic, plastic, creep, microcracking

and fracture, softening and healing under mechanical and environmental (thermal, moisture, etc.) within a single unified and coupled framework.

For the dimensionality problem, a two-dimensional axisymmetric approach is generally regarded as a representative pavement model under ESWL (the Equivalent Single-Wheel Load) with a circular shape (Ayres, 1997; Chen et al, 1995). Since most flexible and composite pavement cases are inherently 3-D, in recent years many researchers are applying 3-D commercial programs or their own program developed using specific constitutive models. The advantages of a 3-D approach include considering multiple wheel loads as well as estimating the moving and flexible behavior of real wheel loads (Gunaratne and Sanders, 1996; Blab and Harvey, 2002). However, axisymmetric models are still reliable for analyzing the mechanical behavior of ESWL in a laboratory condition, and NDT (Non-Destructive testing; e.g., Falling Weight Deflectometer) (Al-Khoury, 2007).

Using a three-dimensional finite element program (ABAQUS), Zaghloul and White (1993) simulated the dynamic behavior of multilayered pavement under traffic loading, and compared the results with an elastic multilayer analysis program called Bitumen Structures Analysis in Roads (BISAR).

For analyzing large scale test, the stress distribution beneath circular loading on an elastic half-space is studied. A homogeneous half-space is generally considered as the simplest method to characterize the behavior of a flexible pavement under wheel loads (Huang, 2004). According to the original Boussinesq (1885) theory, the stress distribution under a circular loaded area on an elastic half-space can be obtained from integrating point loads. However, since the elastic modulus is dependent on the vertical stress, various analytical and numerical solutions for non-homogeneous material are suggested, which are presented in Table 5.

Table 5. Existing Analytical and Numerical Solutions for Inhomogeneous Isotropic Media Due to a Circular Load (After Wang et al., 2006)

Types of non-homogeneity	Author	Analytical and numerical solutions
$E=m_E Z^a$ $G=m_G Z^a$ $(0\leq a\leq 1)$	Rostovtsev (1961)	Settlement due to an elliptical, a circular, and a paraboloid of revolution load
	Popov (1962)	Surface displacement due to a circular load
	Carrier and Christian (1973a)	Displacements and stresses due to a circular load by FEM
	Popov (1973)	Displacements due to vertical/horizontal circular punches
	Booker et al.(1985)	Surface displacement due to strip, ring, and circular loads
	Oner (1990)	Displacements due to vertical/horizontal point, circular, and rectangular loads
	Hemsley (1998)	Vertical displacement and contact pressure due to a rigid circular load
	Doherty and Deeks (2003b)	Circumferential displacement of a rigid circular footing subjected to vertical, horizontal, moment, and torsion loads by using the scaled boundary finite element method
	Doherty and Deeks (2003c)	Displacement response of rigid and flexible circular footings subjected to vertical load by using the scaled boundary finite element method
	Doherty and Deeks (2003a)	Load-displacement response of an embedded rigid circular footing subjected to vertical, horizontal, moment, and torsion loads by using the scaled boundary finite element method
$E=E_0(a+bz)^c$ $G=G_0(a+bz)^c$	Chuaprasert and Kassir (1974)	Displacements and stresses due to a uniform circular load
	Rajapakse and Selvadurai (1989)	Stresses and displacement due to rigid circular and cylindrical foundations
$E=E_0+az$ or $G=G_0+az$	Gibson (1967)	Displacements and stresses due to strip and circular loads
	Brown and Gibson (1972)	Surface displacement due to a strip or circular load
	Carrier and Christian (1973b)	Settlement and stresses due to a rigid circular plate by FEM
	Gibson (1974)	Surface displacement of uniformly circular loads
	Alexander (1977)	Vertical displacement due to a circular load

Types of non-homogeneity	Author	Analytical and numerical solutions
	Rajapakse and Selvadurai (1991)	Axisymmetric elastic response of circular footings and anchor plates
	Yue et al. (1999)	Displacements and stresses due to a circular load for a layered half-space by backward transfer matrix method
$E=E_0+E_1e^{az}$ $G=G_0+G_1e^{az}$	Ter-Mkrtich'ian (1961)	Stresses and displacements due to a circular load
	Selvadurai (1996)	Settlement due to a rigid circular foundation
$G=G^*_0h/(h-z)$ $G=constant$	Awojobi (1975)	Settlement of a circular foundation
	Gibson and Sills (1969)	Stresses and displacements due to point and circular loads

Criteria for establishing required magnitude of undercut

Several aspects of deformation and strain under loading can indicate the condition of subgrade materials and their strength and stiffness. Various indicators include rut depth, maximum surface curvature, and tension crack development. For assessing subgrade quality and the need for undercutting, one of these indicators may be more sensitive than the others to the quality of the subgrade and therefore might be used for development of quantitatively-based undercut criteria. There are however few studies in literature that shed light on this subject. For a paved roadway section, the relationships among deflection, curvature, the compressive strain on the surface of the subgrade, and the tensile strain at the bottom of the asphalt layer were investigated by Huang (1973). Huang mainly used elastic analyses of stress and deformation based on the three-layer elastic theory by Burmister (1945), as shown in Figure 2.

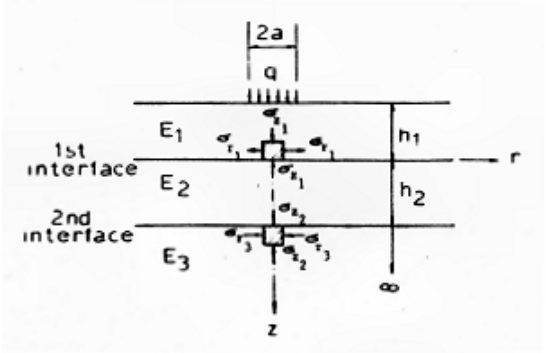

Figure 2. Three-layer elastic system (Huang, 1971)

A number of deformation characteristics including deflection-curvature were calculated and investigated for different layer thicknesses and stiffnesses of the three-layer system shown in Figure 3. Such an approach is a good example of utilizing deformation

characteristics to assess pavement systems, but does not directly apply to roadway sections during the construction stage, the focus of this research. For sections under construction, behavior will predominantly be controlled by inelastic mechanics due to the large deformation induced by construction traffic on the subgrade and base course layers prior to the placement of the asphalt or concrete pavement.

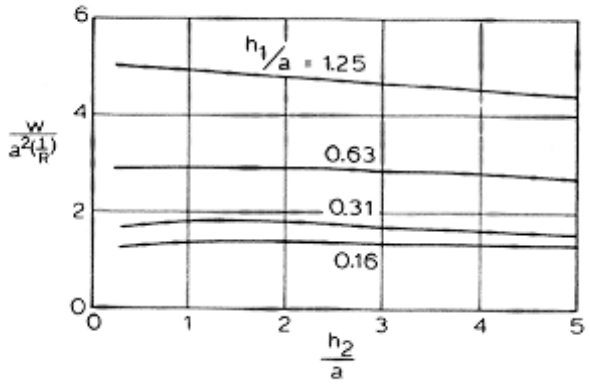

Figure 3. Effect of thickness on deflection-curvature ratio (Huang, 1971)
(h_1=thickness of pavement layer, h_2=thickness of ABC, a=radius of loaded area, R= curvature, and w=maximum settlement)

In order to better simulate subgrade layer response during construction, Maciejewski and Jarzebowski (2004) investigated the deformation of cohesive soil below a rolling cylinder in a laboratory testing program. Figure 4 shows the schematic of the test model they used. The soil used in the test was manufactured to simulate clay and its engineering properties. The testing proceeded by first applying a selected vertical force on the rigid cylinder, simulating a constant weight, and then the cylinder was rolled horizontally. Details of the testing program can be found in Jarzebowski et al. (1995) and Maciejewski and Jarzebowski (2004).

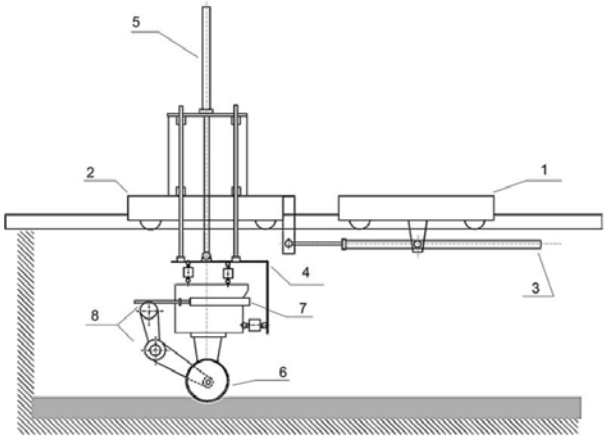

Figure 4. Scheme of the laboratory stand: (1) rear cart; (2) front cart; (3), (5), (7) hydraulic cylinders; (4) rigid frame; (6) rigid cylinder; (8) gear belts (Maciejewski and Jarzebowski, 2004)

During testing, vertical crack lines were noticed in the zone behind the cylinder (moving right to left) as shown in Figure 5. In an attempt to examine the characteristics of crack development, experiments were conducted with varying weight of cylinder as well as height of soil layer. As shown in Figure 6, both crack depth and spacing increased with increasing weight of the cylinder, with a mean distance between cracks of approximately 25 mm. In addition, when the thickness of the soil layer was larger, the crack depth and spacing were also larger (Figure 6).

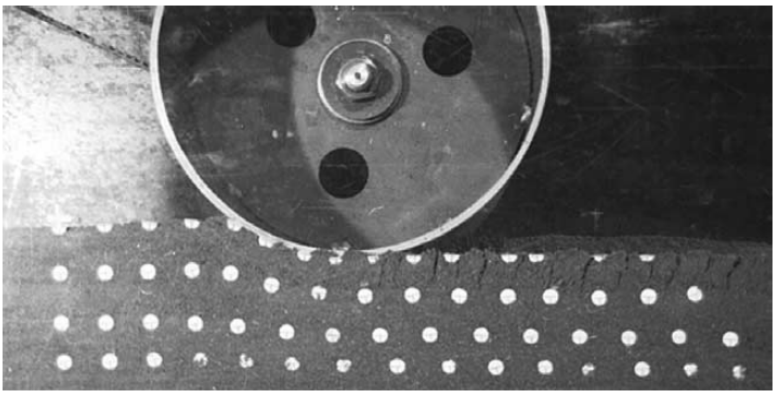

Figure 5. Structure of the soil layer during the towed cylinder test (Maciejewski and Jarzebowski, 2004)

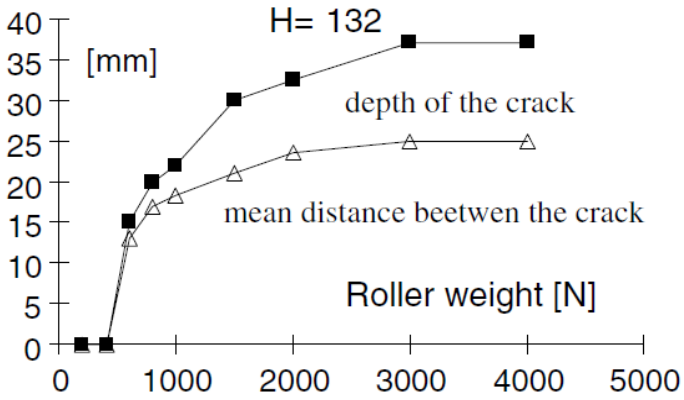

Figure 6. Depth and mean distance between cracks versus weight of the cylinder (Maciejewski and Jarzebowski, 2004)

The same authors (Jarzebowski and Maciejewski, 1998a) conducted numerical simulations of cohesive soil behavior under a rigid rolling cylinder using a finite element code. The authors observed from the numerical analyses that the development of horizontal strain in the soils with two different void ratios, e_0 = 0.9 and 0.55, corresponded to the location of cracks observed during the experiments. It is noted that both depth and spacing of developed cracks are larger for the looser material.

Hambleton and Drescher (2008) established a theoretical relationship between wheel penetration depth and soil strength properties using an approach of ultimate bearing

capacity of shallow foundations. Figure 7 shows the relationship between penetration depth and strength parameters for a rolling wheel load of Qv = 67 kN, d (diameter of wheel) = 1.52m, and b (width of wheel) = 0.46m. The theoretical relation was compared with results from finite element analyses and small scale laboratory experiments. The authors did not provide the dependency of their criteria on the stiffness of the subgrade. If 1 inch (25.4 mm) is assumed as the deformation criterion, the results indicated a minimum value of c=160 kPa for the case of ϕ=0 is required for an acceptable subgrade.

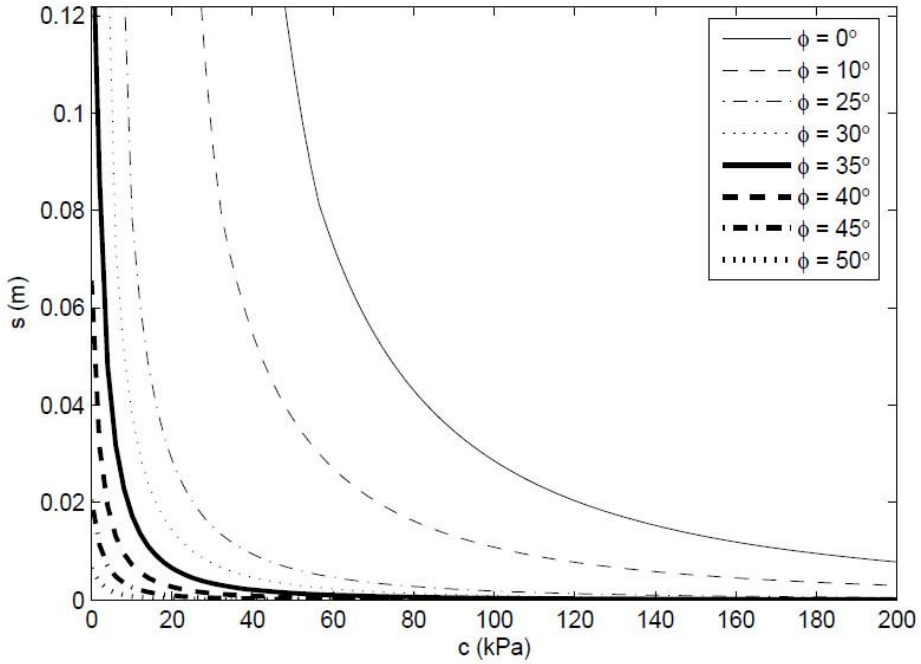

Figure 7. Relationship between penetration depth and strength parameters for rolling wheel with Qv=67 kN, d=1.52 m, b=0.46m, and γ=18 kN/m3 (1mm=0.0394 inch and 1 kPa=20.89 kPa)

There is general agreement among those involved in field observation that acceptance through proof rolling is rather subjective and operator-dependent. It is possible, for example, that weak subgrade areas are not detected if the contact area and applied load from proof roller are inadequate. From the studies previously reviewed, it was shown that deformation, strain, and depth and spacing of developed crack under rolling rigid cylinder (simulating a proof roller) depend on the weight of cylinder, along with the thickness and density of the soil layers. Accordingly, it seems that the indication of deformation, or cracks as manifested by shear strains, can effectively be used as an indicator of the robustness of subgrade under a particular proof rolling load. However there have been no studies that show the implementation of a systematic criteria and its validation based on field performance data. A study is needed to collect field data to show the adequacy of any developed undercut criteria, discerning the need for stabilization measures, and the adequacy of engineered subgrade layers.

Summary

The literature surveyed indicates a significant body of work in all five components related to this current study. There have been considerable and on-going efforts to standardize and generalize design methodologies for geosynthetic reinforced roadways that do not require a specific manufacturer's product or a significant, pre-design phase laboratory study of the interaction between *in situ* soil properties and selected geosynthetics. To this end, the quantification of the benefits of geosynthetics in laboratory box-type tests and full scale field demonstrations have been undertaken by many researchers, with a wide range of results and conclusions.

As a quality control and design tool, many researchers have also looked to the dynamic cone penetrometer as a fast test at various points along a roadway. The approach has traditionally relied on statistical correlations of the DCP index to a range of stiffness or compaction parameters. The literature contains very little coverage of the mechanical behavior of the DCP as it relates to the interaction of the moving penetrometer through the soil.

Stabilization of soils with lime or cement has also received significant research attention over several decades. The mechanisms and behavior of these stabilized soils are well quantified, but a direct comparison between lime or cement stabilization and reinforcement of subgrades with geosynthetics has not been performed.

The literature also contains a number of numerical approaches to modeling layered pavement systems. Typically, axisymmetric models are applied, with a circular footing used to model the wheel load application. Other approaches use axisymmetric plane-strain or full 3-D models with rectangular stress or even moving wheels modeling the application of traffic loading.

As a basis for efforts in all chapters that follow it, the next chapter will describe in detail typical geo-material properties used in areas of North Carolina that require undercut.

CHAPTER 3: TEST MATERIALS CHARACTERIZATION

This chapter summarizes the results of small scale laboratory testing to estimate the physical and engineering properties of the candidate soils provided for the large scale experimental program. The test soils are divided into four main categories: subgrade soil, aggregate base course (ABC), select fill, and lime treated subgrade soil. Geotechnical tests were conducted in accordance with ASTM or AASHTO specifications to define the soils' physical and engineering properties. These tests included grain size analysis, Atterberg limits, specific gravity, standard proctor compaction, shear strength, resilient modulus and permeability tests as appropriate to each soil type. This chapter presents the results of small scale tests performed in this project.

Subgrade soils

Candidate subgrade soils suggested for use in the large scale test pit were provided from two NCDOT undercut project areas. One of the project areas is located in southern Greensboro within the Piedmont Physiographic Province. Topography along the project is typical of the Piedmont area containing gently rolling terrain and well-defined shallow stream valleys. Geologically, the project is underlain by metamorphosed granitic rocks of the Carolina Slate Belt. Soils are derived from the weathering of the underlying bedrock with minor occurrences of metamorphosed gabbro and diorite. These units are generally foliated, and trend in a northeasterly direction. Residual soils are the most prevalent soil type and are derived from the weathering of the underlying metamorphic bedrock. (Geotechnical Inventory Report 2002)

Soil samples were also provided from a project area located north of Greenville, North Carolina within the Coastal Plain Physiographic Province. The topography of the area is nearly flat to gently sloping and generally exhibits poor surface drainage. Surficial soils in this area are generally derived from alluvial deposition and the weathering of existing formational material. Alluvial soils are restricted to areas in and around stream crossings, while the upland sections are composed primarily of oxidized formational soils. These surface units are underlain by the Pliocene marine deposits of the Yorktown Formation. (Geotechnical Inventory Report 2006)

Basic laboratory tests were performed on both the Coastal plain and Piedmont residual soils. The basic testing program included grain size distribution, specific gravity, Atterberg limits, and standard Proctor tests. Table 6 presents the index properties of these soils.

One Piedmont residual soil and five Coastal plain soils were evaluated. The Piedmont residual soil and Coastal plain soil 1 were small samples delivered in two canvas bags in September 2007 for initial characterization. Coastal plain soil 2 was delivered in an approximately 10 cubic yard bulk sample in November 2007 for use in both the small and large scale testing. In early March 2008, it was determined this initial soil volume was

not large enough, and Coastal plain soil 3 was delivered in an 8 cubic yard sample. Coastal plain soil 4 was made by mixing Coastal plain soil 2 and 3 into one approximately 18 cubic yard sample. This mix has been used as main subgrade soil in this research project. Coastal plain soil 5 was delivered to be used as a lime treated subgrade layer in early March, 2009. Gradation curves for all soils are presented in Figure 8. The gradations for coastal plain soil 4 and 5 are the average of two separate grain size analyses. Standard proctor compaction test results are illustrated in Figure 9. The main soil used in the large scale testing program is the Coastal plain soil 4. It is classified as A-6 (6) according to the AASHTO engineering soil classification system, and as CL according to the Unified Soil Classification System. As shown in Figure 9, the maximum dry unit weight of soil 4 is 113.2 pcf at an optimum moisture content of 15.3%

Table 6 Soil Index Properties

Soil Sample	LL	PL	PI	G_s	Maximum dry unit weight, γ_{dmax} (pcf)	Optimum moisture content (%)	Classification	
							USCS	AASHTO
Piedmont soil	44	32	12	2.69	115.7	14.7	ML	A-6(5)
Coastal plain soil 1	20	16	4	2.63	121.6	10.9	CL-ML	A-4
Coastal plain soil 2	29	18	11	2.66	115.1	14.6	CL	A-6(3)
Coastal plain soil 3	36	18	18	-	109.5	15.9	CL	A-6(8)
Coastal plain soil 4	33	17	16	2.70	113.2	15.6	CL	A-6(6)
Coastal plain soil 5	28	15	13	2.65	113.0	15.5	CL	A-6(8)

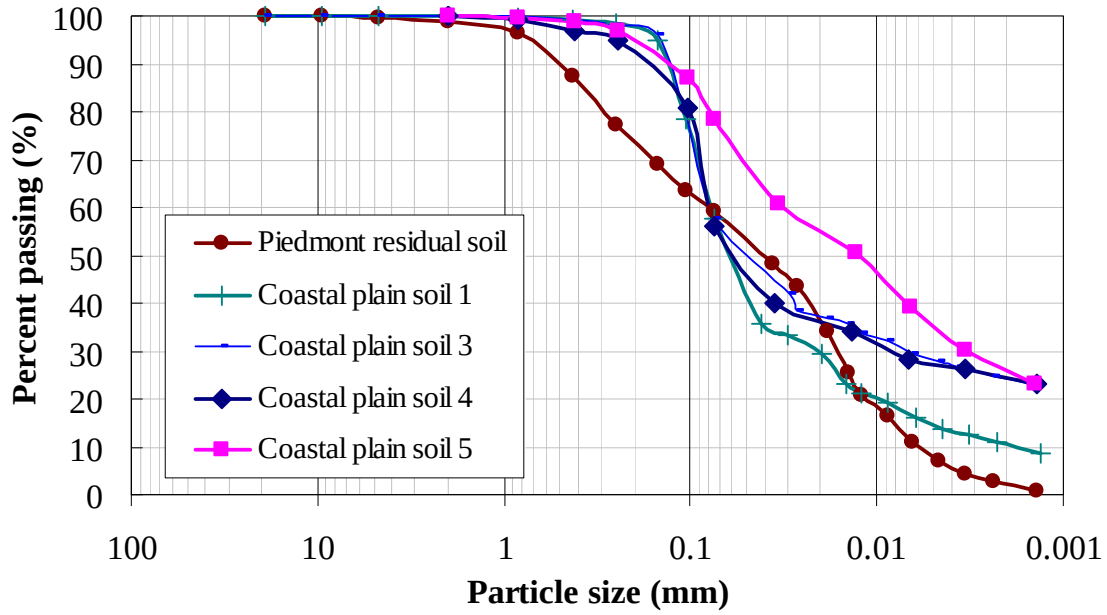

Figure 8. Grain size distribution curves of various soils considered for large scale testing

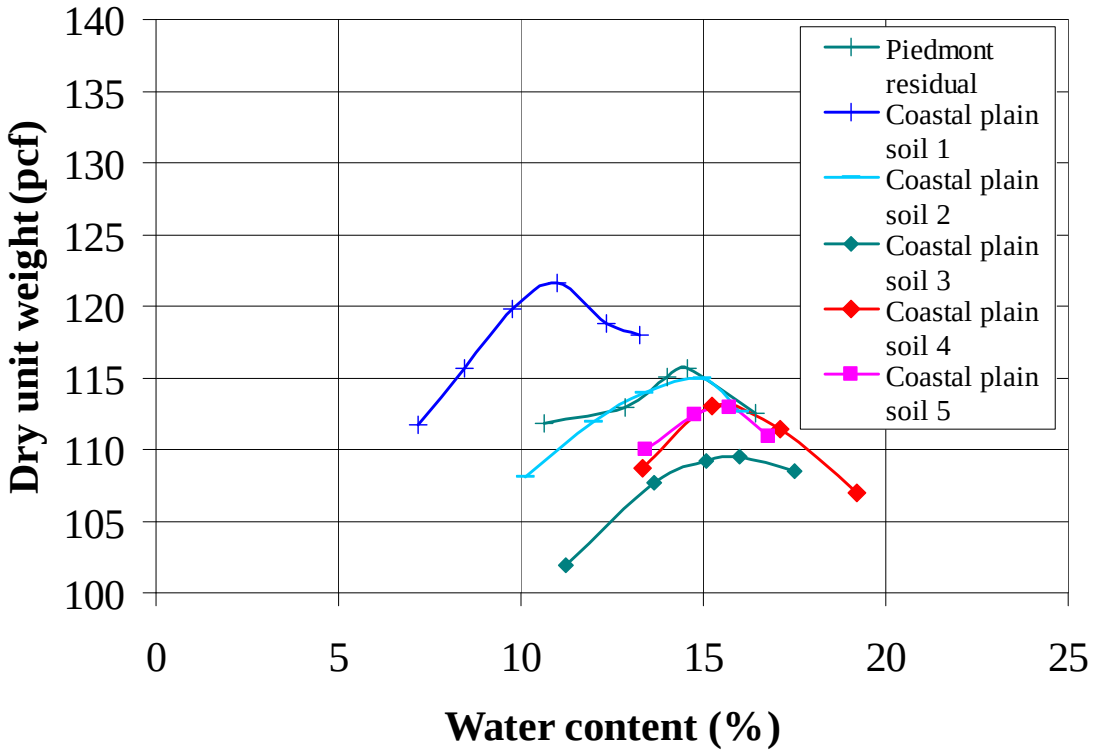

Figure 9. Moisture-density standard compaction test results

California bearing ratio testing

California bearing ratio (CBR) tests (AASHTO T 193-98) were conducted at the NCDOT Material and Testing Unit. Specimens were manually compacted in 150 mm (6 in) molds using a standard proctor hammer (T-99) and then penetrated with 1.95 inch diameter metal piston with and without soaking. The CBR value was measured at 0.1 and 0.2 inch penetration.

Initially, soaked CBR tests using the Piedmont residual soil and Coastal plain soil 1 (remolded with different moisture content and dry unit weight levels) were performed to establish compaction characteristics leading to a CBR equal to 2%. The results are presented in Table 7.

Table 7. Corrected Soaked CBR Values

Soil	Moisture Content (%)	Dry unit weight (pcf)	Relative Compaction (%)	Corrected Soaked CBR (%)
Piedmont soil	13.7	113.7	98.2	9.7
	15.8	113.1	97.7	8.6
	17.6	110.5	95.5	5.2
	19.4	106.8	92.3	1.3
Coastal plain soil 1	10.8	119.7	98.4	26.6
	12.7	116.3	95.6	2.5
	14.5	112.9	92.8	0.8
	16.8	108.1	88.9	0.3

However, the large scale prototype tests were not performed as saturated tests, and unsoaked CBR tests using coastal plain soil 2, 4, and 5 again were carried out to establish the moisture content and dry unit weight level yielding a CBR value on the order of 2%. Test results are reported in Table 8 and Figure 10.

As shown in Figure 10(b), the CBR test results indicate that the sample from coastal plain soil 4, yields a CBR =2% when prepared at water content of 18.8% (at 0.1 in. penetration) or 19.5% (at 0.2 in. penetration).

Resilient modulus testing

The resilient modulus tests were performed at confining and deviator stress levels recommended in the AASHTO T-307 procedure. The load sequence used for testing is presented in Table 9. The moisture content and dry unit weight levels from the CBR tests were adopted as the target values for the specimen preparation of resilient modulus tests. Specimens for the Piedmont residual soil and Coastal plain soil 1 were prepared at the

Table 8. Corrected Unsoaked CBR Values

Soil	Moisture Content (%)	Dry unit weight (pcf)	Relative Compaction (%)	Corrected Unsoaked CBR
Coastal plain soil 2	13.0	113.7	98.8	24.4
	15.1	113.0	98.2	6.8
	16.2	112.1	97.4	3.0
	17.2	109.5	95.2	2.0
	18.6	106.8	92.7	1.6
Coastal plain soil 4	14.0	114.2	100.9	22.5
	15.5	112.2	99.1	13.3
	16.7	--	--	3.8
	17.8	109.3	96.6	3.3
	18.8	106.8	94.3	2.1
	20.7	102.4	90.5	1.0
Coastal plain soil 5	15.3	109.8	24.9	24.1
	17.6	109.2	96.6	3.5
	18.7	107.1	94.8	2.1
	20.6	102.5	90.7	0.8

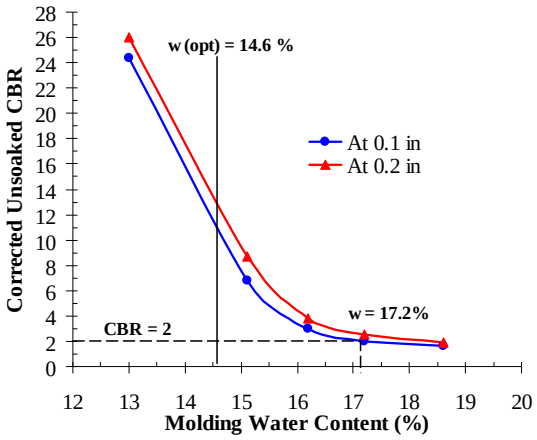

(a) Coastal plain soil 2

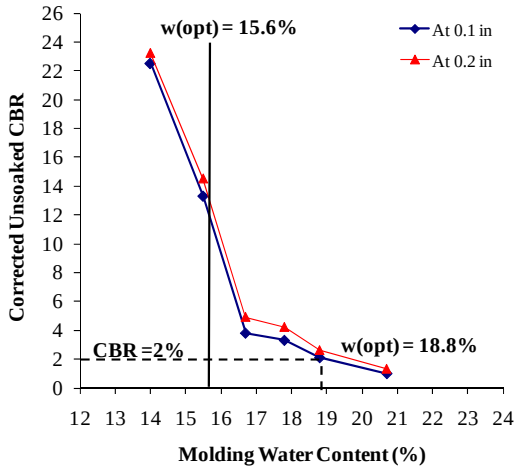

(b) Coastal plain soil 4

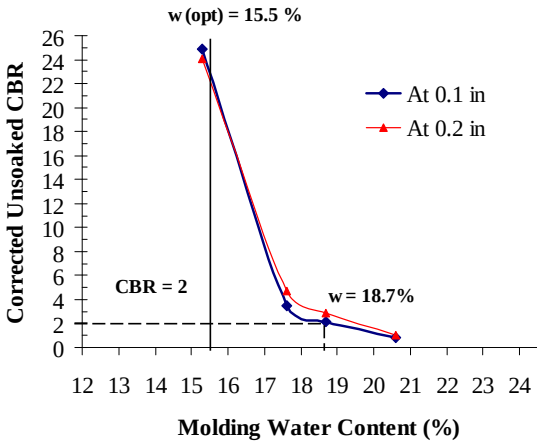

(c) Coastal plain soil 5

Figure 10. Unsoaked CBR test results

moisture content and dry unit weight levels based on the soaked CBR tests. Specimens based on the moisture content and dry unit weight levels from the unsoaked CBR tests for

Coastal plain soil 2 and 4 were also prepared. Specimen preparation data and Mr test results are reported in Appendix A. An example is given below as Figure 11 for Coastal plain soil 4. The resilient modulus increases with an increase in the confining pressure. Generally, it decreases with as water content increases and dry unit weight decreases.

Selection of M_R value

A single test provides 15 resilient modulus values depending on confining pressure and cyclic stress. To select a value of Mr from the testing data, the AASHTO Design Guide (1993) suggests resilient modulus value based on assumed deviatoric stress of 6 psi, or based on actual field stresses. Thompson and Robnett (1976) suggest using a resilient modulus value which occurs at a zero confining pressure and 6 psi deviatoric stress. Rahim (2005) pointed out that Thompson and Robnett's suggestion did not represent in-situ stress states well. In the field, subgrade must sustain the overburden of pavement layers, in addition to the standard 18-kip axle load. Stress analysis by KENLAYER software (Huang 1993), employing the 18-kips standard axle load on a typical Mississippi pavement section comprised of 2 in. asphalt base course and 6 in. lime treated subbase atop subgrade yielded a stress state of 5.4 psi deviator stress and 2 psi lateral stress at the top of subgrade. Therefore, accepting Rahim's suggestion, a resilient modulus value highlighted as sequence 13 in Table 9 (5.4 psi deviatoric stress and 2 psi confining pressure) is used in this study. Figure 11 shows the variation of the Mr values with moisture content for the study soil.

Table 9. Load Sequence for Resilient Modulus Test (AASHTO T-307)

Sequence No.	Confining Pressure, σ_3		Max. Axial Stress σ_{max}		Cyclic Stress σ_{cyclic}		Constant Stress 0.1 σ_{max}		No. of Load Applic.
	psi	kPa	Psi	kPa	psi	kPa	psi	kPa	
0	6	41.4	4	27.6	3.6	24.8	0.4	2.8	500
1	6	41.4	2	13.8	1.8	12.4	0.2	1.4	100
2	6	41.4	4	27.6	3.6	24.8	0.4	2.8	100
3	6	41.4	6	41.4	5.4	37.3	0.6	4.1	100
4	6	41.4	8	55.2	7.2	49.7	0.8	5.5	100
5	6	41.4	10	68.9	9.0	62.0	1.0	6.9	100
6	4	27.6	2	13.8	1.8	12.4	0.2	1.4	100
7	4	27.6	4	27.6	3.6	24.8	0.4	2.8	100
8	4	27.6	6	41.4	5.4	37.3	0.6	4.1	100
9	4	27.6	8	55.2	7.2	49.7	0.8	5.5	100
10	4	27.6	10	68.9	9.0	62.0	1.0	6.9	100
11	2	13.8	2	13.8	1.8	12.4	0.2	1.4	100
12	2	13.8	4	24.8	3.6	24.8	0.4	2.8	100
13	2	13.8	6	37.3	5.4	37.3	0.6	4.1	100
14	2	13.8	8	49.7	7.2	49.7	0.8	5.5	100
15	2	13.8	10	62.0	9.0	62.0	1.0	6.9	100

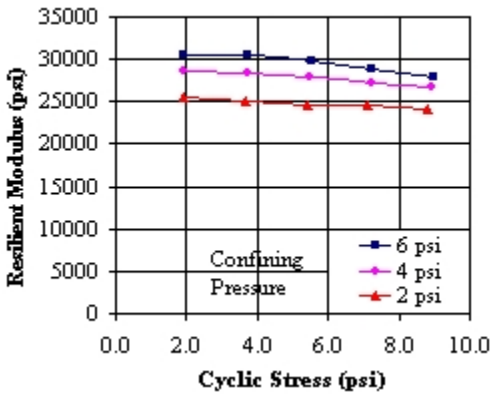

(a) w = 13.8 % and γ_d = 113.7 pcf

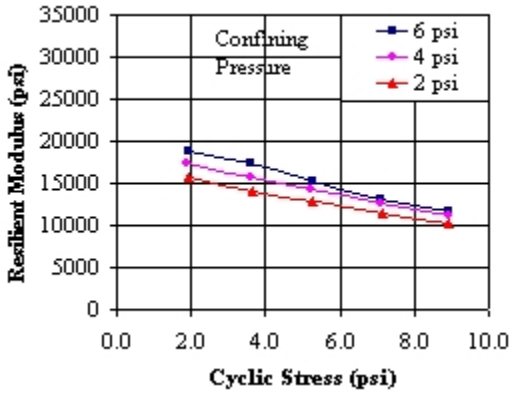

(b) w = 15.9 % and γ_d = 111.6 pcf

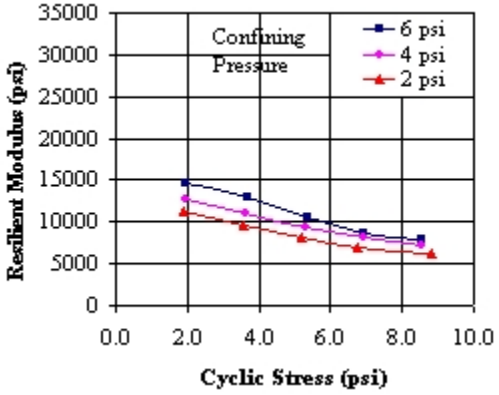

(c) w = 17.9 % and γ_d = 109.9 pcf

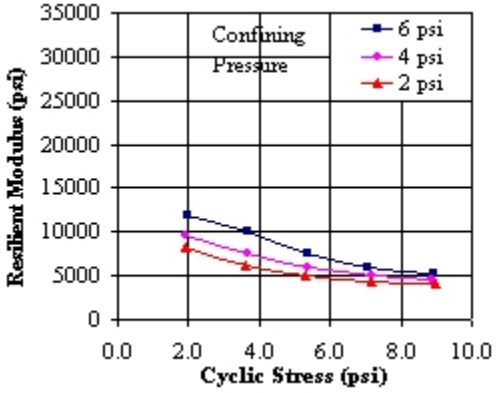

(d) w = 19.4 % and γ_d = 107.2 pcf

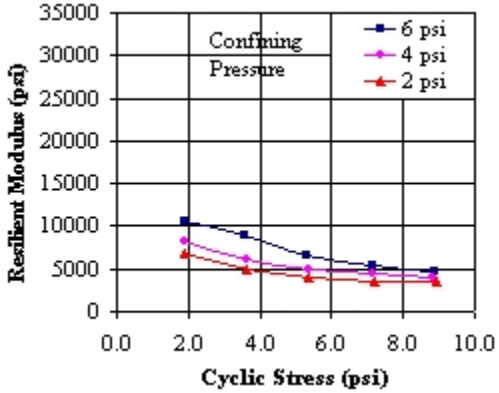

(e) w = 20.3 % and γ_d = 104.7 pcf

Figure 11. MR test results on coastal plain soil 4

Consolidated undrained triaxial testing

Consolidated undrained triaxial tests (ASTM D4767) were performed on the mixed coastal plain soil sample (coastal plain soil 4). Three sets of CU tests were initially performed to measure the variation of shear strength parameters with the change in water content and dry unit weight in June, 2008. Samples for test 1 were prepared at maximum dry unit weight and optimum water content obtained from the standard proctor test. Samples for test 2 and 3 were prepared at moisture content and dry unit weight levels similar to those of subgrade soil in large scale test. Samples for test 2 are very close to the moisture content and dry unit weight level of subgrade in test pit. Specimen moisture content and dry unit weight levels were presented in Appendix A. Stress-strain and pore water pressure-strain curves developed during the shearing stage and Mohr circle charts in terms of both total and effective stresses at the maximum deviator stress criterion are also included in Appendix A. Mohr-Coulomb strength parameters are presented Table 10.

Table 10. Mohr-Coulomb Strength Parameters from CU Tests (June 2008)

Test Series	w (%)	Effective Stress		Total Stress	
		c' (psi)	phi' (deg)	c (psi)	phi (deg)
1	15.6	0	34.5	9.4	20.5
2	19	0	34.5	5.7	19
3	20.7	0	33.5	2	16.5

After all the planned large scale tests for this project were performed, an additional series of CU tests (test #4) was performed in June 2009 on the mixed coastal plain soil under the same moisture content and dry unit weight level as the previous test #2. The objective of this series of testing was to observe any degradation of soil strength due to repetitive re-working of the same soil bulk during the large scale testing. Stress-strain curves, pore water pressure-strain curves, and Mohr circles in terms of both total and effective stresses at the maximum deviator stress criterion are presented in Appendix A. The test results are compared with those of test #2 as shown in Table 11 and Table 12. Figure 12 is the graphical presentation of Table 12.

Table 11. Comparison of Mohr-Coulomb Strength Parameters: Tests 2 and 4

Test #	Test Date	Effective Stress		Total Stress	
		c' (psi)	phi' (deg)	c (psi)	phi (deg)
Test 2	6/2008	0	34.5	5.7	19
Test 4	6/2009	0	37	3.6	15

Table 12. Comparison of Undrained Shear Strength (Su): Tests 2 and 4

Test #2: 6/2008				Test #4: 7/2009			
σ_3 (psi)	σ_1 (psi)	q_f (psi)	Su (psi)	σ_3 (psi)	σ_1 (psi)	q_f (psi)	Su (psi)
3.4	21.1	17.7	8.9	3.4	15.4	12	6.0
20.9	57.6	36.7	18.4	20.7	47.2	26.5	13.3
35.1	82.3	47.2	23.6	34.7	69.4	34.7	17.4

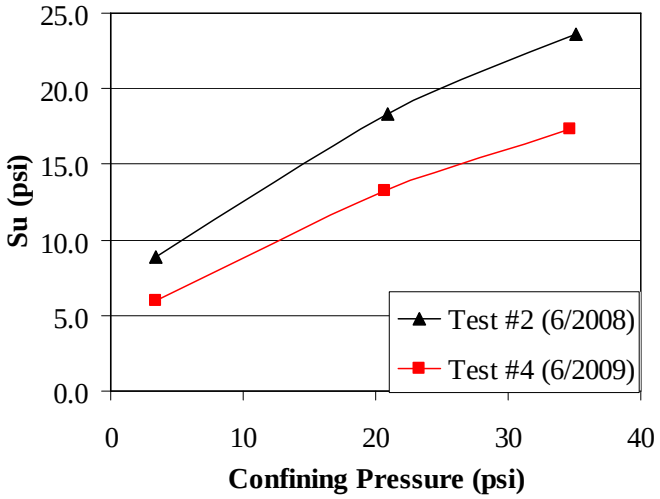

Figure 12. Change in undrained shear strength between test 2 and test 4 at three different confining pressures

The comparative data indicated that the soil strength had decreased by approximately 30% at confining stress of 3.4 psi due to repetitive compaction of the soil in the process of sample preparation for the large scale tests.

Unconfined compressive strength testing

Unconfined compressive strength tests (ASTM D5102) were performed on the mixed coastal plain soil (coastal plain soil 4). Test specimens are prepared at two different conditions: (1) at optimum water content and maximum dry unit weight (w=15.6% and γ_{dmax}=113.2 pcf) and (2) test pit condition (w=19% and γ_d=108.5 pcf). Two tests were performed at each condition. Test results are presented in Table 13. These results will be compared with those from testing on lime-treated subgrade later.

Table 13. UCS Test Results

	Unconfined Compression Strength (psi)			Undrained shear strength (psi)
Water Content	1	2	Mean	Mean
14	38.5	37.4	38.0	19
15.5 (optimum)	33.4	35.6	34.5	17.25
16.7	23.6	24.3	24.0	12
18.8 (Test pit)	16.7	15.5	16.1	8.05
20.7	5.7	5.8	5.8	2.9

Combining the CBR results from Table 8 and the unconfined compressive strength values from Table 13, a correlation between CBR and undrained shear strength, s_u, can be obtained. This correlation is shown as Figure 13 and is distinctly nonlinear.

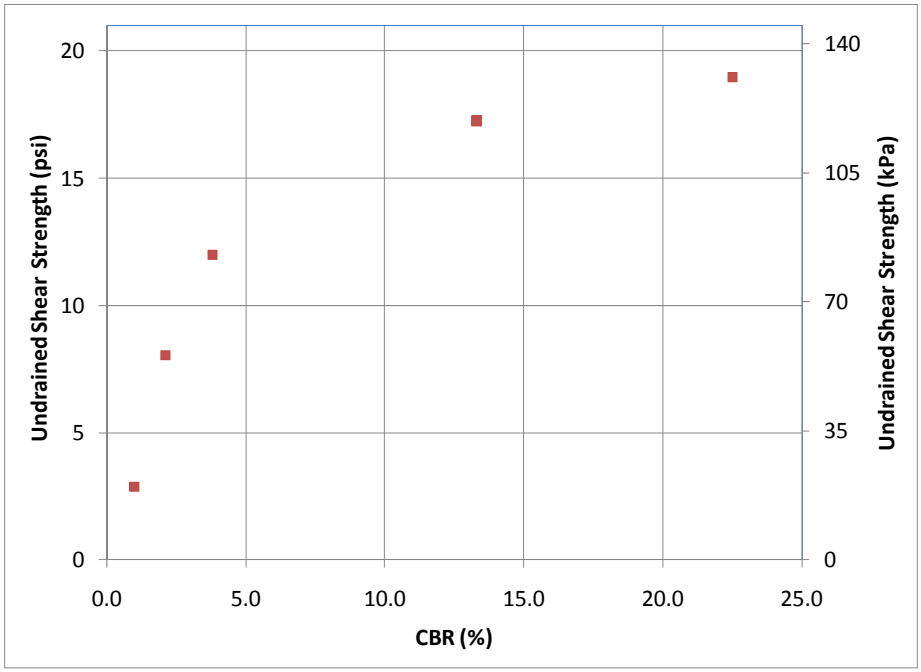

Figure 13. Correlation of undrained shear strength from UCS with CBR

Permeability testing

Falling head permeability tests were performed to determine the permeability of two test soils (Piedmont Residual Soil and Coastal Plain Soil 2).The samples were compacted at optimum moisture content by manual tamping. The results are presented in Table 14, and show that both soils exhibit permeability values, k, less than 10^{-5} cm/s.

Table 14. Permeability Test Results

Soil	Permeability, k (cm/s)
Piedmont Residual Soil	2.2×10^{-6}
Coastal Plain Soil 2	2.8×10^{-7}

Aggregate Base Course (ABC)

Two deliveries of ABC were used for large scale prototype tests. ABC 1 was initially delivered from a local quarry in March 2008, but partial loss of fines was observed during early large scale tests, as described in Chapter 5. Therefore, ABC 2 was delivered for the remaining large scale tests in August 2008. Grain size distribution, specific gravity, Atterberg limit, and modified proctor compaction tests were performed on these two ABC samples. Table 15 presents the index properties of these two soils. Gradation curves

are presented in Figure 14 and the gradations are the average of two grain size analyses. Modified proctor compaction test results are illustrated in Figure 15. Both ABC samples are classified as A-1-a according to AASHTO engineering soil classification system.

Table 15. ABC Index Properties

Soil Sample	LL	PL	PI	Gs	Maximum dry unit weight, γ_{dmax} (pcf)	Optimum moisture content (%)	Classification	
							USCS	AASHTO
ABC 1	20	-	NP	-	137.4	6.4	GW-GM	A-1-a
ABC 2	22	-	NP	-	138.5	5.8	GW-GM	A-1-a

*NP – Non-Plastic

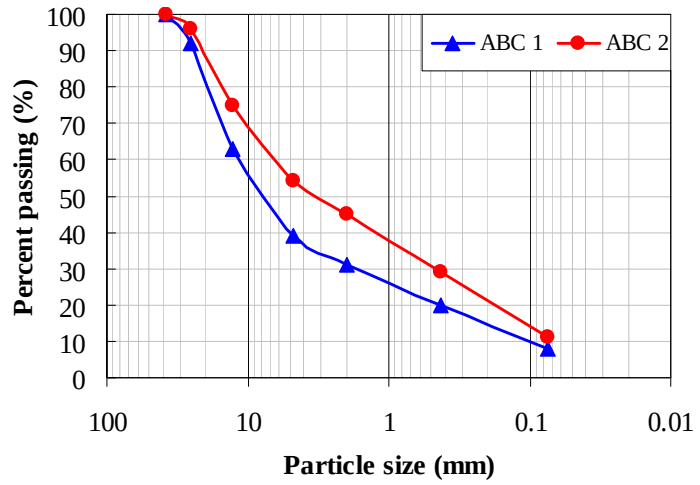

Figure 14. ABC Gradation curves

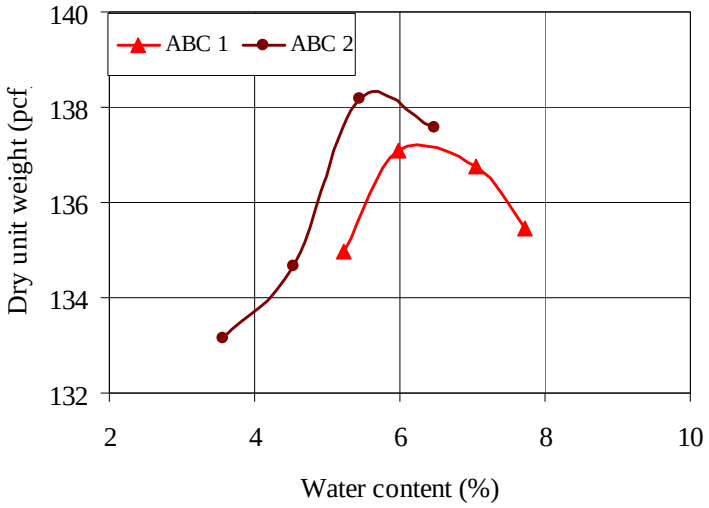

Figure 15. ABC modified proctor compaction test results

Select fill

The select fill material, used as a means of stabilization after cutting soft subgrade, is described as typical by NCDOT and was delivered from a coastal plain borrow site in July, 2007. Grain size distribution, specific gravity, and Standard Proctor tests were performed on this soil. Table 16 presents the index properties, the gradation curve is presented in Figure 16, and moisture content and dry unit weight relationship is illustrated in Figure 17. Select fill is classified as A-1-b according to AASHTO engineering soil classification system.

Table 16. Select Fill Index Properties

Soil Sample	LL	PL	PI	Gs	Maximum dry unit weight, γ_{dmax} (pcf)	Optimum moisture content (%)	Classification	
							USCS	AASHTO
Select fill	-	-	N P	2.64	-	-	SP	A-1-b

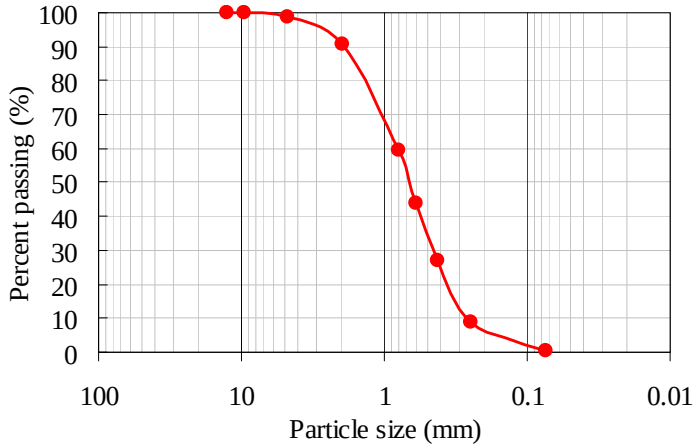

Figure 16. Select fill gradation curve

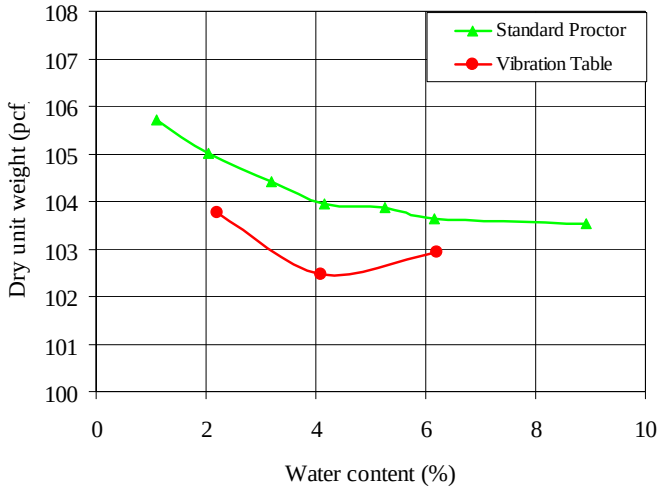

Figure 17. Select fill Moisture content and dry unit weight relationships

California bearing ratio testing

Select fill materials in large scale test pit were prepared at two different moisture contents and dry unit weight levels: (1) a water content of 2% and dry unit weight of 104 pcf and (2) a water content of 4% and dry unit weight 103 pcf. CBR tests were performed on samples made as those moisture content and dry unit weight levels. Samples were prepared under less compactive effort (45 blows per layer) than standard test to achieve those intended moisture content and dry unit weight levels. The test results are reported in Table 17. The results indicate slight difference in CBR value between two different moisture content and dry unit weight levels. The CBR value of select fill is however greater than that of subgrade soil in test pit condition.

Table 17. Select fill Unsoaked CBR Test Results

Test #	Target Value		Achieved Value		Unsoaked CBR Value	
	Moisture Content (%)	Dry unit weight (pcf)	Moisture content (%)	Dry unit weight (pcf)	@ 0.1 in.	@ 0.2 in.
1	2.1	104.0	2.1	104.0	16.5	16.5
2			2.1	104.5	17.2	16.9
3	4.1	103.0	4.1	103.2	15.2	15.2
4			4.2	103.4	16.7	16.9

Resilient modulus testing

Select fill samples were prepared at the same two different moisture content and dry unit weight levels as used in the CBR tests. As mentioned in previous section, these levels are identical to those of the select fill layer prepared in large scale test. The resilient modulus tests are performed on these samples, and test results are reported in Figure 18. Similar to the observation made for the CBR values, the results indicate that there is slight difference in resilient modulus between samples made at two different moisture content and dry unit weight levels.

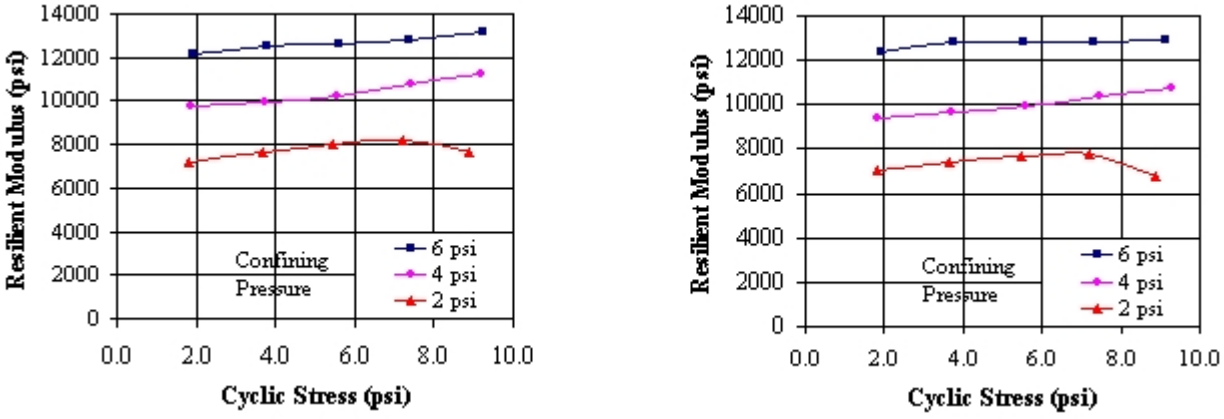

(a) w = 2.1 % and γ_d = 104 pcf (b) w = 4.0 % and γ_d = 103 pcf

Figure 18. Select fill resilient modulus test results

Consolidated undrained triaxial testing

Consolidated undrained triaxial tests (ASTM D4767) were performed on the select fill material. Moisture content and dry unit weight levels for sample preparation with select fill material are presented in Appendix A. These levels are identical to those of select fill in large scale prototype tests. Strain-stress curves and pore water pressures developed during shearing stage and Mohr circle charts in terms of both total and effective stresses at the maximum deviator stress criterion are presented in Appendix A. Mohr-Coulomb strength parameters are presented Table 18.

Table 18. Select Fill Mohr-Coulomb Strength Parameters From CU Tests

Effective Stress		Total Stress	
c' (psi)	phi' (deg)	c (psi)	phi (deg)
0	33.5	15.0	25.0

Lime treated subgrade

Standard proctor compaction testing

Standard proctor compaction tests (ASTM 698) were performed on coastal plain soil 4 containing either 3% or 5% lime by weight. After mixing, the soil-lime mixtures were mellowed for 2 hours in an airtight plastic bag before compaction. An additional compaction test was also carried out using 3% lime treated samples without a mellowing period (immediate compaction) to assess the mellowing effect on moisture content and dry unit weight relationship. The test results are presented in Figure 19.

Compared with an untreated sample, the lime-treated samples exhibited a slight increase in optimum moisture content and decrease in maximum dry unit weight. These results are consistent with Christensen (1969)'s observations. While the mechanism that is causing this behavior has not been fully examined in literature, principles of soil compaction can be used for a possible explanation. As lime is added, the soil is flocculated and forms clumps of particles. Molenaar (2005) stated that higher densities can be achieved when these lumps are softer, and when additional water is added, allowing air to be efficiently expelled from the voids. With the addition of lime and the formation of hydrates, air becomes trapped in the voids and its expulsion may not occur under a given compactive effort. This may lead to the slightly lower densities.

There is also a difference between immediate compaction and delayed compaction as observed for the 3% lime treated sample, as shown in Figure 19, especially at moisture contents dry of optimum. These results are also similar to Christensen (1969)'s results. It seems that more mellowing time for the mixture prior to compaction provides more opportunity for cation exchanges and flocculation and agglomeration. Therefore, the stiffer lumps in the soil-lime mixture make its optimum water content increase and its maximum dry unit weight decrease.

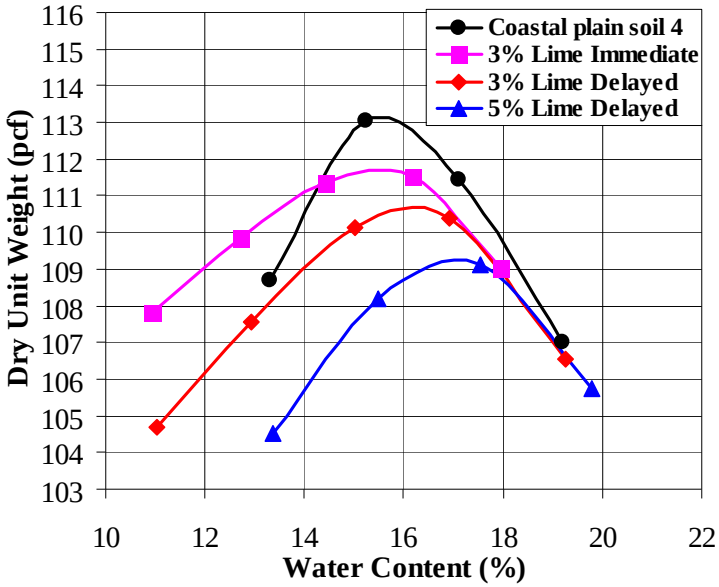

Figure 19. Lime stabilized soil standard proctor compaction test results

Unconfined compressive strength testing

The subgrade soil was treated with 3% lime and cured for 7 days. Three large scale tests were performed using coastal plain soil 4 (2 tests) and 5 (1 test) which were treated with 3% lime and cured for 7 days. For the purpose of providing a more comprehensive understanding of mechanical behavior of coastal plain soil 4 unconfined compressive strength (ASTM D5102) tests were performed on samples with two lime dosages (3 and 5%) and three different curing period (7, 14, and 28 days). The lime treated samples were prepared with appropriate moisture content and dry unit weight levels to each lime dosage shown in Figure 19. The test results are presented in Table 19 and Figure 20. Generally, lime-treated samples show higher unconfined compressive strength than the untreated samples. Unconfined compressive strength slightly increases with increase in lime content and curing period. The sample treated with 5% lime and cured for 28 days shows a striking increase in strength.

Two additional UCS tests were carried out on 3% lime treated samples which cured for 2 days in a drying oven at 105 F. This curing method is per NCDOT soil laboratory specification. The results are included in Table 19 and Figure 20. This rapid curing period significantly increased UCS strength compared to the previously described curing periods (7, 14, and 28 days).

During the large scale testing in the pit, UCS tests were performed on specimens retrieved from the pit to check whether the lime mixture provide an unconfined compressive strength of at least 50 psi, which is the goal in NC DOT field practice. The

samples were cured for 7 days at the same room temperature and conditions as the test pit. The results are presented in Table 20 and show the longer mellowing period (3 days) on coastal plain soil 4 resulted in an increase in unconfined compressive strength, as it allowed for greater cation exchanges and flocculation and agglomeration.

Table 19. UCS Test Results For Lime Treated Subgrade Soils

	UCS (psi)					
	3% Lime			5% Lime		
Curing Days	1	2	Mean	1	2	Mean
7	100.4	94.0	97.2	98.8	105.0	101.9
14	107.0	117.4	112.2	124.5	122.1	123.3
28	124.3	131.7	128.0	179.4	178.4	178.9
NCDOT Rapid Curing (2 days)	197.5	216.2	206.9			

Table 20. UCS Test Result For Test Pit Lime Treated Subgrade Soil

		UCS (psi)			Su (psi)
Soil	Mellowing Time	1	2	Mean	
Coastal Plain Soil 4	1 day	53.1	54.4	53.8	26.9
	3 days	112.1	110.4	111.3	55.6
Coastal Plain Soil 5	3 days	51.8	52.9	52.4	26.2

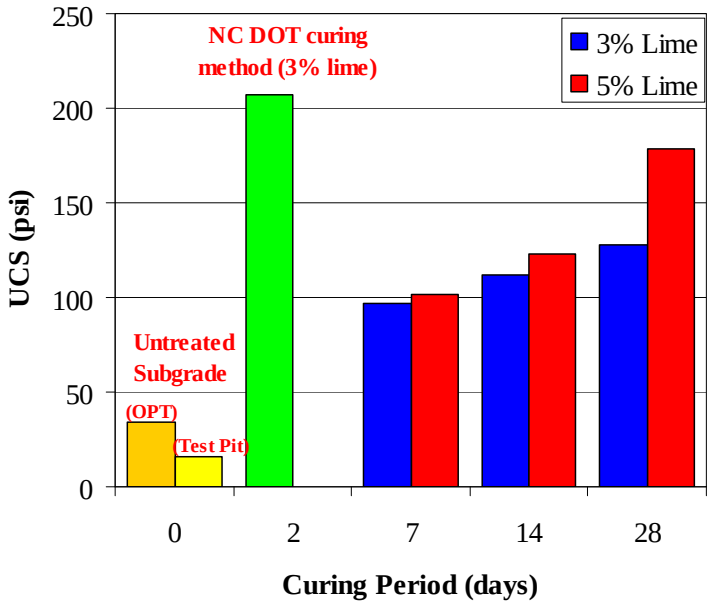

Figure 20. Lime effect on UCS with change in lime dosage and curing period

Resilient modulus testing

The resilient modulus (Mr) tests were performed on lime treated coastal plain soil 4 (mixed coastal plain soil). Lime treated samples were prepared at the same lime dosages (3% and 5%) and curing periods (7, 14, and 28 days) as the UCS tests. The test results are presented in Figure 21 and Figure 22, respectively. For tests with 3% lime, the sample with a 7 day curing period shows the lowest resilient modulus value (Mr). There is not much difference in the values between 14 days and 28 days curing times. In the case of 5% lime treated samples, the Mr value increases with an increase in curing period. The sample cured for 28 days shows a remarkable increase in Mr values. This trend is similar to that of UCS tests performed under same lime content and curing period.

The Mr values (3% lime and 7 days curing) are compared with those of untreated mixed coastal plain soil and select fill as shown in Figure 23. The Mr values of lime treated sample are notably higher than those of the two soils. These results are qualitatively matched with large scale test results in chapter 5.

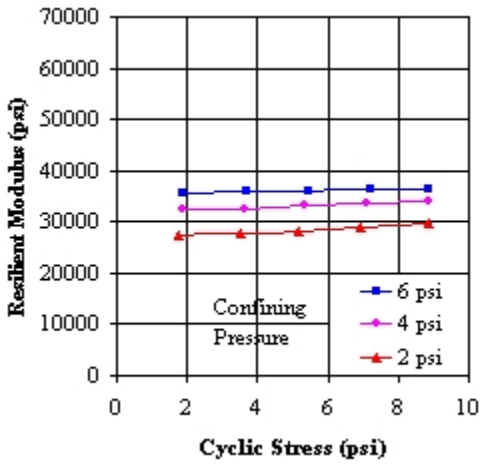

(a) 3% lime and 7 days curing

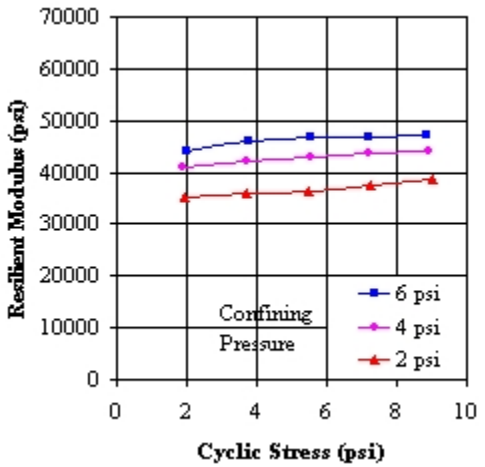

(b) 3% lime and 14 days curing

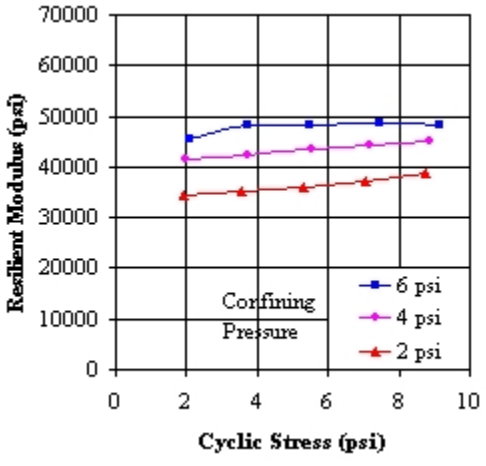

(c) 3% lime and 28 days curing

Figure 21. MR values for 3% lime treated subgrade

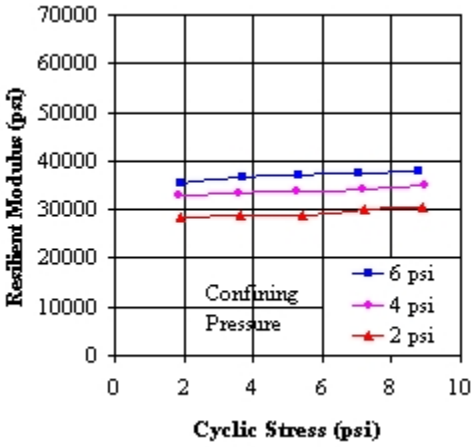

(a) 5% lime and 7 days curing

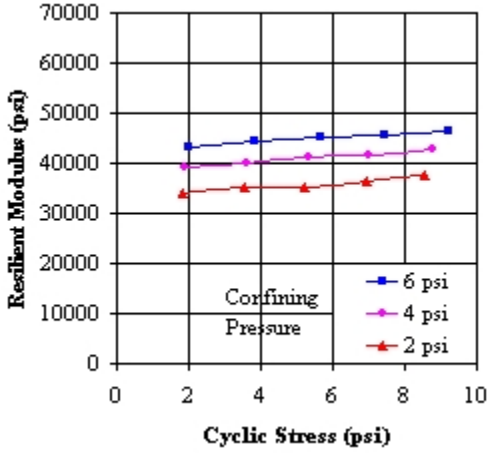

(b) 5% lime and 14 days curing

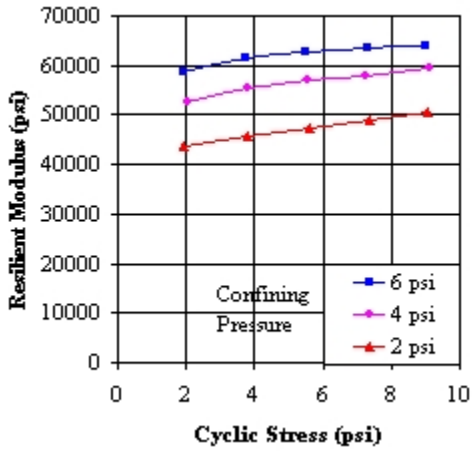

(c) 5% lime and 28 days curing

Figure 22. MR values for 5% lime treated subgrade

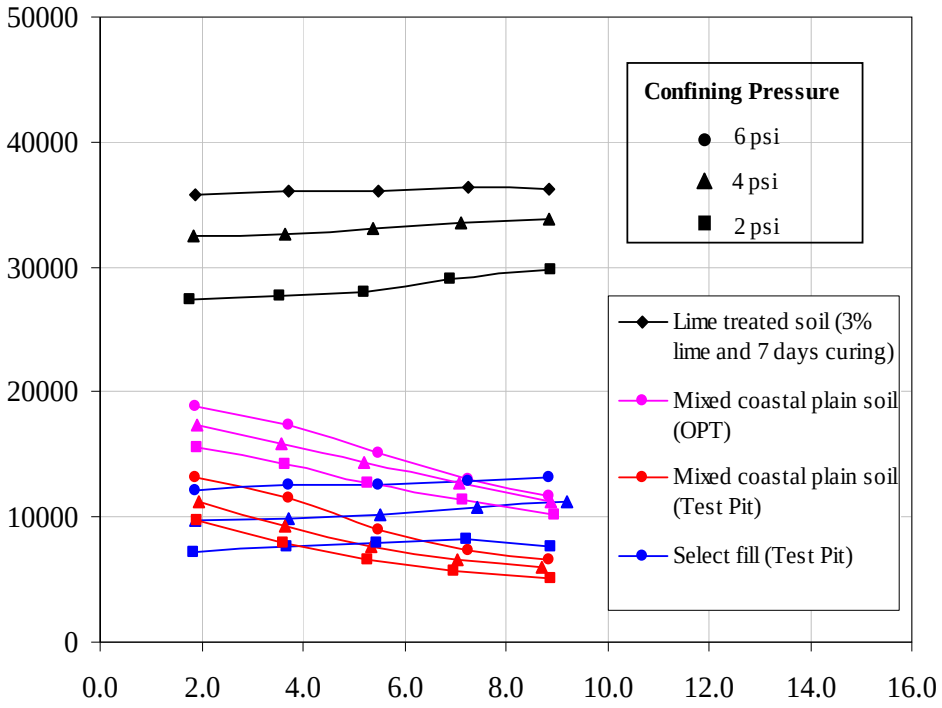

Figure 23. Comparison of Mr values for three different soil conditions

Summary

Characterization tests were performed on four different types of soils used in large scale testing to investigate their physical and engineering properties. These tests include grain size analysis, specific gravity, Atterberg limits, standard proctor compaction, unconfined compressive strength, consolidated undrained triaxial strength, and resilient modulus as appropriate to each soil type. Summary tables for coastal plain soil 4, ABC, select fill, and lime stabilized soil are presented in

Table 21 to Table 25. These test results will guide the selection of input parameters for numerical analysis in chapters 9 through 11 and the parameters needed for preparing for large scale tests described in chapters 5 and 6.

The test results show the low plasticity clay obtained from the coastal plain would typically be undercut in high moisture situations. For coastal plain soil 4, it is classified as A-6 (6) according to the AASHTO system and approximately 56% passes the No. 200 sieve. The value of plasticity index (PI) is 16 and the maximum dry unit weight is 113.2 pcf at an optimum moisture content of 15.3%. A CBR of 2% was measured at water content of approximately 19%. The unconfined compressive strength (UCS) is 16 psi at a CBR 2% condition. The obtained resilient modulus value is 4929 psi at test pit condition assuming that the soil undergoes 2 psi confining pressure and 5.4 psi deviatoric stress.

Table 21. Soil Index Properties

Soil Sample	LL	PL	PI	G_s	Maximum dry unit weight, γ_{dmax} (pcf)	Optimum moisture content (%)	Classification	
							USCS	AASHTO
Coastal plain soil 4	33	17	16	2.70	113.2	15.6	CL	A-6(6)
ABC 1	20	-	NP	-	137.4	6.4	GW-GM	A-1-a
Select fill	-	-	NP	2.64	-	-	SP	A-1-b

*NP – Non-plastic

Table 22. Corrected Unsoaked CBR Values at Test Pit Condition

Soil	Moisture Content (%)	Dry unit weight (pcf)	Corrected Unsoaked CBR
Coastal plain soil 4	18.8	106.8	2.1
Select fill	2.1	104	16.5

Table 23. Mohr-Coulomb strength Parameters from CU Tests at Test Pit Condition

Soil	Effective Stress		Total Stress	
	c' (psi)	phi' (deg)	c (psi)	phi (deg)
Coastal plain soil 4 (06/2008)	0	34.5	5.7	19
Coastal plain soil 4 (06/2009)	0	37	3.6	15
Select fill	0	33.5	15.0	25.0

Table 24. UCS Test Results on Coastal Plain Soil 4

	Sample condition	UCS (psi)
Untreated	At test pit	16.1
	At optimum	34.5
	Curing Period (day)	UCS (psi)
3% Lime treated	7	97.2
	14	112.2
	28	128.0
5% Lime treated	7	101.9
	14	123.3
	28	178.9

Table 25. Resilient Modulus Test Results

		Coastal plain soil 4						Select fill	
		Untreated				Lime treated			
		OPT		Test Pit		3% Lime & 7 days curing		Test Pit (w = 2.1 %)	
Sequence	Confining Pressure psi	Cyclic Stress, psi	Resilient Modulus, psi	Cyclic Stress, psi	Resilient Modulus, psi	Cyclic Stress, psi	Resilient Modulus, psi	Cyclic Stress, psi	Resilient Modulus, psi
1	6	1.9	18870	2.0	11790	1.9	35724	1.9	12163
2	6	3.6	17381	3.7	9983	3.7	36068	3.8	12525
3	6	5.3	15171	5.3	7505	5.5	36145	5.6	12623
4	6	7.1	13073	7.1	5928	7.2	36404	7.4	12824
5	6	8.9	11662	8.9	5274	8.9	36299	9.3	13137
6	4	1.9	17318	1.9	9708	1.9	32519	1.9	9729
7	4	3.6	15815	3.7	7601	3.6	32619	3.7	9939
8	4	5.2	14356	5.4	5959	5.4	33064	5.5	10235
9	4	7.1	12687	7.2	5096	7.1	33472	7.4	10752
10	4	8.9	11224	8.9	4667	8.9	33879	9.2	11200
11	2	1.9	15612	1.9	8306	1.8	27397	1.8	7205
12	2	3.7	14151	3.6	6265	3.5	27637	3.7	7623
13	2	5.3	12788	5.3	4929	5.2	28056	5.4	7972
14	2	7.1	11343	7.2	4275	6.9	29108	7.2	8209
15	2	9.0	10202	9.0	4053	8.9	29717	8.9	7651

CHAPTER 4: PROTOTYPE EXPERIMENTAL DESIGN VIA FIELD MEASUREMENTS AND NUMERICAL MODELS

A series of field measurements were performed to illustrate the current uses of dynamic cone penetrometer (DCP) data for determining or assisting in the decision to undercut and to verify the loading functions applied to the surface of the prototypes. This chapter summarizes several sets of data to assess the field application of general rules to determine undercut based on DCP index and works toward an alternate explanation for the shape of DCP to CBR correlation curves. Literature recommendations for the duration, shape and magnitude of laboratory loads on plates are also compared for large scale prototype test development. Numerical studies were also performed to determine the proper dimensions of the large scale prototype tests.

DCP Field Measurements

NCDOT has provided DCP data from failed proof roll sections in Bladen County, North Carolina and allowed this research team access to proof roll activities on a site in High Point, North Carolina and in northern Wake County, North Carolina. These data are interpreted first in light of the recommendations of Wainaina (2006), who noted that a common metric for considering undercut options is a DCPI of 1.5 inches/ blow (38 mm/blow). The data are also analyzed using wave equation analyses that are typically used to model the pile driving process.

Bladen County

A site in Bladen county was described in an e-mail by Kreider, 2009. An onsite inspector noted that the subgrade "…met compaction, failed quality, and was moving/pumping but did not appear to be overly wet." The comment noting 'failed quality' referred to plasticity indices in excess of 30, which NCDOT defines as unsuitable for borrow applications. Upon observed pumping failure of the proofroll testing (from station 19+00 to 29+00), additional DCP testing was performed as shown in Figure 24.

Figure 24 includes linear regression to determine the overall slope of the collected data, which is the average DCPI over the collected depth. At station 18+50, where failure of the proof roll was not observed, the DCPI was 11 mm/blow. At station 22+50, the average slope is approximately 32 mm/blow. Wainaina (2006)'s undercut consideration based on DCPI of 1.5 inches/ blow (38 mm/blow) is also shown in Figure 24.

Most of the DCP results in Figure 24 have at least a portion of the curve that has a slope of approximately 33 to 39 mm/blow, as illustrated in Figure 25. The majority of high DCPI regions occur in the top 500 mm, but station 21+50 shows a significant deeper soft section with a DCPI of 39 mm/blow, and station 26+00 shows maximum DCPI in the range of 36 mm/blow. Thus, while not exact, the observed values of around 38 mm/blow leading to proof roll failure is supported by these field measurements.

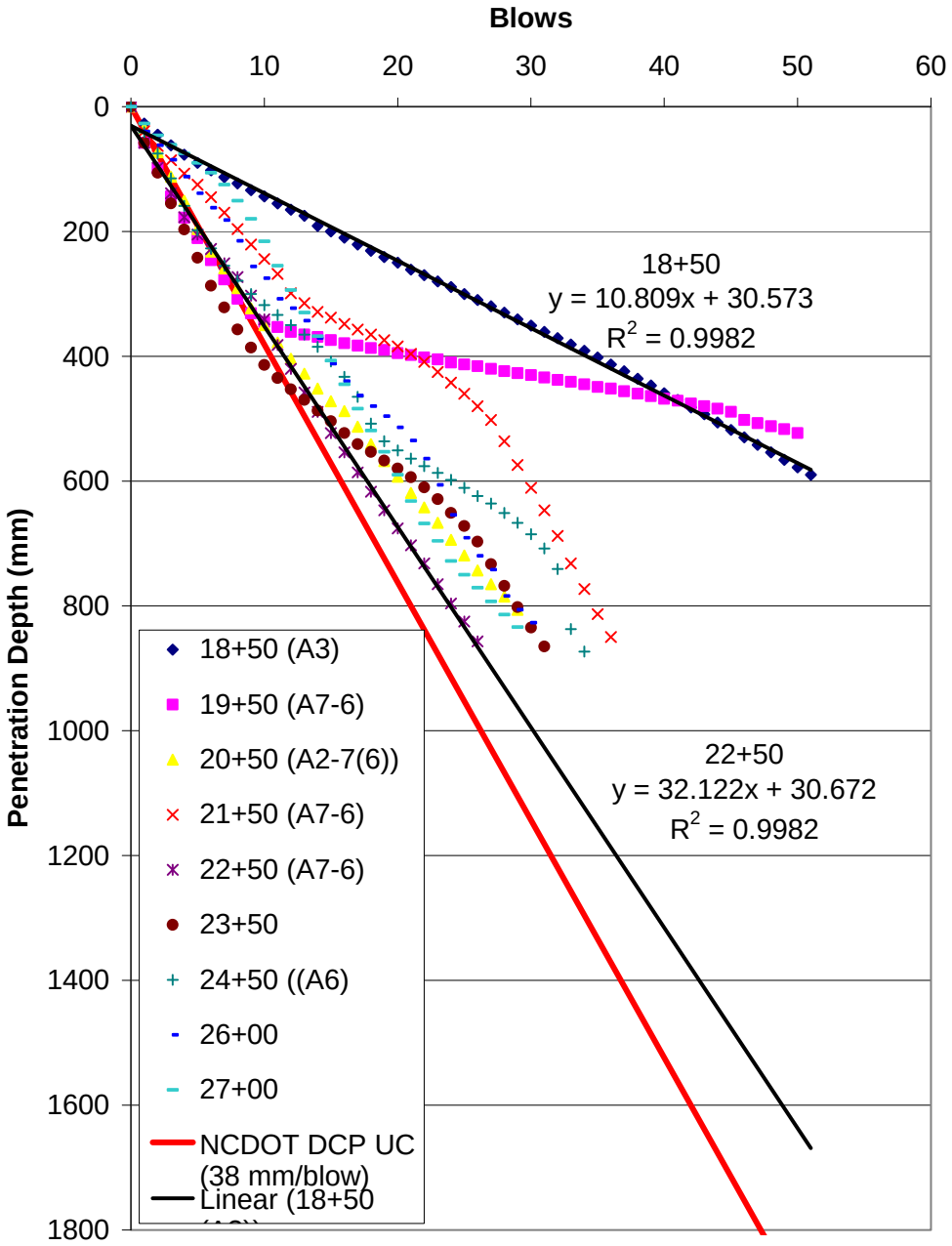

Figure 24. Bladen County DCP results, proof roll fail from station 19+00 to 28+00(Kreider, 2009)

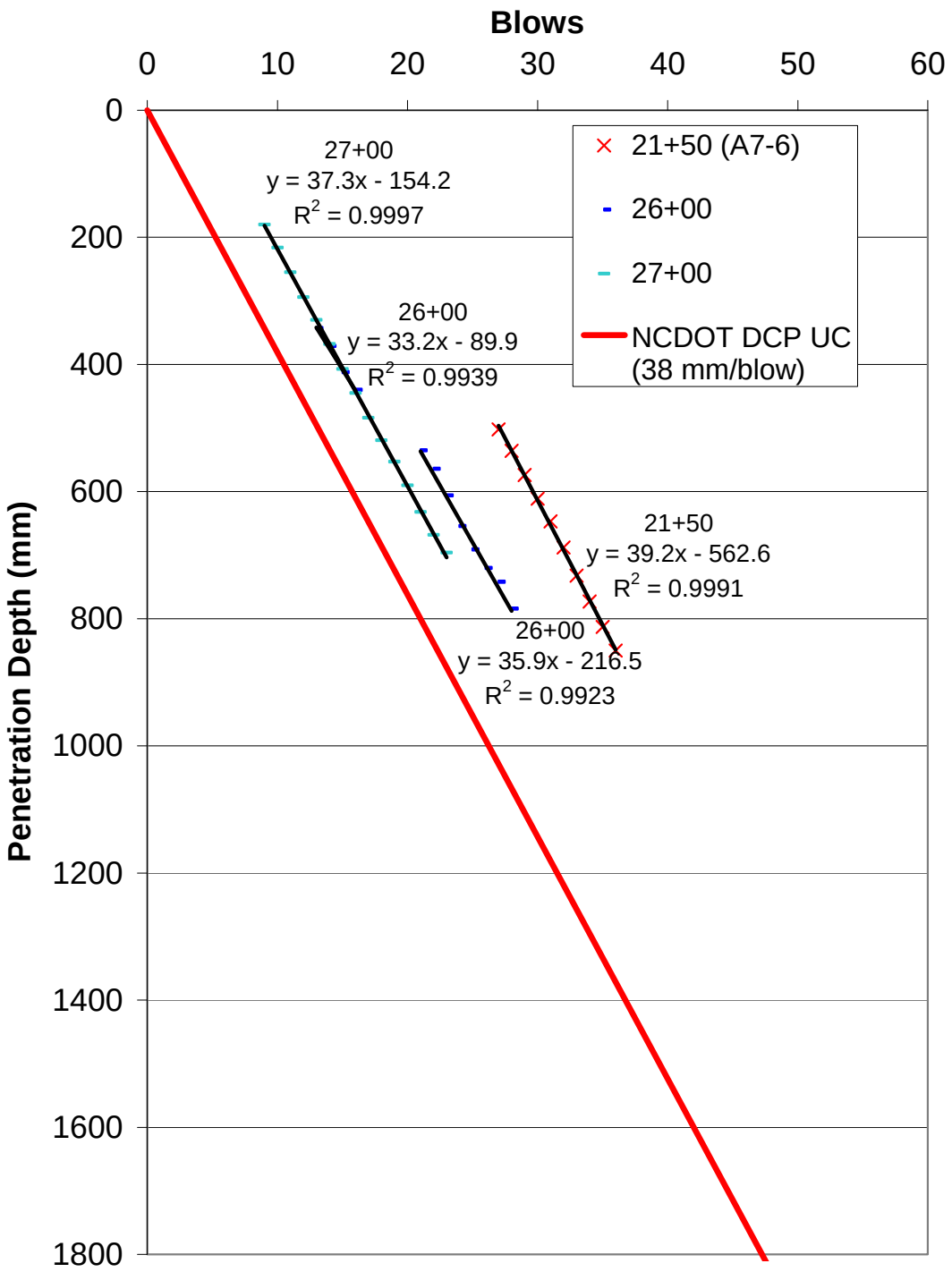

Figure 25. Excerpted data and incremental DCPI from selected data sets shown in Figure 24.

High Point, NC

DCP data were obtained in the northbound lane of US 311 by the project team. Two areas were selected with the assistance of the resident engineer at the site. One area was identified as likely to fail the proof roll, while a second area was not. The area between Stations 67+80 and 68+20 were denoted as the "soft" subgrade location, while the area between Stations 67+40 and 67+80 were denoted as the "stiff" subgrade area. During proof rolling, pumping and excessive rutting were observed at the soft location, indicating a failed proof roll.

To quantify the stiffness of the subgrade, dynamic cone penetrometer measurements were taken at both locations. The results are presented in Table 26, along with a correlation recommended in the NCDOT Pavement Condition Survey Manual (NCDOT, 1998). It is also worth noting that the DCPI at Station 67+80, which failed the proof roll, was 40.6 mm/blow, which is again in line with the recommendation by Wainaina, 2006 that DCPI in excess of 38 mm/blow generally means undercut may be considered.

Table 26. DCP Measurements and CBR Correlations

US 311 Northbound Station 67+40	DCP Index (mm/blow)	Estimated CBR (NCDOT 1998)
"Stiff" Subgrade Location		
Top 5.875 inches	13.6	24
5.875 to 11.4 inches	7.4	46
Station 67+80		
"Soft" Location		
Top 14.375 inches	40.6	8
14.375 to 21.3125 inches	14.7	22

Wake County, NC

On May 22, 2009, proof roll tests were performed on a short portion of the NC 98 Bypass. Seventeen locations were selected for DCP tests in the east and west bound lanes. DCP tests followed the proof roller, and were performed at both sites where the proof roll identified failure. The DCP tests were performed in the ruts of the proof roller, which likely caused slightly lower DCPI values than had the test been performed at a failure location prior to proof rolling. However, as locations of failure or wheel track were not predicted prior to proof rolling, post-proof roll DCP testing was seen as an acceptable compromise.

Of the 17 tests, seven were in locations passing proof roll (Figure 26), while ten were in locations identified as pumping or excessively rutted (Figure 27). In general, the DCPI values at locations that passed proof roll were less than 38 mm/blow, while failed proof roll DCPI were higher than 38 mm/blow. The exceptions are test 1 which was identified as a failed proof roll test in pumping and had a DCPI of 27 mm/blow. The failure may

have been due to deeper soft material, or it may have also been a marginal case. Similarly the proof roll at tests 10 and 18 passed, but had DCPI values on the order of 38 mm/blow. While there was some sign of pumping identified by project team for test 18, test 10 apparently showed no such signs.

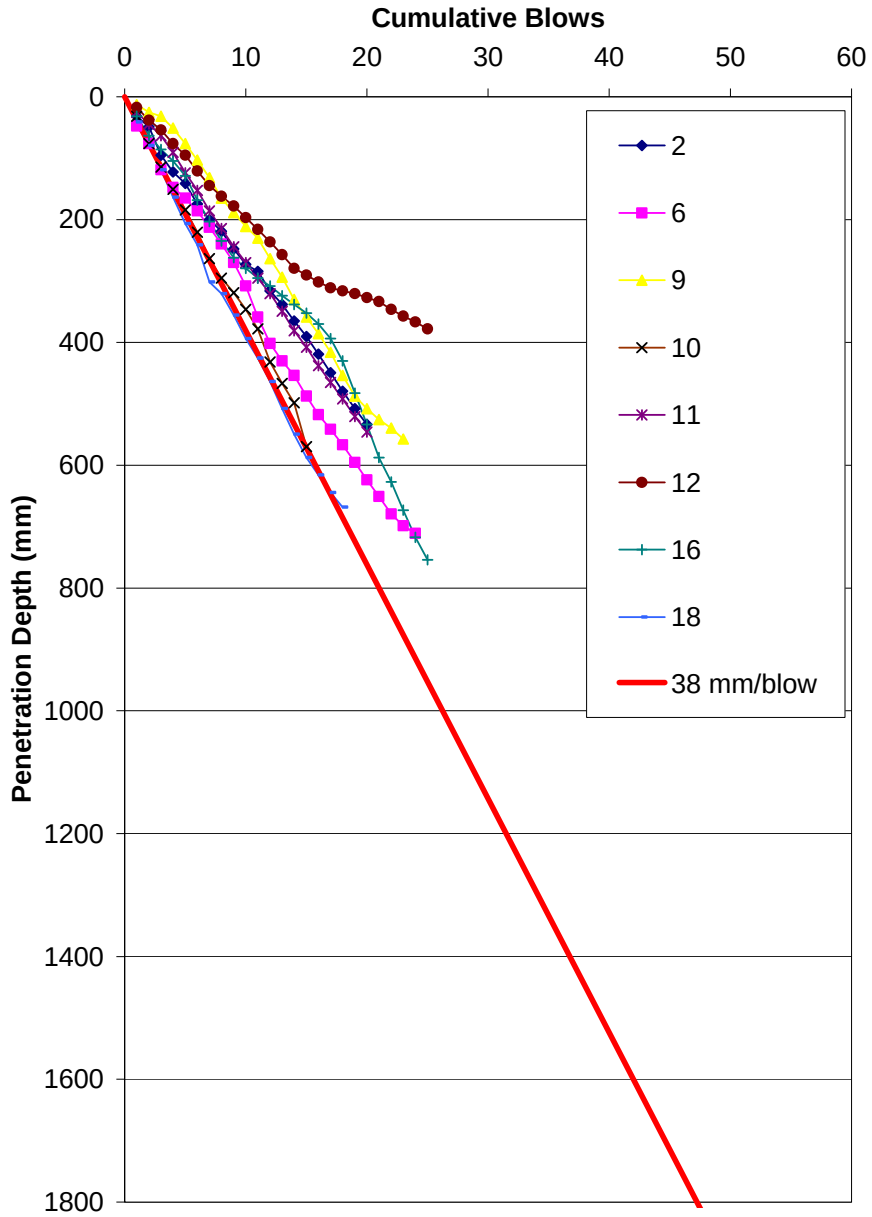

Figure 26. DCPI plot for passed proof roll locations, NC 98 Bypass

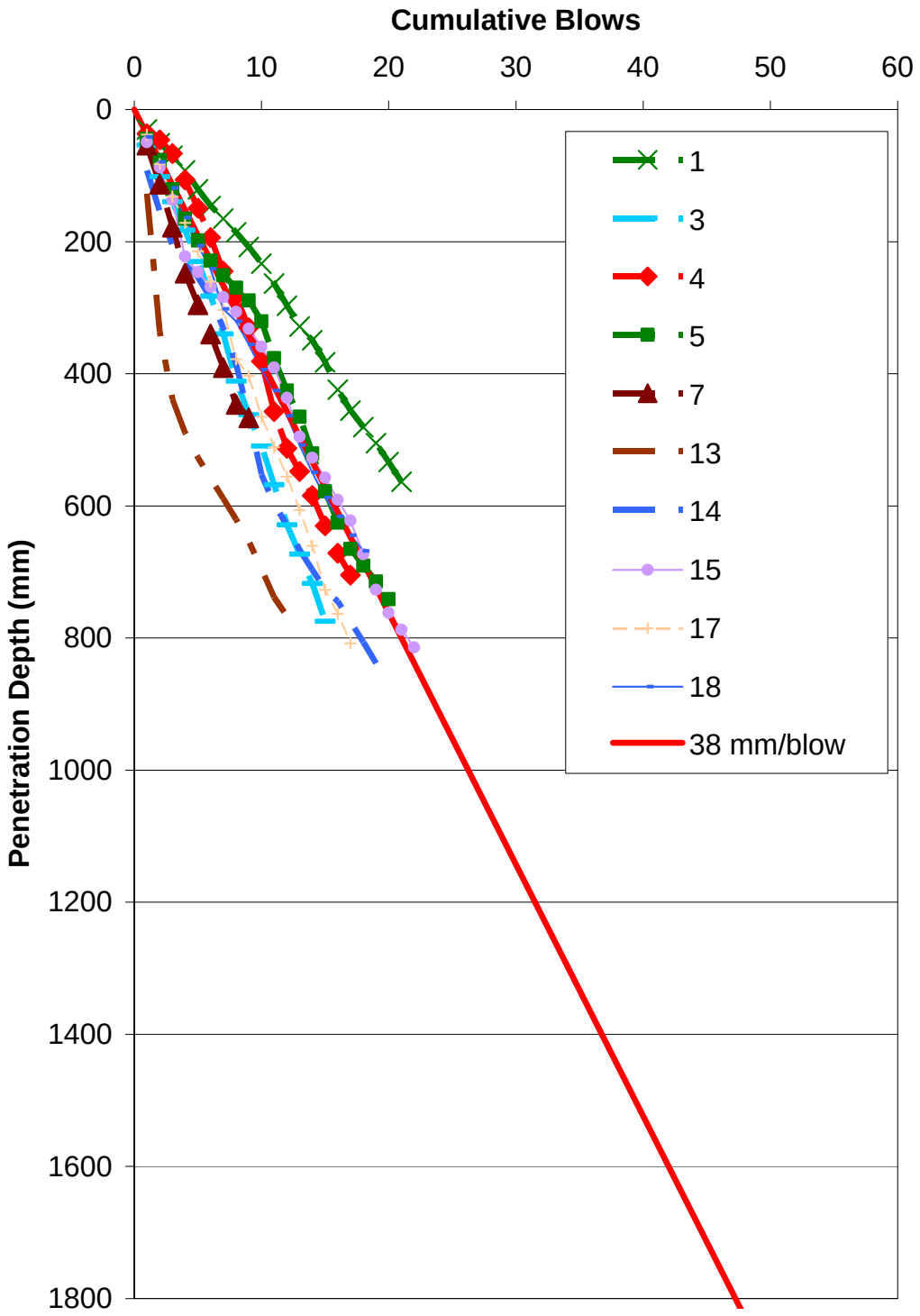

Figure 27. DCPI plot for failed proofroll locations, NC 98 Bypass.

Wave Equation Analysis of the DCP

As discussed in Chapter 2, DCPI is often correlated using statistical regression to a number of subgrade properties, including dry density, water content, resilient modulus, and, most commonly, CBR. With the move toward mechanistic-empirical design in pavements, resilient modulus will be getting more attention in the coming years, while CBR still has the benefit of decades of engineering experience to those currently in practice.

The DCPI to CBR statistical correlations by Coonse (1999), NCDOT (1998) and others should be considered alongside NCDOT's 38 mm/blow DCPI undercut criteria. Several researchers have suggested that the measurements produced by the DCP could be improved through application of the one dimensional wave equation [Minasny, B. and McBratney, A.B. (2005), and Roy (2005)]. As proposed by Smith (1960), the wave equation uses a lumped mass model to discretize the driven elastic rod into a series of masses connected by springs and dashpots. The ram is modeled as a separate mass, while the surrounding soil is modeled as static springs and viscous dampers distributed along the side and at the base of the pile. One commonly used commercial software package for wave equation analysis of pile driving, GRLWEAP (Pile Dynamics, 2005) will be used for this study, which requires: (1) a hammer model, (2) a pile model and (3) soil parameters.

Hammer Model

The hammer model requires a ram weight and geometry, hammer efficiency, and drop height. For this analysis, the 80 N (18 lb) ram is divided up into three segments of 9, 35.5 and 35.5 N (2, 8 and 8 lbs) to account for the change in ram diameter (and therefore stiffness). The rated stroke, or drop height, is 0.57 m (1.875 feet).

The hammer efficiency was an unknown, but subsequent tests measured the DCP ram velocity using a radar based Hammer Performance Analyzer (HPA). This system emits a focused radar signal, which yields a measurement of velocity upon reflection off a moving ram as long as the ram is falling faster than two miles per hour. Given the drop height, gravity and the measured ram velocity from the HPA, the efficiency can be measured over a series of blows.

In all, sixty DCP blows were measured when the ram was dropped on a stiff surface, yielding ram velocities ranging between 3 to 3.34 m/s (9.79 and 10.98 ft/s). The hammer efficiency is defined as:

$$e = \frac{0.5v^2}{gh} \qquad \textbf{(25)}$$

where e is the efficiency, v is the ram velocity, g is the acceleration due to gravity and h is the ram drop height (0.57 m or 1.85 ft). The efficiencies calculated from the

measurements are compiled in a histogram as Figure 28, and the statistics from the test program are summarized in Table 27. Based on the measurements, the efficiency was input in GRLWEAP as the measured average of 92%.

Table 27. Summary of DCP Efficiency Measurement Results

Drops Measured	60
Average Efficiency	92.4%
Standard Deviation	4.7%
Skew	-0.82

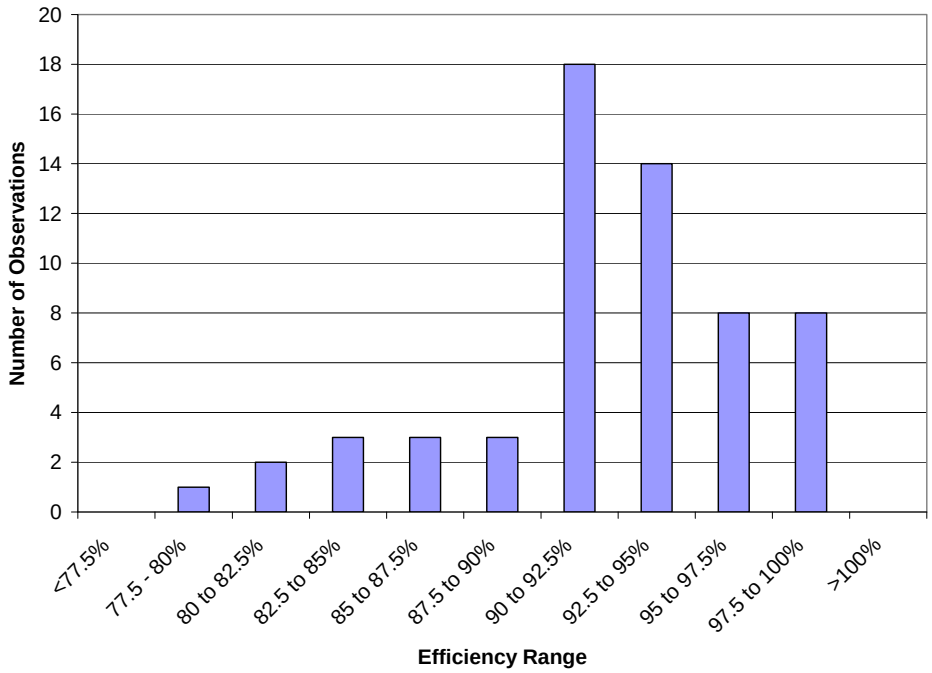

Figure 28. Measured efficiency distribution

.

Pile Model

The 'pile' model is the anvil-rod system. For the DCP used in this study, this corresponds to a 50.8 mm (2 inch) long anvil atop a 1.2 m (47.625 inch) long rod. This steel rod is 16 mm (5/8 inch) in diameter, and discretized into 50, 25.4 mm (1 inch) long sections. The rod material is steel, which has an elastic modulus of 200 GPa (30,000 ksi) and a unit weight of 77.3 kN/m^3 (492 lbs/ft^3).

Soil Model

The soil model consists of a total soil resistance that can be distributed as ultimate static shaft resistance, R_{shaft} and toe resistance, R_{toe}. For the purposes of the DCP, it is assumed that (1) the penetration of the rod into the ground is shallow and (2) for the fine grained materials used to check this model, the oversized DCP tip (4 mm or 0.16 inches larger in

diameter) will create an oversize hole that will also minimize any soil resistance along the side of the rod. Thus, the shaft quake (the displacement at which the linear elastic – plastic resistance model reaches the ultimate resistance) and the shaft damping constant (an empirical value correlated loosely to soil type) will not have an effect on the overall model, since nearly all of the resistance is concentrated at the DCP tip.

The soil model thus leaves only (1) the ultimate resistance at the toe ($R_{toe,\ ult}$), (2) the toe quake (q_t) and (3) the toe damping ($J_{s,toe}$). We also will assume the toe damping will be held constant, at 0.5 s/m (0.15 s/ft), as recommended by Pile Dynamics (2006). It can then be said that the stiffness of the static toe resistance model is ultimate toe capacity, $R_{toe,\ ult}$, divided by the toe quake.

Shear strength estimation using wave equation

First, the quake values were assumed to be that of a soft soil (the DCP diameter divided by 25, 60, and 120) and the ultimate toe resistance was varied. For a cohesive soil where undrained behavior dictates over a very short, dynamic loading time, the ultimate toe capacity was assumed to be 6.5 to 9 times the undrained shear strength, s_u, of 100 to 250 kPa, respectively, per O'Neill and Reese (1999). A common rule of thumb from Black (1961) suggests the undrained shear strength of a soil in kPa is 30 times its CBR value, although other researchers have suggested this is applicable only to relatively low CBR (1-2%, see Cuelho and Perkins, 2009). Cross and Gregory (2007) proposed correlations for undrained shear strength in kPa of approximately 11 times its CBR value, at CBRs of 3.5 to 16%. These differences can be interpreted in light of the data shown in Figure 13, where that curve can be idealized as a series of linear curves depending on the magnitude of CBR.

Upon plotting the results from chapter 3 against the literature values, more references comparing undrained shear strength from UCS and vane shear tests to CBR results were compiled from the literature. Regression of the coastal plain 4 data was used to determine a best fit trendline, as was all data compiled. The results are shown in Figure 29.

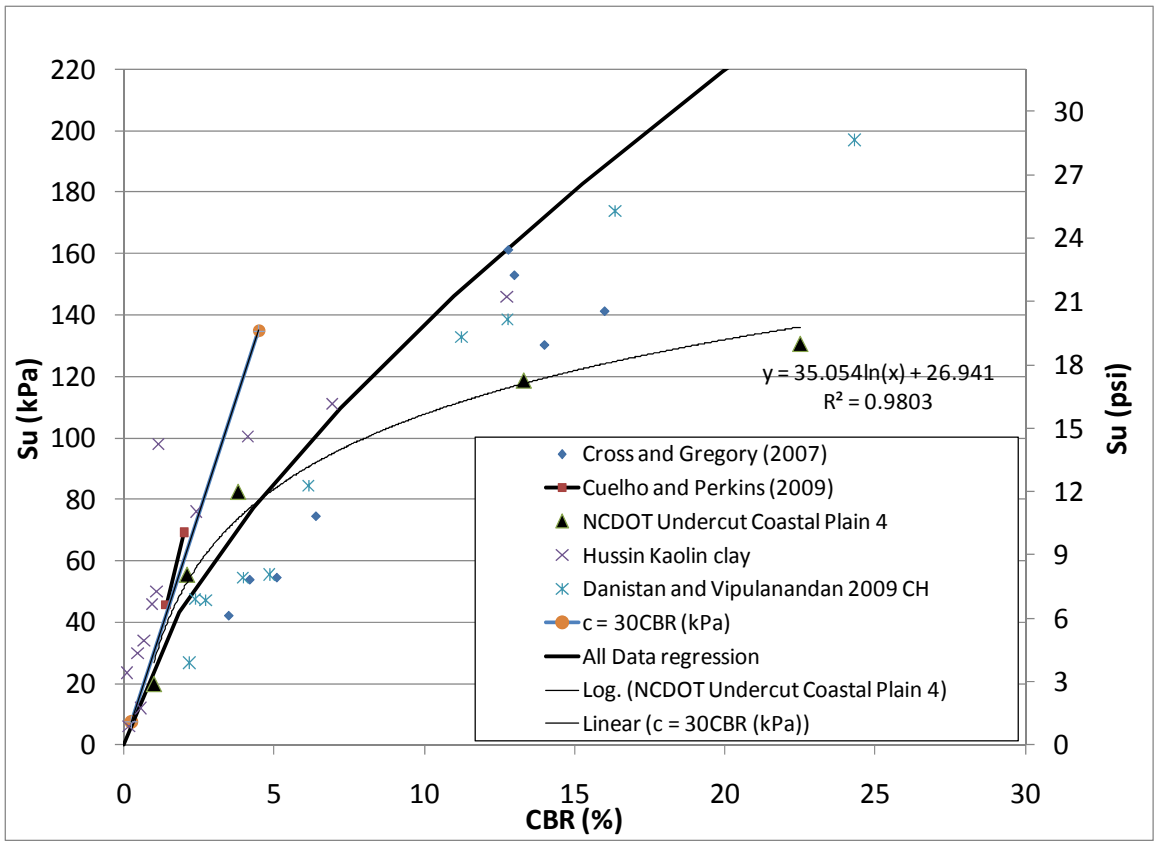

Figure 29. Correlation between CBR and s_u, from multiple sources

The results of this wave equation analysis are shown in Figure 30. Figure 30 shows (1) the lack of dependence on the assumed toe quake, (2) the similarity of the overall shape of all curves, and (3) the similarities between the shape of the correlations of the USACE and Coonse (1999) to the wave equation results when a high toe damping value is used.

The overall shape of the curve has been duplicated using two essentially independent methods—statistical correlation and a physics-based approach. Thus, the DCP appears to be a rational and convenient tool for determining the shear strength or stiffness parameters of the subgrade *in situ*. Further studies are on-going to better calibrate the DCPI and shear strength results to CBR.

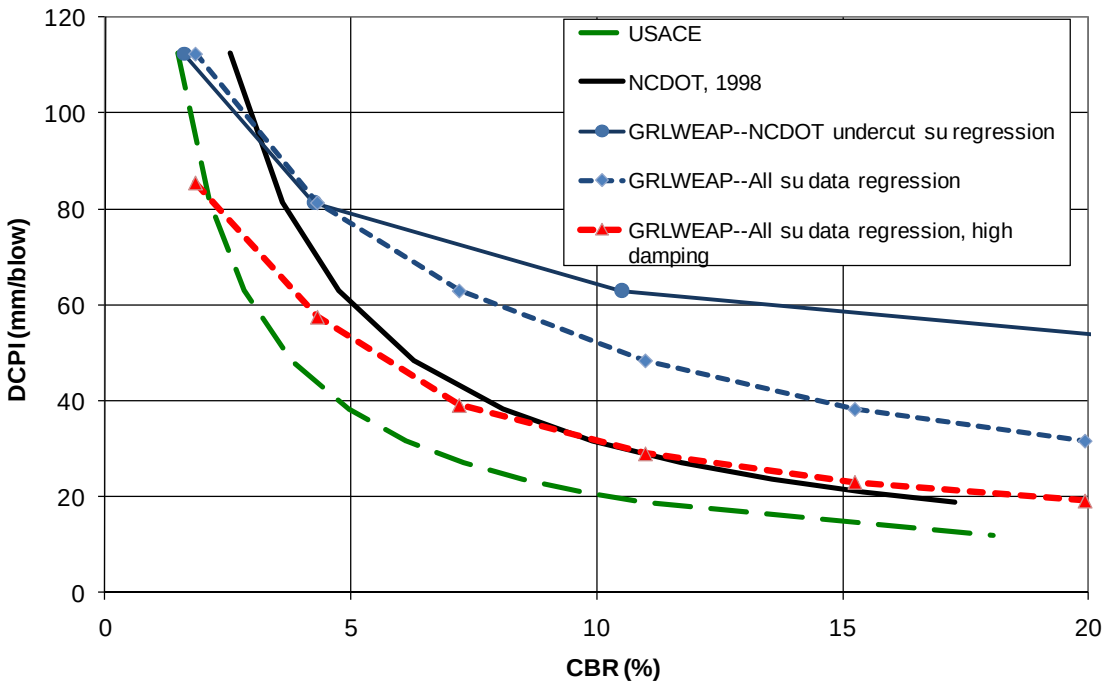

Figure 30. DCPI vs. undrained shear strength from GRLWEAP analysis

Resilient modulus using the wave equation

For mechanistic-empirical design, resilient modulus will become more of a focus. This sub-section will look at the ability of the wave equation approach to determine elastic modulus instead of shear strength. Randolph and Deeks (1992) suggested that the static portion of the base resistance can be determined from the Boussinesq solution of a rigid area on the surface of a half space. For a DCP at the surface or very shallow penetration, this would appear to also be appropriate, given the proximity to the surface and the much higher elastic modulus of steel compared to the soil. The base force is given as:

$$R_{toe,ult} = \frac{2Gdq_t}{(1-\nu)} = \frac{2dq_t}{(1-\nu)} \cdot \frac{E}{2(1+\nu)} = \frac{Edq_t}{(1-\nu^2)} \qquad \textbf{(26)}$$

where G is the shear modulus, E is the Young's Modulus, d is the diameter of the loaded rigid area and ν is Poisson's ratio. Solving for the elastic and shear modulus, with K the stiffness R_{toe}/q_t:

$$E = \frac{R_{toe,ult}(1-\nu^2)}{dq_t} = \frac{K(1-\nu^2)}{d} \qquad \text{or} \qquad G = \frac{R_{toe,ult}(1-\nu)}{2dq_t} = \frac{K(1-\nu)}{2d} \qquad \textbf{(27)}$$

Figure 31 shows the variation in moduli with stiffness for elastic moduli between 0 and 200 MPa, a range of resilient modulus that will be used for a literature comparison later. For elastic moduli less than 100 MPa, Poisson's ratio yields only a small change in required stiffness, even over the range of 0.3 to 0.5

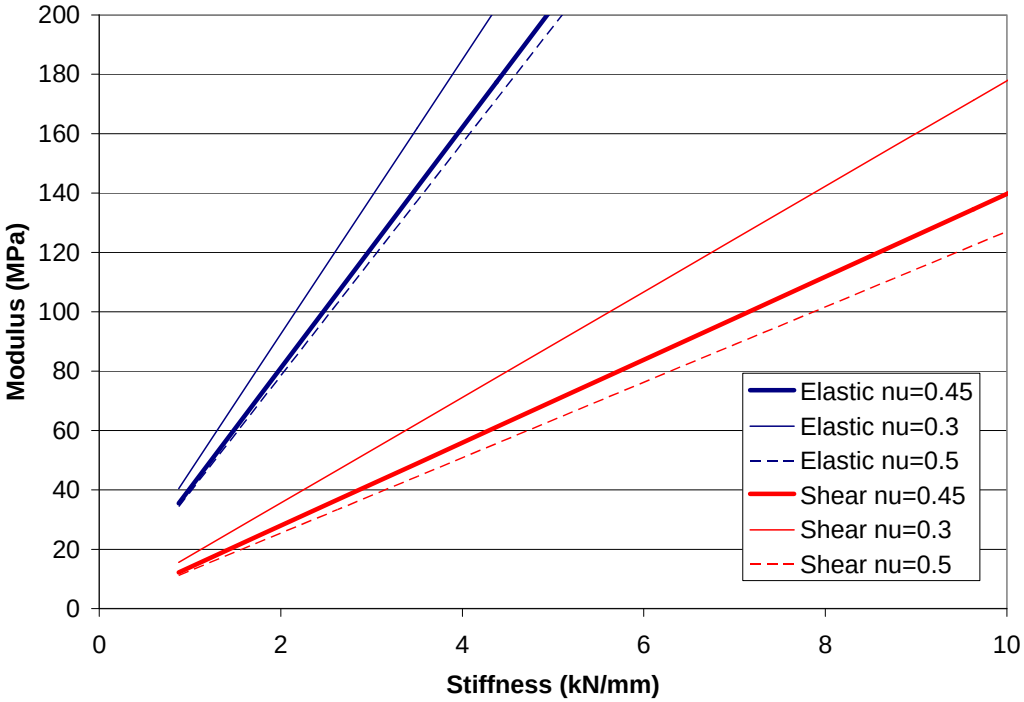

Figure 31. Detail from moduli of 0 to 200 MPa.

Mohammad *et al.* (2007) conducted field and laboratory studies at 31 sites in Louisiana containing soils with AASHTO classifications ranging from A-4 to A-7-6. These authors performed DCP tests at each paved field site (with an additional few performed on compacted samples in a large box), and collected samples for moisture content, gradation, Atterberg limit and standard Proctor tests. Resilient modulus testing was also performed, and correlation of this property was conducted at a 37 kPa cyclic stress (5.4 psi) and a confining stress of 14 kPa (2 psi). This value was selected as a "field representative stress condition at the subgrade layer" under traffic loading, which has been suggested by other researchers.

Mohammad *et al.*(2007) then performed regression analysis of each measured quantity (laboratory tests and DCPI) as a function of the resilient modulus and verified their model using the data of George and Uddin (2000). The data from George and Uddin (2000) appear to be similar to or the same as the DCPI to resilient modulus correlations described in Rahim and George (2002). Mohammad *et al.* (2007) helpfully provided tables of the DCPI and resilient modulus used at each location, which were scanned and exported to Excel for recreation in this study as Figure 32. Note that this plot's scale has been changed to match the previous figures, and that the R-squared value calculated below differs from Mohammad *et al.*(2007)'s because it includes both the model calibration and verification data. The data from George and Uddin (2000) is recreated in Figure 33.

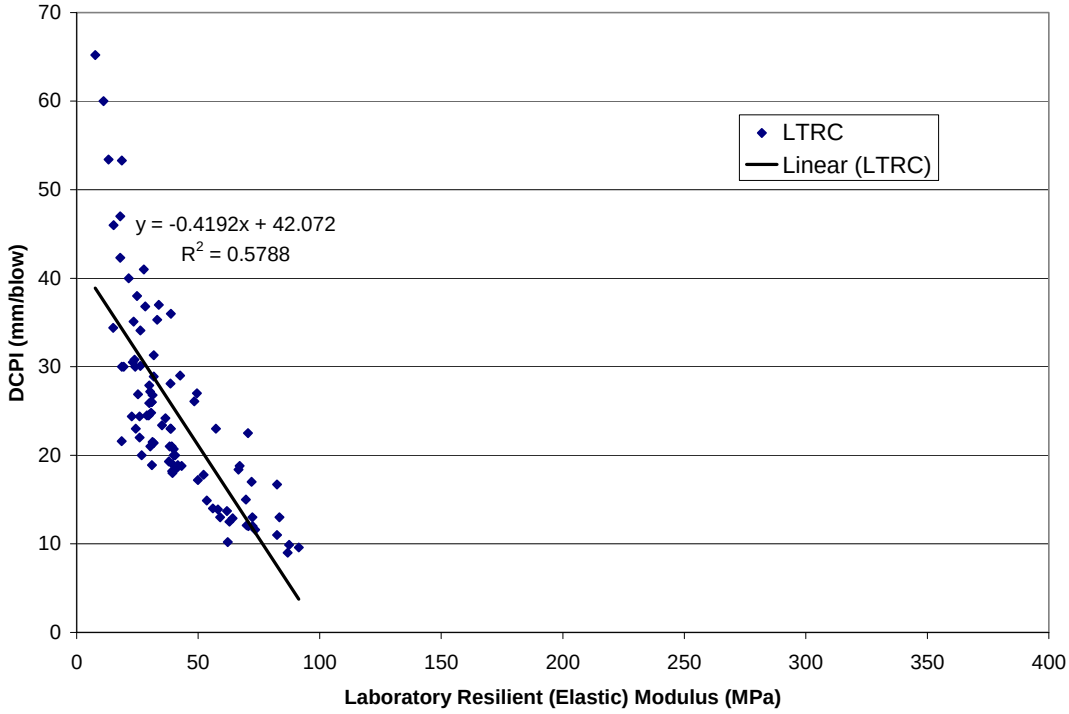

Figure 32. Mohammad et al. (2007) Mr to DCPI correlation.

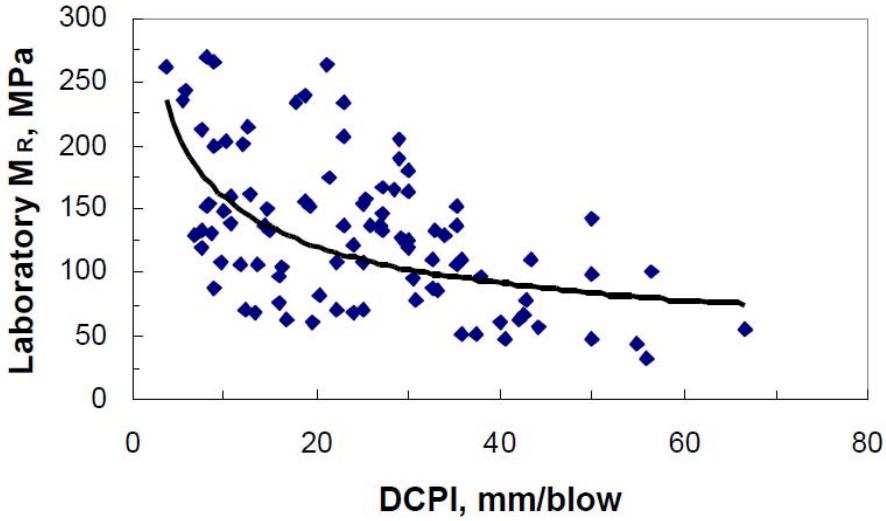

Figure 33. Resilient modulus to DCPI data from George and Uddin (2000)

In Figure 34, the data from the GRLWEAP analyses using the parameters described above are superimposed on Figure 32. A commonly used elastic modulus to undrained shear strength ratio in clays of 200:1 is also included for comparison. The shape of the relationship appears to be captured acceptably, especially when compared with the higher measured moduli results shown in Figure 33 (which also tends to show generally higher

resilient modulus results and greater scatter at DCPI values of between 10 and 30 mm/blow). The magnitude of the elastic modulus predicted by GRLWEAP compared to the measured resilient moduli, however, is initially quite surprising.

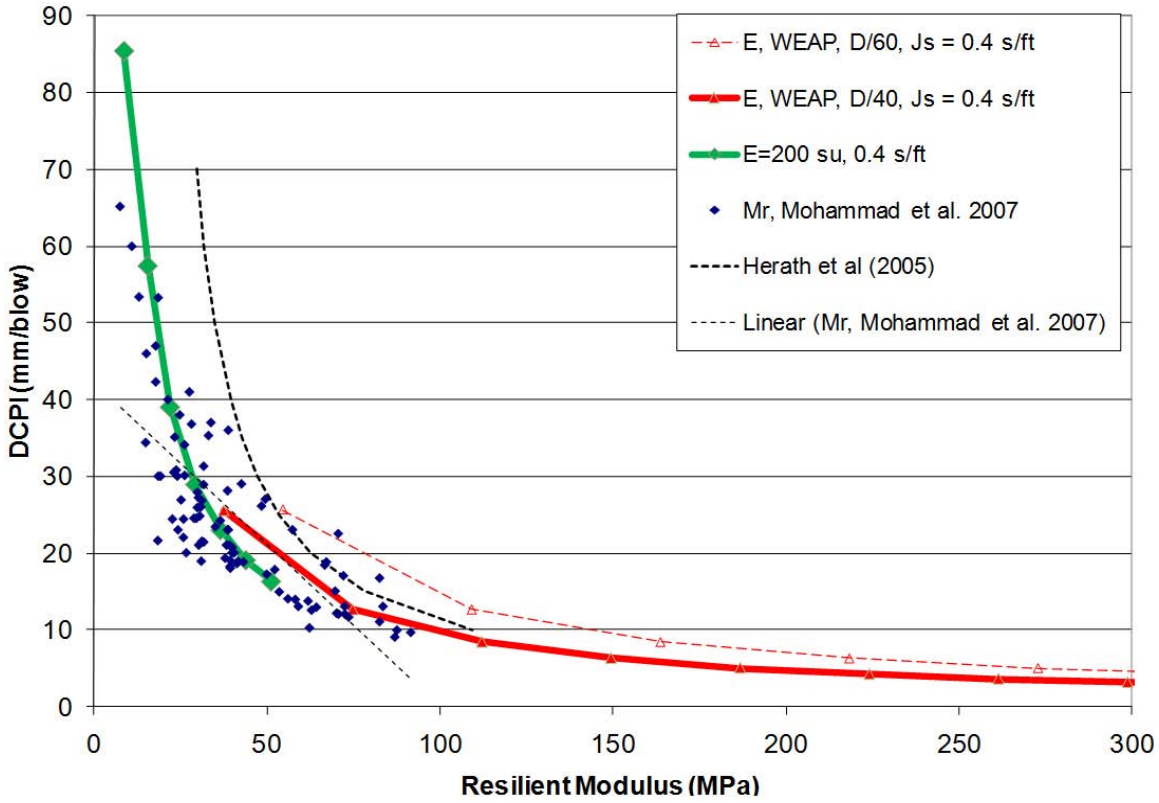

Figure 34. Comparison of measured to GRLWEAP predicted DCPI vs. Mr.

The differences observed in the results using standard recommended toe quake values may be explained by the stress and strain states that exist for each test. First, as shown in clays by Pezo and Hudson (1994), among others, the resilient modulus test occurs at strains of 0.01 to 0.1%, which would tend to predict an elastic modulus of 40 to 90% of the low strain or initial modulus (per a number of sources). The DCP test, however is occurring at strains in excess of 0.1 or 1%, which would imply the modulus should be lower, perhaps as low as 10 to 40% of the low strain modulus. The results Figure 34 would appear to imply quite the opposite—that the DCP moduli predicted by GRLWEAP are higher than those measured and correlated by Mohammad *et al*. (2007).

The state of stress, particularly for the resilient modulus, must also be considered. The resilient moduli above were collected at confining pressures of 2 psi, which is likely acceptable for near surface applications like the DCP. The cyclic stress, however, was 5.4 psi. Under direct traffic loading or proof rolling, this value, at the surface could be as high as 80 psi. Under the tip of the DCP, using the DCP tip velocity predicted by GRLWEAP, the toe damping constant and an ultimate static toe resistance of 0.1 kips and the deviator stress could be as high as 1000 psi. Higher cyclic stresses, however, would also tend to lead to lower resilient moduli, not higher as would be required by Figure 34.

Thus, methods based solely on typical pile driving derived GRLWEAP parameters and the theory of elasticity significantly overpredict the resilient modulus, even if high toe damping values are used. Instead, the differences in strain magnitude were put aside and a best fit approach was taken. In this case, a much lower diameter to toe quake ratio (25:1 instead of 60:1 or 120:1) resulted in a reasonable fit of Mohammad *et al.* (2007)'s data, and the use of correlations of elastic modulus to undrained shear strength tended to fit Herath *et al.* (2005)'s data well. Regardless, the overall shape of the curves is very similar.

Summary

Through field testing, statistical correlations, and wave equation analyses, the dynamic cone penetrometer has been shown to yield relatively consistent results in predicting whether undercut will be necessary. The NCDOT's current DCPI cut-off of 38 mm/blow was generally supported by field observations, and would yield a required CBR of greater than between 5 to 8, depending on the correlation or wave equation result used.

The resilient moduli correlated were performed at confining pressures of 13.8 kPa (2 psi) with a cyclic deviator stress of 37.2 kPa (5.4 psi). At a DCPI of 38 mm/blow, the predicted resilient modulus ranges between 25 and 50 MPa, although scatter in the DCPI and resilient modulus data in the studies surveyed make this difficult to determine exactly.

Prototype Test Design: Load Pulse Magnitude and Duration: Field Measurements

On May 22, 2008, at the request of NCDOT engineers, stress measurements were made on a highway subgrade under construction in High Point, North Carolina. Dynamic earth pressure measurements were collected during proof rolling and passage by a Caterpillar 631 scraper.

Site Description

The subgrade vertical stress increase was measured in the northbound lane of US 311. Two areas were selected with the assistance of the resident engineer at the site. One area was identified as likely to fail the proof roll, while a second area was not The area between Stations 67+80 and 68+20 were denoted as the "soft" subgrade location, while the area between Stations 67+40 and 67+80 were denoted as the "stiff" subgrade area, as was shown in Table 26.

Loading vehicles

A dozer pulled a loaded single axle, four wheeled proof roll trailer conforming to NCDOT specifications (NCDOT, 2002). The proof roll daily report listed the trailer

manufacturer as Blythe-Ferguson, with a gross loaded weight of 48.46 tons. Air pressures of between 68 and 71 psi was measured on all four tires. NCDOT specifications require the proof roller to travel between 2.5 and 3.5 mph.

Figure 35. Proofroll trailer (courtesy M. Valiquette, NCDOT)

A Caterpillar wheel tractor 631 scraper was also used as a subgrade loading vehicle. Current models of this vehicle have a wheelbase of 345.2 inches (28.75 ft) and a maximum published speed of 33 mph. (Caterpillar, 2008). The operator was instructed to drive as fast as practical by the contractor.

Figure 36. Caterpillar 631 scraper (courtesy M. Valiquette, NCDOT)

Instrumentation

In two locations, identified as “soft” (likely to fail proofrolling) and “hard” (likely to pass proofrolling). Two GeoKon model 3500 dynamic earth pressure transducers were buried 6 inches below the ground surface and covered at each location, for a total of four cells. One pressure cell had a nominal maximum measurable pressure of 1000 kPa; three cells had nominal maximum measurable pressures of 400 kPa. The cells were three inches in diameter, and are manufactured with semi-conductor transducers instead of the typical vibrating wire gages. These gages allow the cell to be responsive to dynamic loads.

Excitation voltage for the transducers, as well as signal processing and storage was provided by a Vishay System 7000 data acquisition system. Sample rates of 1000 and 2000 samples per second were used for the proof roll and pan scraper, respectively.

Results

For each vehicle and location, four passes were made over the buried instruments. The system recorded stress with time. Because the distance between the two cells were fixed at six feet, the average speed could be calculated by identifying either the time of initial rise of each loading pulse or the time at the peak. The duration of the pulse was also estimated by noting the time at which the stress was measured above a baseline magnitude.

Proof roll tests

Figure 37 shows a selected stress history for the fourth pass of the proof roll trailer over the soft subgrade. The signal obtained in one pressure cell between 415 and 418 seconds is the passage of the dozer that towed the proof roll trailer. It passed the second pressure cell from 417.5 to 420.5 seconds. The 47 and 55 psi pulses starting at 422 seconds are the results of the proof roll trailer’s wheel passing over the two cells. Figure 38 shows the selected record from the third pass of the proof roll trailer over the stiff subgrade.

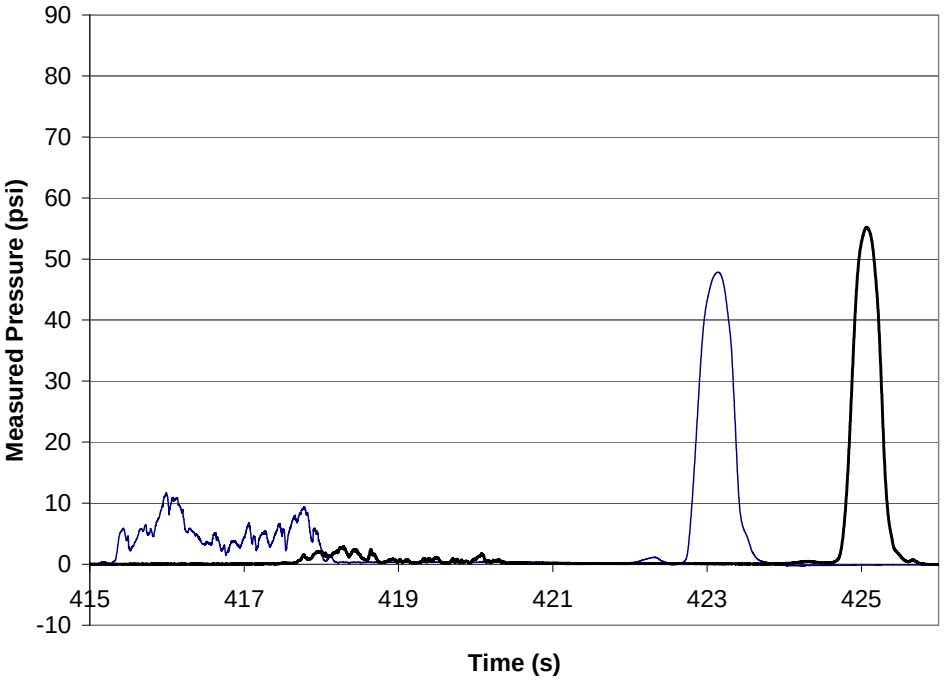

Figure 37. Proof roll trailer over soft subgrade, fourth pass.

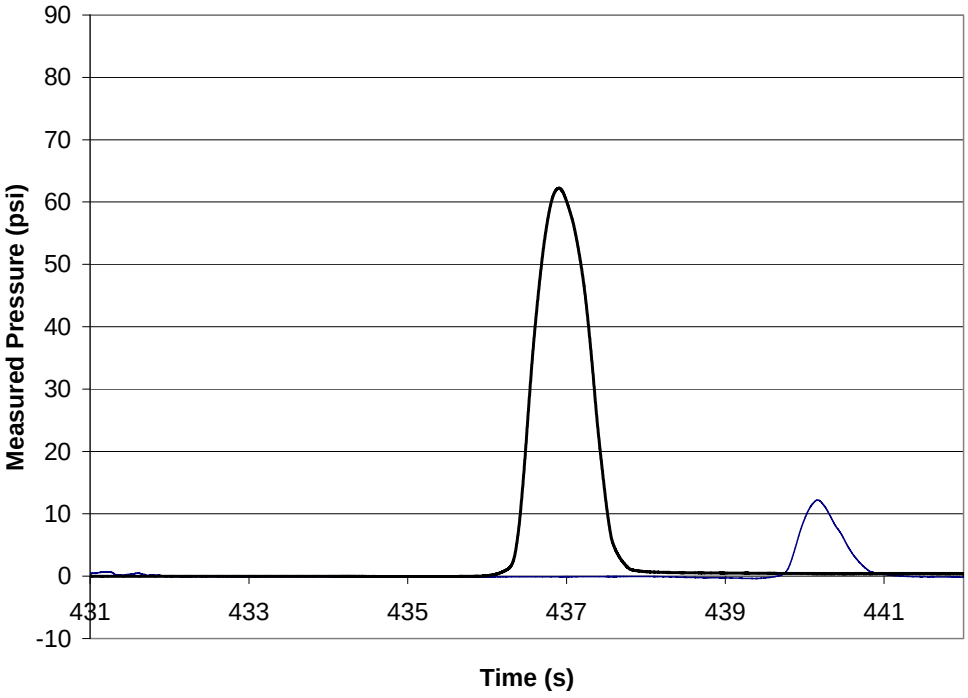

Figure 38. Proof roll trailer over stiff subgrade, third pass.

The results from the proof roll testing are compiled in Table 28. Average speeds ranged from 0.4 to 2.1 mph. These speeds are slower than required by specification, and are reflective of the operator's attempt to ensure the proof roll trailer's wheels passed over the transducers.

Pan Scraper

The pan scraper results are summarized in Figure 39 through Figure 42 with data compiled in Table 29. The results of the testing in the soft subgrade are shown as Figure 39, with a detail of the pulses on a shorter time scale as Figure 40. The stiff subgrade results are shown in the same way in Figure 41 and Figure 42. Compared to the proof roll test, the higher speed of the scraper clearly resulted in shorter duration pulses. Similarly, the two-axle vehicle contributed twice as much data as the single-axle proof roller, in addition to four independent checks of the speed: the time between pulses in adjacent cells for each of the two wheels, and the time between pulses in the same cell between the front and rear axles. Based on the latter, the wheelbase could be calculated. Current models of this pan scraper are built with 28.75 ft between axles; the average of the measurements yielded 27.6 ft.

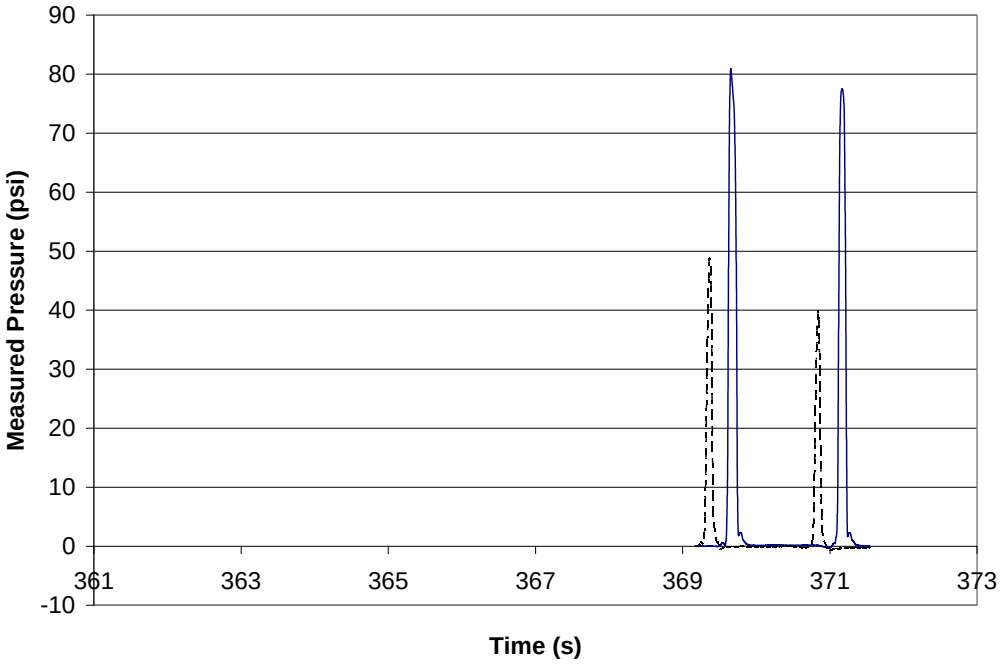

Figure 39. Pan grader over soft subgrade, fourth pass.

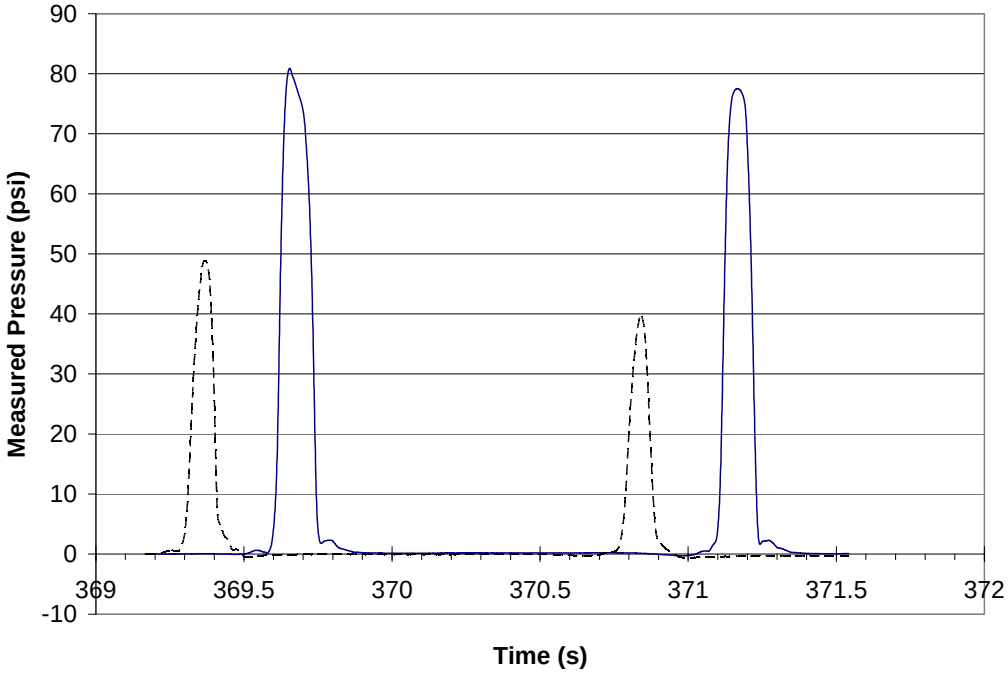

Figure 40. Pan grader over soft subgrade, fourth pass (Detail. Note time scale).

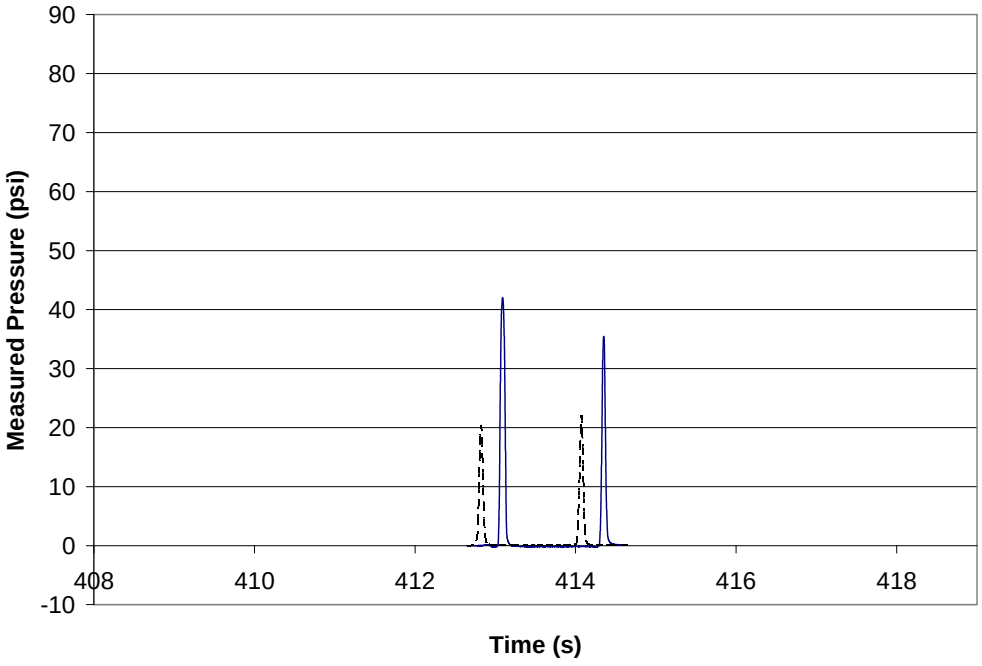

Figure 41. Pan grader over stiff subgrade, fourth pass

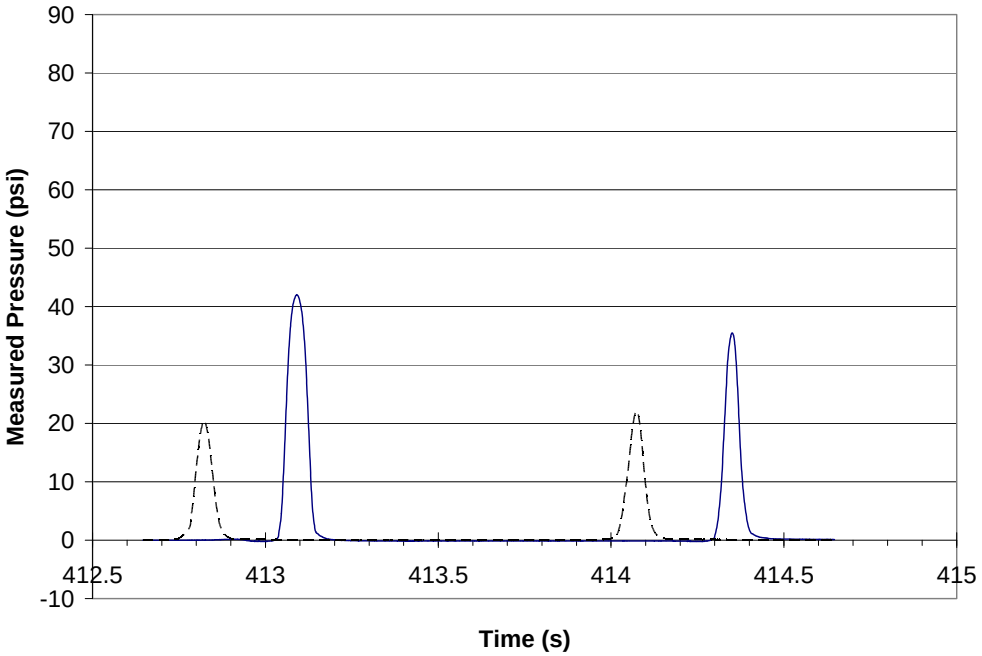

Figure 42. Pan grader over Stiff Subgrade, Fourth Pass (Detail. Note time scale).

Table 28. Proofroll compiled data

SOFT PROOFROLL															
	Pressure Plate 1 Peak			Pressure Plate 2 Peak			Average Speed Calculation--Peak to Peak Plate 2-Plate 1			Average Speed Calculation--Rise to Rise				
Pass	Magnitude psi	Time s	Pulse Duration s	Magnitude psi	Time s	Pulse Duration s	Delta t s	Average speed (6 ft) ft/s	mph	Time s	Time s	Delta t s	Average speed (6 ft) ft/s	mph
1	35.6	54.5	1.2	45.6	51.442	1.399	3.058	2.0	1.3	53.782	50.7	3.082	1.9	1.3
2	6.7	168.405	3.514	7.1	178.777	3.183	10.372	0.6	0.4	166.68	177.404	10.724	0.6	0.4
3	29.6	304.264	1.084	53.5	300.665	2.171	3.599	1.7	1.1	303.715	299.642	4.073	1.5	1.0
4	47.8	423.138	1.127	55.2	425.066	1.033	1.928	3.1	2.1	422.669	424.665	1.996	3.0	2.0

HARD PROOFROLL															
	Pressure Plate 1 Peak			Pressure Plate 2 Peak			Average Speed Calculation Plate 2-Plate 1			Average Speed Calculation--Rise to Rise				
Pass	Magnitude psi	Time s	Pulse Duration s	Magnitude psi	Time s	Pulse Duration s	Delta t s	Average speed (6 ft) ft/s	mph	Time s	Time s	Delta t s	Average speed (6 ft) ft/s	mph
1	14.8	44.722	1.474	2.1	41.279	0.949	3.443	1.7	1.2	44.19	40.822	3.368	1.8	1.2
2	43.8	272.525	1.146	3.3	275.184	1.03	2.659	2.3	1.5	272.016	274.623	2.607	2.3	1.6
3	12.2	440.166	1.425	62.2	436.904	1.826	3.262	1.8	1.3	439.688	436.196	3.492	1.7	1.2
4	6.3	612.747	1.339	8.1	609.974	1.691	2.773	2.2	1.5	612.2	609.28	2.92	2.1	1.4

Table 29. Pan scraper compiled data (rise to rise speeds calculated but not shown due to space constraints)

SOFT PAN

	Pressure Plate 1			Pressure Plate 2			Average Speed Calculation			Check with axle spacing			
		Peak			Peak		Plate 2-Plate 1			Plate 1,1-F	Plate 2,1-Plate 2,2		
Pass	Magnitude	Time	Pulse Duration	Magnitude	Time	Pulse Duration	Delta t	Average speed (6 ft)		Delta t	Delta t	Distance between axles	
	psi	s	s	psi	s	s	s	ft/s	mph	s	s	ft	ft
1	55.4	192.3435	0.2035	70.7	192.6535	0.2315	0.31	19.4	13.2				
1	42.97	193.724	0.1605	60	194.0325	0.197	0.3085	19.4	13.3	1.3805	1.379	26.8	26.8
2	17.68	245.7555	0.2485	2.99	245.439	0.1605	0.3165	19.0	12.9				
2	29.84	247.171	0.2445	4.46	246.8505	0.1805	0.3205	18.7	12.8	1.4155	1.4115	26.5	26.4
3	~~*1.949*~~	~~*309.6125*~~		6.68	309.8615		0.249	~~*24.1*~~	~~*16.4*~~				
3	28.04	310.9285	0.171	56.45	311.2525	0.238	0.324	18.5	12.6	1.316	1.391		25.8
4	80.88	369.654	0.1955	48.83	369.367	0.244	0.287	20.9	14.3				
4	77.53	371.1665	0.192	39.9	370.8415	0.186	0.325	18.5	12.6	1.5125	1.4745	27.9	27.2
										Avg		27.1	26.6
										ST Dev		0.741953	0.62311566

HARD PAN

	Pressure Plate 1			Pressure Plate 2			Average Speed Calculation			Check with axle spacing			
		Peak			Peak		Plate 2-Plate 1			Plate 1,1-F	Plate 2,1-Plate 2,2		
Pass	Magnitude	Time	Pulse Duration	Magnitude	Time	Pulse Duration	Delta t	Average speed (6 ft)		Delta t	Delta t	Distance between axles	
	psi	s	s	psi	s	s	s	ft/s	mph	s	s	ft	ft
1	*0.8*	*239.1915*		*0.1*	*239.4875*		0.296	20.3	13.8				
1	43.2	240.619	0.188	1.8	240.924	0.1455	0.305	19.7	13.4	1.4275	1.4365	28.1	28.3
2	45.7	294.927	0.124	24.8	294.729	0.106	0.198	30.3	20.7				
2	*13.4*	*295.8415*	*0.0935*	42.4	295.64	0.1605	0.2015	29.8	20.3	0.9145	0.911	27.2	27.1
3	34.3	357.941	0.16	2.6	358.2645	0.128	0.3235	18.5	12.6				
3	36.7	359.3725	0.1455	*0.9*	*359.6795*	*0.075*	0.307	19.5	13.3	1.4315	1.415	28.0	27.7
4	42.0	413.091	0.158	20.5	412.822	0.199	0.269	22.3	15.2				
4	35.5	414.3505	0.1945	22.1	414.0735	0.1885	0.277	21.7	14.8	1.2595	1.2515	27.3	27.1
										Avg		27.6	27.5
										ST Dev		0.449048	0.5438798

Analysis

Rise to Rise vs. Peak to Peak

The average speed was calculated by considering two different methods of determining the time between successive pulses. The first, which requires the least judgment, involves identifying the location of the maximum pressure reading for each pulse and recording the time. The distance between cells is divided by the difference between the time of the peak of the first and second cell, yielding an average speed.

The second, which requires a bit more judgment due to the nature of the signals, required identification of the initial rise of each pulse. This was generally done by setting a threshold pressure that, once exceeded, was deemed the beginning of the rise of the pulse. Figure 43 plots the average speeds calculated by both methods against one another. In general, higher speed yielded more scatter.

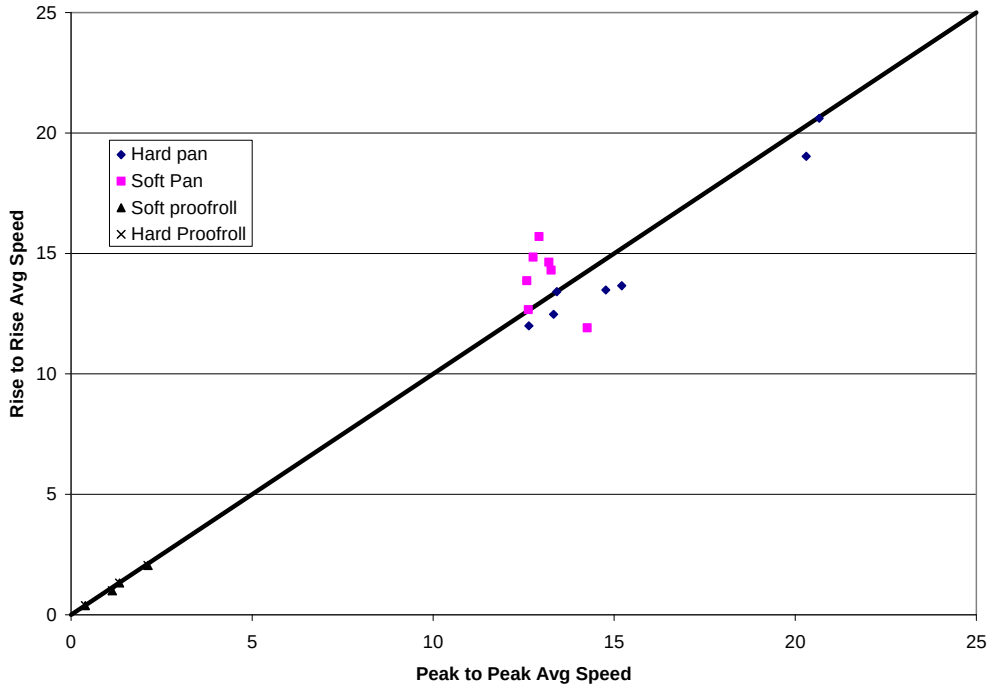

Figure 43. Comparing Rise to Rise and Peak to Peak Methods for Determining Time in Speed Calculations

Pulse Duration

The pulse duration can be plotted against average speed, as shown in Figure 44. To better show the variability in the data for the pan, Figure 45 shows the results on a finer pulse duration scale. The results in Figure 44 are plotted along with the relationship between vehicle speed and pulse time as described by Barksdale (1971) and reproduced in Huang (2004). That reference plots pulse time versus depth below pavement as measured in a layered flexible pavement.

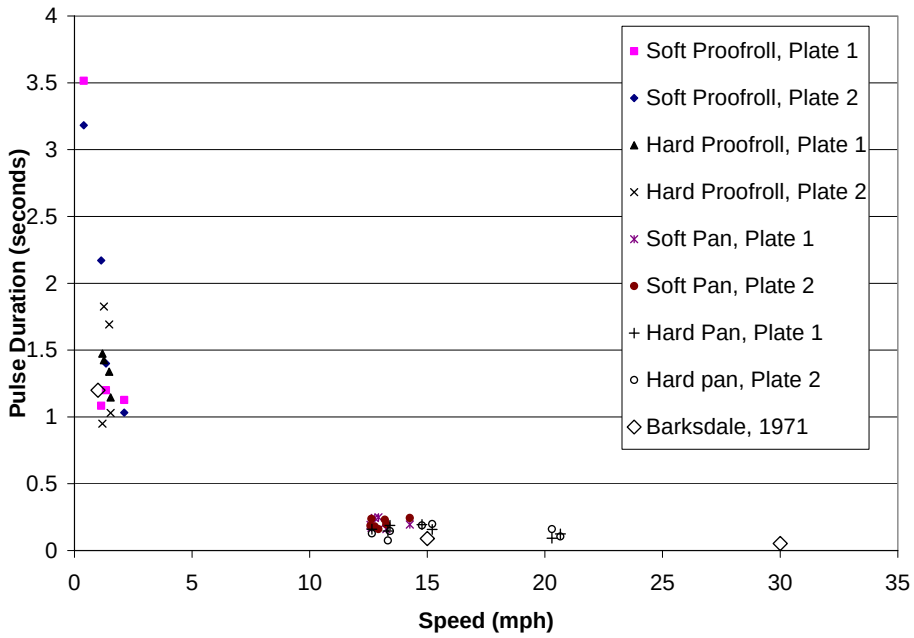

Figure 44. Relationship Between Pulse Duration and Vehicle Speed

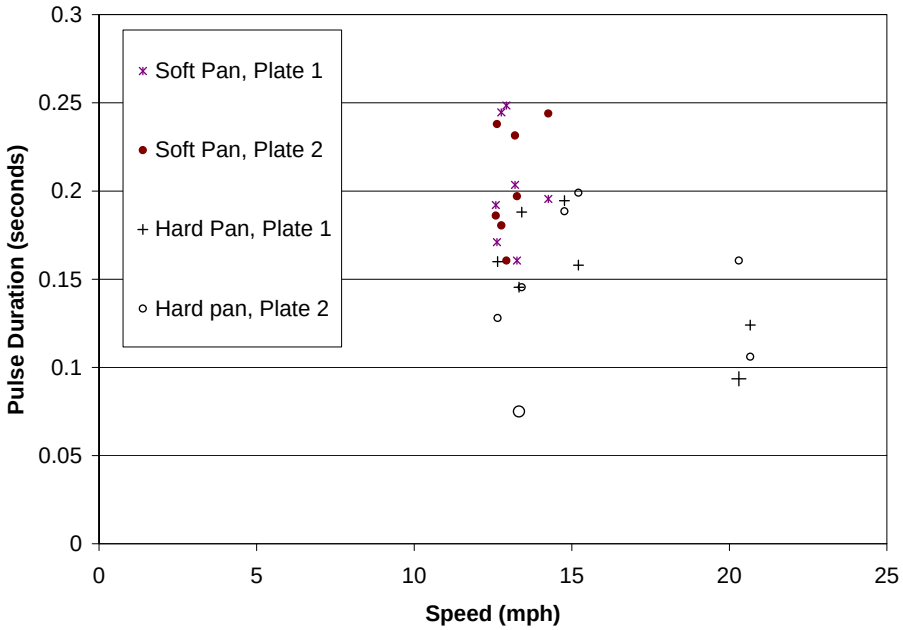

Figure 45. Relationship Between Pulse Duration and Vehicle Speed, Pan Scraper Only

For Figure 44, the pulse durations expected at the measured speeds are shown for 6 inch depths only. In general, the pulses measured at the High Point site are of slightly longer duration than expected by Barksdale, which is probably expected in the subgrade, which undergoes more deformation (some of it plastic) due to its lower strength and stiffness than a layered flexible pavement.

Barksdale (1971) obtained similar results on pavement structures and generated Figure 46. The results from Table 28 and Table 29 at the six inch depth are plotted atop Barksdale's curves and the data compare positively to the previous work.

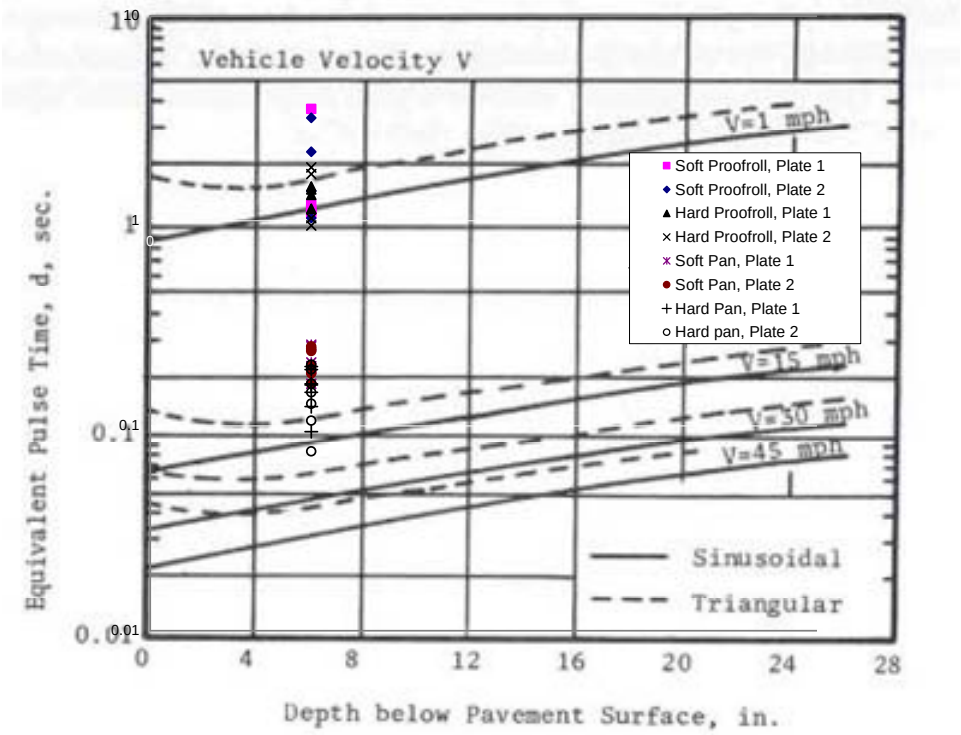

Figure 46. Barksdale (1971) Load Pulse Duration Comparison with Data (Huang, 1993)

Pulse Magnitude

The maximum magnitude of the stress was also plotted against speed for all subgrade conditions, as shown in Figure 47. The pulse magnitude appears to be largely dependent on how close the operator was able to get to the location of the pressure plate. As such, it seems reasonable to conclude the highest measured magnitudes are most similar to those consistently applied to the top of the subgrade. For the pan grader, that yielded a stress of just over 80 psi; and for the proof roll the highest measured stress was just over 60 psi.

Prototype Test Design: Sample Size

A series of axisymmetric elastic FLAC analyses were performed to determine the effects of sample size on test results. The main purpose of the testing was to determine appropriate dimensions of the prototype tests, such that side wall and concrete floor boundaries in the test pit would have minimal effects on the measured stresses and displacements compared to a typical of roadway section with large area and extent.

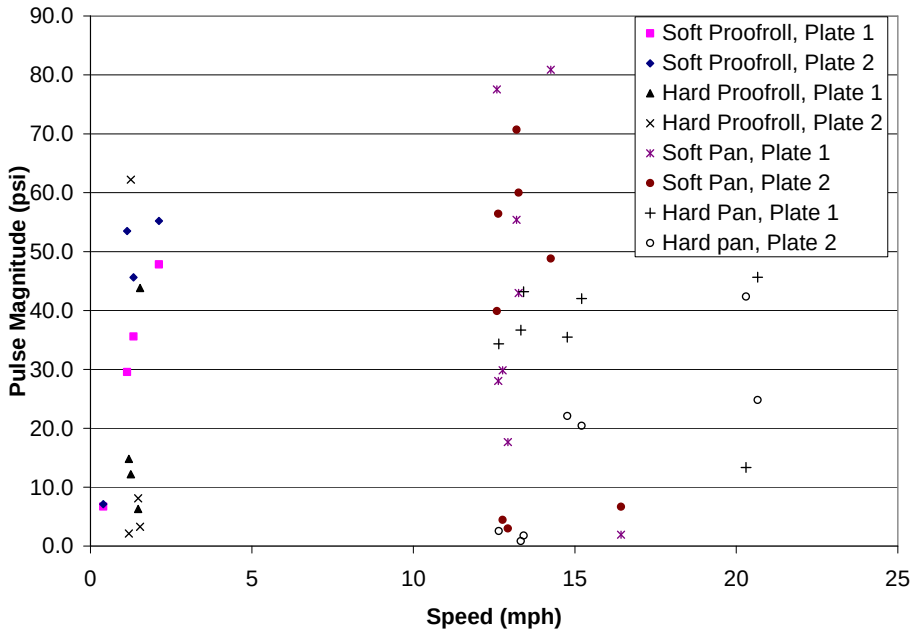

Figure 47. Pulse magnitude versus speed

In FLAC, a model was built prior to the small scale laboratory testing in Chapter 3 with an 8 inch layer of ABC overlying a soft subgrade with a CBR of approximately 3%. Assumed material properties are shown in
Table **30**. An 80 psi surface stress with a radius of six inches was applied at the center of the mesh, and the stress contours were plotted for subgrade depths of 3, 4, 5 and 10 feet, respectively. In all cases, the radial extent of the model was 3 feet, and the side and bottom boundaries were fixed against displacement. The resulting vertical stress contours for the four foot deep subgrade analyses are shown in Figure 48. As can be seen in this figure, the vertical stress dissipates to 10% of the applied surface stress approximately 1.72 feet from the bottom of the pit. Radially, a 90% reduction in vertical stress was predicted approximately 1 foot from the center of the loading for all four modeled cases.

Table 30. Assumed Material Properties for Flac Prototype Models

Soil	E in ksi (MPa)	ν	c in psf (kPa)	ϕ (deg)	Comment
ABC	29 (200)	0.15	100 (4.8)	44	-
Subgrade	12.3 (85)	0.35	1,880 (90)	0	Medium Clay

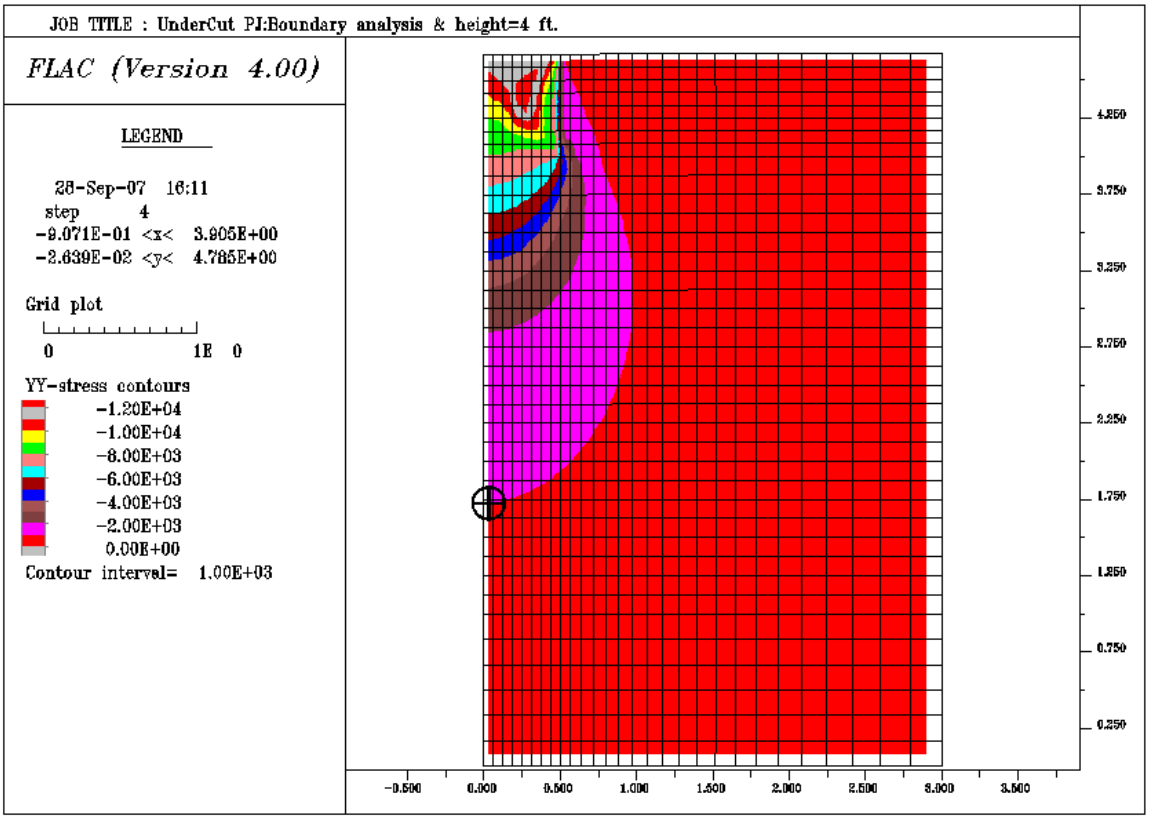

Figure 48. FLAC Results, 4 foot deep subgrade section

The estimated vertical stress results from the FLAC analyses were compiled as Table 31. From these results, the difference between a subgrade height of four and five feet was negligible, with both geometries showing a depth to 90% reduction of around 2.25 feet. Because the test pit in CFL could not reasonably hold more than 5 feet, and the difference in results between 4 and 5 was so small, the 4-foot subgrade thickness was selected.

Table 31. Depth to Vertical Stress Equal to 10% of the Applied Stress for Subgrade Depths of 3, 4, 5 and 10 ft.

Cases	Depth of σ_v = 0.1q (ft)
H=10 ft	2.05
H=5 ft	2.23
H=4 ft	2.28
H=3 ft	2.74

Prototype Test Design Summary

Based on the field measurements taken and summarized above, the proof roll test appears to load the subgrade over a 1.5 to 2.5 second pulse, with magnitudes of between 60 and 70 psi. For construction loading, a pan scraper traveling between 12 and 20 mph loads the subgrade over a 0.15 to 0.25 second pulse with magnitudes as high as 80 psi. The strength of the subgrade (soft or stiff) does not appear to affect significantly the magnitude of the pulse: for the proof roll test, the highest magnitude was observed in stiff soils; for the pan scraper, the highest stress was observed in the soft soils.

Based on axisymmetric numerical studies, the 6 ft x 9 ft x 8 ft deep test pit in the Constructed Facilities Laboratory was large enough to minimize the effects of side and bottom boundaries compared to a deep layer. The analysis showed the height of the subgrade sample for a thin ABC stabilization layer could be four feet.

Summary

This chapter has reviewed dynamic cone penetrometer data from three field sites in North Carolina. The recommendation by Wainaina (2006) is that a DCPI of 38 mm/blow or greater generally results in replacement of the subgrade. The DCP measurements, coupled with the inspector's interpretation of the proof roll, generally confirmed this recommendation. Further analysis using the wave equation showed existing literature correlations to both shear strength and, to a lesser extent, resilient modulus, could be explained using the physical model included in GRLWEAP. These results helped confirm the decision to place the clay subgrade described in Chapter 3 at high water contents and thus DCPI in excess of 38 mm/blow.

Field measurements and numerical studies were used to also determine load pulse magnitude and duration and prototype size. The field measurements generally confirmed the pulse durations with speed and measurement depth suggested by Barksdale (1971). Measured pulse magnitudes determined by field measurements were much more scattered, but maximum values were very close to the tire pressure of the pan scraper or proof roll trailer measured.

To determine the proper size for the full scale prototype tests, axisymmetric numerical studies in FLAC were developed. These analyses showed a significant difference in the depth to 90% reduction in applied static surface stress between 3 and 4 feet subgrade thickness, but very little difference in the depth to 90% reduction between 4 and 5 feet subgrade. Stresses at the side boundary showed considerably less than 10% of the applied surface stress at a radius of 3 ft from the center of the applied load.

The prototype test geometry, subgrade condition and loading functions discussed above were used to develop the full scale prototype tests described in Chapter 5.

CHAPTER 5: PROTOTYPE TESTING AND QUALITY CONTROL

Large-scale tests were conducted in a concrete test pit at the Constructed Facilities Laboratory (CFL) located on the Centennial Campus of North Carolina State University in Raleigh, North Carolina. The overall dimensions of the test pit were 9 feet wide, 12 feet long, and 7 feet deep. The test pit was recessed into the floor of the laboratory approximately 3 feet, and was accessible by a 6 foot wide ramp that led down to the test pit floor.

The test pit was made smaller to decrease the amount of soil needed to fill the pit. Three concrete panels, each 7 feet tall, 3 feet wide, and 8 inches thick were placed along one side of the test pit and shored with wooden braces. A pre-fabricated wall consisting of bolted wooden beams was braced against the back wall to decrease the length dimension. The final dimensions of the reduced test pit area were 6 feet wide, 9 feet long, and 7 feet deep.

The soil was retained along the ramp side of the test pit by wooden beams with a nominal 4 inch square cross section. The beams were stacked gradually as the section was constructed and held in place by two C-shape channels embedded in the test pit walls. A picture of a completed test is shown as Figure 49, and additional photos and schematic plans are given in Appendix B.

The test sections were loaded with an MTS Systems Corporation hydraulic actuator. The actuator was model number 244.22, and had 20 inches of dynamic stroke with a load cell capacity of 22 kips. The actuator had an internal linear variable differential transducer (LVDT) and was controlled with an MTS FlexTest Digital ServoController. The system elements were calibrated before the start of testing on March 20, 2008 by an MTS technician. During testing, the actuator was held in place with a ratcheting strap to keep it from sliding in the direction of the hydraulic lines, which had a tendency to pull on the actuator. This is also shown below in Figure 49.

The actuator was connected to a reaction frame that spanned over the test pit. This is shown above in Figure 49. Two W10 x 88 shape steel columns, each 20 feet high, were bolted to the concrete strong floor with four embedded 5/8” diameter threaded rods. A 14-foot long W24 x 76 section steel beam was bolted between the columns with eight 7/8” diameter steel bolts on each side. The actuator was hung slightly to one side of the beam (6 feet) to load the middle (horizontal direction) of the test pit below. Because of the column mounting positions in the strong floor, though, the actuator was not able to load the sections directly in the middle of test pit (long/ramp direction). However, the minimum resulting dimension was still greater than half of the width of the test pit.

Figure 49. Completed Test Section Showing Test Pit, Load Actuator, and Reaction Frame

The actuator loaded the test sections through a steel load plate. The plate was 12 inches in diameter by 1 inch thick. An 8 by 8 inch square, 1 inch thick steel plate was welded to the top of the circular plate. Three hooks were threaded into the plate for attachment of string-potentiometers. An elastomeric bearing pad 12-1/8 inches in diameter by 0.53 inches thick was placed beneath the steel plate assembly. This was done to reduce the stress concentrations generated on the test surface. Stiffness testing of these elements will be described previously. Although the pad helped to level the load plate, a thin layer of fine sand was also placed beneath the rubber pad as a final leveling mechanism. A picture of the load plate is shown below as Figure 50.

Figure 50. Typical load plate and pad configuration

Instrumentation

The instrumentation described here does not include the LVDT and force transducer mounted directly on or within the load actuator.

Earth Pressure Cells

Eight semiconductor strain gauge Earth Pressure Cells (EPCs) were buried within the subgrade soil to measure changes in horizontal and vertical stress during testing. All of the EPCs were either model number 3500 or 3510 from GeoKon® and had zero to five volts of DC output. The calibration gauge factors given in the manufacturers' calibration reports were used.

One of the EPC's was nine inches in diameter with a 250 kPa (35 psi) capacity and was placed at the interface of the sand buffer layer and the subgrade to measure the boundary stresses near the bottom of the test pit. Horizontal boundary stresses were measured with another nine inch diameter EPC with 250 kPa (35 psi) capacity with a rigid back-plate that was mounted to the concrete sidewall at the minimum horizontal dimension from the load plate.

The other 6 EPC's were 4-inches in diameter with capacities of either 250 kPa (35 psi), 400 kPa (60 psi), or 1 Mpa (150 psi). The EPCs with higher load capacity were placed in the soil at locations closer to the load plate. To measure horizontal soil stress, the EPC's were oriented vertically. The two EPC's on the left of Figure 51 are placed in such a manner. All of the EPC cables were protected with PVC piping.

Figure 51. Installed Earth Pressure Cells (EPCs)

Surface Displacement

During testing, surface displacements of the load plate and the nearby soil surface were continually measured. All of the instruments were calibrated before use and hung from an independent beam over the test pit to avoid disturbance from the load actuator.

Three string potentiometers (string pots) measured the displacement of the load plate at three locations equidistant from the plate center and 120-degrees apart. The string pots were Celesco® model number SP 1-12, with 12.5 inches of stroke. The cables were attached to hooks fixed to the plate. Three short longfellow linear variable displacement transducers (LVDT's) were mounted at distances from the edge of the load plate to measure soil surface deformation during loading. The LVDTs were manufactured by

Honeywell® and had approximately 4 inches of stroke. Initial tests had less instrumentation (discussed later in Section 4.1.4).Figure 52 shows a typical surface instrumentation setup.

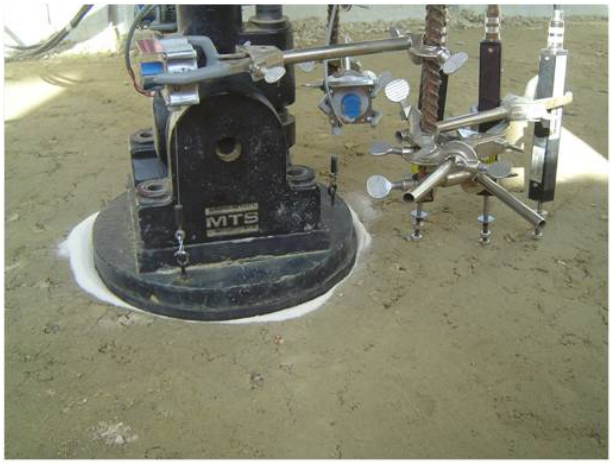

Figure 52. Typical surface displacement instrumentation setup

Data Acquisition

All of the instrumentation data was collected by a control system from Vishay Micro-Measurements®. The control box housed a voltage calibration card, two analog input cards, a scanner card, a high level card, and a strain gauge card. This provided 16 channels for data acquisition, which were occupied by the eight EPCs, three string-pots, three LVDTs, the actuator load cell, and the actuator internal LVDT. Data were fed into a PC computer with StrainSmart© software for recording. The sample rate of data acquisition was changed and dependent on the load sequence.

Surface Profile Measurements

Although surface deformation was continuously monitored during testing by surface-mounted LVDT's and string-pots attached to the load plate, the individual deformations of the subgrade and granular layers were desired. This was accomplished by measuring the distance between a fixed string-line grid on a wooden frame and the soil surface. The grid was placed on the stationary concrete walls around the test pit. The grid consisted of perpendicularly-oriented strings that crossed every 3 inches in a 3 foot square around the center of the load. The measurements were read and recorded by one tester, while another lowered a plum-bob with an attached tape measure at each string intersection. The graduations on the tape were in millimeters. A typical test reading is shown as Figure 53.

Figure 53. Typical surface profile measurement

Measurements were taken of the soil layers before and after testing to determine the change in profile that occurred during loading. Taking the difference in readings of layers before loading also gave a measure of constructed layer thickness, assuming that compaction of the upper layer did not compress the lower layer. Any leveling sand on the granular layer surface was removed with a shop-vacuum before measurement.

Test Section Construction

Soil Preparation

To prepare it for the test pit, soil was spread on the paved loading dock outside the laboratory with a Bobcat® Model 773 skid-steer loader. A Poulan-Pro® Model HDF800 front-tine tiller was used to break up soil clods of the Coastal Plain Subgrade until no further particle size reduction was observed, as shown in Figure 54. The tiller also aided in distributing additional moisture that added with a spray hose until within target values, which were verified by several readings on back-scatter mode from a nuclear moisture-density gauge. For both the select fill and ABC, additional moisture was distributed throughout the prepared soil by simply flipping it with the loader.

Once the soil had uniform moisture distribution and within target values, it was brought inside and placed in the test pit with the loader. The loose soil was approximately leveled with shovels and rakes before compacting.

Figure 54. Soil Preparation with Front-Tine Tiller

Chemical Stabilizer Addition

For test sections with LSS, hydrated lime was added to the Coastal Plain subgrade. First, a quantity of soil for the prescribed depth of stabilization was brought outside. After water was added to generate the same moisture content as the unstabilized subgrade, an amount of lime to produce 3% lime content by weight was added incrementally by spreading over the subgrade surface. This is shown in Figure 55. LSS was mixed on days when the ambient air temperature was above 45 degrees-F, and care was taken not to fly a significant amount of the lime while spreading. The lime was then tilled into the soil until it was visibly uniform, and brought inside the laboratory to mellow for 1 to 3 days. The laboratory was kept at an average temperature of 70 degrees-F.

After the mellowing period, the soil was brought back outside of the test pit and tilled to break down the soil clods. Quality control testing of the LSS was performed before it was into the test pit and compacted. The LSS was left to cure for 7 days in the test pit and sprayed periodically with water to keep the surface from drying out.

Figure 55. Spreading of Hydrated Lime on Coastal Plain Subgrade

Hydrated lime was added to the Coastal plain subgrade to simulate the creation of Lime Stabilized Subgrade (LSS) in the field. The hydrated lime used was Type N manufactured by Southern Lime Company® in Calera, Alabama and purchased in 50-lb bags. The hydrated lime was stored inside the laboratory to prevent moisture infiltration.

LSS test specimens were prepared at both 3 and 5 percent lime for Standard Proctor, Unconfined Compressive Strength (UCS) per ASTM D 2166. Standard Proctor specimens were compacted both immediately after adding the lime and after a 2 hour waiting period (termed "delayed") to determine the effects of initial flocculation on compaction. UCS samples were cured for 7, 14, and 28 days to determine the effects of prolonged hydration on strength and resilient behavior, respectively. UCS tests also used an NCDOT rapid oven curing method.

The test sections with LSS were scheduled last since the stabilized subgrade could not be reused for testing. After disposing of the tested LSS from several tests, it became apparent that the number of LSS tests originally desired would not be possible with the given supply of subgrade. Thus, additional subgrade excavated at a site in the Coastal Plain region close to the original location was delivered to the laboratory in February 2009. Because the new subgrade was gray in color rather than brown like the previous Coastal Plain subgrade, it is referred to as "gray subgrade" (or "gray LSS") even though it was also from the Coastal Plain region. This soil was only used as LSS for the last test (Test 21) to mimic the effects of differing stabilized layers over a given subgrade. Testing on the gray subgrade included grain size distribution, specific gravity, Atterberg limit, Standard Proctor, and CBR tests. UCS tests were performed on the gray LSS at 3% lime content.

Compaction

All soils were compacted in 6 inch lifts, except for the 3 inch surfacing of ABC on the select fill sections and 4 inch lifts for the LSS. The compaction equipment included a Northern Industrial Equipment® Model JPC-60 plate compactor. The plate compactor had a weight of 69 kg, a 510 mm by 310 mm plate area, and a centrifugal force of 1030 kg-f. The compactor was engaged until no further settlement was apparent. This is shown as Figure 56.

For the Coastal Plain Subgrade and for the LSS in one test (Test 19), additional compaction was required to achieve sufficient density. This was accomplished using a Bosch® Model 110304 electric jack-hammer with an 8 inch square tamping plate, as shown in Figure 57. The jack-hammer impacted at 1400 beats per minute at 43 foot-pounds of force, and tamped against the soil until settlement appeared to cease. The plate compactor was used after jack-hammering to finish compaction of the lifts. After the first LSS test (Test 19), it was apparent that further compactive effort beyond the Bosch jack-hammer was needed to achieve adequate density. A Multiquip® model MTX-70 Tamping Rammer (Jumping-Jack) was used to compact the stiff LSS closer to target values, as shown in Figure 58. The rammer had an impact force of 2,855 lbs over a 13.4 by 11.2 inch wide tamping plate.

Figure 56. Initial Soil Compaction using Vibratory Plate Compactor

Figure 57. Additional Soil Compaction using Jack-Hammer

Figure 58. Additional compaction on LSS using Jumping-Jack Rammer

Geosynthetic Installation

Test sections with geosynthetics located at the subgrade/granular layer interface were first prepared by cutting a 6 foot wide by 11 foot long piece of geosynthetic out of the larger roll. The longer dimension was cut in the machine direction, which was laid length-wise against the subgrade and stapled against the back wooden wall. In the front of the test pit, the geosynthetic was lapped between wood beams and stapled. This was not done for anchorage purposes, but to keep the geosynthetic flat while the granular layer was placed. Pictures of typically installed geogrid and geotextile test sections before granular layer placement are shown in Figure 59 and Figure 60, respectively.

Figure 59. Installed Geogrid B before granular layer placement

Figure 60. Installed Geotextile A before granular layer placement

Four geosynthetics (two geotextiles and two geogrids) were tested at the granular layer/subgrade interface. The two geotextiles were manufactured by Mirafi®, with the less stiff geotextile (HP270) serving the primary function of separation. The stiffer fabric (HP570) was used to provide both reinforcement and separation. The geogrids used were

biaxial model numbers BX-1100 and BX-1500 manufactured by Tensar®, with the BX-1500 geogrid having higher stiffness.

All of the geosynthetics used are within specifications of the NCDOT for subgrade stabilization. The geosynthetics will be referred to as “Geogrid A” and “Geogrid B” for the BX-1500 and BX-1100, and “Geotextile A” and “Geotextile B” for the HP570 and HP270, respectively. The notation ‘A’ will be used for the stiffer of the two geosynthetics.

Quality Control Testing

The test pit was divided into 9 equal sections in plan (each 3 feet long by 2 feet wide) for quality control testing. This section describes the testing that was conducted in these locations.

Nuclear Moisture-Density Gauge

Soil moisture prior to compaction, and both moisture and density post-compaction were measured using a Troxler® Model 3440 nuclear moisture-density gauge (nuclear gauge). The nuclear gauge was calibrated before each use on a resin calibration block provided by Troxler®, the records of which are given in Appendix B. Before all readings, the soil surface was leveled using a steel field plate. Holes for direct transmission (DT) readings with the nuclear gage probe rod were created with a steel spike.

For the Coastal Plain subgrade, nuclear gauge readings were taken every 12 inches (2 lifts) within each of the 9 sections. The subgrade of early test sections was tested with the nuclear gauge at 15 second reading durations in back-scatter mode, as well as DT readings at 3, 6, 9, and 12 inches. Later sections were checked with DT readings at 6 and 12 inches, but at 1 minute reading times.

For the select fill, nuclear gauge readings were taken in each section at 6 and 12 inch DT with a 1 minute reading duration. For the LSS and ABC, the soil was too dense to drive the steel spike and only back-scatter readings were taken on the ABC every 6-inch lift, 3 inch surface lift for select fill sections, and every 4 to 6 inch surface lift for LSS sections. All DT testing holes were refilled prior to placing the next lift of soil.

The collection of soil samples for oven moisture content determination enabled moisture content correction (K) factors to be used. Data were compiled throughout testing to determine an average representative value for each soil type.

Sand Cone

Sand cone tests were performed according to ASTM D 1556 as an additional measurement of soil density and to verify the nuclear gauge readings (ASTM, 2007). Two tests were performed every 12” (two lifts) next to a nuclear gauge reading location for comparison. Sand cone tests were not performed on the ABC and select fill contained

voids that allowed sand to escape, thus increasing the apparent volume and decreasing the measured density.

Two different sands were used for sand cone testing. The first was fine GS-40 sand, but it was realized after initial tests that it did not meet gradation specifications set forth in ASTM D 1556. The specification regulates the fine portion of the sand in order to prevent sand from escaping into the surrounding voids, but since the subgrade was a tightly compacted clayey soil, this was not thought to be a problem. Nevertheless, later sand cone tests were switched to Ottawa 20-30 sand that met specifications. The sand cone device was according to specifications. Figure 61 gives the grain size distribution of each sand used, and Figure 62 shows a test setup.

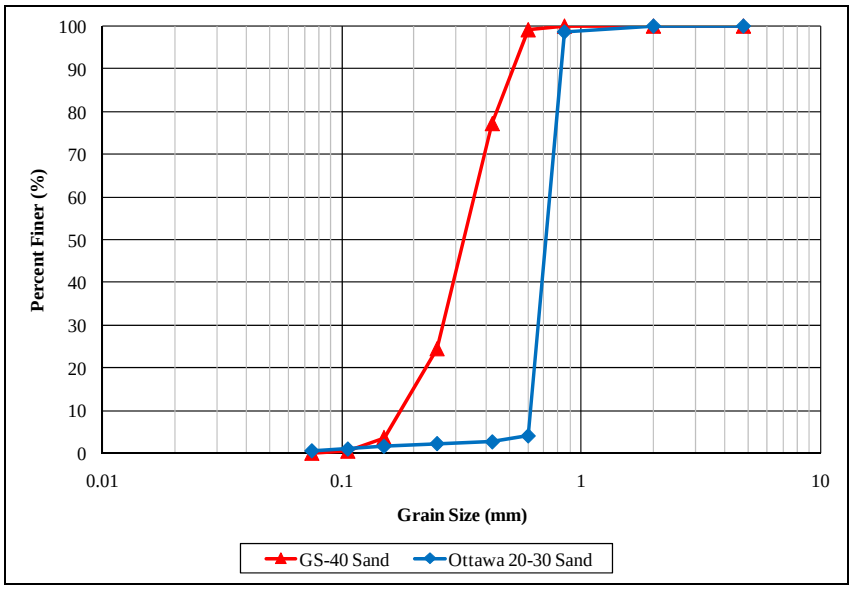

Figure 61. Grain size distribution curves of sands used in sand cone testing

Figure 62. Typical Sand Cone Test Setup

Rubber Balloon

Rubber Balloon density tests were performed according to ASTM D 2167. The balloon device was a Volumeasure Model 29-4522 from ELE International®. Like the sand cone tests, two tests were performed every foot (2 lifts) of Coastal Plain subgrade next to a nuclear gauge test location for comparison. Two tests were also performed every lift (6 inches) of select fill and two lifts (8 inches) of LSS as a comparison to nuclear gauge measurements. Although balloon tests were performed on several test sections with ABC, the sharp stones popped the inflated balloon during testing. Testing was thus stopped to avoid further problems. Figure 63 shows a typical test setup,.

Figure 63. Typical Rubber Balloon Test Setup

Dynamic Cone Penetrometer (DCP)

Dynamic Cone Penetrometer (DCP) readings were taken as an additional quality control measure to ensure constant subgrade construction and to calculate soil properties through empirical correlations. The DCP is used by dropping a weight along a rod of specified height onto an anvil to drive a cone into the underlying soil. The model used for this testing consisted of an 8 kg (17.6 lbs) weight with a drop height of 576 mm (22.6 inches) and a 60-degree cone. This form of the DCP is specified in ASTM D 6951. All readings for the DCP are given as distance per blow (usually mm/blow) and referred to as the DCP Index (DCPI).

DCP testing was performed with two operators. One dropped the weight and ensured that the DCP remained vertical and perpendicular to the soil surface. The other used a wooden stake to record the individual blow penetrations based on the position of the horizontal handle attached to the DCP anvil. A typical test is shown as Figure 64. After the DCP was driven approximately two feet, the DCPI was calculated by measuring the total penetration depth on the stake and dividing it by the total number of blows. Five DCP readings, one each within the test pit corner sections and one in the middle of the test pit, were taken every two feet of subgrade. DCP readings were taken on the LSS after testing to ensure that its integrity would not be compromised beforehand.

Figure 64. Typical Dynamic Cone Penetrometer (DCP) Test

The DCP results were used to empirically derive CBR values using published equations. The two equations used were developed by Coonse (1999) for Piedmont residual soils (Equation 12), and another by the NCDOT (1998) for both ABC and cohesive soils (Equation 13).

$$\text{Log(CBR)} = 2.53 - 1.14*\text{Log(DCPI)} \quad \textbf{(28)}$$

$$\text{Log(CBR)} = 2.60 - 1.07*\text{Log(DCPI)} \quad \textbf{(29)}$$

Lime Stabilized Subgrade (LSS) Quality Control

Prepared LSS was analyzed before compaction in the test pit. First, oven water content samples were taken to quantify the amount of drying that occurred during the initial mellowing period. Back-scatter nuclear gauge measurements, which gave instantaneous readings, determined whether or not extra water needed to be added to the LSS to bring back up to optimum moisture content.

Next, samples were obtained to check the gradation of the mellowed LSS versus NCDOT specifications. Samples were also taken to prepare specimens for UCS testing. The specimens were cured for 2 days under accelerated oven curing conditions or 7 days under normal curing.

The exact percentage of lime in the LSS was not determined. Instead, the UCS of the test pit was checked against the UCS of laboratory prepared specimens (at a known lime percentage). If the test pit value was within tolerance of the laboratory value, the constructed LSS was deemed adequate. This was similar to the rationale used for field situations, where lime percentages over design are often added to subgrades to ensure high strength.

Depth of the placed LSS was determined using surface profile measurements. This was performed instead of using phenolphthalein indicators. Surface profile measurements will be described later, as will measured layer thicknesses.

Loading Sequence

Static Loading

Before cyclic loading was conducted, static loads were applied to determine section responses under static conditions and to help seat the load plate. Applied pressures between 0 to 40 psi or 80 psi in 10 psi increments were applied and held until plate displacements were less than 0.001 inches per minute for three consecutive minutes, per ASTM D 1196. The displacements were monitored with the actuator internal LVDT and the string pots attached to the load plate. The sampling rate from the data acquisition system was 10 readings per second during static loading.

Cyclic Loading

Cyclic loads were applied to the test sections to mimic construction traffic on stabilized subgrades before the placement of final pavement layers. This was accomplished by applying 10,000 load pulses at 80 psi (9.048 kips on the 12-inch diameter plate), at a rate of 0.1 seconds of load application, followed by 0.9 seconds of rest with a residual load of 250 pounds to maintain contact with the load plate. This was based on past large scale tests reported in the literature, the rate of loading during small scale resilient modulus testing, and field verification testing. The sample rate from the data acquisition system was 200 readings per second during the cyclic loading.

Proof-Roll Loading

Simulated proof-roll loads were applied to the test sections. The pulse was 70 psi for a 2 second duration, as based on field verification testing described previously. A residual load of 250 pounds was kept on the load plate to maintain contact. The sampling rate from the data acquisition system was 1000 readings per second during the proof-roll loading.

Section Demolition

After the sections were tested, surface instrumentation was removed and soil was carefully excavated to avoid damaging the buried earth pressure cells. Layers were individually excavated to reuse as much soil as possible. All LSS and any mixed soils at the layer interfaces were discarded.

Several tests were excavated down to 24 inches of subgrade to avoid a complete rebuild of the test section. The measured stresses at these depths were deemed low enough to not have drastically changed the stress state of the soil. Again, post density readings were taken to ensure that the bottom subgrade layers had not substantially dried out or compacted during testing. The bottom 24 inches of subgrade was not reused for more than two consecutive tests. This will be discussed further in Chapter 6.

Large Scale Testing

A total of 22 test sections were constructed to evaluate different subgrade stabilization measures on soft Coastal Plain subgrade.
Table 32 outlines the subgrade and stabilization layer thicknesses and types investigated.

Multiple replicate test sections were constructed. Tests 3 and 4 were intended to be replicates of Test 2, and Test 18 an intended replicate of Test 16. Tests above with select fill and LSS (Tests 8 through 11 and 19 through 21) included a thin layer of ABC to provide a stable wearing surface. A test not shown was performed on the select fill after removing the ABC from Test 9 (called Test 9a).

Different subgrade depths were constructed so that the final test section surface elevation was within range of the overhanging actuators' stroke (with additional stroke for anticipated displacement). The cross-beam supporting the actuator remained at a fixed height for all tests.

Applied Loading

Table 33 gives the loadings applied to each of the test sections. The static load test column reports the maximum pressure applied after increasing in 10 psi increments. The loading sequence for most tests consisted of a static load increased from 0 to 40 psi in 10 psi increments. Static testing was followed by 2 proof-roll pulses to simulate inspection immediately after undercut and before construction trafficking (pre proof-roll). Then, the test sections were cyclically loaded until 10,000 cycles to simulate construction was obtained or significant deformation and/or plate rotation occurred. The resulting deformation rut was then refilled with surface material (usually ABC) and recompacted to simulate repair of stabilized subgrade before final paving operations. The sections

were again proof-roll loaded twice to simulate final inspection (post proof-roll), and then loaded with additional cyclic pulses (typically 10,000 cycles) to mimic construction traffic during final paving (Cyclic 2).

Table 32. Summary of Constructed Test Sections

Test No.	Date Tested	Subgrade Thickness (in)	Stabilization Layer Type	Stabilization Layer Thickness (in)	Geosynthetic
1	4/2/2008	48	ABC	6	None
2	5/8/2008	48	ABC	18	None
3	6/4/2008	48	ABC	18	None
4	6/27/2008	48	ABC	18	Geogrid B
5	7/15/2008	48	ABC	12	None
6	8/5/2008	48	ABC	18	Geotextile A
7	8/12/2008	24	Select Fill	36	None
8	9/3/2008	48	Select Fill and ABC	18 and 3	Geotextile A
9	9/12/2008	24	Select Fill and ABC	36 and 3	None
10	10/8/2008	36	Select Fill and ABC	24 and 3	Geotextile B
11	10/22/2008	48	Select Fill and ABC	12 and 3	Geotextile A
12	10/27/2008	60	None	None	None
13	11/12/2008	48	ABC	18	Geotextile B
14	11/24/2008	48	ABC	12	Geotextile B
15	12/18/2008	48	ABC	18	None
16	1/19/2009	48	ABC	12	Geotextile A
17	1/30/2009	48	ABC	12	Geogrid A
18	2/16/2009	48	ABC	12	Geotextile A
19	3/6/2009	48	LSS and ABC	8 and 6	None
20	3/30/2009	36	LSS and ABC	8 and 3	None
21	4/17/2009	36	Gray LSS and ABC	8 and 3	None
22	4/20/2009	36	Gray LSS	8	None

Table 33. Applied Loading Outline

Test No.	Static Load Test	Pre Proof-Roll	Post Proof-Roll	Cyclic 2
1	80 psi	No	No	No
2	No	No	No	No
3	40 psi	No	No	No
4	40 psi	No	No	No
5	40 psi	No	Yes	Yes
6	40 psi	Yes	Yes	Yes
7	40 psi	Yes	Yes	Yes
8	40 psi	Yes	Yes	Yes
9	40 psi	Yes	Yes	Yes
10	40 psi	Yes	Yes	Yes
11	40 psi	Yes	Yes	Yes
12	After Pre-Proof Roll	Yes	No	No
13	40 psi	Yes	Yes	Yes
14	40 psi	Yes	Yes	Yes
15	40 psi	Yes	Yes	Yes
16	40 psi	Yes	Yes	Yes
17	40 psi	Yes	Yes	Yes
18	40 psi	Yes	Yes	Yes
19	40 psi	Yes	Yes	Yes
20	40 psi	Yes	Yes	Yes
21	40 psi	Yes	Yes	Yes
22	40 psi	Yes	No	No

The loading sequence was revised as testing progressed. The final static load increment of 80 psi used in Test 1 was reduced to 40 psi to avoid significantly compacting the subgrade prior to proof-roll and cyclic loading. Proof-roll loads were not applied to Tests 1 through 4 because the load function was not identified until after processing data collected from field testing in late May 2008 (from Section 3.6.2). Loading on Test 12 (unstabilized Coastal Plain subgrade) consisted of a single proof-roll pulse followed by a static load test to bearing capacity failure. The same load procedure but in reverse order was used for Test 22, which reused LSS from Test 21 after the surface ABC lift was removed. A static-only test not listed in Table 32 was performed on Test 9 after testing and removing the surface ABC layer to quantify the bearing capacity of the select fill.

Measured Layer Thicknesses

The as-constructed stabilization layer thicknesses were determined from surface profile measurements by taking the difference in readings of the subgrade and stabilization layer surfaces before loading. The measurements assume that the subgrade did not compact under granular layer addition. This was verified because the subgrade surface around the load displacement bowl did not deform from post-loading measurements. Reported thicknesses are the average of readings taken over a 3-foot grid around the load plate in 3 inch intervals. The measured and intended layer thicknesses are reported below in Table 34. The percent error is calculated based on the intended layer thickness.

The layer thickness of Test 9 could not be determined because a surface profile measurement was not taken at the subgrade surface. Test 22 has the same layer thicknesses as Test 21 minus the ABC layer.

It can be seen from Table 34 that it was difficult to determine the amount of loose stabilization material to place in the test pit to obtain the final compacted thickness. Test 1 had a thicker than intended ABC layer predominately due to the lack of reaction from the soft underlying subgrade, which did not enable the ABC to be adequately compacted to the intended thickness. Although this was somewhat expected, the magnitude of this effect was difficult to quantify. This was overcompensated for in Test 2 by reducing the amount of loose material placed and resulted than a thin ABC layer. This pattern continued for the next several tests. However, the percent error gradually reduced during testing because familiarity with ABC compaction was gained. As with all experiments, the general reduction in percent error reflects experience with the materials and equipment.

Unfamiliarity with materials can also be seen in the tests with LSS (Tests 19 through 21). Test 19 had a thick LSS layer because the equipment used (jackhammer) did not have enough compactive effort. This also gave the LSS a lower than desired dry density (as will be seen later in Section 4.2.1). Tests 20 and 21 used a jumping-jack rammer to compact the LSS, giving it a closer to intended thickness and higher dry density. The thickness still remained high due to the lack of reaction from the subgrade. Differences in stabilization layer thicknesses between replicate test sections hampers reproducibility, but will be used to help quantify differences in performance later in this report.

Table 34. Intended versus Measured Stabilization Layer Depths

Test No.	Stabilization Material	Intended (in)	Measured (in)	% Error
1	ABC	6	7.7	28.3
2	ABC	18	16.1	-10.6
3	ABC	18	19.8	10.0
4	ABC	18	16.4	-8.9
5	ABC	12	13.5	12.5
6	ABC	18	19.0	5.6
7	Select Fill	36	35.8	-0.6
8	Select Fill and 3" ABC	21	19.9	-5.2
9	Select Fill and 3" ABC	39	N/A	N/A
10	Select Fill and 3" ABC	27	27.6	2.2
11	Select Fill and 3" ABC	15	17.3	15.3
13	ABC	18	20.2	12.2
14	ABC	12	12.7	5.8
15	ABC	18	17.9	-0.6
16	ABC	12	12.9	7.5
17	ABC	12	10.7	-10.8
18	ABC	12	12.4	3.3
19	LSS	8	11.8	47.5
	ABC	6	5.4	-10.0
20	LSS	8	9.3	16.3
	ABC	3	4.4	46.7
21	LSS	8	8.5	6.3
	ABC	3	3.6	20.0
22	LSS	8	8.5	6.3

Based on the measured layer thicknesses, the test section designations are listed below in Table 35. This will make comparisons easier with less reference to Table 32 to determine the layer configurations. The designations below use the layer thicknesses from Table 34 rounded to the nearest whole inch. The test number is retained in parenthesis.

Instrumentation Locations

The buried EPC's remained in fixed locations because the protective PVC pipe housing was bolted to the back wood wall. Thus, depending on the stabilization layer thicknesses, the depth of the buried EPC's relative to the test section surface (z) changed. The individual EPC radial distances (r) were not recorded, but were consistently placed during construction at set distances from the concrete sidewalls. Figure 65 shows the final EPC locations for Test 1 (with intended layer thickness), while Appendix C gives dat for the remaining tests.

Table 35. Test Section Designations Reflecting Measured Layer Thicknesses

Test Configuration (Test No.)
8" ABC (1)
16" ABC (2)
20" ABC (3)
16" ABC with Geogrid B (4)
14" ABC (5)
19" ABC with Geotextile A (6)
36" Select Fill (7)
17" Select Fill/3" ABC with Geotextile A (8)
36" Select Fill/3" ABC (9)
25" Select Fill/3" ABC with Geotextile B (10)
14" Select Fill/3" ABC with Geotextile A (11)
Subgrade (12)
20" ABC with Geotextile B (13)
13" ABC with Geotextile B (14)
18" ABC (15)
13" ABC with Geotextile A (16)
11" ABC with Geogrid A (17)
12" ABC with Geotextile A (18)
12" LSS/5" ABC (19)
9" LSS/4" ABC (20)
9" Gray LSS/4" ABC (21)
9" Gray LSS (22)

Several EPC's were broken as a result of test section demolition, including 24V-250 during Tests 13 and 14 and 48V-250 during Tests 15 through 22. The EPCs were broken for multiple tests because they were buried in reused subgrade (Section 4.2.4), and therefore could not be accessed between consecutive tests. For Tests 13 and 14, 48V-250 was moved closer to the load plate to measure stress increase where 24V-250 would have been.

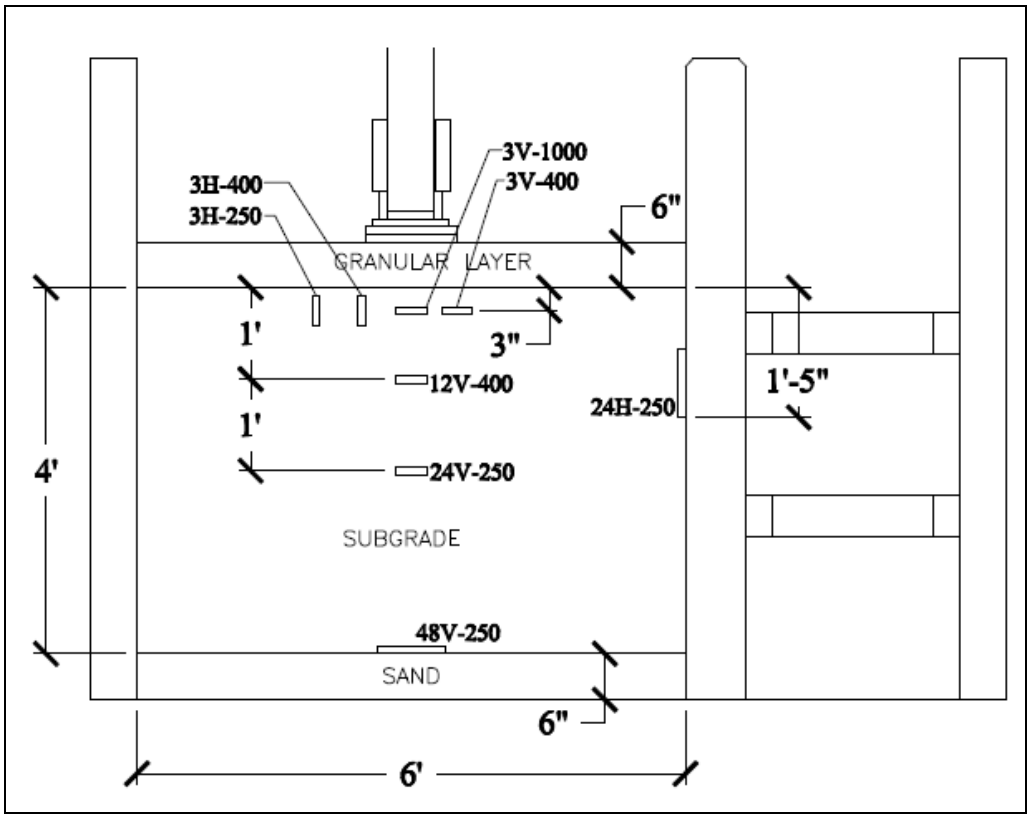

Figure 65. Instrumentation cross section for Test 1 (Not to Scale)

CHAPTER 6: PROTOTYPE TEST QUALITY CONTROL

A number of quality control measures were instituted in order to carefully assess the as-built properties of the subgrade, ABC, select fill, and lime stabilized soils. This chapter describes the quality control efforts to determine the density, water content, CBR and strength of the subgrade, ABC and select fill.

Moisture Content and Unit Weight

The large-scale tests were performed on soft Coastal Plain subgrade to evaluate different stabilization measures. Nuclear density gauge, sand cone, rubber balloon, and DCP readings were taken to ensure that the subgrade remained consistent throughout testing. For the Coastal Plain subgrade, the target CBR was 2.0% at a dry unit weight of approximately 108 pcf and a water content of 18.7%, as was determined from laboratory data.

Table 36 gives the average dry unit weight and water content with standard deviations from both uncorrected and corrected nuclear gauge measurements. The number of tests (N) performed for each prepared large scale sample changed because the depth of subgrade in each test might be different. Although 22 large scale samples were prepared, measurements were not taken on Test 22 because it reused the LSS and subgrade from Test 21.

A correction factor (K) was used to correct water content readings and was calculated as a running average as testing progressed. The K-value was calculated using oven water contents from sand cone and balloon test samples taken close to nuclear gauge reading locations. Equation 14 gives an approach for estimating the K-value equation as was presented in the Troxler® owner's manual.

The uncorrected water content readings from the nuclear gage were greater than the oven-based water content values (shown later). The uncorrected dry unit weights were lower because the nuclear gauge measured the total unit weight and then calculated the dry unit weight from a separate electronic measurement of the water content. Thus, a high water content measurement decreases the calculated dry unit weight.

Based on the average of all tests, the final K-value was found to be -17.2 for the Coastal Plain subgrade. This number was back-applied to uncorrected readings to determine a more accurate dry unit weights and water contents for the test samples.

Table 36. Average Subgrade Dry Unit Weight and Water Content from Uncorrected and Corrected Nuclear Gauge Measurements

Test No.	Uncorrected Values					Corrected Values					
	Avg. γ_d (pcf)	σ	Avg. w%	σ	N	Avg. γ_d (pcf)	σ	Avg. w%	σ	N	K
1	102.8	3.9	20.9	1.9	153	N/A	N/A	N/A	N/A	0	N/A
2	102.7	2.9	21.6	1.6	180	N/A	N/A	N/A	N/A	0	N/A
3	103.1	2.7	21.4	0.9	180	N/A	N/A	N/A	N/A	0	N/A
4	103.6	1.7	20.9	0.8	72	105.9	1.2	18.6	0.8	72	-21.0
5	104.6	1.9	20.6	0.9	54	106.7	2.0	18.2	0.9	54	-21.0
6	103.7	2.0	21.0	1.1	72	105.5	2.1	19.1	1.1	72	-21.0
7	104.8	1.6	20.4	1.0	14	107.0	1.9	18.4	1.0	14	-15.4
8	104.3	1.3	21.0	0.8	72	105.8	1.4	19.2	0.9	72	-15.4
9	105.5	1.1	20.5	0.7	10	107.1	1.2	18.6	0.6	10	-15.4
10	105.2	1.4	20.7	0.8	54	107.1	1.6	18.5	0.9	54	-19.0
11	104.9	1.9	20.6	0.9	50	107.0	2.0	18.3	1.1	50	-19.0
12	105.2	2.1	20.2	1.1	36	107.3	2.2	18.1	1.0	36	-19.0
13	104.4	1.5	20.8	0.6	72	106.5	1.9	18.5	0.8	72	-19.0
14	104.5	1.3	20.8	0.9	54	106.9	1.4	18.5	0.9	54	-19.0
15	104.0	1.6	21.1	1.0	72	105.8	1.6	19.0	1.0	72	-17.4
16	104.6	1.5	20.5	0.7	72	106.4	1.4	18.4	0.9	72	-17.4
17	105.8	0.7	20.4	0.5	50	107.9	1.0	18.2	0.6	50	-17.4
18	104.0	1.0	20.8	0.6	72	106.4	1.1	18.6	0.7	72	-17.4
19	105.3	1.1	20.5	0.6	50	107.2	0.9	18.3	0.6	50	-17.4
20	105.3	0.8	20.5	0.4	50	108.1	0.9	17.8	0.4	50	-17.4
21	104.7	1.2	20.8	0.5	50	107.1	1.2	18.3	0.6	50	-17.4

$$K = \left(\frac{w\%_{oven} - w\%_{gauge}}{100 + w\%_{gauge}} \right) * 1000$$

The results of this correction are presented below in Table 37 with calculated coefficients of variation (C_v).

Table 37. Average Subgrade Dry Unit Weight and Water Content from Corrected Nuclear Gauge Measurements Using Average K-Value of -17.2

Test No.	γ_d (pcf)			w%		
	Avg.	σ	C_v	Avg.	σ	C_v
1	104.6	4.0	0.04	18.8	1.9	0.10
2	104.4	3.1	0.03	19.5	1.7	0.09
3	104.8	2.8	0.03	19.3	0.9	0.05
4	105.4	1.7	0.02	18.8	0.7	0.04
5	106.4	1.9	0.02	18.5	0.9	0.05
6	105.5	2.0	0.02	18.9	1.1	0.06
7	106.7	1.7	0.02	18.3	0.9	0.05
8	106.1	1.3	0.01	19.0	0.8	0.04
9	107.4	1.2	0.01	18.4	0.7	0.04
10	107.0	1.4	0.01	18.6	0.8	0.04
11	106.7	1.9	0.02	18.5	0.9	0.05
12	107.0	2.1	0.02	18.2	1.1	0.06
13	106.3	1.6	0.02	18.7	0.7	0.04
14	106.3	1.4	0.01	18.7	0.9	0.05
15	106.2	1.7	0.02	19.0	1.0	0.05
16	106.5	1.5	0.01	18.4	0.7	0.04
17	107.7	0.7	0.01	18.3	0.5	0.03
18	105.7	1.0	0.01	18.7	0.6	0.03
19	107.1	1.2	0.01	18.4	0.6	0.03
20	106.3	1.2	0.01	18.6	0.5	0.03
21	106.5	1.2	0.01	18.7	0.5	0.03

Table 38 below gives the average results of sand cone and balloon tests on Coastal Plain subgrade. The number of readings (N), standard deviations, and coefficients of variation are also shown. One value of water content is reported since both used a single water content reading from samples sand cone tests. Since the tests were always performed within one foot of each other, the water content should be representative to use for both tests. Balloon tests were not performed until after Test 3.

Table 38. Average Subgrade Dry Unit Weight and Water Content from Sand Cone and Balloon Density Tests

Test No.	Sand Cone				Balloon				w%	σ	C_v
	γ_d (pcf)	σ	C_v	N	γ_d (pcf)	σ	C_v	N			
1	108.3	0.7	0.01	2	N/A	N/A	N/A	0	18.0	2.9	0.16
2	108.3	4.3	0.04	8	N/A	N/A	N/A	0	18.9	0.9	0.05
3	107.5	4.1	0.04	8	N/A	N/A	N/A	0	18.2	0.9	0.05
4	107.8	4.1	0.04	8	105.5	3.3	0.03	8	18.9	0.6	0.03
5	109.2	2.8	0.03	6	111.2	2.6	0.02	6	18.3	0.5	0.03
6	108.7	1.6	0.01	8	112.5	1.8	0.02	8	18.3	0.8	0.04
7	108.9	1.3	0.01	2	106.0	4.1	0.04	2	18.3	0.3	0.02
8	107.4	3.8	0.04	8	100.5	3.2	0.03	8	18.7	0.5	0.03
9	112.2	1.5	0.01	2	102.5	0.6	0.01	2	18.5	0.6	0.03
10	110.5	3.9	0.04	6	100.3	1.6	0.02	6	19.2	0.4	0.02
11	107.5	1.0	0.01	6	98.2	3.2	0.03	6	19.0	0.8	0.04
12	108.1	1.5	0.01	4	96.9	2.3	0.02	4	18.8	0.6	0.03
13	109.5	3.0	0.03	8	95.9	2.7	0.03	8	18.7	0.7	0.04
14	108.5	1.8	0.02	6	96.4	5.6	0.06	6	18.2	1.1	0.06
15	109.7	3.3	0.03	8	118.1	2.8	0.02	8	18.7	1.0	0.05
16	108.0	2.7	0.03	8	109.9	3.1	0.03	8	18.2	0.8	0.04
17	107.5	3.7	0.03	6	108.4	2.9	0.03	6	19.0	0.7	0.04
18	107.8	1.9	0.02	8	106.1	4.3	0.04	8	18.4	0.8	0.04
19	108.1	2.4	0.02	6	104.9	2.7	0.03	6	18.9	0.8	0.04
20	110.1	2.2	0.02	6	111.0	4.6	0.04	6	17.9	0.8	0.04
21	109.8	1.3	0.01	6	112.5	3.5	0.03	6	18.1	1.0	0.06

It can be seen that the standard deviations for sand cone and balloon testing are much higher than nuclear gauge readings. This was partly due to the low number of tests performed in comparison, as well as user's error generally associated with direct measurement methods. A graphical comparison of uncorrected nuclear gauge dry unit weight to both sand cone and balloon measurements is shown below in Figure 66 for all tests. The sand cone density measurements are shown for both of the sand types used. The GS-40 sand did not meet test specifications but that apparently did not greatly affect test results. Ottawa 20-30 sand was used for most of the test sections. Figure 66show an underestimation of dry unit weight by the nuclear gauge compared to the sand cone, as well as scatter in the balloon measurements. The scatter in the balloon density measurements was primarily an artifact of conducting the tests in soft soil. If the balloon was over-inflated, the high pressure exerted on the walls of the excavated hole increased the apparent volume and decreased the calculated dry unit weight. The opposite was true for under-inflated balloons.

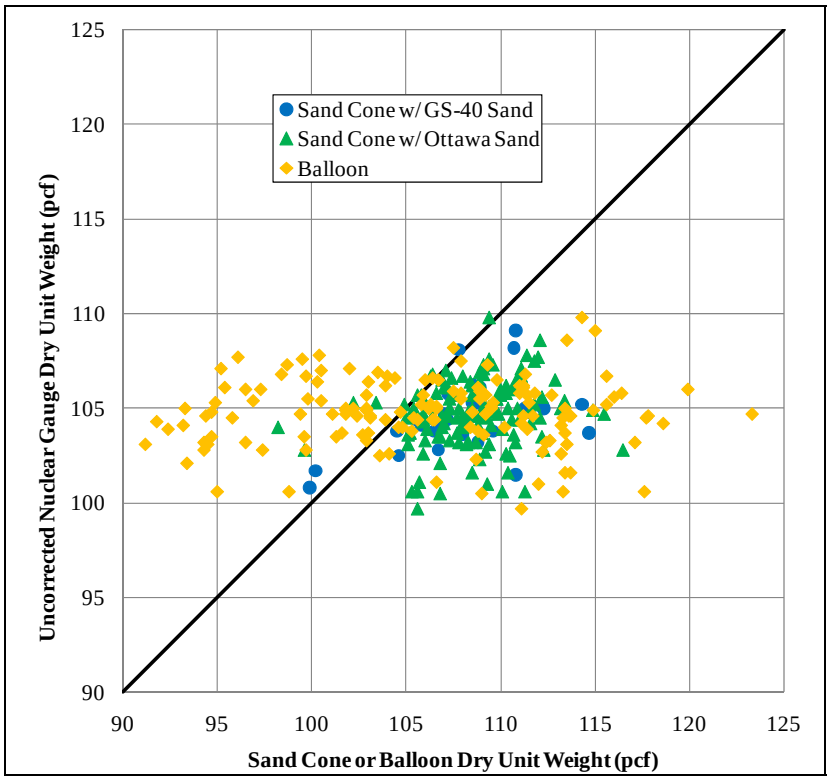

Figure 66. Sand Cone and Balloon versus Uncorrected Nuclear Gauge Dry Unit Weight for Coastal Plain Subgrade

Figure 67 compares oven water content to uncorrected nuclear gauge water content readings. The plot shows that the oven water contents were consistently less than the uncorrected nuclear gauge water content values. The uncorrected nuclear gauge water content readings needed to be reduced (through a K-value) to more accurately measure the true water content. The oven water content readings, although still an experimental measurement, are believed to be a more accurate measure of the true water content in the test pit.

Applying the final averaged K-value of -17.2, Figure 68 shows corrected nuclear gauge water content versus oven water content. In comparison to data in Figure 67, the correction factor reduced the nuclear gauge water content readings much closer to actual values, as shown in Figure 68 . When this was applied to the dry unit weight measurements, as shown in Figure 69, the measured values are also much closer to the sand cone dry unit weights, but still vary widely for the balloon measurements. The relatively large scatter associated with many of the balloon measurements are most likely due to disturbance of the excavated hole by the inflated balloon, which was not an issue with sand cone measurements.

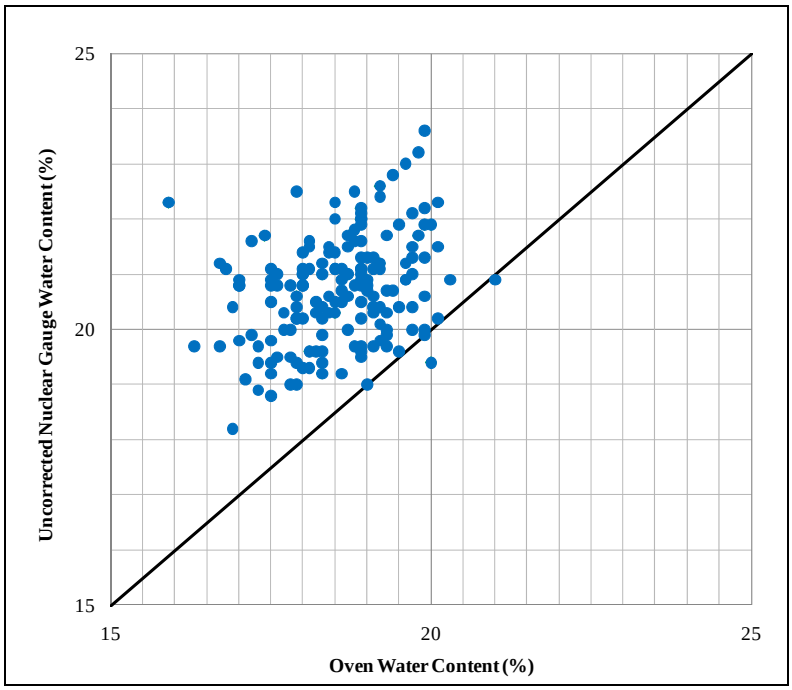

Figure 67. Oven versus Uncorrected Nuclear Gauge Water Content for Coastal Plain Subgrade

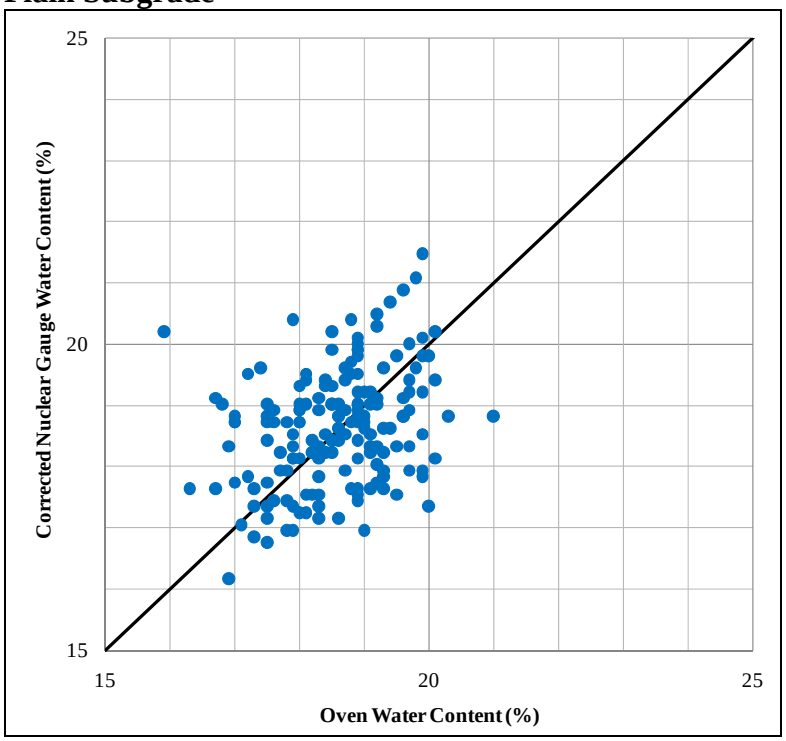

Figure 68. Corrected Nuclear Gauge versus Oven Water Content for Coastal Plain Subgrade

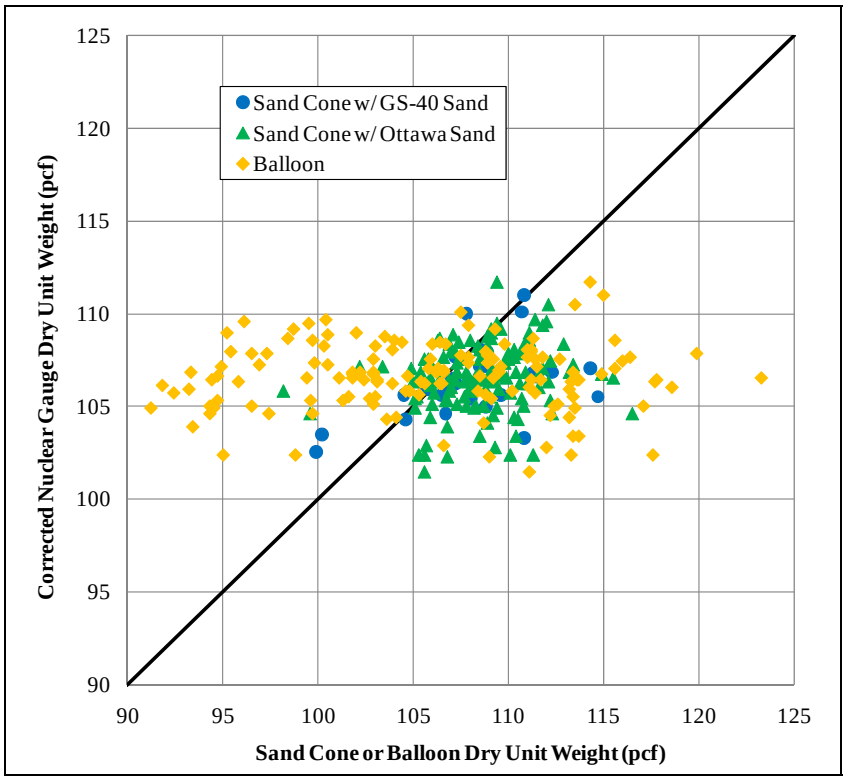

Figure 69. Corrected Nuclear Gauge versus Sand Cone and Balloon Dry Unit Weight for Coastal Plain Subgrade

Dynamic Cone Penetrometer (DCP)

Dynamic Cone Penetrometer (DCP) readings were also taken during each test to provide an indication of sample consistency with depth. The DCP Index (DCPI in mm/blow) was used in conjunction with empirical models to estimate CBR values. Table 39 below gives the average, standard deviation, coefficients of variation, and number of readings for each large scale sample tested Correlated. CBR values are based on the Coonse (1999) and NCDOT (1998) models given previously in Equations 12 and 13. Readings were not taken on Test 12 but can be assumed to be similar to those of Test 11, since it reused the subgrade. Values are not reported for Test 22 since it reused the subgrade and LSS from Test 21. The relatively high standard deviations reflect the user error associated with keeping the DCP oriented vertically during testing. DCP readings were not taken on the ABC layers to prevent damage to the cone tip.

Table 39. Average Coastal Plain Subgrade DCPI

Test No.	Avg. DCPI (mm/blow)	σ	C_v	N	Correlated CBR (%)	
					Coonse (1999)	NCDOT (1998)
1	53.5	8.8	0.16	9	3.6	5.6
2	87.5	8.9	0.10	10	2.1	3.3
3	80.5	8.6	0.11	10	2.3	3.6
4	102.2	6.3	0.06	10	1.7	2.8
5	90.6	14.6	0.16	10	2.0	3.2
6	100.8	14.4	0.14	10	1.8	2.9
7	91.9	5.3	0.06	5	2.0	3.2
8	117.1	13.9	0.12	10	1.5	2.4
9	110.5	8.9	0.08	5	1.6	2.6
10	102.3	7.1	0.07	5	1.7	2.8
11	110.4	26.4	0.24	10	1.6	2.6
12	N/A	N/A	N/A	0	N/A	N/A
13	115.1	13.0	0.11	10	1.5	2.5
14	108.5	16.5	0.15	10	1.6	2.6
15	114.0	16.4	0.14	10	1.5	2.5
16	114.8	10.3	0.09	10	1.5	2.5
17	111.9	13.4	0.12	10	1.6	2.6
18	110.1	15.6	0.14	10	1.6	2.6
19	102.5	9.1	0.09	10	1.7	2.8
20	95.7	12.1	0.13	5	1.9	3.0
21	98.2	9.3	0.09	5	1.8	2.9

Aggregate Base Course (ABC) and Select Fill

All ABC and select fill layers were intended to be placed at optimum water content to achieve the maximum dry unit weight. Table 40 and Table 41 give the average dry unit weight and water content measured from uncorrected nuclear gauge readings for ABC and select fill layers, respectively. The number of tests reflects the depth of the layers. Relative density (D_R) based on maximum dry unit weight of approximately 137.5 pcf is also given.

Table 40. Uncorrected Nuclear Gauge Dry Unit Weight and Water Content of ABC Layers

Test No.	γ_d (pcf)			w%			N	D_R (%)
	Avg.	σ	C_v	Avg.	σ	C_v		
1	116.6	5.3	0.05	5.9	0.4	0.07	9	84.8
2	120.1	4.4	0.04	6.4	0.7	0.11	27	87.3
3	119.5	5.1	0.04	6	0.2	0.03	27	86.9
4	125.8	6.1	0.05	6.4	0.5	0.08	27	91.5
5	128.6	4.1	0.03	6.8	0.3	0.04	9	93.5
6	121.7	6.2	0.05	7.1	0.6	0.08	27	88.5
7	N/A	N/A	N/A	N/A	N/A	N/A	0	N/A
8	N/A	N/A	N/A	N/A	N/A	N/A	0	N/A
9	127.6	2.8	0.02	7.0	0.4	0.06	9	92.8
10	126.6	2.3	0.02	6.6	0.4	0.06	9	92.1
11	128.6	3.3	0.03	6.2	0.2	0.03	9	93.5
12	N/A	N/A	N/A	N/A	N/A	N/A	0	N/A
13	126.7	2.9	0.02	7.1	0.4	0.06	27	92.1
14	126.9	3.3	0.03	7.4	0.2	0.03	18	92.3
15	127.7	2.3	0.02	7.3	0.5	0.07	27	92.9
16	126.4	2.4	0.02	6.1	0.3	0.05	18	91.9
17	127.2	2.8	0.02	6.5	0.3	0.05	18	92.5
18	126.8	2.1	0.02	6.4	0.2	0.03	18	92.2
19	128.8	1.8	0.01	7.9	0.4	0.05	9	93.7
20	126.2	1.8	0.01	6.3	0.3	0.05	9	91.8
21	126.6	2.9	0.02	6.6	0.4	0.06	9	92.1

Table 41. Uncorrected Nuclear Gauge Dry Unit Weight and Water Content of Select Fill Layers

Test No.	γ_d (pcf)			w%		
	Avg.	σ	C_v	Avg.	σ	C_v
7	103.2	2.2	0.02	2.3	0.3	0.13
8	104.8	0.5	0.00	1.9	0.1	0.05
9	103.4	1.0	0.01	3.0	0.4	0.13
10	104.0	1.0	0.01	3.7	0.3	0.08
11	103.2	1.2	0.01	3.7	0.2	0.05

The moisture content of the select fill varied between 2 and 4% because it was stored outside and could not be dried to 2% for Tests 9 through 11. Laboratory testing showed that the optimum dry unit weight and other soil material properties did not change over this range in moisture content, and dry unit weight did not vary significantly between tests.

Data in Table 41show that the select fill was much closer to maximum dry unit weight (105 pcf for 2% moisture and 104 pcf for 4% moisture) than tests with ABC layer (137.5

pcf). The ABC layers were typically much thinner than the select fill layer and therefore it was challenging to compact it over the soft Coastal Plain subgrade. The ABC was also placed slightly over optimum moisture content (approximately 6.0%) because it was stored outside of the laboratory.

Direct measurements of dry unit weight were difficult for ABC and select fill layers. At the recommendation of NCDOT field personnel, sand cone tests were not performed in either layer type because the sand had a tendency to escape into voids, increasing the apparent volume and decreasing the calculated dry unit weight. Balloon tests were also discouraged because the sharp stones in the ABC had a tendency to pop inflated balloons. Balloon tests were performed in the select fill without difficulty, although some values were low from the same over-inflation problems encountered in the Coastal Plain subgrade (cavity expansion in soft soil). Table 42 shows the balloon unit weight data for select fill layers.

Table 43. Balloon Dry Unit Weight and Water Content of Select Fill

Test No.	γ_d (pcf)			w%			N
	Avg.	σ	C_v	Avg.	σ	C_v	
7	103.8	6.0	0.06	2.7	0.2	0.07	4
8	103.3	2.1	0.02	2.0	0.1	0.05	3
9	99.3	2.0	0.02	3.7	0.4	0.11	6
10	96.4	3.5	0.04	4.4	0.3	0.07	4
11	88.0	1.3	0.01	4.4	0.1	0.02	2

Similar to Coastal Plain subgrade, the oven water content values were compared to uncorrected nuclear gauge readings for the ABC and select fill. The combined data are presented in Figure 70. It can be seen that neither soil type required a correction factor. The average calculated K-values were only -1.8 and 4.0 for ABC and select fill, respectively. Thus, K-values were not used. The uncorrected nuclear gauge water content and dry unit weight are graphed versus the balloon measured values for both soil types in Figure 70 and Figure 71.

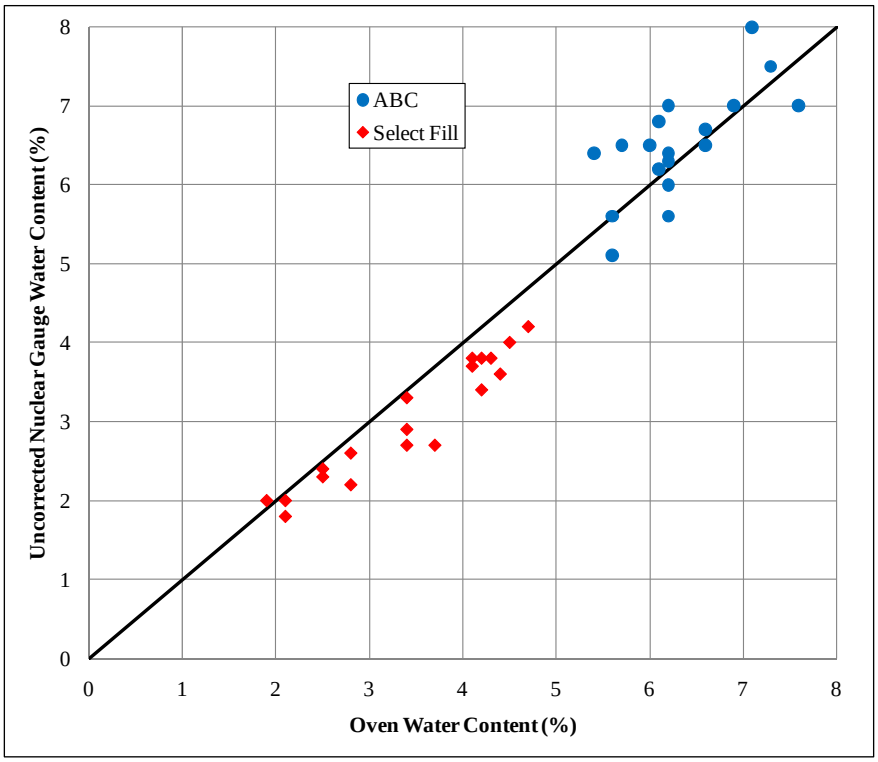

Figure 70. Uncorrected Nuclear Gauge versus Oven Water Content

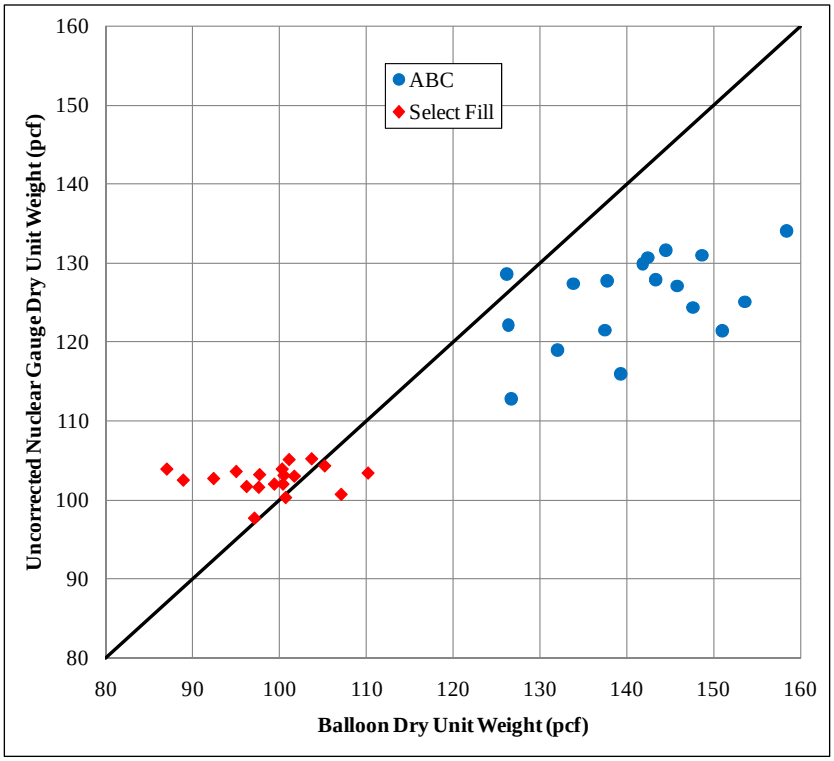

Figure 71. Uncorrected Nuclear Gauge vs. Balloon Dry Unit Weight :ABC and Select Fill

Lime Stabilized Subgrade (LSS)

Quality control of the LSS was performed before it was placed into the test pit. This included oven water content and grain size tests to determine change in water content and gradation during mellowing. Table 44 presents the average oven water content values of Tests 19 through 21. Values for Test 22 are not reported since it used the same LSS as Test 21. Percent change is based on the water content before mellowing. The water content before mellowing reflects the same water content as untreated subgrade to simulate placement of lime stabilization in the field.

Table 45 gives the average percent passing compared to NCDOT specifications. Tests 19 and 20 used Coastal Plain LSS, while Test 21 (and 22) used gray LSS, as previously described in Chapter 3. LSS quality control data are reported in Appendicies B and C.

Table 44. Average Oven-Water Content of LSS Before and After Mellowing

Test No.	Before (%)	After (%)	% Change
19	18.8	18.4	2.1
20	18.9	16.2	14.3
21	19.1	18.3	4.2

Table 45. Average Percent Passing of LSS After Mellowing Compared to NCDOT Specifications

Sieve No.	NCDOT Spec.	Test 19 (%)	Test 20 (%)	Test 21 (%)
1/2"	100.0	86.4	86.4	94.7
#4	80.0	36.9	35.3	50.8

Test 19 mellowed only for 1 day. Mellowing was increased to 3 days for Tests 20 and 21 to allow the water content to decrease closer to optimum (approximately 16.0% for Coastal Plain LSS and 15.4% for gray LSS) and to allow the clay particles to further breakdown to meet gradation specifications. It can be seen that prolonged mellowing helped water content reduce for Test 20, but a significant decrease was not seen for Test 21 with gray LSS. This was probably a result of the finer gradation of the gray subgrade in comparison to the Coastal Plain subgrade used in the first 20 tests.

For Tests 20 and 21, the grain size distribution was not significantly improved by increasing the mellowing period. This was mainly an artifact of the tilling equipment used in the laboratory, which had much less power than field rotovators. After mellowing, the LSS was compacted in the test pit and tested by nuclear gauge, sand cone, and balloon methods for dry unit weight and water content. There were too few tests to accurately determine a K-value to change uncorrected nuclear gauge water content measurements, so Table 46 gives the corrected nuclear gauge measurements using the Coastal plain subgrade K-value of -17.2. Table 47 presents the combined sand cone and balloon test values. Balloon tests were not performed on Test 19.

Table 46. Corrected Nuclear Gauge Dry Unit Weight and Water Content of LSS

Test No.	γ_d (pcf)			w%			N	K
	Avg.	σ	C_v	Avg.	σ	C_v		
19	101.4	4.0	0.04	21.7	1.4	0.06	9	-17.4
20	97.8	5.7	0.06	19.1	1.8	0.09	9	-17.4
21	104.3	2.4	0.02	18.9	0.6	0.03	9	-17.4

Table 47. Sand Cone and Balloon Dry Unit Weight and Water Content of LSS

Test No.	Sand Cone				Balloon				w%	σ	C_v
	γ_d (pcf)	σ	C_v	N	γ_d (pcf)	σ	C_v	N			
19	104.6	5.3	0.05	2	N/A	N/A	N/A	0	20.0	0.3	0.02
20	104.9	1.0	0.01	2	61.0	0.8	0.01	2	15.1	0.2	0.01
21	99.2	2.0	0.02	2	108.7	2.4	0.02	2	18.1	0.4	0.02

Nuclear gauge measurements of the LSS were inconsistent because the jumping-jack rammer left the LSS surface uneven. The nuclear gauge required flat surfaces for accurate measurements. Sand cone and balloon tests results were also sporadic because digging test cavities in the dense LSS was extremely difficult. In most instances, the cavity was unable to meet ASTM specifications for minimum volume.

As previously stated, the lime percentage of the in-place LSS was not checked. Rather, UCS specimens were prepared, tested, and compared to laboratory test values. Preliminary calculations of lime quantities were still performed, though. It was determined that approximately three 50 pound bags were needed for the thicknesses of LSS prescribed.

Table 48 gives the test pit (grab sample before compaction) UCS versus the laboratory test values. All values are averages of two tests. The percent difference is based on the laboratory value.

Table 48. Test Pit Versus Laboratory 7-day UCS for LSS

Test No.	Test Pit (psi)	Laboratory (psi)	% Difference
19	53.8	97.2	- 44.7
20	111.3	97.2	14.5
21	52.4	117.8	- 55.5

It can be seen that the increased mellowing period between Tests 19 and 20 led to an increase in the UCS beyond laboratory values for Test 20. However, the high water content after mellowing in Test 21 resulted in a low test pit UCS. Although longer mellowing periods would have helped decrease the water content, the NCDOT only recommends mellowing periods between 1 and 4 days.

DCP readings were taken on the LSS after loading to avoid compromising the layer integrity. Table 49 gives the average DCPI values for each test and correlated CBR

values, even though the correlations may not be appropriate for LSS. A decreased DCPI can be seen for Test 20 versus Test 19 due to the longer mellowing period and an increased compactive effort. Test 21 had a comparatively high DCPI, matching the low UCS from Table 48.

Table 49. LSS Average DCPI

Test No.	Avg. DCPI (mm/blow)	σ	C_v	N	Correlated CBR (%)	
					Coonse (1999)	NCDOT (1998)
19	17.8	1.0	0.06	5	12.8	18.3
20	9.5	0.5	0.05	5	26.0	35.8
21	19.8	1.0	0.05	5	11.3	16.3

Section Reuse

Several of the sections reused the Coastal Plain subgrade from the previous test to expedite the testing program. This was done by excavating half of the previous test (down to 2 feet) and replacing it with 2 feet of newly prepared subgrade. This was not done for more than two consecutive tests (in other words, the subgrade was completely rebuilt every other test). Table 50 gives the corrected nuclear gauge readings of the tests that reused Coastal plain subgrade. Table 51 gives the same data for sand cone and balloon tests, and Table 52 does so for DCP results. The "previous test" values are the layer averages of the prior test, while the "reused values" are the averages of measurements made on the subgrade after the half of the previous test was removed before replacing with new subgrade.

Test 12 (subgrade only test) reused 4 feet of subgrade from Test 11 with an extra foot of new subgrade placed on top of it. For each reuse, there was an expected reduction in water content and increase in dry unit weight. The percent change is based on the previous test value. The change in dry density was a result of loading and overburden of placed layers. The low percent change values justify the reuse of subgrade in that it was not significantly denser or drier than the previous test. The reused subgrade was also far enough away from load application to not significantly influence test results.

Table 50. Corrected Nuclear Gauge Dry Unit Weight and Water Content Values for Tests with Reused Test Section

Test No.	Previous Test				Reused Value				% Change	
	γ_d (pcf)	σ	w%	σ	γ_d (pcf)	σ	w%	σ	γ_d (pcf)	w%
5	106.2	1.5	18.3	0.6	107.9	2.1	17.8	0.9	1.6	-2.7
7	104.6	1.9	19.4	0.9	106.7	1.7	18.3	0.9	2.0	-5.7
9	106.5	1.7	18.5	0.9	107.4	1.2	18.4	0.7	0.8	-0.5
11	107.9	1.3	18.1	0.6	107.9	2.3	17.8	1.0	0.0	-1.7
12	106.9	1.4	18.6	0.6	108.5	1.7	17.3	0.8	1.5	-7.0
14	106.7	1.4	18.4	0.7	107.2	1.3	17.9	0.6	0.5	-2.7
17	106.1	1.0	18.8	0.6	107.9	0.7	18.0	0.5	1.7	-4.3
19	106.6	0.8	18.2	0.4	107.9	0.7	18.1	0.5	1.2	-0.5

Table 51. Sand Cone and Balloon Dry Unit Weight and Water Content Values Loading for Tests with Reused Test Section

Test No.	Previous Test						Reused Value						% Change		
	$\gamma_{d,SC}$ (pcf)	σ	$\gamma_{d, Ball}$ (pcf)	σ	w%	σ	$\gamma_{d,SC}$ (pcf)	σ	$\gamma_{d, Ball}$ (pcf)	σ	w%	σ	$\gamma_{d,SC}$ (pcf)	$\gamma_{d, Ball}$ (pcf)	w%
5	108.7	2.5	104.2	0.8	19.7	0.6	108.3	1.5	110.1	2.3	18.5	0.2	-0.4	5.7	-6.1
7	108.9	0.6	112.7	1.0	17.5	0.5	108.9	1.3	106.0	4.1	18.3	0.3	0.0	-5.9	4.6
9	109.7	1.7	102.0	0.3	18.5	0.7	112.2	1.5	102.5	0.6	18.5	0.6	2.3	0.5	0.0
11	108.2	0.3	100.0	0.4	19.0	0.2	107.6	1.7	100.7	3.2	18.1	0.2	-0.6	0.7	-4.7
12	107.4	0.4	98.1	3.3	19.3	0.1	109.2	0.2	97.3	3.0	18.8	0.1	1.7	-0.8	-2.6
14	106.8	4.8	93.6	1.7	18.6	0.4	109.8	1.4	93.8	0.8	17.7	0.2	2.8	0.2	-4.8
17	105.0	0.1	107.5	2.3	19.4	0.2	107.0	0.5	109.4	2.2	19.5	0.3	1.9	1.8	0.5
19	108.6	1.1	110.0	4.8	18.1	1.5	106.4	1.2	107.3	2.0	18.3	0.7	-2.0	-2.5	1.1

Table 52. DCPI for Tests with Reused Test Section

Test No.	Previous Test				Reused Value				% Change in DCPI
	Avg. DCPI (mm/blow)	σ	Correlated CBR (%)		Avg. DCPI (mm/blow)	σ	Correlated CBR (%)		
			Coonse (1999)	NCDOT (1998)			Coonse (1999)	NCDOT (1998)	
5	97.2	4.3	1.8	3.0	77.3	4.9	2.4	3.8	-20.5
7	112.5	7.9	1.6	2.5	92.0	5.3	2.0	3.2	-18.2
9	127.2	5.7	1.4	2.2	110.5	8.9	1.6	2.6	-13.1
11	102.3	7.1	1.7	2.8	85.5	4.1	2.1	3.4	-16.4
12	135.3	4.0	1.3	2.1	109.6	6.9	1.6	2.6	-19.0
14	119.5	11.6	1.5	2.4	110.9	15.8	1.6	2.6	-7.2
17	115.3	11.7	1.5	2.5	112.0	9.8	1.6	2.6	-2.9
19	99.3	0.7	1.8	2.9	96.3	0.4	1.9	3.0	-3.0

Subgrade Remolding

The Coastal Plain subgrade sample (approximately 9 yd^3) was reused throughout the testing program. The question arose of what effect tilling, compacting, and excavation over the course of 22 tests had on the subgrade strength. This first became apparent upon the analysis of the corrected nuclear gauge and DCP data presented in Figure 72 and Figure 73, respectively. It can be seen that, for fairly constant water content, the dry unit weight and DCPI both increased over the first seven tests, and then remained fairly consistent throughout the remainder of testing.

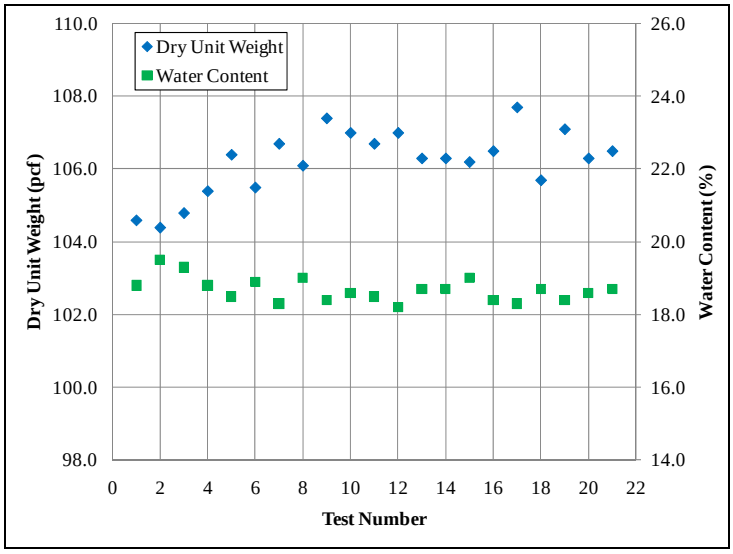

Figure 72. Corrected nuclear gauge dry unit weight and water content versus test number

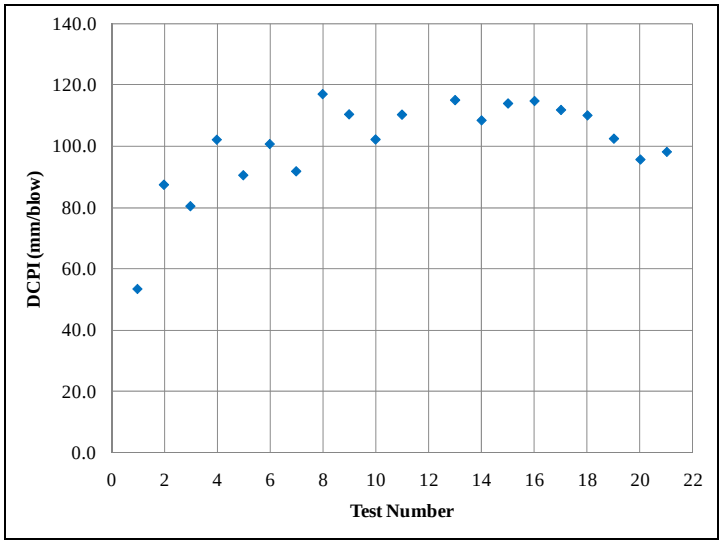

Figure 73. Coastal Plain subgrade DCPI versus test number

To quantify the change in undrained shear strength over the course of testing, additional CU triaxial tests were performed on the Coastal Plain subgrade at the end of testing in June 2009 by Pyo (2009). The Mohr-Coulomb strength parameters compared to the June 2008 values are compared below in Table 53, and the undrained shear strength for various confining pressures are given in Figure 74. The data show an approximate 30% decrease in undrained shear strength over the testing program.

Table 53. Coastal Plain Subgrade Mohr-Coulomb Strength Parameters from CU Triaxial Testing performed by Pyo (2009)

	Effective Stress		Total Stress	
	c' (psi)	phi' (deg)	c (psi)	phi (deg)
June 2008	0	34.5	5.7	19
June 2009	0	37	3.6	15

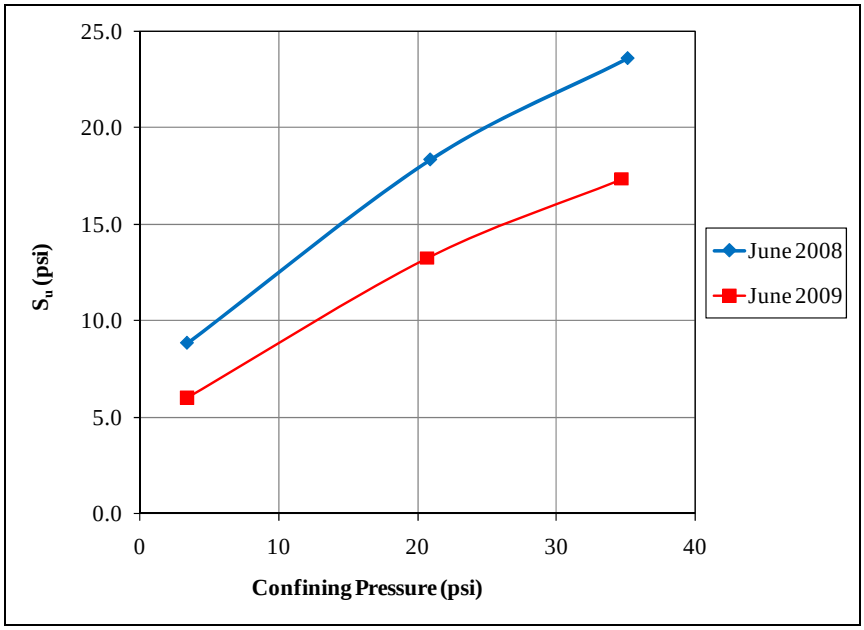

Figure 74. Coastal Plain Subgrade Undrained Shear Strength (S_u) for various confining pressures from CU Triaxial Testing performed by Pyo (2009)

While changes in strength between each individual test cannot be quantified, tilling, compacting, and excavation of the same Coastal Plain subgrade over the 22 test program caused a higher increase in pore-water pressure under loading. This reduced the undrained shear strength and the total stress Mohr-Coulomb strength parameters, while increasing the effective friction angle. The resulting quality control testing showed a higher DCPI, corresponding to less resistance to the DCP cone tip under penetration. The higher dry unit weight also suggests a more efficient particle arrangement in the remolded state. While most of this remolding apparently over the first seven tests, it cannot be proven with laboratory test data. The later tests would have an apparently weaker subgrade under cyclic loading, which will be important during analysis later.

ABC Gradations

The grain size distribution of the ABC was monitored throughout testing to quantify any degradation that may have occurred from compaction or loading. Samples were taken from within the layer after testing at a location beneath the load plate. Figure 75 shows the gradations measured for Tests 2 through 6. The NCDOT specification bounds are also given. According to data in Figure 10, the ABC seems to have lost fines as testing progressed. It was thought that this was due to outdoor stockpiling of the material and loss of fines due to precipitation (even though it was covered). Thus, a new batch of ABC was ordered and delivered to the laboratory in August 2008 after Test 6. Analyses were not performed for Tests 7 through 11 since they only had thin surface lifts of ABC over select fill.

Test 14 was the first test with the new ABC to have a measured gradation. Figure 76 shows that Test 14 contained less fines than expected even though it was performed not long after the delivery of the new ABC. This raised questions about the grain size sieving technique. Previously, ABC fines that had conglomerated after oven drying were simply pulverized with a pestle and mortar. For Test 15, the ABC was wash sieved through a #200 sieve after oven drying. This helped release fines adhered to larger particles and brought the gradation curve closer to the original line. Wash sieving was performed for the remaining tests. The gradation curves for Tests 15 through 21 show that the material did not fall out of specification as previously suspected, and that little degradation of ABC was measured. Small variations are due to sample differences rather than degradation.

Whether or not degradation occurred in Tests 2 through 6 is uncertain but doubtful since it was from the same quarry and did not increase in fines content (even though wash sieving was not performed to accurately determine this). One would have expected for the fines content to at least remain constant if degradation was occurring

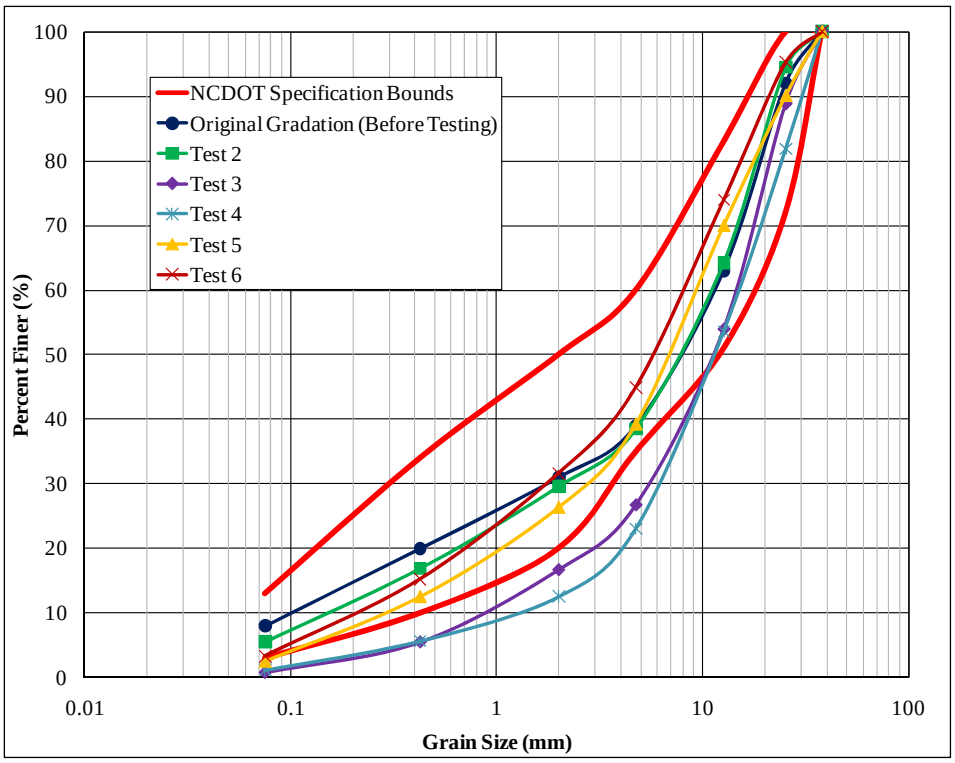

Figure 75. ABC Gradations for Tests 2 through 6

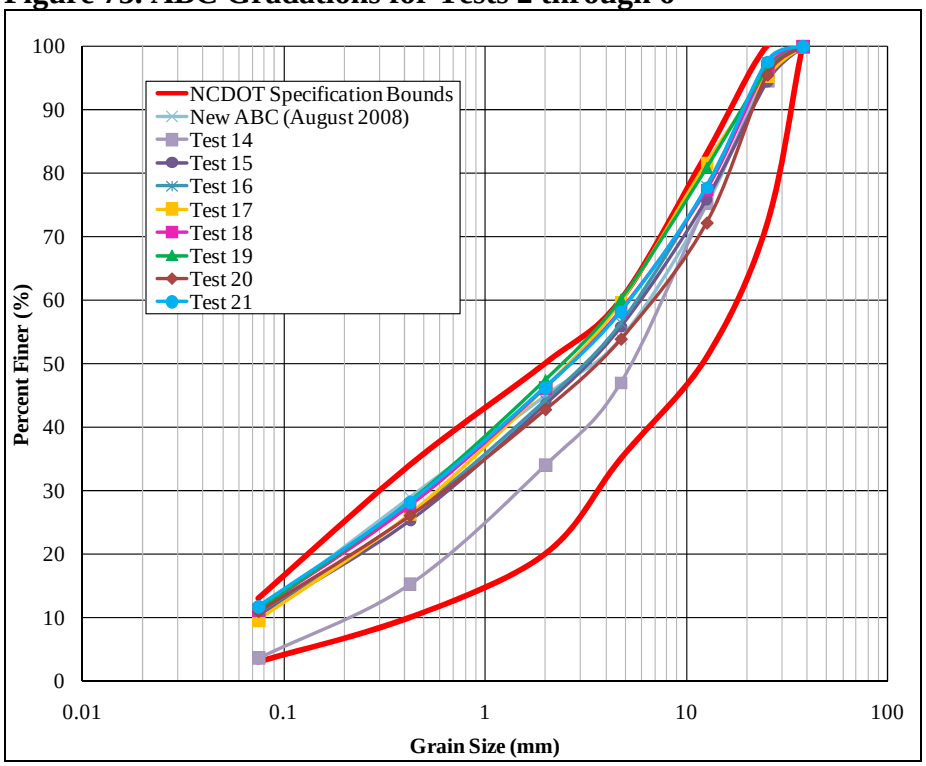

Figure 76. ABC Gradations for Tests 14 through 21

Summary

This chapter has described the quality control efforts performed on this project. The calibration of the nuclear density gage water content and unit weight for coastal plain subgrade, select fill and ABC were described. Granular material showed close correlation between oven dried and nuclear density gage water content, while the bulk of the corrected water contents from the coastal plain subgrade were within approximately +/- 1% of the oven dried water content. Sand cone density tests on the subgrade also compared relatively well with nuclear density gage dry density, particularly once enough data was collected to determine a stable correction factor for the nuclear density gage readings. On average, nuclear density gage readings tended to be between +2 and -5 pcf of the sand cone test results. Balloon density tests on both subgrade and granular materials were highly variable compared to both sand cone and nuclear density gage density tests.

The effects of subgrade remolding (i.e. higher measured dry density, lower CBR and lower shear strength as the soil was reused and remolded) was also described. The quality control data indicated an approximately 30% decrease in shear strength over the first seven to eight test sections. ABC Gradations were also shown to be consistent throughout the tests in which ABC stabilized sections were used.

CHAPTER 7: TESTING RESULTS

Static Load-Deformation Response

The center load plate displacements during static testing are presented below in Table 54. The values at each load increment are after reaching steady state displacement per ASTM D 1196 and calculated from the average of the three string-pots attached to the load plate. The table gives cumulative (from the start of static load testing), incremental (during that load increment), and resilient (amount recovered after unloading) displacements for each applied pressure. Unlike the other tests, Test 3 was not unloaded back to residual load (250 pounds) between static load increments.

In addition to results of each static load test (as presented in Table 54) surface deformation graphs for each test (similar to data in Figure 77), as well as vertical pressure distributions from all buried EPC measurements (similar to data in Figure 78) are presented in Appendix C. The connected data points on the left side of Figure 77 denote the deformation associated with the load plate. The load plate extends from -6 to +6 inches on the radial distance axis (x). Because the plate deformation was usually greater than the soil deformation from short long-fellow measurements (on the right side of the figure), the two sets of data were not connected with a line to avoid confusion.

For data in Figure 78, the EPC measurements are connected with lines that do not extend to the surface (depth 0 inches). The surface point only shows the applied surface pressure and is thus not associated with EPC stress distribution. The EPC's were zeroed before the start of static testing and thus denote an increase in vertical stress not accounting for geostatic stresses. The dark horizontal line in Figure 78 denotes the ABC-subgrade layer interface, at the bottom of the ABC, from measured layer thicknesses.

Table 54. Static Load Test Plate Displacements (inches)

Pressure	10 psi			20 psi			30 psi			40 psi		
Test No.	Cumul.	Increm.	Resil.	Cumul.	Increm.	Resil.	Cumul.	Increm.	Resil.	Cumul.	Increm.	Resil.
1	N/A	N/A	N/A	0.155	0.155	N/A	0.216	0.061	N/A	0.314	0.098	N/A
2	N/A	N/A	N/A	N/A	N/A	N/A	N/A	N/A	N/A	N/A	N/A	N/A
3	0.009	0.009	N/A	0.032	0.022	N/A	0.048	0.017	N/A	0.063	0.015	N/A
4	0.022	0.022	0.011	0.060	0.037	0.023	0.091	0.032	0.036	0.132	0.040	0.045
5	0.007	0.007	0.010	0.035	0.027	0.025	0.078	0.044	0.043	0.133	0.054	0.053
6	0.010	0.010	0.010	0.014	0.005	0.022	0.020	0.005	0.033	0.030	0.010	0.046
7	0.006	0.006	0.010	0.038	0.032	0.020	0.075	0.036	0.027	0.118	0.044	0.037
8	0.003	0.003	0.015	0.013	0.010	0.016	0.043	0.030	0.022	0.076	0.033	0.035
9	0.013	0.013	0.010	0.031	0.018	0.025	0.053	0.023	0.033	0.078	0.024	0.043
10	0.004	0.004	0.008	0.009	0.005	0.015	0.020	0.011	0.027	0.046	0.026	0.035
11	0.016	0.016	0.004	0.048	0.033	0.015	0.087	0.039	0.027	0.135	0.048	0.042
13	0.014	0.014	0.008	0.032	0.018	0.020	0.054	0.023	0.035	0.085	0.031	0.050
14	0.034	0.034	0.008	0.090	0.055	0.026	0.153	0.063	0.045	0.235	0.082	0.057
15	0.037	0.037	0.012	0.087	0.050	0.029	0.134	0.047	0.044	0.181	0.047	0.062
16	0.005	0.005	0.010	0.031	0.026	0.027	0.079	0.048	0.046	0.152	0.073	0.066
17	0.028	0.028	0.009	0.066	0.038	0.031	0.122	0.055	0.053	0.188	0.067	0.079
18	0.022	0.022	0.009	0.057	0.035	0.026	0.102	0.046	0.044	0.173	0.070	0.064
19	0.033	0.033	0.005	0.064	0.031	0.010	0.087	0.023	0.023	0.106	0.019	0.030
20	0.027	0.027	0.010	0.044	0.016	0.015	0.054	0.010	0.022	0.067	0.013	0.029
21	0.018	0.018	0.007	0.027	0.009	0.016	0.038	0.011	0.029	0.054	0.017	0.040

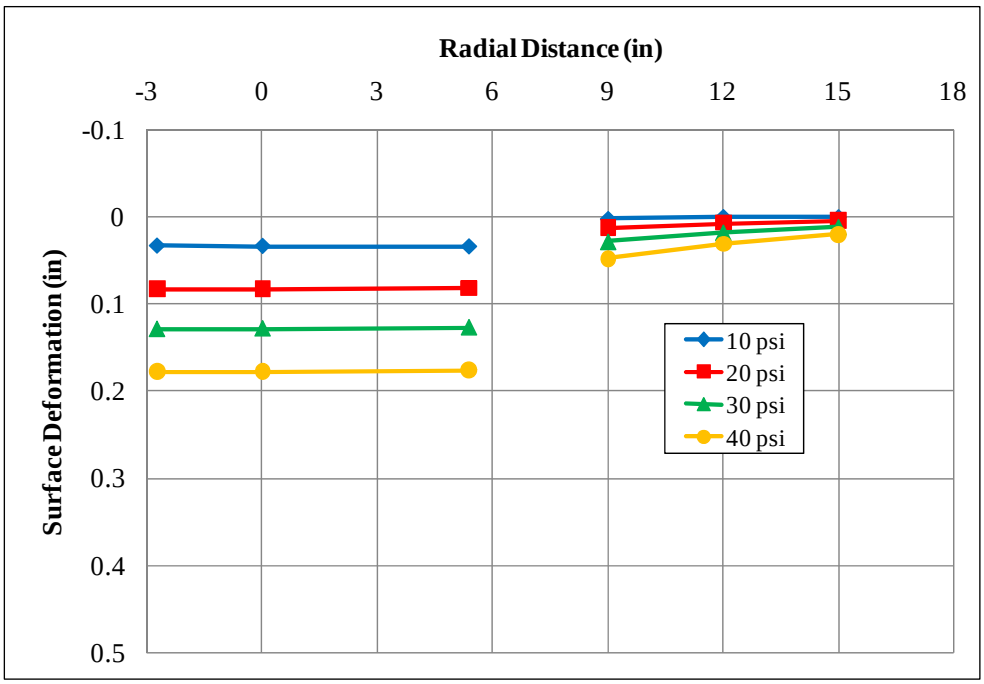

Figure 77 Static Load Test Surface Displacement for 16" ABC with Geogrid B (4) Test Section

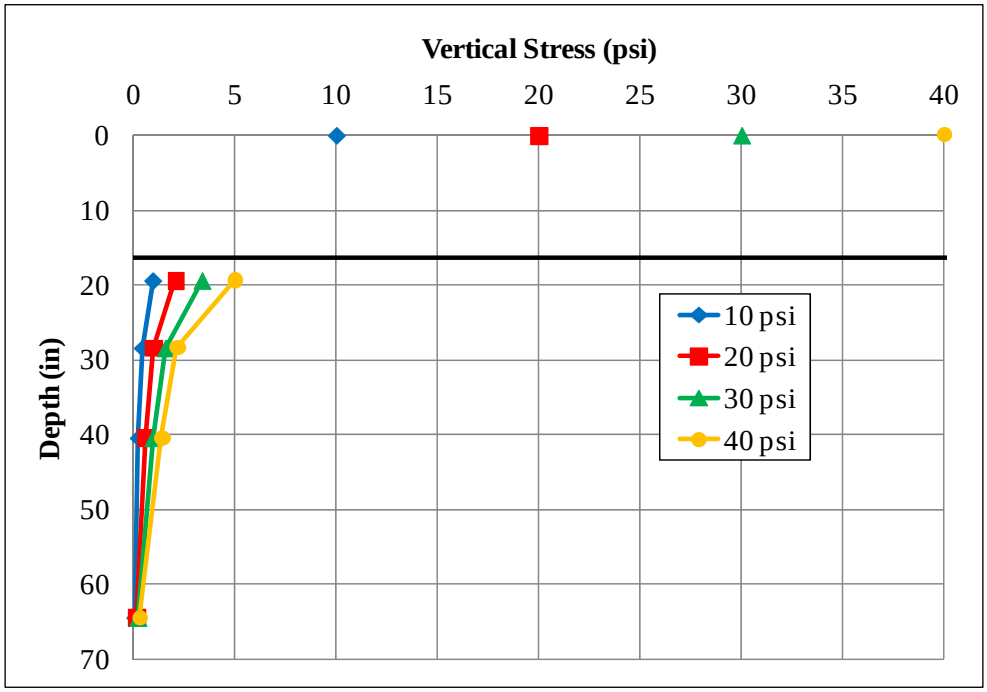

Figure 78 Static Load Test Vertical Stress Increase Distribution for 16" ABC with Geogrid B (4) Test Section

BEARING CAPACITY TESTS

Static load tests were also performed on several sections to evaluate subgrade to failure. These tests were loaded past the typical 40 psi load increment to either sudden bearing capacity failure or until deformation rates were dramatically high.

Table 55 presents the cumulative displacements at each applied pressure for the material level tests. The first test (called Test 9a) was performed after Test 9 is completed by removing the 3 inch ABC layer that was placed over 36 inches of select fill. The select fill was loaded until bearing capacity failure occurred at approximately 130 psi of applied pressure. Another test was performed on Coastal Plain subgrade (Test 12) by statically loading the prepared samples to 80 psi. At that load, significant punching of the plate had occurred and deformation was nearing 3 inches.

Table 55. Cumulative Displacements (inches) Bearing Capacity Tests

Applied Pressure (psi)	Test 9a	Test 12	Test 22
10	0.033	0.038	0.006
20	0.089	0.111	0.020
30	0.122	0.190	0.036
40	0.153	0.271	0.053
50	0.185	0.545	0.103
60	0.219	1.007	0.125
70	0.255	1.965	0.157
80	0.296	2.954	0.192
90	0.343	-	0.271
100	0.395	-	0.395
110	0.471	-	0.669
120	0.577	-	1.032
130	0.739	-	-
130	-	-	-

Lastly, a static test was performed on 9 inches of gray LSS after removing 4 inches of ABC; this was a sequence of Test 21, and is labeled as Test 22. The sample was loaded up to 120 psi before deformation rates continued to increase.

For Test 9a, displacement measurements were only taken with the actuator internal LVDT to avoid breaking instrumentation during a sudden bearing capacity failure. However, string-pots were kept on for Tests 12 and 22 because the strain rates close to failure were much slower. Appendix C presents the surface deformation and vertical stress increase with depth values, as well remaining tabulated data for these static load tests. The scales vary between these graphs because of the wide range of deformations and pressures that occurred.

Static Analysis

Static plate load testing per ASTM D 1196 are commonly performed to determine the coefficient or modulus of subgrade reaction (k). The value is the applied pressure divided by the steady state deformation and typically has units of psi/in. Subgrade reaction moduli are commonly used in rigid pavement designs when PCC pavement is placed directly on subgrade. The values are the stiffness of springs that are modeled as the support system for slabs on grade.

Subgrade reaction moduli were calculated in this study as secant moduli from the start of testing to the end of each increment. The slope of this line on an applied pressure-deformation plot is the modulus value. Because these tests were unloaded back to 0 psi between each increment, subgrade reaction moduli were also calculated on an incremental basis using the restart of loading. An unloading modulus was also calculated by using the 0 psi value of each load increment. Figure 79 shows how each modulus was calculated. The moduli are referred to as “Initial Subgrade Modulus”, “Incremental Subgrade Modulus”, and “Unloading Subgrade Modulus”. The initial and incremental subgrade moduli are the same over the first load interval.

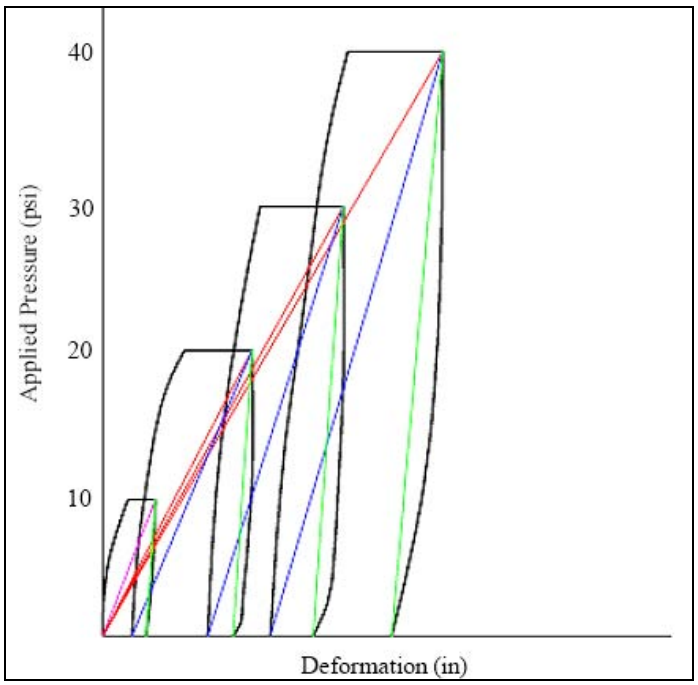

Figure 79. Initial (red), Incremental (blue), and Unloading (green) Subgrade Reaction Modulus (k, psi/in) Calculation

Upon analysis of the calculated values, it was apparent that for many tests that the initial subgrade reaction moduli increased between 10 and 20 psi and then decreased for the remaining increments. This also occurred for the incremental moduli. Although a portion of this may be due to the recovered deformation during unloading, this is counter intuitive in the context of data presented in Figure 79. Since the 10 psi increment was the first load applied

to the test sections, the logical explanation was that seating effects caused significant plate movements that decreased reaction moduli values.

To address this effect, the origin point was changed to the end of the 10 psi increment rather than using the start of testing to calculate the initial subgrade modulus. The calculated initial subgrade reaction moduli are presented in Table 56. The revised subgrade moduli could not be calculated for Tests 1, 2, and 3 because they were not unloaded back to zero. The initial values tared at 10 psi now match the incremental subgrade reaction moduli during the 20 psi load increment. Subgrade reaction values and both initial and incremental subgrade reaction moduli are presented in Appendix C.

Table 56. Estimated Initial Subgrade Moduli (psi/in)

Test/Pressure	20 psi	30 psi	40 psi
16" ABC with Geogrid B (4)	307	271	243
14" ABC (5)	353	246	215
19" ABC with Geotextile A (6)	668	636	550
36" Select Fill (7)	338	290	251
17" Select Fill/3" ABC with Geotextile A (8)	674	450	336
36" Select Fill/3" ABC (9)	411	376	351
25" Select Fill/3" ABC with Geotextile B (10)	860	636	486
14" Select Fill/3" ABC with Geotextile A (11)	378	282	232
Subgrade (12)	179	161	139
20" ABC with Geotextile B (13)	462	369	305
13" ABC with Geotextile B (14)	219	170	147
18" ABC (15)	214	195	183
13" ABC with Geotextile A (16)	332	232	175
11" ABC with Geogrid A (17)	256	190	158
12" ABC with Geotextile A (18)	296	223	176
12" LSS/5" ABC (19)	434	362	366
9" LSS/4" ABC (20)	567	578	537
9" Gray LSS/4" ABC (21)	713	564	492
9" Gray LSS (22)	1087	836	751

The static load data from Test 22 is given between 0 to 40 psi and then reloaded again starting at 50 psi. Sorting of performance response is performed using the data in Table 56 to determine the stiffest test sections. Comparing the reaction moduli at 40 psi (in order to eliminate any effects caused by seating the plate at the lower load increments) yield the highest k value of 751 psi/in for the 9" Gray LSS (test 22) and the lowest of 139 psi/in for the subgrade soil. From a chart presented by Huang (1993), the range of subgrade reaction moduli correspond to CBRs between 85% and 4.5% for the 9 inch gray LSS and subgrade only static tests, respectively.

The vertical stress increase measurements near the top of the Coastal Plain subgrade layer, under the applied pressure of 40 psi, are plotted on a two-layered system graph presented in Poulos and Davis (1974) based on Fox (1948). This gives an equivalent E_1/E_2 ratio for each test even though the tests did not necessarily have two layers and often contained geosynthetics. The values of h are based on the measured layer thicknesses, and 'a' represents the plate radius of 6 inches. Table 57 gives the calculated E_1/E_2 for each test.

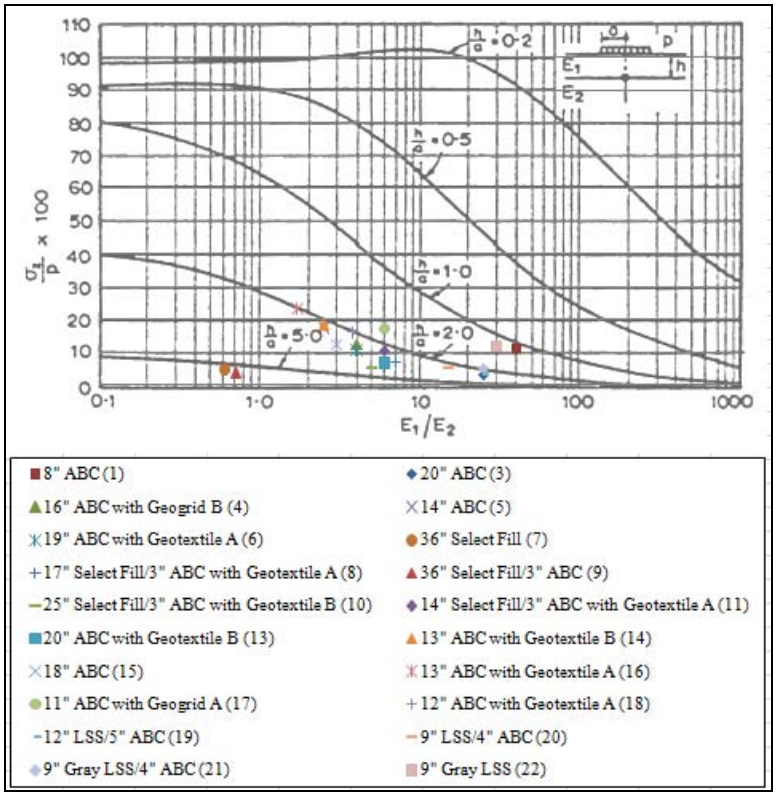

Figure 80. Static Test Data at 40 psi Plotted on Fox (1948) Graph

Data in Table 57 show that the E_1/E_2 of ABC over subgrade ranged from 2.5 to 40. Tests 5 and 15 yielded similar values (2.5 and 3.0). For all ABC depths, geosynthetic reinforcement increased the ratio to values typically between 4.0 and 6.0 (with some lower exceptions). Geosynthetic-reinforced select fill (between 14 and 25 inches) with thin ABC surface layers yielded ratios between 5.0 and 7.0 while unreinforced select fill (36 inches) with and without ABC had ratios less than 1.0. A modulus ratio less than one designates that most of the deformation occurred in the upper layer, and therefore the lower modulus in comparison to the subgrade value. All LSS and thin ABC layer tests had high ratios between 15.0 and 30.0. In all cases except for the deep select fill, the stabilization provided a stiffer response to loading than pure subgrade.

Proof-Roll Loading

Two simulated proof-roll, pulses were applied to the test sections after static loading and before the first 10,000 cycle increment, and then again (two pulses) after the rut from the first cyclic increment had been refilled with material and compacted. These were done to simulate

inspection immediately after subgrade stabilization and after grading, or may be repairs, had been made to a pavement section that had seen construction traffic, respectively.

Table 57. Layered Elastic Analysis of Static Test Results: 40 psi using Fox (1948) Graph

Test Configuration (Test No.)	h (in)	h/a	Measured σ (psi)	(σ/p) *100	E_1/E_2
8" ABC (1)	7.7	1.3	4.5	11.3	40.0
20" ABC (3)	19.8	3.3	3.2	8.0	25.0
16" ABC with BX1100 (4)	16.4	2.7	5.0	12.5	4.0
14" ABC (5)	13.5	2.3	7.0	17.5	2.5
19" ABC with HP570 (6)	19.0	3.2	4.3	10.8	4.0
36" Select Fill (7)	35.8	6.0	1.9	4.8	0.6
17" Select Fill/3" ABC with HP570 (8)	19.9	3.3	2.8	7.0	7.0
36" Select Fill/3" ABC (9)	39.0	6.5	1.6	4.0	0.7
25" Select Fill/3" ABC with HP270 (10)	27.6	4.6	2.1	5.3	5.0
14" Select Fill/3" ABC with HP570 (11)	17.3	2.9	4.2	10.5	6.0
20" ABC with HP270 (13)	20.2	3.4	2.7	6.8	6.0
13" ABC with HP270 (14)	12.7	2.1	7.4	18.5	2.5
18" ABC (15)	17.9	3.0	5.0	12.5	3.0
13" ABC with HP570 (16)	12.9	2.2	9.3	23.3	1.7
11" ABC with BX1500 (17)	10.7	1.8	6.9	17.3	6.0
12" ABC with HP570 (18)	12.4	2.1	6.4	16.0	3.8
12" LSS/5" ABC (19)	17.2	2.9	1.4	3.5	25.0
9" LSS/4" ABC (20)	13.7	2.3	2.1	5.3	15.0
9" Gray LSS/4" ABC (21)	12.1	2.0	2	5.0	25.0
9" Gray LSS (22)	8.5	1.4	4.8	12.0	30.0

Based on discussions with NCDOT engineers, it appeared that the proof-roll displacements important to field inspectors are the pumping and rut values. The pumping value alerts inspectors that the subgrade is “moving”. The rut values are the permanent displacements remaining after some amount of the maximum displacement is recovered from pumping. Even if a subgrade does not permanently rut, it may undergo significant maximum displacement that leads to tension cracks left on the surface adjacent to or within the wheel paths. Table 58 gives the measured permanent and recovered deformations from the tested sections. Pulse 1 and 2 measurements signify the two proof-roll loads applied between static and the first set of cyclic loads. Pulse 3 and 4 are the proof-roll pulses after repairing the rut created by the first 10,000 cycles. Instruments were tared between each pulse. It can be seen that only the unstabilized Coastal Plain subgrade section (Test 12) displaced significantly under proof-roll loading. Only one pulse was applied to this test. Pulses were not applied to the first four tests because field measurements used to determine the proof-roll function were not taken until May 2008. The data show that each test generally stiffened between Pulses 1 and 2. Displacement from Pulse 3 (applied after “repairing” the rut) was usually higher than the first two pulses because of seating effect from resetting the load plate after rut repair. Unlike the first two proof-roll pulses, Pulse 3 did not have the “benefit” of a prior static load to seat the load plate.

Table 58. Proof-Roll Test Displacement Data (inches)

Test No.	Pulse 1			Pulse 2			Pulse 3			Pulse 4		
	Permanent	Recovered	Maximum	Permanent	Recovered	Maximum	Permanent	Recovered	Maximum	Permanent	Recovered	Maximum
1	N/A	N/A	N/A	N/A	N/A	N/A	N/A	N/A	N/A	N/A	N/A	N/A
2	N/A	N/A	N/A	N/A	N/A	N/A	N/A	N/A	N/A	N/A	N/A	N/A
3	N/A	N/A	N/A	N/A	N/A	N/A	N/A	N/A	N/A	N/A	N/A	N/A
4	N/A	N/A	N/A	N/A	N/A	N/A	N/A	N/A	N/A	N/A	N/A	N/A
5	N/A	N/A	N/A	N/A	N/A	N/A	0.064	0.091	0.155	0.018	0.094	0.111
6	0.028	0.069	0.097	0.018	0.061	0.079	0.032	0.087	0.119	0.003	0.086	0.089
7	0.219	0.040	0.259	0.088	0.053	0.141	0.109	0.043	0.152	0.029	0.045	0.074
8	0.198	0.051	0.249	0.015	0.076	0.092	0.014	0.063	0.077	0.005	0.064	0.069
9	0.051	0.052	0.102	0.022	0.055	0.077	0.107	0.043	0.149	0.013	0.048	0.061
10	0.050	0.049	0.099	0.020	0.056	0.076	0.057	0.046	0.103	0.011	0.048	0.059
11	0.176	0.070	0.246	0.037	0.080	0.117	0.020	0.074	0.094	0.004	0.075	0.080
12	1.617	0.158	1.776	N/A	N/A	N/A	N/A	N/A	N/A	N/A	N/A	N/A
13	0.033	0.067	0.100	0.016	0.075	0.091	0.062	0.077	0.139	0.009	0.081	0.091
14	0.063	0.075	0.138	0.024	0.088	0.112	0.144	0.112	0.256	0.033	0.117	0.150
15	0.054	0.075	0.129	0.026	0.078	0.105	0.085	0.075	0.160	0.010	0.086	0.096
16	0.108	0.108	0.216	0.061	0.122	0.183	0.136	0.093	0.229	0.011	0.093	0.105
17	0.093	0.100	0.193	0.051	0.115	0.166	0.103	0.143	0.246	0.017	0.154	0.171
18	0.090	0.092	0.183	0.058	0.102	0.159	0.036	0.093	0.130	0.013	0.000	0.013
19	0.029	0.041	0.070	0.010	0.047	0.057	0.037	0.069	0.107	0.008	0.095	0.103
20	0.016	0.043	0.059	0.006	0.051	0.056	0.028	0.076	0.104	0.000	0.073	0.073
21	0.021	0.075	0.097	0.012	0.081	0.093	0.051	0.093	0.144	0.011	0.097	0.108
22	0.005	0.083	0.089	0.008	0.083	0.092	N/A	N/A	N/A	N/A	N/A	N/A

The displacement data for Test 6 are presented in Figure 81. The bar chart shows the proportional amount of permanent (red) and recovered (blue) displacement for each pulse. The sum of the two gives the maximum displacement. Test 12 which failed proof-roll testing and had a significantly larger displacement than the other tests. Data for the remaining tests are given in Appendix C.

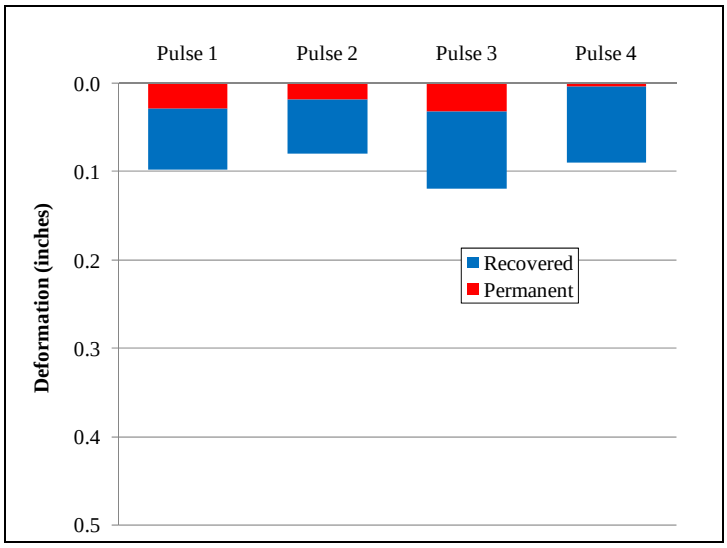

Figure 81. Proof-roll Displacement for 19" ABC with Geotextile A (6) Section

The displacements in Table 58 can be sorted based on permanent and recovered deformations. The pulse that is the most tell-tale of section stiffness is Pulse 1 which benefitted from seating from the static load, and is representative of a field inspection of a newly stabilized subgrade. The values for this pulse sorted from least to greatest permanent displacement are presented inTable 59 (whicj also include the results from first pulse of Test 12 for comparison.) Test configurations are given for reference.

Table 59. Proof-Roll Test: Displacement Sorted by Permanent Displacement (inches)

Test Configuration (Test No.)	Permanent	Recovered	Maximum
9" Gray LSS (22)	0.005	0.083	0.089
9" LSS/4" ABC (20)	0.016	0.043	0.059
9" Gray LSS/4" ABC (21)	0.021	0.075	0.097
19" ABC with Geotextile A (6)	0.028	0.069	0.097
12" LSS/5" ABC (19)	0.029	0.041	0.070
20" ABC with Geotextile B (13)	0.033	0.067	0.100
25" Select Fill/3" ABC with Geotextile B (10)	0.050	0.049	0.099
36" Select Fill/3" ABC (9)	0.051	0.052	0.102
18" ABC (15)	0.054	0.075	0.129
13" ABC with Geotextile B (14)	0.063	0.075	0.138
12" ABC with Geotextile A (18)	0.090	0.092	0.183
11" ABC with Geogrid A (17)	0.093	0.100	0.193
13" ABC with Geotextile A (16)	0.108	0.108	0.216
14" Select Fill/3" ABC with Geotextile A (11)	0.176	0.070	0.246
17" Select Fill/3" ABC with Geotextile A (8)	0.198	0.051	0.249
36" Select Fill (7)	0.219	0.040	0.259
Subgrade (12)	1.617	0.158	1.776

Cyclic Loading

Two sets of 10,000 cycles simulating construction traffic were applied onto the test sections. The first set simulated traffic on newly stabilized and proof-rolled subgrade (will be referred to as Cyclic 1) and the second set simulated final “paving” construction traffic after subgrade rut repair and inspection (will be referred to as Cyclic 2). Table 60 and Table 61 give the displacement measurements of the load plate during both cycle sets at log intervals. The ‘minimum’ values represent conditions during rest periods between pulses, and ‘maximum’ values were under the 80 psi cyclic pressure. Cyclic loading was not performed on Tests 12 and 22, and Cyclic 2 was not performed on Tests 1 through 4, as the need for such a scheme was later specified after these tests were completed. Tests with a dash mark ‘-‘ at certain cycle intervals did not reach that cycle number because of either significant plate displacement or rotation. The test was then stopped to avoid damaging the actuator. As illustration of data plots, Figure 82 and Figure 83 plot surface displacement and vertical stress increase for 13” ABC with Geotextile B (Test 14). The data plotted represent minimum (between 80 psi load pulses) for each set of cycles. Boussinesq and Westergaard stress distribution curves are given for visual reference even though the cyclic stresses represent neither static nor elastic conditions. In Figure 83, the layer interface is again shown as a black line. Data for the remaining tests are presented in Appendix C.

Table 62 gives the maximum boundary stresses at the bottom and sides of the test pit for each test during the first set of cycles (when subgrade stresses were highest). It can be seen that the measured values were less than 10% of the applied surface pressure of 80 psi, with maximum values only near 4% in Test 5. This indicates that the test pit was adequately sized and boundary effects from the concrete sidewalls were negligible. Pressure readings were not taken on several tests because of broken EPCs. Figures showing plate displacement per number of applied cycles and tables sorted according to displacement magnitudes will be presented in Chapter 8 as performance comparisons.

Table 60. Load Plate Displacement During Cyclic 1 Loading (inches)

Test Configuration (Test No.)	Minimum Displacement					Maximum Displacement				
Cycle No.	1	10	100	1000	10000	1	10	100	1000	10000
8" ABC (1)	0.000	0.221	-	-	-	0.049	0.263	-	-	-
16" ABC (2)	0.000	0.097	0.415	1.206	2.355	0.081	0.172	0.492	1.288	2.432
20" ABC (3)	0.000	0.072	0.252	0.692	1.537	0.024	0.097	0.277	0.721	1.568
16" ABC with Geogrid B (4)	0.000	0.120	0.485	1.458	2.761	0.034	0.156	0.524	1.500	2.782
14" ABC (5)	0.000	0.236	0.826	2.077	-	0.043	0.279	0.869	2.124	-
19" ABC with Geotextile A (6)	0.000	0.064	0.282	0.767	1.766	0.027	0.092	0.313	0.801	1.786
36" Select Fill (7)	0.000	1.533	3.805	5.188	-	0.045	1.588	3.813	5.190	-
17" Select Fill/3" ABC with Geotextile A (8)	0.000	0.124	0.564	1.820	-	0.033	0.155	0.591	1.844	-
36" Select Fill/3" ABC (9)	0.000	0.128	0.455	1.156	2.108	0.026	0.152	0.477	1.177	2.129
25" Select Fill/3" ABC with Geotextile B (10)	0.000	0.032	0.246	0.881	2.283	0.022	0.056	0.268	0.901	2.307
14" Select Fill/3" ABC with Geotextile A (11)	0.000	0.232	0.906	2.768	-	0.039	0.270	0.940	2.799	-
Subgrade (12)	N/A	N/A	N/A	N/A	N/A	N/A	N/A	N/A	N/A	N/A
20" ABC with Geotextile B (13)	0.000	0.081	0.345	1.098	2.361	0.029	0.115	0.381	1.138	2.401
13" ABC with Geotextile B (14)	0.000	0.220	0.744	2.066	4.878	0.056	0.261	0.789	2.118	4.944
18" ABC (15)	0.000	0.120	0.493	1.260	2.476	0.034	0.154	0.530	1.296	2.511
13" ABC with Geotextile A (16)	0.000	0.273	1.086	2.296	3.540	0.054	0.329	1.136	2.343	3.582
11" ABC with Geogrid A (17)	0.000	0.208	0.979	2.737	4.865	0.052	0.264	1.041	2.807	4.939
12" ABC with Geotextile A (18)	0.000	0.253	1.183	3.299	5.699	0.047	0.304	1.234	3.345	5.743
12" LSS/5" ABC (19)	0.000	0.059	0.202	0.524	-	0.019	0.078	0.226	0.552	-
9" LSS/4" ABC (20)	0.000	0.016	0.061	0.146	0.228	0.016	0.033	0.081	0.169	0.251
9" Gray LSS/4" ABC (21)	0.000	0.055	0.192	0.512	0.875	0.031	0.087	0.230	0.553	0.917
9" Gray LSS (22)	N/A	N/A	N/A	N/A	N/A	N/A	N/A	N/A	N/A	N/A

Table 61. Load Plate Displacement During Cyclic 2 Loading (inches)

Test Configuration (Test No.)	Minimum Displacement					Maximum Displacement				
Cycle No.	1	10	100	1000	10000	1	10	100	1000	10000
8" ABC (1)	N/A	N/A	N/A	N/A	N/A	N/A	N/A	N/A	N/A	N/A
16" ABC (2)	N/A	N/A	N/A	N/A	N/A	N/A	N/A	N/A	N/A	N/A
20" ABC (3)	N/A	N/A	N/A	N/A	N/A	N/A	N/A	N/A	N/A	N/A
16" ABC with Geogrid B (4)	N/A	N/A	N/A	N/A	N/A	N/A	N/A	N/A	N/A	N/A
14" ABC (5)	0.000	0.053	0.198	0.474	-	0.037	0.092	0.236	0.511	-
19" ABC with Geotextile A (6)	0.000	0.029	0.115	0.272	-	0.031	0.059	0.145	0.302	-
36" Select Fill (7)	0.000	0.215	2.284	-	-	0.027	0.240	2.307	-	-
17" Select Fill/3" ABC with Geotextile A (8)	0.000	0.058	0.183	0.388	-	0.027	0.085	0.201	0.410	-
36" Select Fill/3" ABC (9)	0.000	0.054	0.167	0.330	-	0.021	0.074	0.184	0.346	-
25" Select Fill/3" ABC with Geotextile B (10)	0.000	0.049	0.159	0.338	0.607	0.020	0.068	0.177	0.354	0.623
14" Select Fill/3" ABC with Geotextile A (11)	0.000	0.037	0.174	0.478	1.218	0.028	0.066	0.201	0.504	1.245
Subgrade (12)	N/A	N/A	N/A	N/A	N/A	N/A	N/A	N/A	N/A	N/A
20" ABC with Geotextile B (13)	0.000	0.034	0.110	0.231	-	0.030	0.066	0.141	0.262	-
13" ABC with Geotextile B (14)	0.000	0.079	0.289	0.779	1.804	0.051	0.130	0.342	0.831	1.848
18" ABC (15)	0.000	0.057	0.194	0.406	0.783	0.036	0.091	0.227	0.438	0.814
13" ABC with Geotextile A (16)	0.000	0.036	0.121	0.263	0.464	0.036	0.072	0.157	0.298	0.499
11" ABC with Geogrid A (17)	0.000	0.081	0.288	0.726	1.444	0.061	0.145	0.355	0.792	1.510
12" ABC with Geotextile A (18)	0.000	0.031	0.101	0.216	0.443	0.038	0.069	0.140	0.255	0.482
12" LSS/5" ABC (19)	0.000	0.036	0.104	0.191	0.413	0.028	0.063	0.130	0.216	0.438
9" LSS/4" ABC (20)	0.000	0.004	0.020	0.051	0.092	0.028	0.034	0.051	0.080	0.120
9" Gray LSS/4" ABC (21)	0.000	0.031	0.082	0.156	0.292	0.038	0.072	0.123	0.198	0.334
9" Gray LSS (22)	N/A	N/A	N/A	N/A	N/A	N/A	N/A	N/A	N/A	N/A

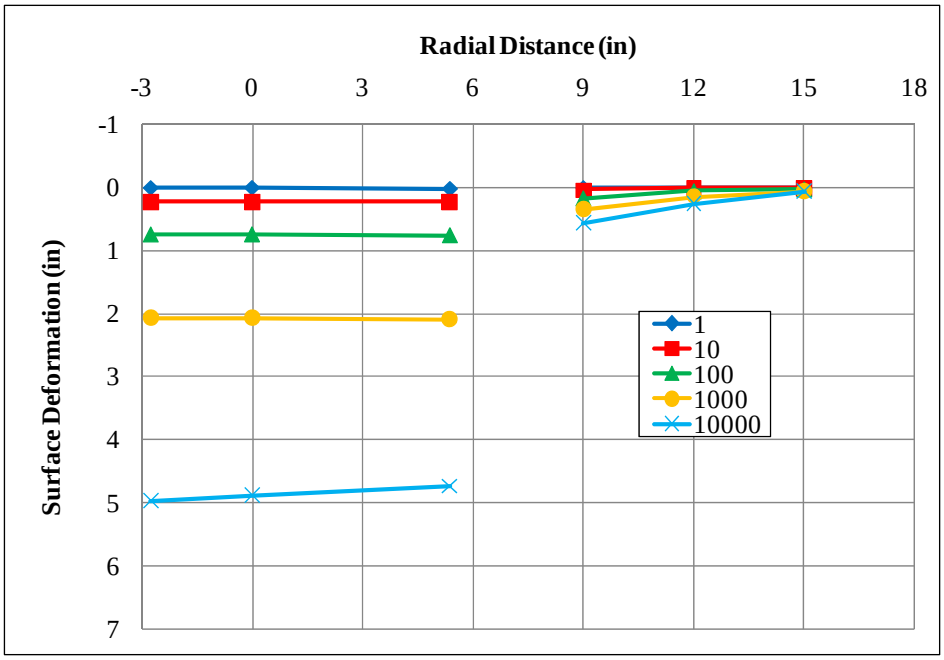

Figure 82. Surface Displacement per Log Cycles for 13" ABC with Geotextile B (14) Cyclic 1 Test

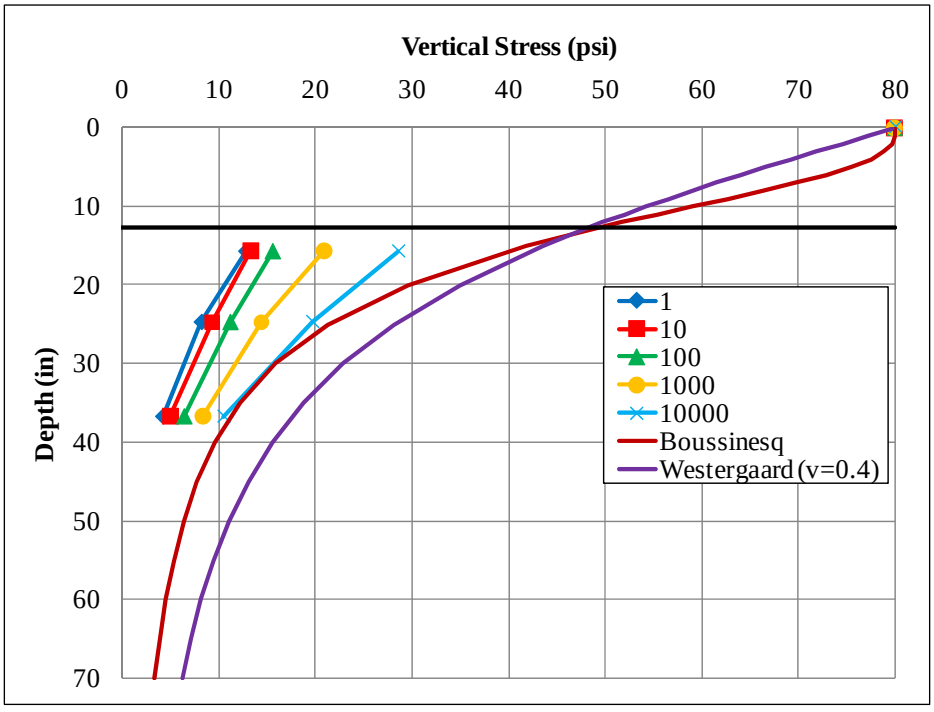

Figure 83. Vertical Stress Increase per Log Cycles for 13" ABC with Geotextile B (14) Cyclic 1 Test

Table 62. Maximum Test Pit Boundary Stresses (psi) at Log Cycles for Cyclic 1

Test Configuration (Test No.)	Cyclic 1									
	Maximum Stress at Bottom of Pit					Maximum Stress at Side of Pit				
Cycle No.	1	10	100	1000	10000	1	10	100	1000	10000
8" ABC (1)	1.17	1.18	-	-	-	1.17	1.31	-	-	-
16" ABC (2)	1.04	1.18	1.38	1.78	1.91	1.41	1.81	2.04	2.38	2.46
20" ABC (3)	0.65	0.60	0.61	0.72	0.85	1.03	1.51	1.96	2.44	2.74
16" ABC with Geogrid B (4)	0.90	1.05	1.36	1.83	1.94	1.35	1.93	2.54	3.13	3.06
14" ABC (5)	0.90	1.19	1.58	2.09	-	1.61	2.27	2.80	3.14	-
19" ABC with Geotextile A (6)	0.94	0.98	1.12	1.34	1.34	1.10	1.36	1.69	2.15	2.05
36" Select Fill (7)	0.93	0.95	1.40	1.57	-	0.18	0.18	0.43	0.50	-
17" Select Fill/3" ABC with Geotextile A (8)	0.77	0.81	0.91	1.02	-	0.33	0.57	0.87	1.02	-
36" Select Fill/3" ABC (9)	0.94	0.96	0.95	1.02	1.11	0.19	0.32	0.38	0.42	0.33
25" Select Fill/3" ABC with Geotextile B (10)	1.19	1.21	1.30	1.37	1.48	0.74	0.75	0.76	0.70	0.52
14" Select Fill/3" ABC with Geotextile A (11)	0.99	1.25	1.61	1.93	-	0.60	0.97	1.22	1.35	-
Subgrade (12)	N/A	N/A	N/A	N/A	N/A	N/A	N/A	N/A	N/A	N/A
20" ABC with Geotextile B (13)	-	-	-	-	-	0.52	0.80	0.99	1.12	1.03
13" ABC with Geotextile B (14)	-	-	-	-	-	0.60	0.78	0.95	1.13	1.08
18" ABC (15)	-	-	-	-	-	0.28	0.66	1.03	1.17	1.21
13" ABC with Geotextile A (16)	-	-	-	-	-	0.64	1.09	1.42	1.51	1.41
11" ABC with Geogrid A (17)	-	-	-	-	-	0.64	0.92	1.26	1.32	1.17
12" ABC with Geotextile A (18)	-	-	-	-	-	0.29	0.64	1.13	1.27	1.18
12" LSS/5" ABC (19)	-	-	-	-	-	0.14	0.10	0.14	0.28	-
9" LSS/4" ABC (20)	-	-	-	-	-	0.27	0.29	0.42	0.53	0.52
9" Gray LSS/4" ABC (21)	-	-	-	-	-	0.41	0.49	0.67	0.99	1.13
9" Gray LSS (22)	N/A	N/A	N/A	N/A	N/A	N/A	N/A	N/A	N/A	N/A

Displacement Contours

Displacement of the samples surface and the underlying interface layers were measured with a string-line grid. The displacements were measured every three inches in both lateral directions over a three foot square around the center of the load plate. The contour plots were created in Microsoft Excel© as a one-dimensional surface graph. The displacement scales are in inches. The 12 inch diameter load plate extended from -6 to +6 in both directions. A typical plot for Test 6 is shown as Figure 84. Appendix C includes data for surface displacement plans for each test.

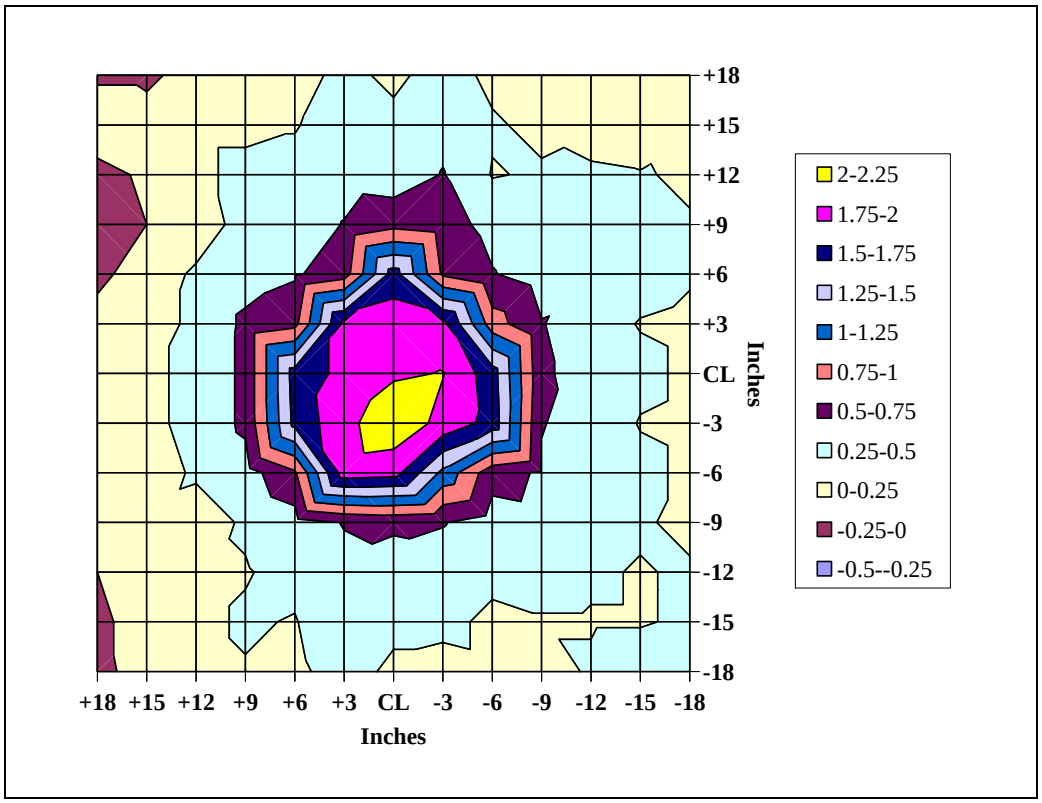

Figure 84. 19” ABC with Geotextile A (6) ABC Surface Displacement Contour Plan (inches)

The displacement measurements of the test pit surface (usually ABC, or select fill for Test 7) were taken after the static load test, first two proof-roll pulses, and first set of 10,000 load cycles. The measurements of the underlying surfaces (Coastal Plain subgrade or LSS) were taken after removing the upper layers during section demolition. Thus, the underlying displacement measurements account for an additional two proof-roll pulses and Cyclic 2 loading sequence that occurred after the deformation rut was refilled.

Subgrade surface displacement measurements were not taken on Test 9 (36” Select Fill/3” ABC) and Test 7 (36” Select Fill) where bearing capacity type failure occurred. Test 12 (Subgrade only) did not have a stabilization layer displacement profile.

Cumulative Displacements

The plate displacement was tared at the beginning of each load sequence. This allowed for the relative displacements under static, proof-roll, and cyclic loading to be compared between tests. However, it is important to consider how much cumulative (total) displacement occurred for each test since the loading regimes were applied consecutively. Figure 85 is similar to Figure 81 but shows cumulative permanent displacement from static loading as well as the permanent and recovered displacements from the first two proof-roll pulses.

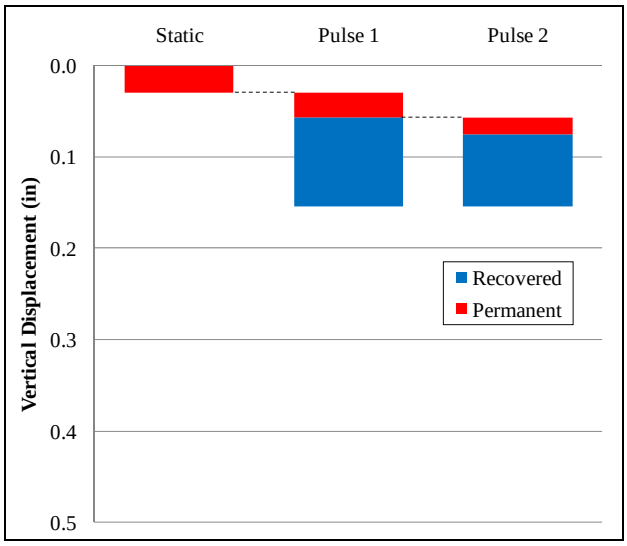

Figure 85. Cumulative Permanent Displacements from Static and Proof-roll Loads for 19" ABC with Geotextile A (6) Test Prior to Cyclic 1

Cumulative displacements were used to compare observed tension cracking between tests. Tension cracks alert field inspectors to unstable subgrades under proof-rolling. For these large scale tests, the tension cracks were seen during the first set of cyclic loading (after static and proof-roll loading). Tension cracks were also observed during the second set of cycles after proof-rolling. Figure 86 shows a picture of typical tension cracking observed during cyclic loading.

Table 63 gives the number of cycles to observed tension cracks for both sets of cycles and the cumulative plate displacement at that cycle. This is from the start of static loading for Cyclic 1 and from the start of proof-roll Pulse 3 for Cyclic 2. The values reflect the maximum displacements since these are what initiate the formation of tension cracks. The number of cycles to tension crack formation was not recorded for Tests 1 through 3. Tests with no observed tension cracks are listed as 'none'. Ranges are given for several tests where tension cracks were not detected until some time after they had initially formed.

Figure 86. Tension Crack Formation During Cyclic 1 of 17" Select Fill/3" ABC with Geotextile A (8) Test

Table 63. Cumulative Plate Displacements to Observed Tension Cracks

Test Configuration (Test No.)	Cyclic 1		Cyclic 2	
	No. Cycles	Cum. Displ. (in)	No. Cycles	Cum. Displ. (in)
8" ABC (1)	N/A	N/A	N/A	N/A
16" ABC (2)	N/A	N/A	N/A	N/A
20" ABC (3)	N/A	N/A	N/A	N/A
16" ABC with Geogrid B (4)	450	1.20	N/A	N/A
14" ABC (5)	250 to 300	1.41 to 1.50	None	None
19" ABC with Geotextile A (6)	1500	0.99	None	None
36" Select Fill (7)	1	0.16	30	0.69
17" Select Fill/3" ABC with Geotextile A (8)	90	0.84	None	None
36" Select Fill/3" ABC (9)	60	0.54	None	None
25" Select Fill/3" ABC with Geotextile B (10)	200	0.52	4850	0.58
14" Select Fill/3" ABC with Geotextile A (11)	80	1.18	1000	0.53
20" ABC with Geotextile B (13)	277 to 379	0.78 to 0.88	None	None
13" ABC with Geotextile B (14)	150	1.29	273 to 1061	0.69 to 1.04
18" ABC (15)	750	1.45	5000	0.76
13" ABC with Geotextile A (16)	35	1.03	2405	0.51
11" ABC with Geogrid A (17)	50	1.08	50	0.40
12" ABC with Geotextile A (18)	40	1.08	3000	0.39
12" LSS/5" ABC (19)	261	0.30	1300	0.27
9" LSS/4" ABC (20)	None	None	None	None
9" Gray LSS/4" ABC (21)	755 to 900	0.59 to 0.62	2000 to 3100	0.29 to 0.32

CHAPTER 8: COMPARATIVE STABILIZATION PERFORMANCE

Performance of the 22 large scale prototype tests is compared first considering the type of stabilization (i.e. ABC replacement, select fill replacement, mechanical reinforcement, or lime stabilization). Next, the comparisons are made by considering the depth of stabilization (i.e., comparing all stabilization layers of approximately 12 inches to one another).

Comparison by Stabilization Type

Unreinforced Granular Layer Tests

Seven tests were performed on Coastal Plain subgrade stabilized with unreinforced granular layers comprised of ABC, select fill, or a combination of both. The first test with 8 inches of ABC was used for system and load function calibration. Although the test underwent large displacement, the results were suspect and are excluded from all performance analyses. Figure 87 presents the displacement curves for the remaining six tests. Test numbers 2 and 3 were not loaded with secondary cycles. Test 5 experienced significant plate rotation and was stopped before 5,000 initial cycles to prevent damaging the actuator.

As mentioned earlier, combined quality control and displacement data showed how reusing the same Coastal Plain subgrade throughout testing effected results. For the first seven tests, the soil had been remolded (through tilling and compaction) very few times. The 14, 16, and 20 inch ABC tests in Figure 87 are thus comparable.

However, the 16 inch ABC (Test 2) displaced less than the 18 inch ABC (Test 15) section. The quality control data show a higher average corrected nuclear gauge dry unit weight (106.2 pcf) and DCPI (114.0 mm/blow) for the 18 inch ABC test compared to the 16 inch test (104.4 pcf and 87.5 mm/blow, respectively). The thicker stabilization test was performed later in the program and had a more remolded subgrade, explaining why it had more displacement than the 16 inch ABC test.

A system response observed on all ABC test sections was intrusion of larger stones (generally greater than 0.5 inches nominal) into the Coastal Plain subgrade surface in areas immediately beneath the load plate.

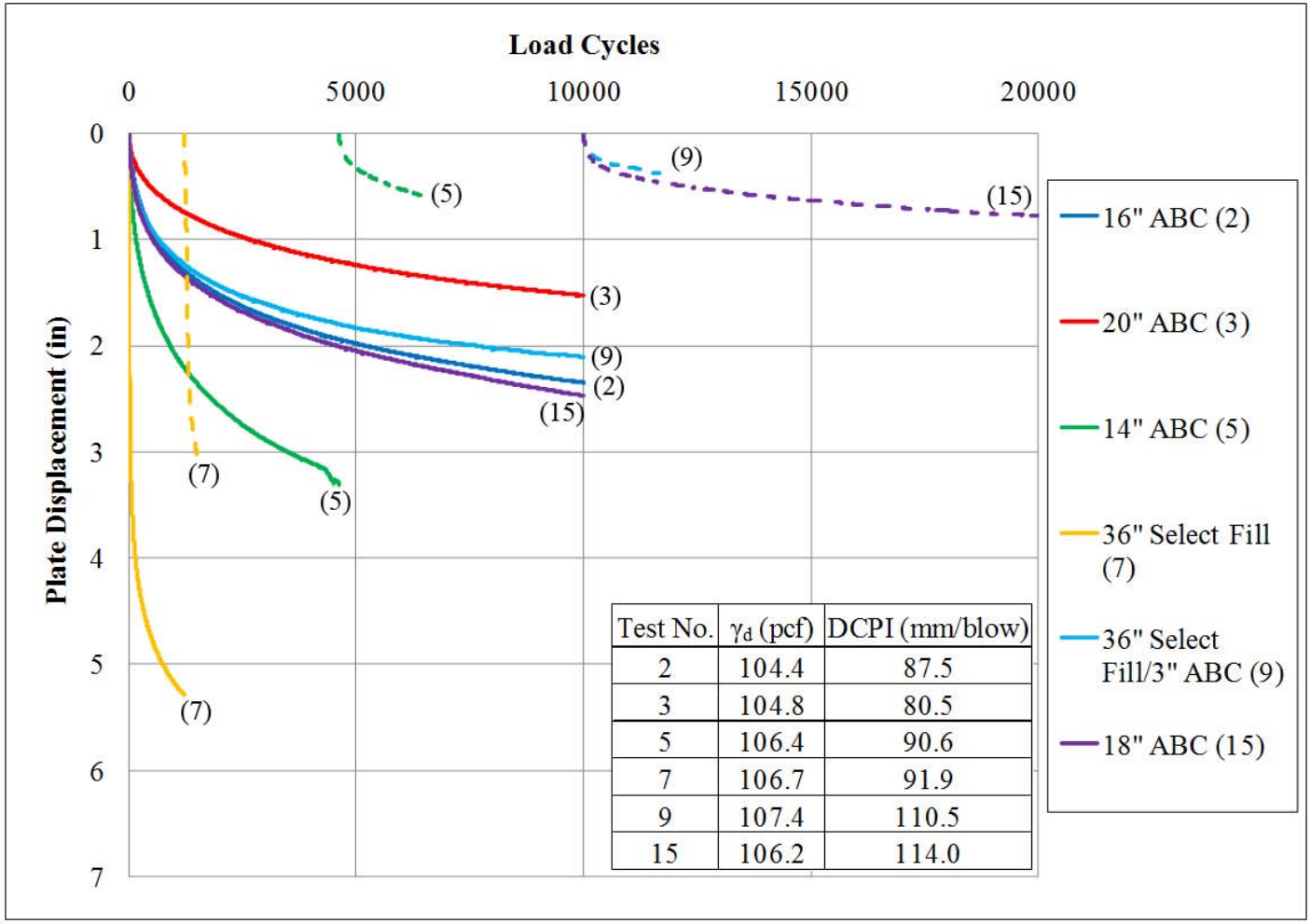

Test No.	γ_d (pcf)	DCPI (mm/blow)
2	104.4	87.5
3	104.8	80.5
5	106.4	90.6
7	106.7	91.9
9	107.4	110.5
15	106.2	114.0

Figure 87. Displacement Curves for Unreinforced Granular Layer Test

Tests with thicker ABC layers experienced less intrusion but over a greater area than tests with thinner layers because of load spreading and reduction in vertical stress increase with depth. Figure 88 shows typical ABC intruded with Coastal Plain subgrade at the layer interface. The picture was taken after testing, and is backlit for contrast to clearly show the stone particles.

Figure 88. Intrusion of ABC into Coastal Plain Subgrade Surface - Post 14" ABC (5) Test

ABC intrusion was most likely concurrent with ABC densification during initial cycles. Data from laboratory testing showed that compacted ABC ranged between 84 and 93 percent relative density (with thicker ABC tests having higher values) due to a combination of small laboratory compaction equipment and soft underlying subgrade. As it was cyclically loaded, the ABC compacted only slightly because the soft underlying subgrade could not provide sufficient bearing capacity Thus, stones at the bottom of the ABC intruded into the subgrade surface as the subgrade experienced increased vertical stress and deformation of its own (tests with less ABC experienced higher measured subgrade deformation). Surface displacements eventually exhibited a slower rate of increase after some amount of cycles has been applied. The rate of displacement increase depended on the ABC layer thickness. At some point, ABC compaction and layer mixing could no longer occur, and rate of increase in displacement becomes entirely due to the accumulated strain within the subgrade layer. Accordingly, smaller displacement accumulation at higher cycles was not due to any measurable degradation of the ABC and likely related to subgrade deformation.
During secondary cycles for ABC tests, there was initially a high displacement rate due to compaction under loading of the ABC that was used to refill the rut. These tests had lower displacement rates at earlier cycles because the previously compacted ABC (from initial

cycles) confined the newly placed ABC. Layer mixing likely continued during cyclic 2 because the subgrade stress increase under loading was usually just as high or higher than during cyclic 1. The refilled rut also meant that the section had a thicker stabilization depth than during cyclic 1, but the tests are not renamed.

The rut refilling depths should be considered when analyzing data in Figure 87. According to data in Figure1, it appears as though the 14 inch ABC test would reach approximately the same rate of change in displacement during the second stage of cyclic loading as the 18 inch ABC test. From the rut refilling, the 14 inch test had approximately 17 inches of ABC after the 3 inch initial cycle rut was repaired, and the 18 inch test would be about 20.5 inches ABC with the 2.5 inch rut. Again, the effects of subgrade strength remolding are seen because the 14 inch ABC test was performed earlier in the program than the 18 inch ABC test.

Test number 7 was the first test to use select fill, so it was unclear how the section would behave under cyclic loading. At a low number of cycles (1212), the load plate displaced 5.3 inches and the actuator slid off the rotated load plate. The select fill failed in a general bearing capacity mode and significant heave was observed around the load plate. Under the second set of cycles, the plate displaced somewhat less because of select fill densification, but eventually also experienced heave and excessive deformation at low cycle numbers.

After consulting with the NCDOT regarding standard field practices, a thin lift of ABC (~3 inches) was placed on the remaining select fill tests. This provided vertical confinement on the select fill to prevent heave and decrease plate displacement. Comparing the 36 inch select fill tests with and without ABC (Tests 7 and 9) shows that the presence of the ABC significantly improved performance. Differences in Coastal Plain subgrade from remolding did not change surface displacement because the increased stabilization depth meant that the subgrade had little influence on surface response.

The test sample with 36 inches of select fill and 3 inches of ABC (Test 9) displaced an amount about half way between that observed during the tests on 18 and 20 inches of ABC at 10,000 cycles. The displacement during Test 9 approximately matched with that observed during the 18 inch ABC test over the first 500 cycles, but then showed stiffer behavior for the remainder of Cyclic 1. As mentioned earlier, the 14, 16, and 20 inch ABC test samples had different subgrade conditions from 36 inch select fill test section. It is speculated that if subgrade conditions were similar, the select fill test displacement would be more in line with the test with 20 inches of ABC.
The 36 inch select fill with 3 inches ABC ample displayed a slight punching failure of the load plate through the thin ABC surface layer. However, it did not occur immediately; it was likely because of the relatively deep stabilization depth. It will be shown later that thinner select fill tests underwent punching failure of the ABC at low cycles because of the closer proximity of the underlying subgrade. After refilling ruts from Cyclic 1, the 36 inch select fill with 3 inches ABC test displaced much less, because the ABC layer was stiffer due to previous loading and rut refilling.

Conclusions that can be made about unreinforced granular layer sections are:

- In general, greater stabilization layer depths decreased surface displacements over all cycles.

- Thin ABC surface layers over select fill decreased surface displacement by reducing heave seen when only select fill was cyclically loaded.

- Stabilization with 36 inches of select fill and 3 inches ABC performed about the same as test sections with between 18 and 20 inches of ABC during initial 10,000 cycles. Secondary cycles showed marked improvement because the repaired ABC was denser and thicker beneath the load plate.

- Mixing at the ABC/subgrade layer interface occurred by larger stones intruding downward into the subgrade surface. This was likely simultaneous with ABC layer densification during initial cycles, which resulted in large initial surface deformation followed by smaller displacements, likely associated with subgrade consolidation.

- The subgrade seemed to have more consistent strength values after Test 7 and for the remainder of testing due to reworking and compacting it.

Reinforcement Geotextile A Tests

Five tests were performed on subgrade stabilized with granular layers and reinforcement Geotextile A at the layer interface. Figure 89 gives the displacement curves for these tests. Loading was stopped before 10,000 cycles for Tests 8 and 11 because significant deformation caused plate rotation and slippage of the actuator. The load plate was re-leveled after rotating at approximately 6,000 cycles for Test 6, creating a slight jump in the displacement curve.

The load plate was also re-leveled for Test 18 (12 inches ABC with Geotextile A) at 5,000 cycles, but the jump in displacement was much higher because the rotation magnitude was large. More sand was needed to re-level the load plate. This resulted in a high displacement rate initially upon reloading, due perhaps to compaction of the leveling sand before it returned to the same rate as before the stoppage. To ‘correct’ for this leveling effect, the first 1,000 cycles after the re-load (between 5,000 and 6,000 cycles) was removed and the remaining data were offset downward to match the earlier curve because it was reasonable to assume that it would represent the sample behavior. The original data are shown in light blue and the corrected trend is in pink. All future graphs with this test will use the corrected graph with the 1,000 cycle gap in the data.

The 17 inches select fill with 3 inches ABC and Geotextile A test displaced less initially than the tests with 12 and 13 inches of ABC. This was because the overall stabilization depth was greater, so the stresses on the subgrade were less (12.2 psi versus 22.1 psi for 12 inches and 18.6 psi for 13 inches at 1,000 cycles, respectively). However, punching failure of the load plate occurred at relatively few cycles for both select fill tests, as shown in Figure 89, which prevented displacement rates from decreasing at higher load cycles. A picture of this is shown in Figure 90. Punching failure was not as drastic as for the previous deep select fill test (36 inch select fill with 3 inch ABC) because the subgrade stress increase was less (3.5 psi versus 12.2 psi and 15.6 psi at 1,000 cycles for Tests 8 and 11, respectively).

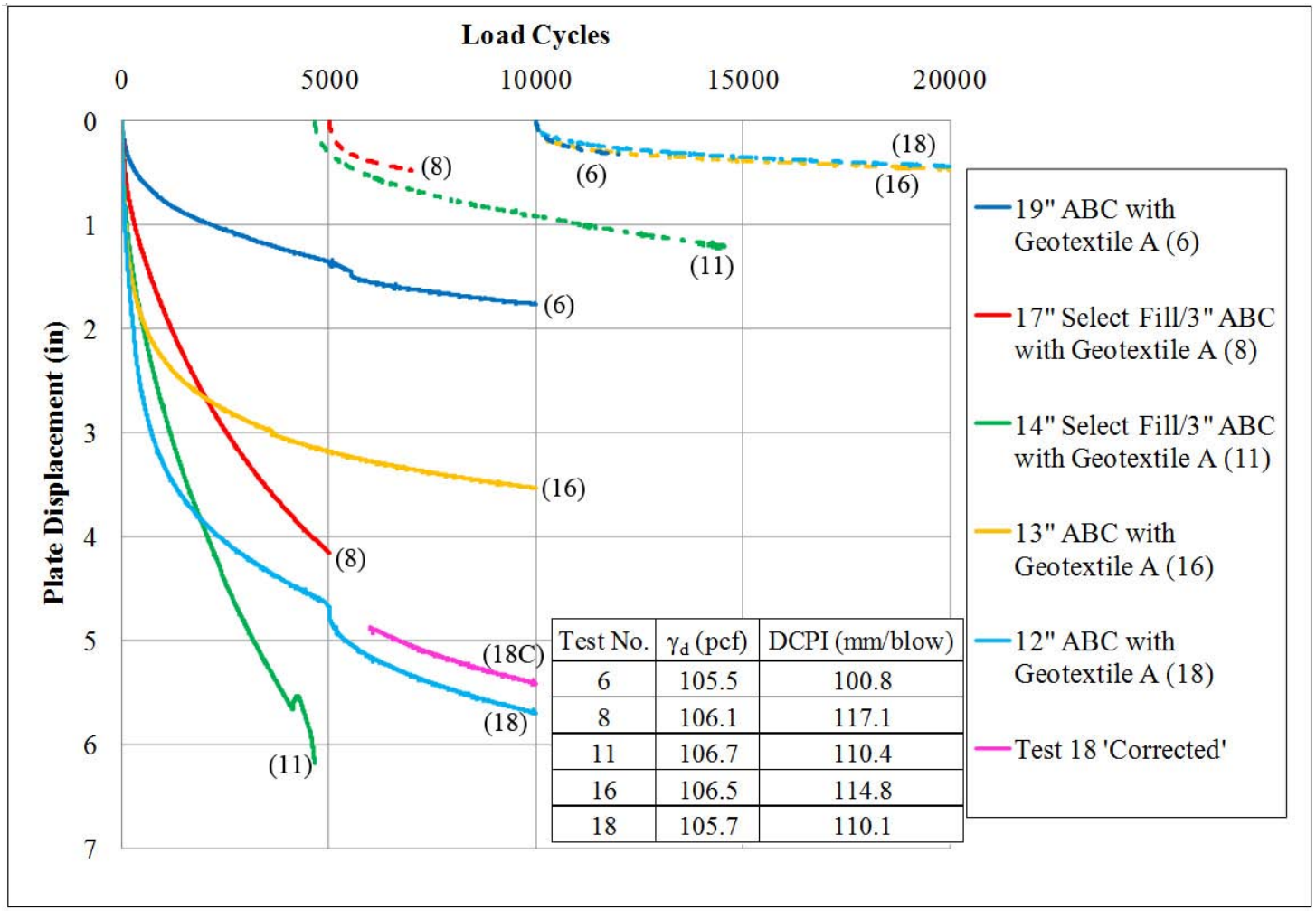

Figure 89. Displacement Curves for Tests Reinforced with Reinforcement Geotextile A

Although large vertical plate displacement was measured, it was likely that Geotextile A was mobilized very little because the select fill simply displaced laterally between the bottom of the ABC and the top of the fabric. In other words, the rounded select fill sand particles simply rolled horizontally over the reinforcement surface without engaging it. The subgrade surface deformation measurements shed light on this behavior. The test with 17 inches of select fill with 3 inches ABC (20 inches total stabilization) had only 0.5 to 0.75 inches of subgrade surface deformation, but with over 4 inches of plate displacement. Similar ABC depths (19 inch test number 6) had subgrade deformations of 0.75 to 1.0 inches with only 1.5 inches of plate displacement. Because the relative magnitude of surface deformation for the select fill test was greater than for the ABC test and no "heave" was measured on the surface around the load plate, the only place the select fill could have displaced was laterally. This relative difference in magnitude between surface and subgrade deformation also occurred in the 14 inch select fill with 3 inches ABC test sample. In this test, the surface displaced over 5.5 inches and yet only 1 to 1.25 inches of subgrade deformation was measured.

The initial performance of the three Geotextile A tests with ABC must be analyzed in the context of subgrade reuse. The test with 19 inches of ABC over Geotextile A was performed early in the test program and had an average dry unit weight and DCPI of 105.5 pcf and 100.8 mm/blow, respectively. The DCPI values increased for the 12 inch ABC with Geotextile A (110.1 mm/blow) and 13 inch ABC with Geotextile A (114.8 mm/blow) tests due to the remolding effects. Thus, the 19 inch ABC test may have displaced more had the subgrade been in the same condition, making the benefits of having the stiff reinforcement geotextile at depths similar to the load plate diameter (12 inches) more significant.

Figure 90. Punching Failure during 14" Select Fill/3" ABC with Geotextile A (11) Test

During secondary cycling, this influence was magnified because initial cycles caused tensioning and mobilization of Geotextile A strength. After adding the depth of rut repair, the test with 12 inch ABC with Geotextile A had approximately 17.5 inches of ABC, the test with 13 inch ABC with Geotextile A about 16.5 inches, and the 19 inch ABC with Geotextile A test about 21 inches. However, all three tests had about the same deformation over secondary cycles, even with the less remolded subgrade and thicker ABC in Test 6. Thus, for stabilization depths similar to the load plate diameter, Geotextile A underwent more tensioning and strength mobilization during cyclic 1 that proved beneficial during cyclic 2.

The displacement curves for unreinforced ABC tests and Geotextile A are presented in Figure 91. The Geotextile A test with 19 inches ABC (Test 6) can be compared to 20 inches of unreinforced ABC (Test 3). Both tests were performed early in the testing program and had similar nuclear gauge dry unit weights, but the 20 inch ABC test had slightly lower DCPI. The similar curves show that the presence of Geotextile A provided slight improvement over the initial 10,000 cycles. Even with similar subgrades, Geotextile A would have likely shown little additional benefit because of the thick stabilization depth relative to the load plate diameter. A comparison cannot be made during Cyclic 2 loading because the 20 inch ABC test was not subjected to the additional cycles.

For Geotextile A tests with thinner ABC layers (12 and 13 inches for Tests 16 and 18, respectively), a comparison can be made to results from the test with 18 inches of ABC (Test 15). Both thin tests displaced more over the initial cycles because the subgrade stresses were higher (18.6 psi and 26.2 psi versus 17.4 psi at 10,000 cycles) and any layer mixing that occurred in the 18 inch unreinforced ABC test did not offset the layer thickness differences. However, over the second set of cycles, the 12 and 13 inch ABC tests had ABC depths from rut refilling of 17.5 and 16.5 inches, respectively. The 18 inch unreinforced test had approximately 20.5 inches ABC after rut repair. So, even with less ABC, the Geotextile A-reinforced tests displaced less during cyclic 2 because of the mobilized strength in the reinforcement.

As was shown by the quality control data, the tests with thicker ABC layers only had slightly higher average dry unit weights, and that the presence of Geotextile A did not seem to increase compaction compared to unreinforced tests. Heavier field equipment may mobilize the fabric strength more, and subsequently less surface displacement during initial cycles. However, the lack of subgrade reaction due to its lower strength may still hamper this effect.

Excavation of tests with Geotextile A revealed no ABC stone mixing at the layer interface as was seen with unreinforced tests. So, during initial cycles, ABC and subgrade compaction occurred without ABC intrusion. However, in all tests, the geotextile was stained with brown subgrade fines over a circular area with diameter slightly greater than twice the stabilization depth. Figure 92 shows a stained Geotextile A sample. Subgrade deformations apparently caused upward pumping of excess pore water and erosion of fines. Some fines were trapped in Geotextile A, which was a reinforcing and not a filtering fabric. According to the AASHTO Criteria, Geotextile A did not meet the filtration requirements because its Apparent Opening Size (AOS) was too large (#30 sieve) for soils with more than 50%

passing the #200 sieve (AASHTO, 1991). Geotextile A managed to trap a significant amount of eroded soil, so the fabric may have allowed some pore-water to escape upward into the ABC if it remained unclogged. This would have decreased the excess pore water pressure at the interface and strengthened the subgrade.

In conclusion, the following can be stated about the reinforcement Geotextile A tests:

- The presence of Geotextile A did not dramatically increase initial density of stabilization layers. Larger field compaction equipment may have been able to mobilize the reinforcement more, but soft underlying subgrades might still limit the extent and ability to achieve high density for the ABC.

- Stiffer initial performance of select fill tests with thin ABC surface layers resulted from greater overall stabilization depths than the ABC. This resulted in less subgrade stress and deformation. However, after punching failure of the ABC layer, high surface deformations resulted without mobilization of the reinforcement because the select fill simply displaced laterally over the fabric surface without engaging it.

- Geotextile A tests with ABC displaced less than select fill tests after approximately 2,000 cycles. After some initial ABC compaction and subgrade surface displacement, the displacement of the ABC was able to mobilize the reinforcing effects of the fabric.

- The most improvement of test samples performance with Geotextile A, compared to unreinforced ABC tests, occurred when ABC depth was closest to the load plate diameter (12 inches). Improvement was less pronounced for thicker layers near 20 inches. The fabric strength was mobilized with continued deformation.

- Geotextile A improvements were most dramatic during additional cycling after rut refilling due to the tensioning and mobilization of the fabric strength during initial cycles. Again, this improvement was greater for tests with ABC depths similar to the load plate diameter.

- Geotextile A did not meet filter criteria for the Coastal Plain subgrade, but because the openings were large, excess pore water pressure generated during loading may have dissipated upward into the granular layers if the fabric remained unclogged.

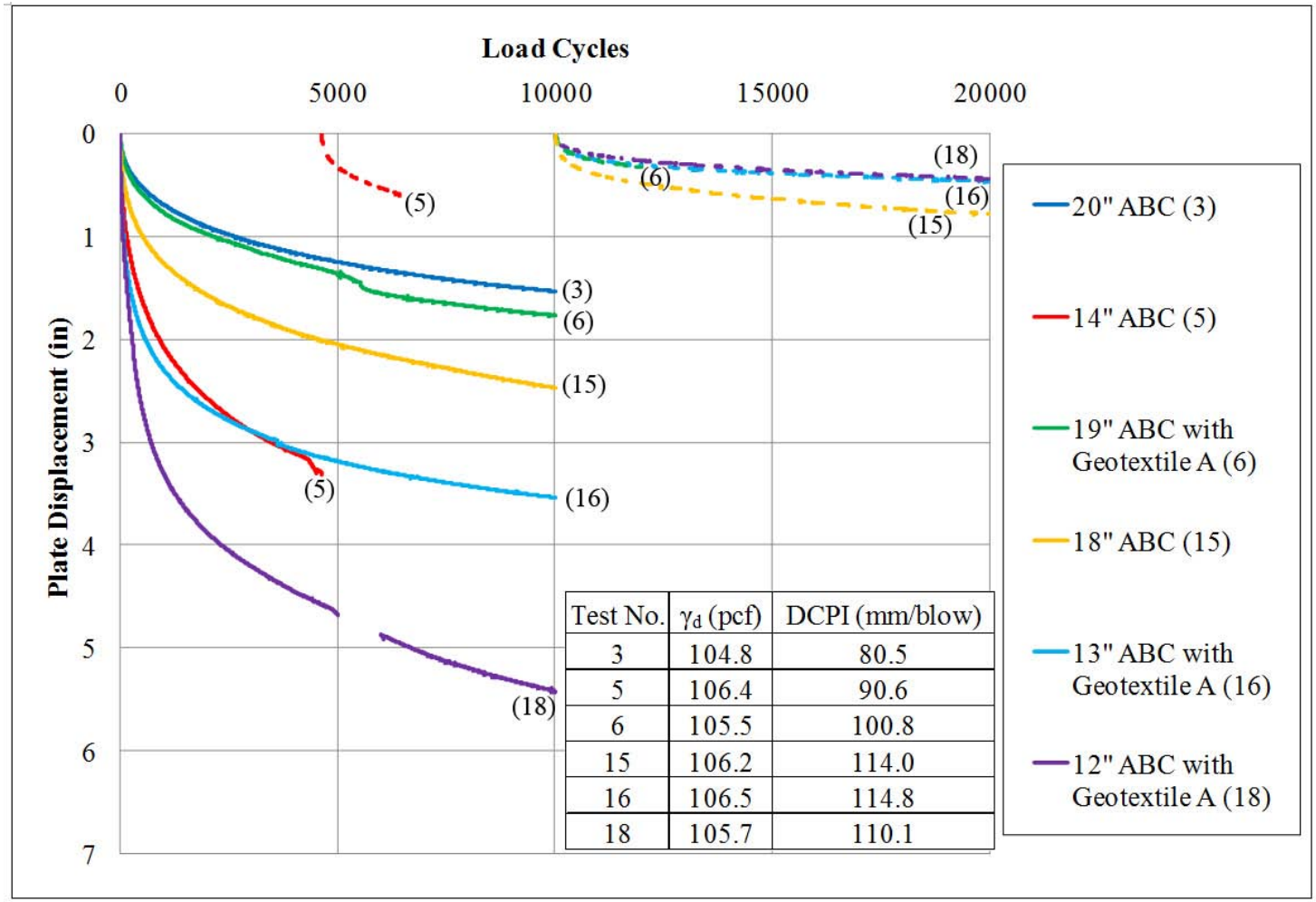

Figure 91. Displacement Curves for Unreinforced and Reinforcement Geotextile A ABC Tests

Figure 92. Fabric Stained by Pumped Subgrade Fines - Post 19" ABC with Geotextile A (6) Test

Separation Geotextile B Tests

Three tests were performed on granular layers reinforced with Geotextile B, which was a separation fabric that had lower stiffness than Geotextile A. Figure 93 shows the displacement curves for these tests.

Performance was very comparable between the 25 inches select fill with 3 inches ABC and 20 inches ABC tests. The effect of the slightly lower DCPI for the select fill test was likely less influential because of the relatively deep stabilization depth. The two tests also displaced the same amount during the second set of cycles. Rut repair depths do not need to be accounted for since both experienced the same amount of rutting during cyclic 1. The select fill test did not exhibit a punching failure because the overall stabilization depth was greater than that existing in the Geotextile A select fill tests.

With a refilled rut of 5 inches, the 13 inch ABC test with Geotextile B became 18 inches during cyclic 2. The initial displacement rate during secondary cycles was high because load cycles compacted the deeply repaired rut depth. In comparison to the 20 inch ABC test, which became 22 inches under the loading plate during cyclic 2, inclusion of Geotextile B did not produce the improvement during secondary cycles shown by Geotextile A because it lacked reinforcing contribution (i.e., Geotextile B is much less stiff than Geotextile A).

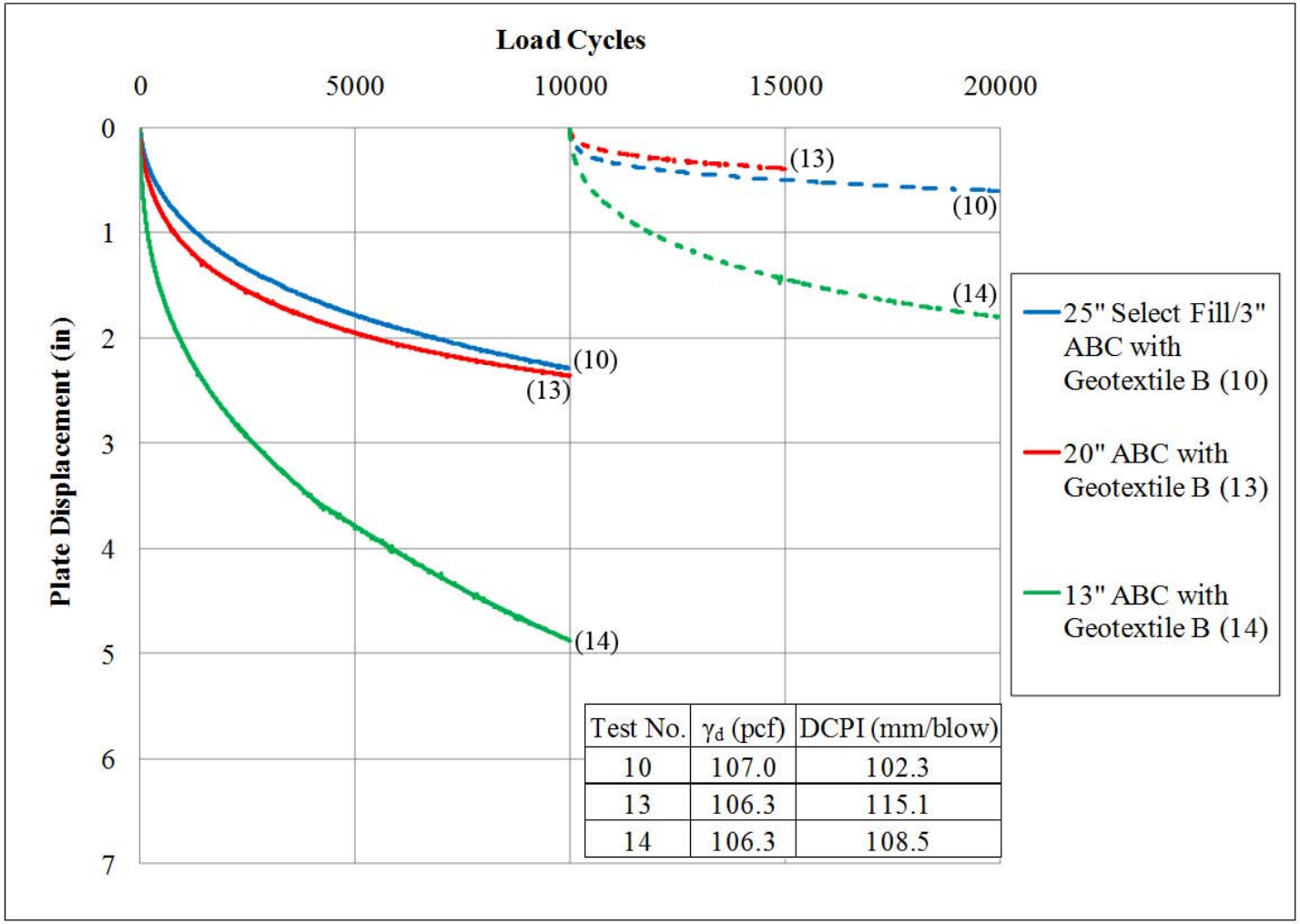

Figure 93. Displacement Curves for Tests Reinforced with Separation Geotextile B

However, Geotextile B experienced staining by subgrade fines similar to that seen in the Geotextile A tests. This behavior can be seen in Figure 94. Tears in the fabric were created during section demolition and did not result from testing. Geotextile B had the same AOS as Geotextile A and therefore also did not meet the filter criteria for the Coastal Plain subgrade. Little staining occurred during the select fill test because the greater stabilization depth created less increase in vertical stress at the fabric depth (6.7 psi versus 28.7 psi at 10,000 cycles for Tests 10 and 14, respectively). Little in-plane drainage likely occurred because Geotextile B, like Geotextile A, is not a drainage fabric.

Figure 95 presents the displacement as a function of load cycles for Geotextile B-reinforced and unreinforced ABC tests of similar depth. It can be seen that the 20 inch ABC test sample with Geotextile B actually displaced more than the unreinforced 20 inch ABC test. The quality control data show that the 20 inch ABC unreinforced test had lower average subgrade corrected nuclear gauge and DCPI (104.8 pcf and 80.5 mm/blow) than the later reinforced test (106.3 pcf and 115.1 mm/blow). A more remolded soil structure may have allowed for a higher dry unit weight but less resistance to DCP penetration.

Figure 94. Fabric Stained by Subgrade Fines - Post 13" ABC with Geotextile B (14) Test

The unreinforced test with 18 inches ABC, though, was performed later in the program and had similar subgrade conditions to the 20 inch ABC with Geotextile B test. The two tests performed similarly over the first 10,000 cycles, and the 20 inch ABC with Geotextile B test showed little improvement over cyclic 2 loading. Rut repair depths did not need to be considered since initial rutting was similar.

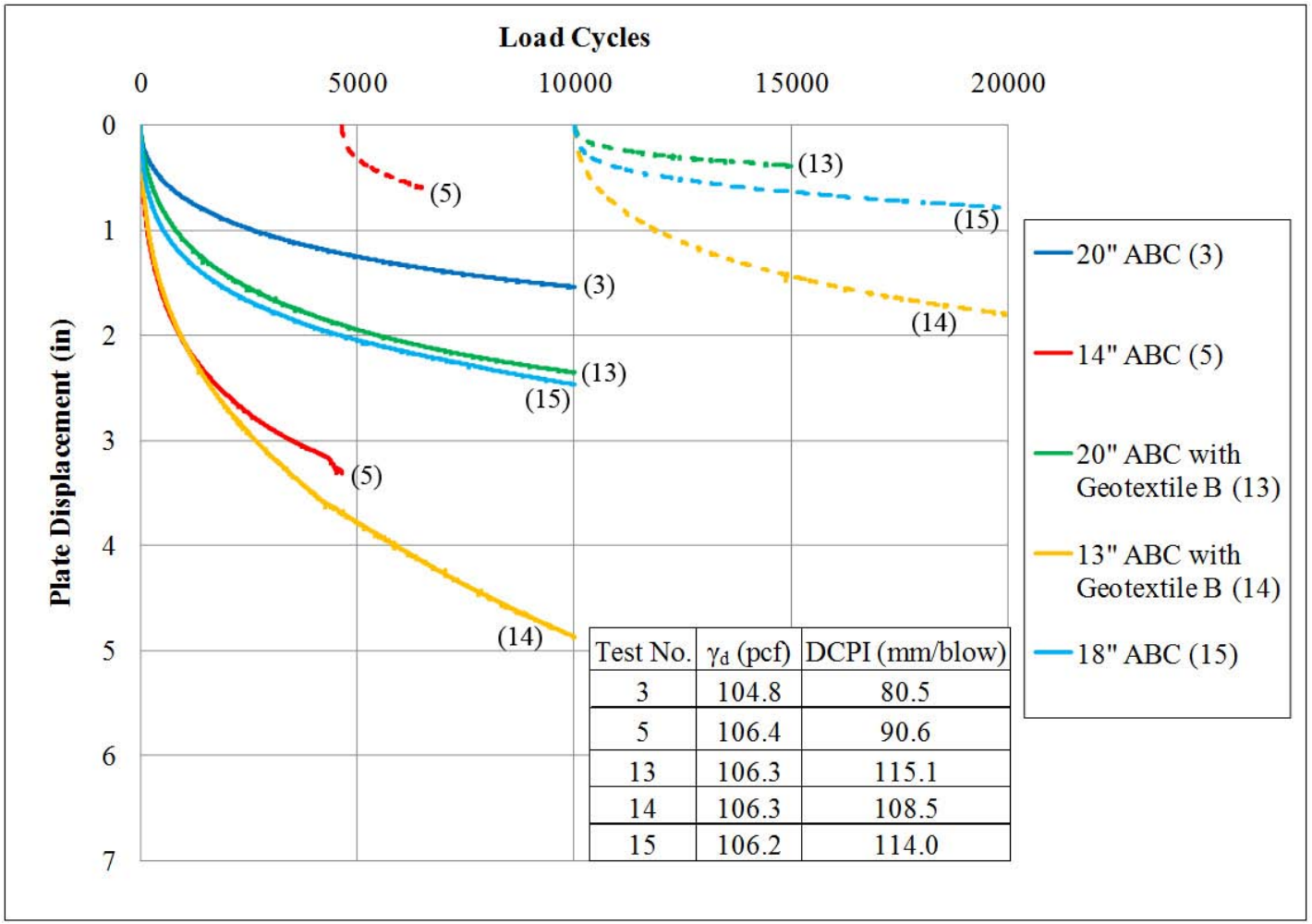

Test No.	γ_d (pcf)	DCPI (mm/blow)
3	104.8	80.5
5	106.4	90.6
13	106.3	115.1
14	106.3	108.5
15	106.2	114.0

Figure 95. Displacement Curves for Unreinforced and Separation Geotextile B ABC Tests

Analysis of the thinner reinforced test section with 13 inches of ABC (Test 14) showed that subgrade remolding effects also had to be considered when compared to the 14 inch unreinforced ABC section (Test 5). The unreinforced 14 inch ABC section test was performed early in the test program, and although it had comparable average subgrade dry unit weight to Test 14 (106.4 to 106.3 pcf for the unreinforced and reinforced tests, respectively), the DCPI was lower (90.6 to 108.5 mm/blow). Despite having a softer remolded subgrade and an inch less of ABC, the 13 inch ABC test with Geotextile B displacement response tracked similarly to the unreinforced test over the first 1,200 cycles.

In comparison to the 18 inch unreinforced test over similar subgrade, the 13 inch ABC test with Geotextile B had more displacement during initial cycles. After rutting, the reinforced test had approximately 18 inches of ABC, while the unreinforced test had 20.5 inches of ABC. With high initial deformation from compaction of the rut repair with ABC, Geotextile B test sample still had more displacement than the unreinforced section.

Even as a separator fabric, Geotextile B did not improve ABC compaction. The lack of support from the soft underlying subgrade and the small laboratory equipment used in compaction likely minimized the separation benefits. Geotextile B did help prevent aggregate punching into the soft subgrade in testing.

In conclusion, the test sections reinforced with separation Geotextile B showed that:

- Stabilization with 25 inches of select fill and 3 inches of ABC produced a system that displaced similarly to 20 inches of ABC, when both were placed over Geotextile B. This held true over initial and post-rut repair cycles.

- The performance benefits of sections reinforced with Geotextile B versus unreinforced ABC layers were minimal. The fabric did not have enough tensile strength to stiffen reinforced systems during initial cycling, nor were sufficient improvements seen after rut refilling.

- The benefits of Geotextile B as a separator fabric were limited to prevention of significant intermixing of the two layers (ABC and subgrade). Compaction density of ABC, even with Geotextile B, may also be low in field situations because the soft subgrade simply does not provide enough reaction.

- Geotextile B prevented downward punching of ABC stones into soft subgrade. The fabric was also stained with subgrade fines that are piped during upward movement of excess pore water in the subgrade. If Geotextile B remained unclogged, it may have helped increase the shear strength of the subgrade near the interface by allowing drainage.

Geogrid A and Geogrid B Tests

Two tests were performed on ABC reinforced with geogrid (one each with Geogrids A and B). Geogrid A had a higher stiffness than Geogrid B. Figure 96 gives the displacement

curves for these two tests, as well as displacement curves of similar unreinforced ABC sections. Secondary cycles were not applied on Test 4.

The first comparison can be made between 16 inch ABC unreinforced (Test 2) and 16 inch ABC reinforced with Geogrid B (Test 4). Both tests were performed early in the testing program and had similar subgrade dry unit weights from corrected nuclear gauge readings (104.4 and 105.4 pcf, respectively). However, the later reinforced test had a higher average subgrade DCPI (102.2 mm/blow) compared to the unreinforced test (87.5 mm/blow). While this explains why the unreinforced test had less displacement than the Geogrid B reinforced test, the differences are small enough to believe that Geogrid B did not provide substantial benefits. This was most likely due to depth of placement and the relatively low stiffness of Geogrid B.

The comparison between Test 17 with 11 inch ABC and Geogrid A and Test 5 with 14 inches of unreinforced ABC is influenced by the same experimental factors. The average subgrade dry unit weight from corrected nuclear gauge readings for this test (107.7 pcf) was similar to the value from 14 inch unreinforced ABC (106.4 pcf). The average subgrade DCPIs, though, were higher for the reinforced test (111.9 mm/blow) in comparison (90.6 mm/blow) because the remolded soil later in the testing program had less resistance to DCP penetration.

Disregarding subgrade differences, a comparison over secondary cycles shows that the displacement curves for Tests 5 and 17 samples would have possibly converged at 15,000 cycles. Considering rut repair, the Geogrid A test had approximately 16 inches of ABC and the unreinforced test had about 17.5 inches of ABC during secondary loading. Both tests gave apparent similar performance at 20,000 cycles

From the results shown, the stiffer Geogrid A provided more benefit than Geogrid B. This was also magnified by the shallow ABC depth. As was seen in the geotextile tests, when the geogrid was placed at a depth similar to the loading plate diameter, the surface displaced less as the reinforcement strength was mobilized with deformation.

The inclusion of either geogrids did not appear to increase ABC compaction on the soft subgrade. A difference between the geotextile and geogrid tests was the inability of geogrids to prevent intermixing of the ABC and the subgrade layers. Small ABC stones could fit between the geogrid ribs and intruded into the subgrade, as shown in Figure 97.
The comparison between Test 17 with 11 inch ABC and Geogrid A and Test 5 with 14 inches of unreinforced ABC is influenced by the same experimental factors. The average subgrade dry unit weight from corrected nuclear gauge readings for this test (107.7 pcf) was fairly similar to the value from 14 inch unreinforced ABC (106.4 pcf). The average subgrade DCPIs, though, were higher for the reinforced test (111.9 mm/blow) in comparison (90.6 mm/blow) because the remolded soil later in the testing program had less resistance to DCP penetration.

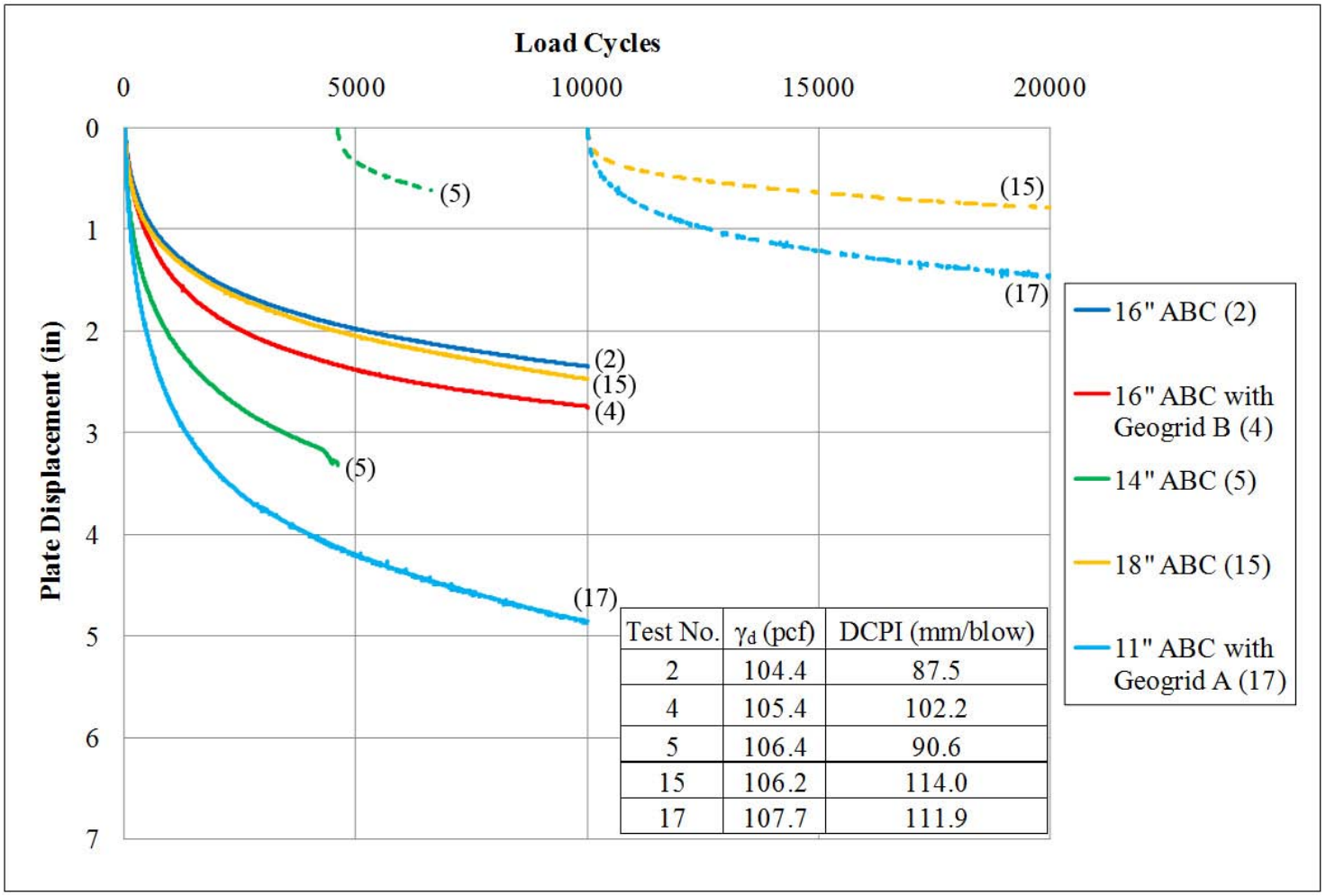

Test No.	γ_d (pcf)	DCPI (mm/blow)
2	104.4	87.5
4	105.4	102.2
5	106.4	90.6
15	106.2	114.0
17	107.7	111.9

Figure 96. Displacement Curves for Unreinforced and Geogrid Reinforced ABC Tests

Figure 97. Layer Mixing (Geogrid Removed) - Post 16" ABC with Geogrid B (4) Test

Disregarding subgrade differences, a comparison over secondary cycles shows that the displacement curves for Tests 5 and 17 would have possibly converged at 15,000 cycles. Considering rut repair, the Geogrid A test had approximately 16 inches of ABC and the unreinforced test had about 17.5 inches of ABC during secondary loading. Since both tests gave apparent similar performance at 20,000 cycles, the Geogrid A provided same stabilization as an additional 1.5 inches of ABC after initial mobilization.

Overall, subgrade variations made quantification of Geogrids A and B inclusion difficult. From the results shown, the stiffer Geogrid A apparently gave more benefit than Geogrid B. This was also magnified by the shallow ABC depth. As was seen in the geotextile tests, when the geogrid was placed at a depth similar to the loading plate diameter, the surface displaced less because the reinforcement underwent more mobilization and potentially intercepted shear failure surfaces.

Although neither geogrid appeared to increase the ability to compact ABC over the soft subgrade layer, a difference between the geotextile and geogrid tests was the inability of geogrids to separate the ABC from the subgrade in this case, and given the size distribution of the ABC layer. Small ABC stones could fit between the geogrid ribs had intruded into the subgrade, as shown as Figure 97.

Small ABC stones intruded into the subgrade during initial layer compaction before ABC began to catch and interlock with the geogrid ribs. Subsequent cycles pushed the interlocked mass further downward, impregnating the geogrid into the subgrade surface. This caused significant permanent strain in the Geogrid A test, as shown by Figure 98. During excavation of the test specimen, the geogrid was turned over and placed upside down on the lab floor. The figure shows a large hump (measured 3 inches), which was a depression in the otherwise flat geogrid. This occurred directly beneath the load plate, and was not seen with Geogrid B

because it had a thicker stabilization layer and less subgrade displacement (1 to 1.25 inches versus 2.75 to 3 inches for Geogrid A).

Figure 98. Permanent Deformation - Post 11" ABC with Geogrid A (Test 17)

Based on the tests with Geogrids A and B, the following conclusions can be made:

- The benefits of the reinforcement were more apparent when placed at depths similar to the load plate diameter where the reinforcement was effectively mobilized. However, differences in subgrade made geogrid inclusion benefits over unreinforced tests difficult to quantify. Given the soft subgrade used in this study, it seems that the geogrid inclusion did not impact ABC compaction level.

- During initial cycles, small ABC stones pushed between the geogrid apertures and into the soft subgrade in both tests. It seems that the geogrid strength was mobilized after larger stones interlocked with the ribs, allowing the ABC mass to compact and displace downward as a whole.

- When placed over soft subgrade, geogrid stiffness was important because the geogrid held the interlocked ABC mass above it from displacing downward. Permanent deformation in Geogrid A occurred because of large subgrade deformations.

Lime Stabilized Subgrade (LSS) Tests

Three tests were performed on Coastal Plain subgrade mixed with hydrated lime which created the Lime Stabilized Subgrade (LSS). Figure 99 presents the vertical displacement as a function of load cycles for each test. On comparative scales, it can be seen that these tests deformed much less than all other tests. All three LSS tests deformed less than 1.25 inches during the initial 10,000 cycles and less than 0.5 inches after rut repair. The load plate significantly rotated around cycle 9,500 during initial loading of Test 19.

The thickest test section with 12 inches LSS and 5 inches ABC (Test 19) had the highest deformation during the initial 10,000 cycles. This reflects a change in LSS construction

procedures. The 9 inch LSS with 4 inches ABC test displaced less than the thicker test because a longer mellowing period (which produced a final water content closer to optimum) and greater compactive effort (jumping-jack rammer instead of a jack hammer) were used. This resulted in UCS values of 53.8 and 111.3 psi for the thicker and thinner LSS, respectively, even though both used the same Coastal Plain subgrade and lime percentage.

The surface profiles of the 12 inch LSS with 5 inches of ABC test showed that nearly all of surface deformation occurred within the ABC layer itself. When the ABC layer thickness was reduced for the 9 inch LSS with 4 inches ABC test, less surface deformation may have occurred because of the higher quality LSS or because the stiffer LSS allowed for greater ABC compaction.

Test 21 with 9 inches Gray LSS and 4 inches ABC displaced more than the same test with Coastal Plain LSS (Test 20). This was because the Gray LSS had a lower UCS (52.4 versus 111.3 psi for Test 20) and this lower strength was verified by higher DCPI values (19.8 versus 9.5 mm/blow). Even though both LSS layers underwent similar mellowing and compaction procedures, the lower plasticity of the Gray subgrade resulted in lower strength LSS despite the higher fines content. Surface profile measurements also showed that about 0.75 inches of deformation occurred in the Gray LSS layer surface as opposed to none in the Coastal Plain LSS. Because the two sections produced similar subgrade stress measurements, it appears that the differences in surface deformations were only due to different LSS strengths. Conclusions that can be made from the LSS tests were:

- Longer mellowing time (3 days versus 1) allowed for greater flocculation of the lime/subgrade mixture and reduced the water content closer to optimum.
- Greater compactive effort on LSS increased the resulting UCS at fixed curing times.
- Higher quality LSS resulted in less surface deformation even when less ABC was placed above it.

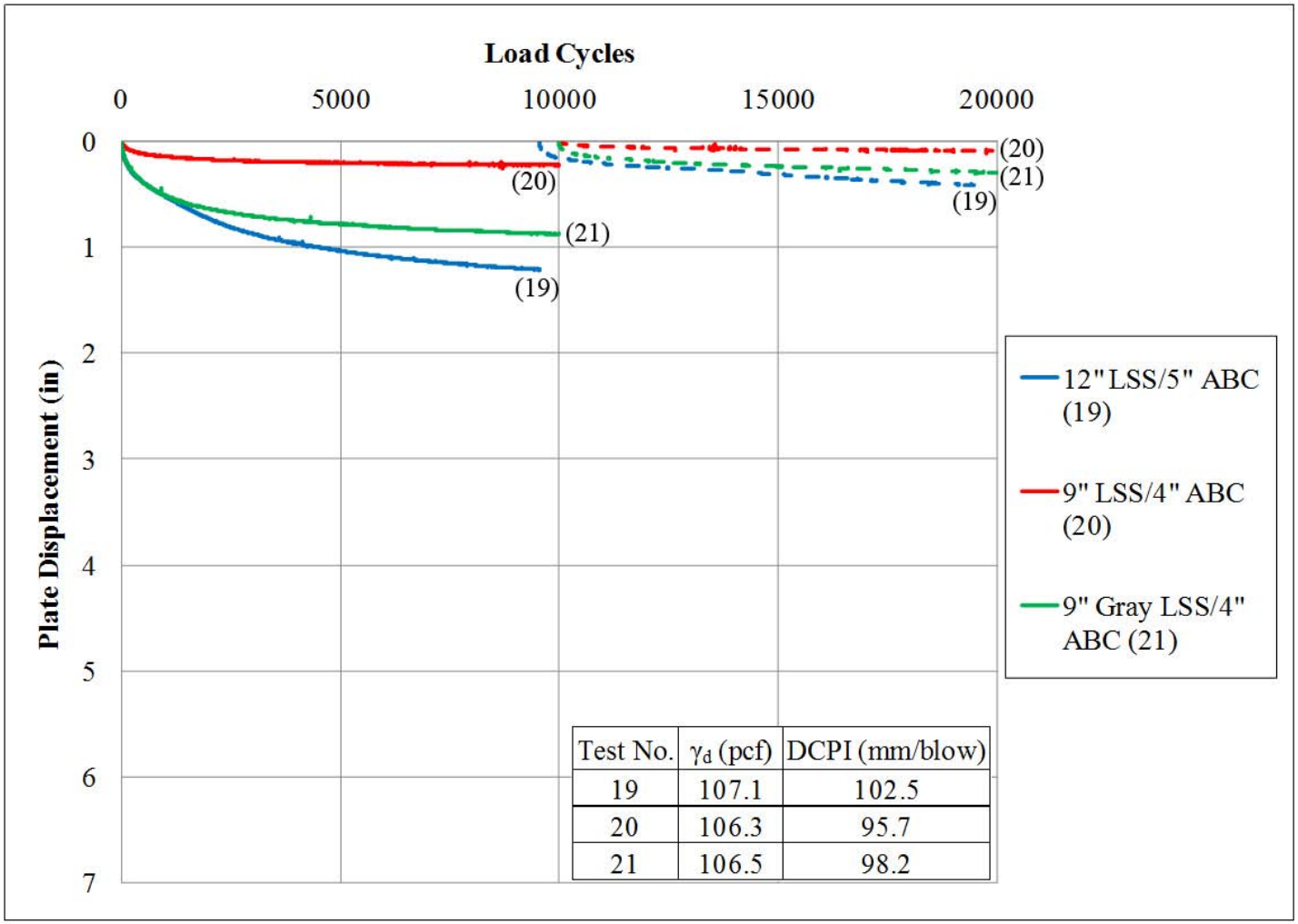

Figure 99. Displacement Curves for LSS Tests

Comparisons by Stabilization Depth

12 inch Undercut Stabilization Tests

Five tests were performed on sections with intended 12 inches of stabilization. The sections had average measured layer depths that were all within 2 inches. Test 5, which had 14 inches of unreinforced ABC, was performed early in the testing program. Because sample exhibited the same subgrade remolding effects discussed previously, it was removed from this comparison. The displacement curves for the remaining four tests are presented as Figure 100.

The test with the least displacement at low initial cycles was the 13 inch ABC test with Geotextile B and was surpassed in displacement by the 13 inch ABC with Geotextile A sample only after 1,800 cycles. This was not expected, but compaction may have mobilized a higher percentage of the fabric's tensile strength for Geotextile B. Geotextile A only had less displacement rate change after cycling mobilized its reinforcing capabilities.

The 13 inch ABC test with Geotextile B experienced less displacement than the 11 inch ABC test with Geogrid It should be mentioned that the tensile strength of Geogrid A and Geotextile B is comparable. However, near the end of 10,000 cycles, both test samples exhibited similar final displacements. Geotextile B was mobilized more during compaction and prevented layer mixing, but the higher stiffness of Geogrid A allowed it provide resistance to limit displacement to the same level as the 13 inch ABC test with Geotextile B, once the geogrid strength is mobilized with deformation. The Geogrid A test also had an inch less of ABC in comparison to the 12 inches ABC with Geotextile The shallower ABC apparently led to higher stress magnitude at the reinforcement level and mobilize at a lower number of cycles.

During the second 10,000 cycles, all of the tests had higher ABC depths beneath the load plate from rut repair. The 12 and 13 inch ABC tests with Geotextile A became 17.5 and 16.5 inches of ABC, respectively. The 11 inch ABC with Geogrid A test increased to about 16 inches of ABC, and the 13 inch ABC test with Geotextile B increased to 18 inches of ABC.

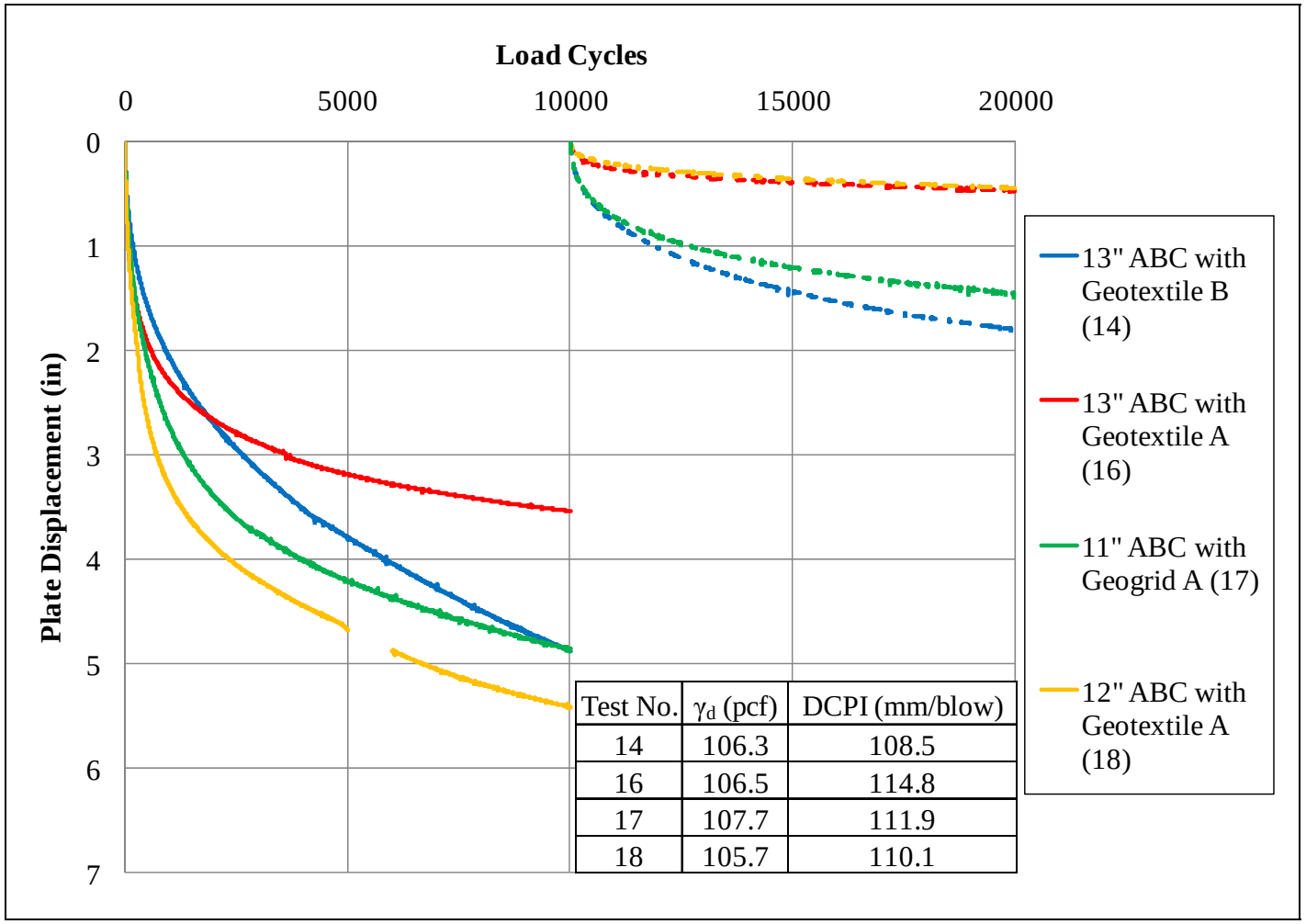

Test No.	γ_d (pcf)	DCPI (mm/blow)
14	106.3	108.5
16	106.5	114.8
17	107.7	111.9
18	105.7	110.1

Figure 100. Displacement Curves for 12 inch Stabilization Tests

Both Geotextile A test samples showed the lowest amount post-rut repair displacement because the reinforcement was sufficiently mobilized over initial cycles. The test samples also needed a lower number of secondary cycles to reach a steady-state even though they had deep repaired ruts.

The Geogrid A and Geotextile B tests performed similarly over secondary cycles, even though they had repaired ABC depths of 16 and 18 inches, respectively. Analysis of the manufacturer-reported ultimate tensile strengths revealed that Geogrid A had less than half the strength value of Geotextile A. So, while the thin ABC depth allowed for high reinforcement mobilization, Geogrid A did not have sufficient strength to withstand high deformation after ABC interlock occurred.

In conclusion, for shallow subgrade stabilization in the realm of 12 inches:

- For low initial cycles (less than 1,800), the test with 13 inches of ABC and Geotextile B had the least displacement. This may have been due to the larger percent mobilization during compaction in comparison to the stiffer reinforcements.

- At higher initial cycles (greater than 1,800), 13 inches of ABC with Geotextile A had the least displacement. This occurred only after displacement took place during initial cycles for mobilization of the reinforcement.

- The test sample with 11 inches ABC and Geogrid A displaced less than the test sample with 12 inches ABC and Geotextile A over the initial 10,000 cycles, and had a final displacement equal to that of 13 inches ABC with Geotextile B. A larger percent mobilization of Geogrid A occurred over early cycles as it had approximately half the ultimate reinforcing capacity of Geotextile A.

- During secondary cycles, both ABC tests with Geotextile A displaced less because the fabric provided both separation and reinforcement. Geotextile A had higher manufacturer-reported tensile strength than either Geotextile B or Geogrid A.

18 inch Undercut Stabilization Tests

Seven tests were performed on sections with intended 18 inches of stabilization. The sections had actual layer depths that were all within 4 inches. Test 3, which had 20 inches of unreinforced ABC, was performed early in the test section and was removed from this comparison. Two of the tests (Tests 4 and 6) were also performed early in the program, but differences that did exist will be noted. The displacement curves for these tests are presented as Figure 101. Cyclic 2 loading was not performed on Test 4 with 16 inches of ABC and Geogrid B.

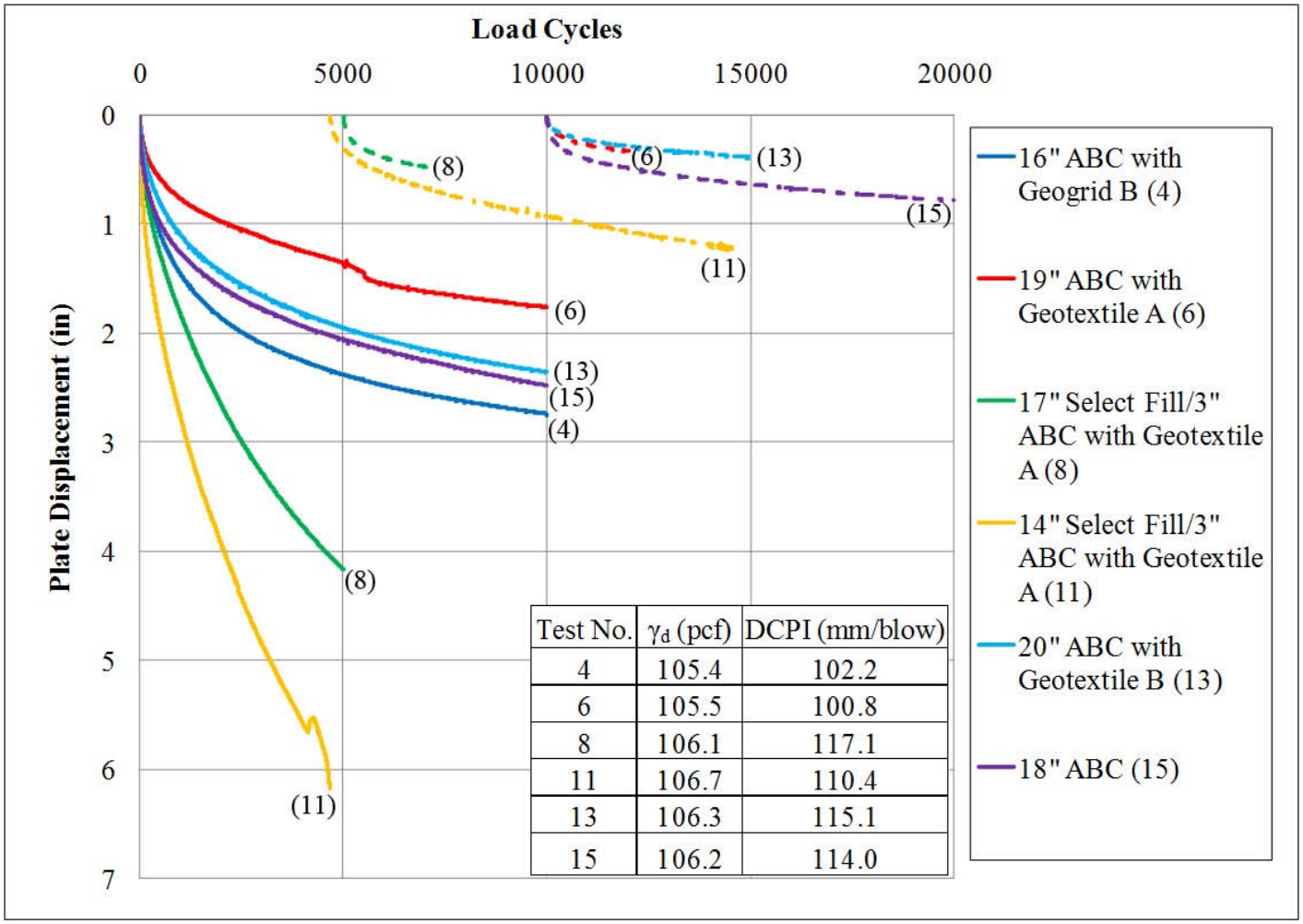

Figure 101. Displacement Curves for 18 inch Stabilization Tests

The select fill tests displaced more than all ABC tests during initial cycles. The presence of the reinforcement did not prevent the select fill from spreading laterally after the upper ABC failed in punching shear. The tests only displaced less when the ABC did not punch through during secondary cycling.

Subgrade remolding slightly affected the comparison between the 19 inch ABC with Geotextile A (Test 6) and the 20 inch ABC with Geotextile B (Test 13) section. The early test had an average subgrade dry unit weight of 105.5 pcf. This was similar to the average 106.2 pcf dry unit weight of the 20 inch ABC with Geotextile B, but the DCPI for this test was higher (114.0 mm/blow) than the earlier section (105.5 mm/blow). The lack of difference in displacement between these test samples again shows how placing the fabric at depths greater than the loading width minimized any effects.

During secondary cycles, all ABC tests showed high initial displacement rate associated with compaction of the repaired rut. Confinement of the compacted ABC refill helped the test reach a constant displacement rate much quicker. The 19 inch ABC test with Geotextile A, which increased to approximately 20.5 inches ABC after rut repair, performed similarly to the 20 inch ABC test with Geotextile B that became 22.5 inches of ABC during secondary cycles. Considering the differences in subgrade strength due to remolding effect, this again shows that the benefits of the stiff fabric reinforcement were not as significant as in the 12 inch tests.

Of the three reinforced ABC tests, the section with 16 inches of ABC and Geogrid B displaced most during initial cycles. While it had the thinnest amount of ABC, it also had a stiffer subgrade because it was performed early in testing. This again showed the importance of the separation function of the geotextile when ABC layers are placed over soft subgrades. The less stiff geogrid could not prevent downward movement of the interlocked ABC mass above it. Even though secondary cycles were not performed on this section, it is doubtful that any mobilization effects would have been seen.

Based on the performance data, conclusions about tests with approximately 18 inches of stabilization were:

- Subgrades stabilized with select fill and thin ABC layers displaced more than purely ABC sections because lateral densification of select fill after punching failure of the upper ABC. The select fill tests showed improvement over the secondary cycles because the repaired ABC layer did not punch through as easily. These effects were not likely due to any mobilization of the reinforcement because the select fill did not seem to engage the reinforcement.

- Tests with deeper ABC layers and geotextile displaced the least during secondary cycles. However, these tests had layer thicknesses greater than the loading plate diameter, so the reinforcement benefits were less than for thinner test sample because of less mobilization.

Deep Undercut Tests

Three tests were performed on sections with deep undercut stabilization (greater than 24 inches). The displacement curves for these tests are presented as Figure 102. Although there were some differences in subgrade displacement, the effect on surface displacement was less pronounced as the subgrade layer was not subjected to significant stress influence (because of the stabilization layer thickness). The Geotextile B reinforced test with less stabilization (25 inches select fill and 3 inches ABC) performed similarly to the 36 inch select fill and 3 inches ABC test over both initial and post-rut repair cycles. Accordingly, it might be inferred that the presence of Geotextile B is equivalent to 11 inches of select fill. However, the maximum vertical stresses at the subgrade surface for these tests were only 1.96 and 0.43 psi at 10,000 cycles for the 25 inch select fill test and the 36 inch select fill test, respectively. Thus, the interface layers were deep enough from the load plate that they had little effect on resulting surface displacement. The deep undercut, though, prevented ABC punching failure during initial cycles as compared to the case during shallower select fill tests.

Test 7 with 36 inches of select fill was the first test to use select fill. The test sample yielded significant heave at low initial cycles. The 3 inch ABC layer on the top of the surface in Test 9 provided enough confinement to limit the heave and decrease plate displacement significantly. As mentioned earlier, differences in subgrade did not greatly influence surface displacement because of the significant stabilization depth.

The presence of Geotextile B did not help with select fill compaction and did not reduce the long term displacement rates because the fabric was not meant as a reinforcement type. In this case, select fill sand particles never intruded into the subgrade and no interlayer mixing was observed.

In conclusion, the test sections with deep undercut showed that:

- Sample with 25 inches of select fill and 3 inches of ABC over Geotextile B performed similarly to 36 inches of select fill and 3 inches of ABC over both initial and post-rut repair cycles. It was more likely that differences in stabilization configurations at depth greater than the load plate diameter did not significantly alter surface deformation. This was explained by low vertical stress increase at the subgrade level.

- Thin ABC surface lifts helped prevent surface heave of the select fill and significantly improved select fill performance.

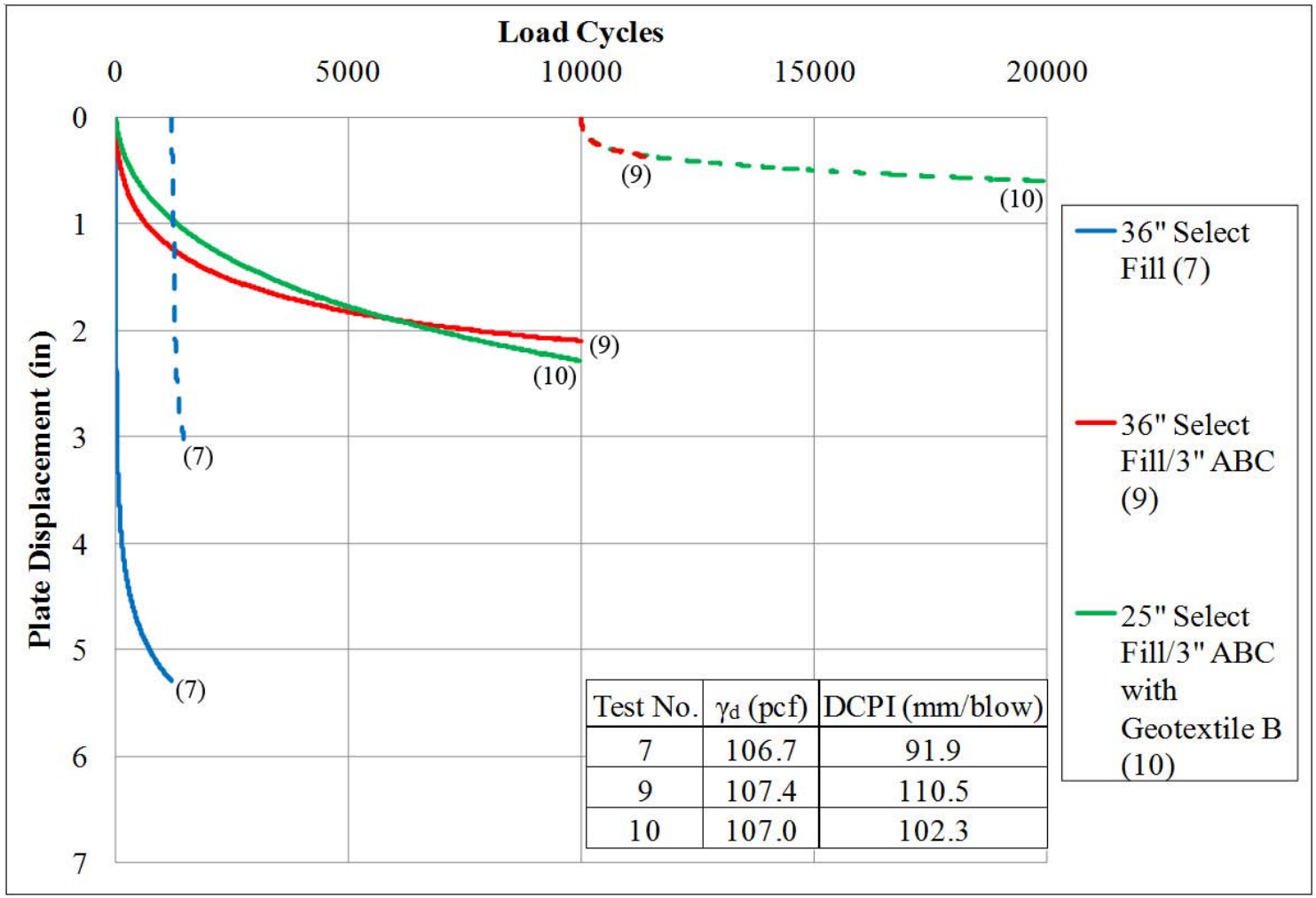

Figure 102. Displacement Curves for Deep Stabilization Tests

Comparison to Results in Literature

Unreinforced Granular Layer Tests

Performance aspects of the unreinforced granular layers reported in this study were compared to applicable results presented in the literature. Only cyclic 1 data were compared to exclude any effects of rut refilling. Comparisons were made to sections tested by Tingle and Jersey (2005) and Christopher and Lacina (2008). Aside from different soil type is these tests, a significant difference is a longer load pulse used by Christopher and Lacina (2008). The ESALs used for data presentation by Tingle and Jersey (2005) had to be divided by two to obtain number of cycles.

These tests produced displacements significantly greater than the obtained data for the 14 inch ABC test because of the softer subgrade, smaller stabilization depth, and perhaps because of the slightly longer load pulse duration.

Figure 103 compares the literature to the 14 inch ABC test (5). The figure uses a reduced vertical and horizontal scale from previous graphs for easier comparison at low cycles. Two tests performed by Christopher and Lacina (2008) consisted of 12 inches of aggregate over a subgrade with CBR equal to 1.0%. These tests produced displacements significantly greater than the obtained data for the 14 inch ABC test because of the softer subgrade, smaller stabilization depth, and perhaps because of the slightly longer load pulse duration.

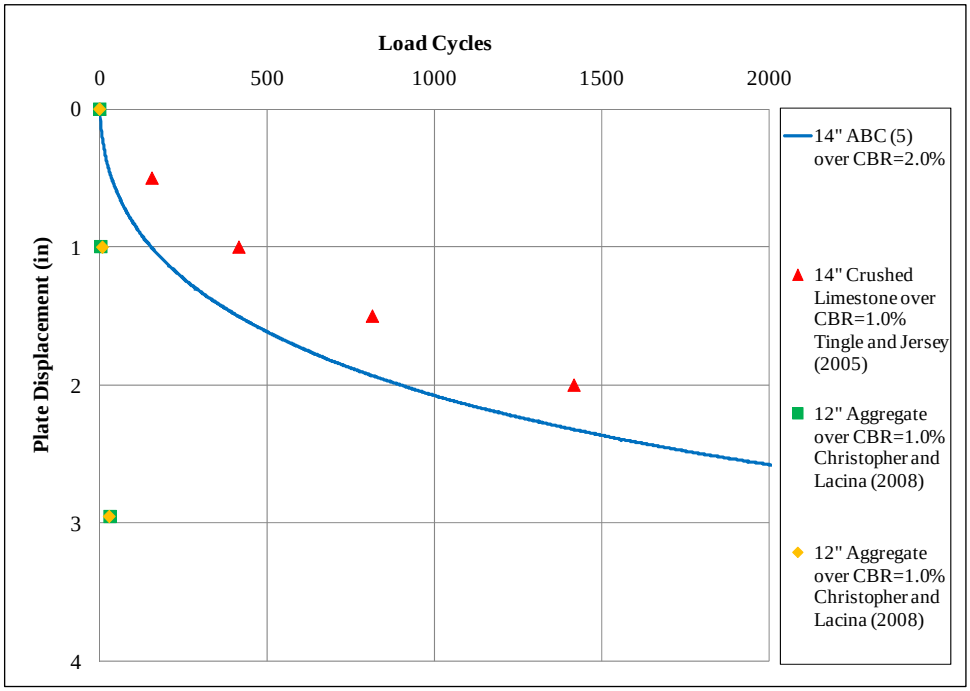

Figure 103. 14" ABC (5) Displacement Curve Compared to Literature Test Results

The test from Tingle and Jersey (2005) had 14 inches of granular material, but it was placed over a CH subgrade with CBR of 1.0%. This test displaced less than the comparable test from this research, despite having a lower CBR subgrade. This may be due to the fact that crushed limestone was used rather than ABC as the stabilization layer. Although not shown, this performance difference was also seen between the 20 inch ABC (3) test and a 20 inch crushed limestone test from Tingle and Jersey (2005). The number of cycles to 0.5 inches surface deformation was approximately 16,000 for the Tingle and Jersey (2005) test versus about 400 cycles for Test 3 in this study.

Geosynthetic-Reinforced Tests

Displacement curves from geotextile and geogrid are compared to literature test results in Figure 104 and Figure 105, respectively. Figure 104 shows the results from Christopher and Lacina (2008), in which they used Geotextiles A and B between aggregate and subgrade with a CBR of 1.0%. The 13 inch ABC with Geotextile B (Test 14) displaced less than the Christopher and Lacina (2008) Geotextile B test with 1 inch less aggregate over the first 250 cycles. However, their test had a dramatic decrease in displacement rate and had less displacement than Test 14 during the remaining 750 cycles. Similarly, Tests 13 and 14 with 12 and 13 inches of ABC with Geotextile A (respectively) displaced less than the comparable section from Christopher and Lacina (2008) over initial 100 load cycles before the literature results had less displacement.

Although the subgrade used by Christopher and Lacina (2008) had lower CBR than the subgrade used here (CBR approximately 2.0%) as well as a longer load pulse duration, their tests likely displaced less because of differences in the granular stabilization material. The reported dry density of their aggregate was approximately 145 pcf, much higher than the average 128.5 pcf of the ABC in this testing. This was probably accomplished using heavier laboratory compaction equipment, and not only decreased the amount of granular layer compaction, but helped increase geotextile mobilization under initial cyclic loading. Christopher and Lacina (2008) performed tests on Geotextile A and B at the same stabilization depth. This was also done in this program with Tests 14 and 16 (both with 13 inches of ABC), where the lower strength Geotextile B displaced less than the reinforcing Geotextile A over the first 1,000 load cycles similar to their test response. Since this testing carried out loading to more cycles, it appears that Geotextile A mobilized under further cycles producing a stiffening effect with the resulting displacement matching Geotextile B at approximately 1,800 cycles.

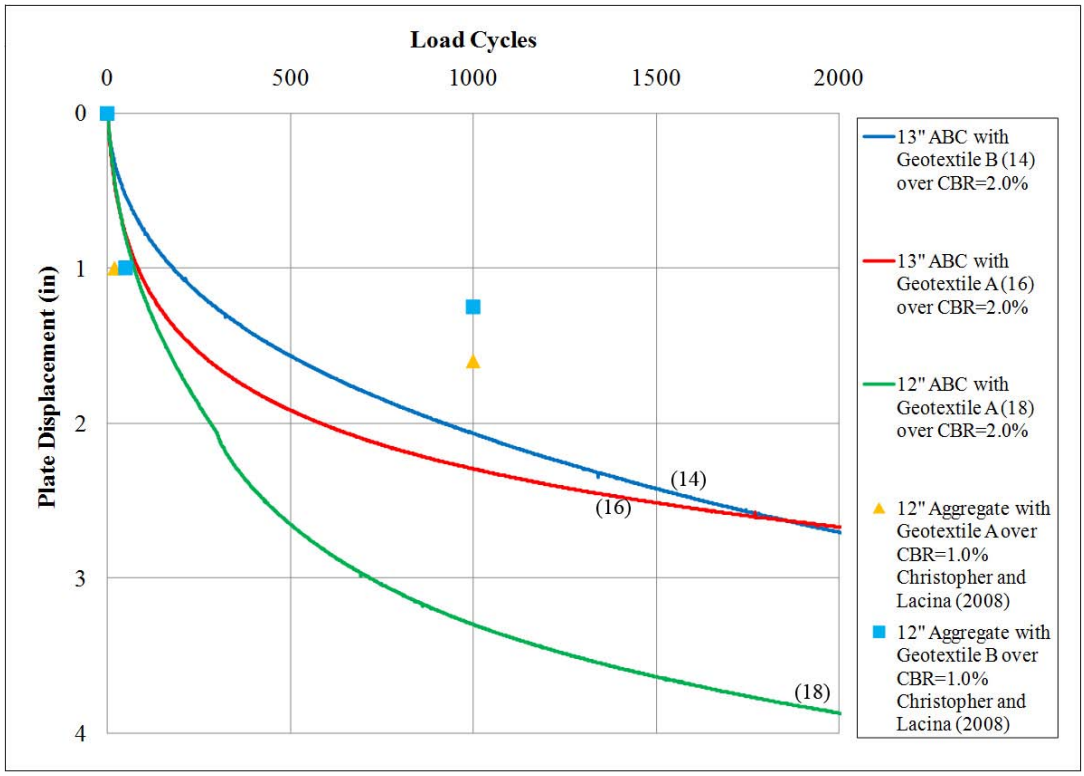

Figure 104. Geotextile Tests compared to Literature Test Results

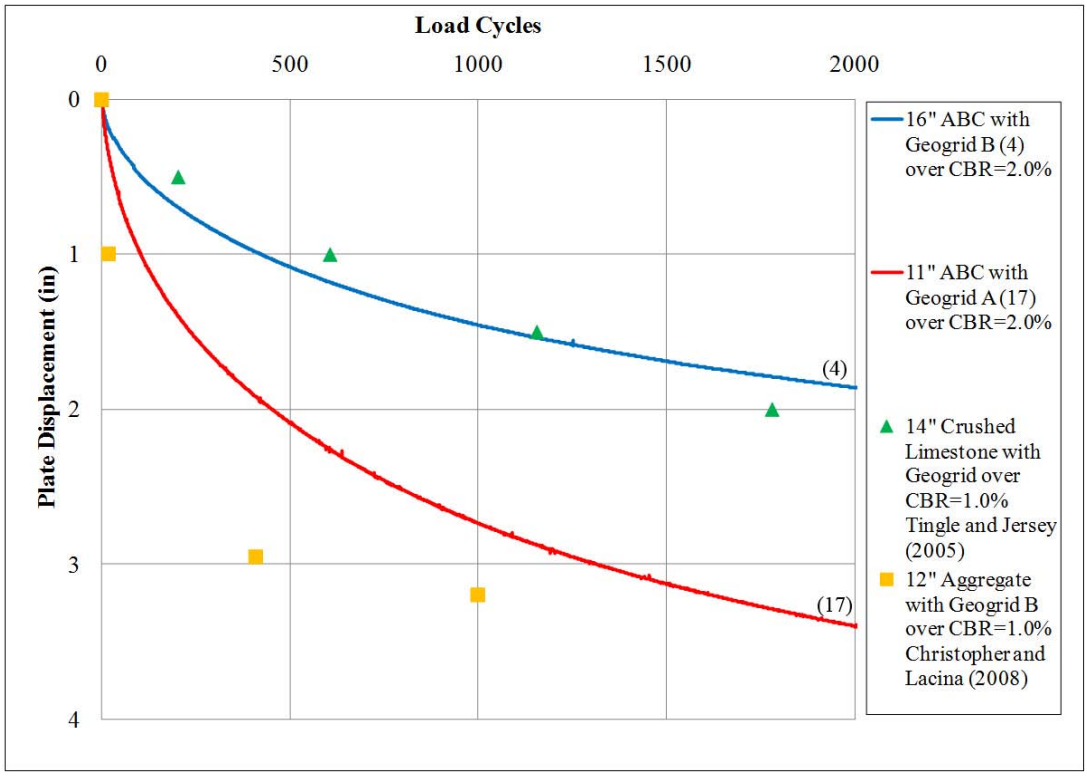

Figure 105. Geogrid Tests compared to Literature Test Results

From Figure 105, it can be seen that the sample test with 12 inch aggregate with Geogrid B performed by Christopher and Lacina (2008) displaced more than the 16 inch ABC with Geogrid B (Test 4) section. Despite having a stiffer granular layer, the Christopher and Lacina (2008) test had higher surface deformation because with a thinner stabilization layer a higher stress increase is transmitted to the softer (CBR of 1.0%) subgrade.

The test performed by Tingle and Jersey (2005) used a geogrid with strength properties between Geogrids A and B, as well as an intermediate stabilization layer thickness. The results from Tingle and Jersey (2005) test were comparable to the results from the 16 inch ABC with Geogrid B section performed in this study as shown in Figure 19.

Equivalent Stabilization Comparison Methodology

Stabilization layer compaction, layer mixing, and geosynthetic mobilization depended on the number of applied cycles. Thus, the number of applied cycles and whether or not the rut has been repaired must be considered before making an equivalence comparison. To facilitate the comparison, the highly non-linear displacement curves were most appropriately linearized into three intervals. The intervals chosen were 0 to 200 cycles, 200 to 1,000 cycles, and 1,000 to 10,000 cycles for both cyclic 1 and 2 load sets because they represented the approximate point of displacement rate change for most tests. Incremental change in plate displacement was calculated for each test between these cycle intervals. The values were then sorted to determine which sections had equivalent performance over certain cycle intervals. An example is shown in Figure 106 for Test 15.

For tests that did not reach 10,000 cycles, displacements were extrapolated using best fit function to the measured displacements. First, the curve fitting function was determined by fitting it to data that reached 10,000 cycles, then curves that did not reach 10,000 cycles were fit and extrapolated. An example of two extrapolated curves for a given test is shown in Figure 107. The figures present the fitted equation and coefficient of determination to the measured data. Cyclic 2 displacements were only extrapolated to an additional 10,000 cycles regardless of the cyclic 1 end point. All extrapolated displacements used in the equivalence comparison will be noted by an asterisk.

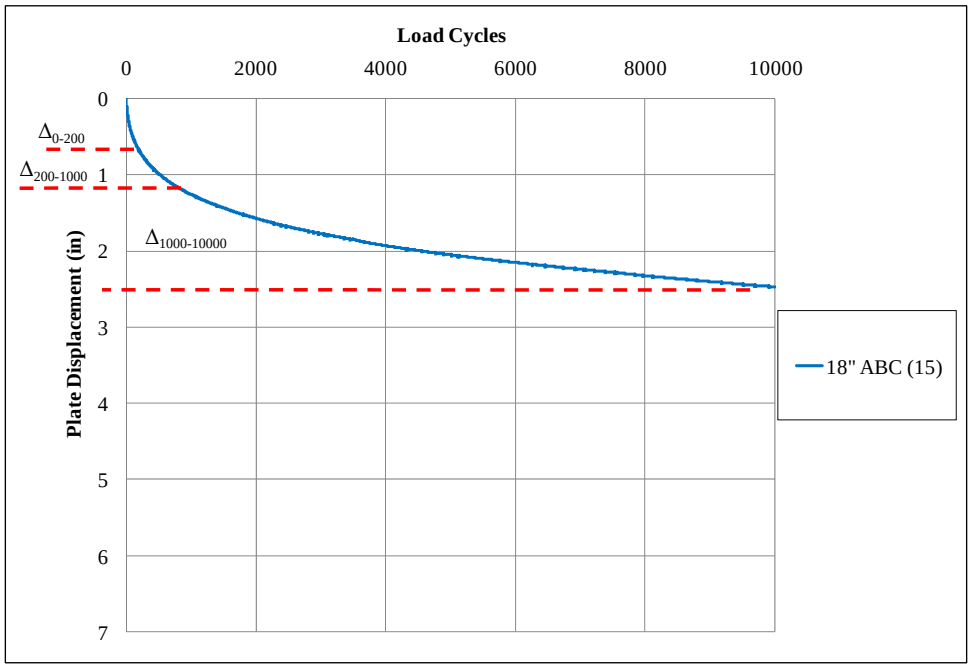

Figure 106. Incremental displacement calculation example for 18" ABC (15) Test

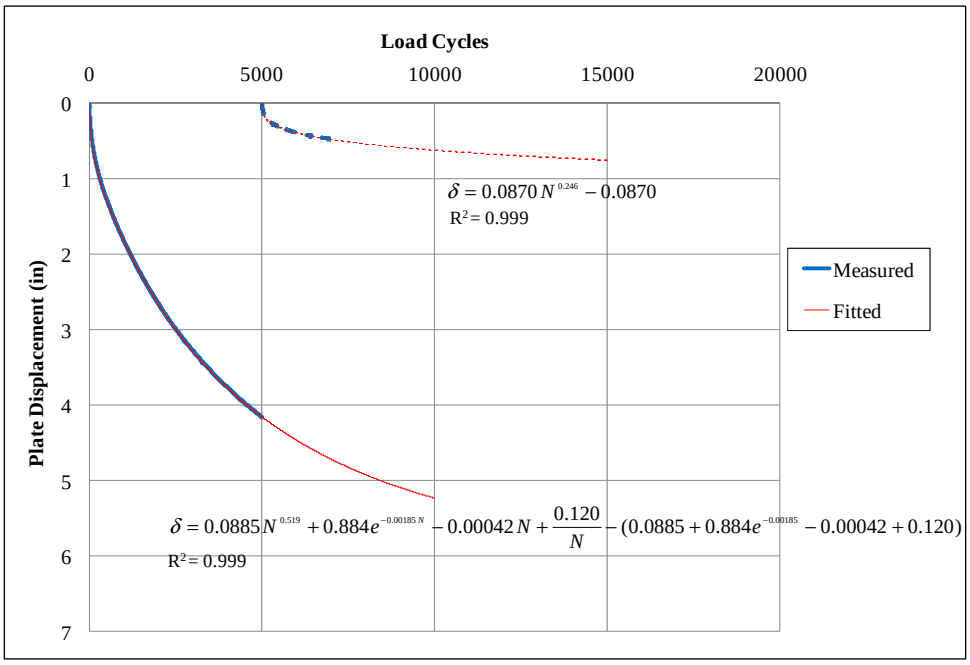

Figure 107. Extrapolated Displacements from 17" Select Fill/3" ABC with Geotextile A (8) Tests

Equivalence Comparison during Initial Cycles

Table 64 presents the sorted displacement results between 0 and 200 cycles of initial loading. Grouped tests with similar displacements have similar shaded cells. Based on the displacements in Table 64, stabilization methods can be grouped into configurations with similar incremental surface deformations. The equivalent stabilization methods were:

Table 64. Tests Sorted by Cyclic 1 Displacement between 0 and 200 Cycles

Test Configuration (Test No.)	Displacement (in)
9" LSS/4" ABC (20)	0.086
9" Gray LSS/4" ABC (21)	0.261
12" LSS/5" ABC (19)	0.274
20" ABC (3)	0.348
25" Select Fill/3" ABC with Geotextile B (10)	0.378
19" ABC with Geotextile A (6)	0.393
20" ABC with Geotextile B (13)	0.502
16" ABC (2)	0.594
36" Select Fill/3" ABC (9)	0.618
18" ABC (15)	0.677
16" ABC with Geogrid B (4)	0.693
17" Select Fill/3" ABC with Geotextile A (8)	0.804
13" ABC with Geotextile B (14)	1.052
14" ABC (5)	1.119
14" Select Fill/3" ABC with Geotextile A (11)	1.262
11" ABC with Geogrid A (17)	1.385
13" ABC with Geotextile A (16)	1.427
12" ABC with Geotextile A (18)	1.684

<u>0.0 to 0.5 inches:</u>
9 inches LSS with 4 inches ABC, 9 inches Gray LSS with 4 inches ABC, 12 inches LSS with 5 inches ABC, 20 inches ABC, 25 inches select fill with 3 inches ABC and Geotextile B, and 19 inches ABC with Geotextile A.

<u>0.5 to 1.0 inches:</u>
20 inches ABC with Geotextile B, 16 inches ABC, 36 inches select fill with 3 inches ABC, 18 inches ABC, 16 inches ABC with Geogrid B, and 17 inches select fill with 3 inches ABC and Geotextile A.

<u>Greater than 1.0 inches:</u>
13 inches ABC with Geotextile B, 14 inches ABC, 14 inches select fill with 3 inches ABC and Geotextile A, 11 inches ABC with Geogrid A, 13 inches ABC with Geotextile A, and 12 inches ABC with Geotextile A.

Table 65 presents the sorted displacement results between 200 and 1000 cycles of initial loading. Grouped tests with similar displacements have similar shaded cells. The stabilizations with equivalent performance between 200 and 1,000 initial cycles were:

0.0 to 0.5 inches:
9 inches LSS with 4 inches ABC, 12 inches LSS with 5 inches ABC, 9 inches Gray LSS with 4 inches ABC, 20 inches ABC, and 19 inches ABC with Geotextile A.

0.5 to 1.0 inches:
25 inches select fill with 3 inches ABC and Geotextile B, 36 inches select fill with 3 inches ABC, 18 inches ABC, 20 inches ABC with Geotextile B, 16 inches ABC, 16 inches ABC with Geogrid B, 13 inches ABC with Geotextile B, and 14 inches ABC.

Greater than 1.0 inch:
13 inches ABC with Geotextile B, 17 inches select fill with 3 inches ABC and Geotextile A, 11 inches ABC with Geogrid A, 14 inches select fill with 3 inches ABC and Geotextile A, and 12 inches ABC with Geotextile A.

Table 66 presents the tests sorted by surface displacement between 1,000 and 10,000 initial cycles. Test numbers 5, 8, and 11 did not reach 10,000 cycles and used curve-fits to find extrapolated displacements. Larger displacement intervals were used for grouping than previous tables. Based on the table, the stabilization methods with equivalent performance were:

Table 65. Tests Sorted by Cyclic 1 Displacement between 200 and 1,000 Cycles

Test Configuration (Test No.)	Displacement (in)
9" LSS/4" ABC (20)	0.059
12" LSS/5" ABC (19)	0.250
9" Gray LSS/4" ABC (21)	0.252
20" ABC (3)	0.344
19" ABC with Geotextile A (6)	0.373
25" Select Fill/3" ABC with Geotextile B (10)	0.503
36" Select Fill/3" ABC (9)	0.538
18" ABC (15)	0.583
20" ABC with Geotextile B (13)	0.595
16" ABC (2)	0.612
16" ABC with Geogrid B (4)	0.765
13" ABC with Geotextile A (16)	0.870
14" ABC (5)	0.959
13" ABC with Geotextile B (14)	1.014
17" Select Fill/3" ABC with Geotextile A (8)	1.016
11" ABC with Geogrid A (17)	1.352
14" Select Fill/3" ABC with Geotextile A (11)	1.507
12" ABC with Geotextile A (18)	1.614

0.0 to 0.5 inches:
9 inches LSS with 4 inches ABC, and 9 inches Gray LSS with 4 inches ABC.

0.5 to 1.0 inches:
12 inches LSS with 5 inches ABC, 20 inches ABC, 36 inches select fill with 3 inches ABC, and 19 inches ABC with Geotextile A.

Table 66. Tests Sorted by Cyclic 1 Displacement between 1,000 and 10,000 Cycles

Test Configuration (Test No.)	Displacement (in)
9" LSS/4" ABC (20)	0.082
9" Gray LSS/4" ABC (21)	0.363
12" LSS/5" ABC (19)	0.693
20" ABC (3)	0.846
36" Select Fill/3" ABC (9)	0.952
19" ABC with Geotextile A (6)	0.999
16" ABC (2)	1.149
18" ABC (15)	1.216
13" ABC with Geotextile A (16)	1.244
20" ABC with Geotextile B (13)	1.263
16" ABC with Geogrid B (4)	1.303
25" Select Fill/3" ABC with Geotextile B (10)	1.402
14" ABC (5)	1.423*
11" ABC with Geogrid A (17)	2.128
12" ABC with Geotextile A (18)	2.401
13" ABC with Geotextile B (14)	2.812
17" Select Fill/3" ABC with Geotextile A (8)	3.407*
14" Select Fill/3" ABC with Geotextile A (11)	5.701*

1.0 to 2.0 inches:
16 inches ABC, 18 inches ABC, 13 inches ABC with Geotextile A, 20 inches ABC with Geotextile B, 16 inches ABC with Geogrid B, 25 inches select fill with 3 inches ABC with Geotextile B, and 14 inches ABC.

Greater than 2.0 inches:
11 inches ABC with Geogrid A, 12 inches ABC with Geotextile A, 13 inches ABC with Geotextile B, 17 inches select fill with 3 inches ABC and Geotextile A, and 14 inches select fill with 3 inches ABC and Geotextile A.

In summary, data in these three tables showed that over initial cycle increments:

- Tests with LSS had lowest initial displacement over all cycle intervals compared to all granular layer tests.

- Generally, tests with greater stabilization depth displaced less over all intervals. Geosynthetic reinforcement had minimal effect on displacement during initial cycles. Some of these tests showed improvement during later cycle intervals, but most of these tests also had greater stabilization depths that minimized the effects of reinforcement inclusion.

- Tests with thin select fill stabilization layers and geotextile reinforcement experienced punching failure of the load plate through the thin ABC surface layer. The stabilized subgrade was too shallow, and the reinforcement did not mobilize as the plate displaced because the select fill spread laterally without engaging the reinforcement. These tests had high incremental displacements even during later cycle intervals.

- . Overall greater stabilization depth reduced the deformations in the subgrade.

Equivalence Comparison: Post-Repair Cycles

Table 67 presents test sections sorted by surface displacements between 0 and 200 cycles during the second loading after rut repair. Secondary cycles were not performed on test numbers 2 through 4. Added thickness of ABC for rut repair is also given for reference. The values are actual rut repair depths and not based on extrapolated displacements.

The range of deformations was less than during initial loading. All test samples for which data are available experienced a deformation range from 0.0 to 0.5 inches in this case. Table 68 presents test sections sorted by surface displacements between 200 and 1,000 cycles during the second loading period. Again up the 1000 cycles, deformation did not exceed 0.5 inch.

Table 67. Tests Sorted by Cyclic 2 Displacement between 0 and 200 Cycles

Test Configuration (Test No.)	Displacement (in)	Add. ABC (in)
9" LSS/4" ABC (20)	0.029	0.228
9" Gray LSS/4" ABC (21)	0.100	0.875
12" LSS/5" ABC (19)	0.128	1.217
12" ABC with Geotextile A (18)	0.130	5.699
20" ABC with Geotextile B (13)	0.139	2.361
19" ABC with Geotextile A (6)	0.155	1.766
13" ABC with Geotextile A (16)	0.159	3.540
25" Select Fill/3" ABC with Geotextile B (10)	0.208	2.283
36" Select Fill/3" ABC (9)	0.215	2.108
17" Select Fill/3" ABC with Geotextile A (8)	0.231	4.163
14" Select Fill/3" ABC with Geotextile A (11)	0.243	6.181
18" ABC (15)	0.250	2.476
14" ABC (5)	0.262	3.296
11" ABC with Geogrid A (17)	0.392	4.865
13" ABC with Geotextile B (14)	0.395	4.878
16" ABC (2)	N/A	N/A
20" ABC (3)	N/A	N/A
16" ABC with Geogrid B (4)	N/A	N/A

Table 69 presents test sections sorted by surface displacement between 1,000 and 10,000 cycles during the second loading period. Several tests did not reach 10,000 secondary cycles have extrapolated displacements and are noted with an asterisk. The table shows that the stabilization methods that produced similar surface deformations were:

Table 68. Tests Sorted by Cyclic 2 Displacement between 200 and 1,000 Cycles

Test Configuration (Test No.)	Displacement (in)	Add. ABC (in)
9" LSS/4" ABC (20)	0.021	0.228
9" Gray LSS/4" ABC (21)	0.056	0.875
12" LSS/5" ABC (19)	0.063	1.217
12" ABC with Geotextile A (18)	0.086	5.699
20" ABC with Geotextile B (13)	0.092	2.361
13" ABC with Geotextile A (16)	0.104	3.540
36" Select Fill/3" ABC (9)	0.115	2.108
19" ABC with Geotextile A (6)	0.117	1.766
25" Select Fill/3" ABC with Geotextile B (10)	0.129	2.283
18" ABC (15)	0.156	2.476
17" Select Fill/3" ABC with Geotextile A (8)	0.157	4.163
14" ABC (5)	0.212	3.296
14" Select Fill/3" ABC with Geotextile A (11)	0.235	6.181
11" ABC with Geogrid A (17)	0.334	4.865
13" ABC with Geotextile B (14)	0.383	4.878
16" ABC (2)	N/A	N/A
20" ABC (3)	N/A	N/A
16" ABC with Geogrid B (4)	N/A	N/A

<u>0.0 to 0.5 inches:</u>
9 inches LSS with 4 inches ABC, 9 inches Gray LSS with 4 inches ABC, 13 inches ABC with Geotextile A, 12 inches LSS with 5 inches ABC, 36 inches select fill with 3 inches ABC, 12 inches ABC with Geotextile A, 20 inches ABC with Geotextile B, 19 inches ABC with Geotextile A, 25 inches select fill with 3 inches ABC and Geotextile B, 17 inches select fill with 3 inches ABC and Geotextile A, and 18 inches ABC.

<u>0.5 to 1.0 inches:</u>
14 inches ABC, 11 inches ABC with Geogrid A, and 14 inches select fill with 3 inches ABC and Geotextile A.

<u>Greater than 1.0 inch:</u>
13 inches ABC with Geotextile B.

In summary, the equivalence comparisons over secondary cycles yielded the following:

- Tests with LSS continued to have the lowest displacements over all cycle intervals.
- Table 67 showed that sections with highest rut refill depths did not necessarily have the highest initial displacements during the first 200 secondary cycles. Thus, it appears that the benefit of Geotextile A reinforcement was primarily due to mobilization during initial cycles and not due to increased ABC depth.

Table 69. Tests Sorted by Cyclic 2 Displacement between 1,000 and 10,000 Cycles

Test Configuration (Test No.)	Displacement (in)	Add. ABC (in)
9" LSS/4" ABC (20)	0.041	0.228
9" Gray LSS/4" ABC (21)	0.136	0.875
13" ABC with Geotextile A (16)	0.201	3.540
12" LSS/5" ABC (19)	0.222	1.217
36" Select Fill/3" ABC (9)	0.226*	2.108
12" ABC with Geotextile A (18)	0.227	5.699
20" ABC with Geotextile B (13)	0.243*	2.361
19" ABC with Geotextile A (6)	0.253*	1.766
25" Select Fill/3" ABC with Geotextile B (10)	0.269	2.283
17" Select Fill/3" ABC with Geotextile A (8)	0.361*	4.163
18" ABC (15)	0.377	2.476
14" ABC (5)	0.601*	3.296
11" ABC with Geogrid A (17)	0.719	4.865
14" Select Fill/3" ABC with Geotextile A (11)	0.740	6.181
13" ABC with Geotextile B (14)	1.025*	4.878
16" ABC (2)	N/A	N/A
20" ABC (3)	N/A	N/A
16" ABC with Geogrid B (4)	N/A	N/A

- Geotextile A Tests with ABC depths close to the load plate diameter (12 inches) showed marked improvement over all cyclic intervals.

- All unreinforced ABC tests showed high incremental displacements because of layer mixing and high vertical stress increase in the soft subgrade. With increasing number of cycles, the incremental displacement increased at a higher rate than for the reinforced tests

- Geotextile B and both Geogrids showed slight benefit when reinforcing thick ABC layers. Geotextile B tests performed well with thicker ABC layers because it helped prevent layer mixing.

- Select fill tests with thin stabilization depths did not fail in punching shear because of the thicker “repaired” ABC layer. However, the test samples yielded high displacements with increasing number of cycles because the stabilization depth was not sufficient to reduce the vertical stress increase on the soft subgrade.

- Select fill samples with deeper stabilization depths slightly displaced over all cycle intervals due to significant reduction in vertical stresses imposed on the subgrade. The repaired ABC layer also underwent less punching than during initial cycles.

CHAPTER 9: NUMERICAL MODEL: INPUT PARAMETERS AND CALIBRATION

Numerical modeling using the finite difference method was used for the analysis of the prototype test results and simulations of field applications of the selected stabilization methods. Five prototype tests using different stabilization methods were selected and simulated for the backcalculation of the relevant modeling parameters of the soil materials. The model calibration utilized the results from three testing schemes: static loading, proof rolling, and cyclic loading. The computed settlements were compared to the measured values obtained from the three testing schemes using the various stabilization methods. The results of these simulations will be used later for the study of various conditions in the field.

Material Properties

The material properties required for the large-scale simulations were estimated initially from information obtained from a literature review, small-scale laboratory tests, and inverse analysis. The properties to be simulated included density, stiffness, and strength parameters, such as cohesion (c) and friction (ϕ). The density (ρ) or unit weight (γ) of each layer was obtained from test pit sample measurements taken by nuclear gauge and sand cone devices, as previously described in Chapter 5. The stiffness parameters are the elastic modulus (E) and Poisson's ratio, and the Mohr-Coulomb strength parameters are cohesion and the friction angle. These values are required for the elastic – perfectly plastic model (Mohr –Coulomb model) used in the simulation.

The geosynthetics were simulated using interface elements between the aggregate base course (ABC) and subgrade soil layers. For the interface elements, the spring coefficients for normal and shear forces and the strength of the springs are required. In addition, the dynamic material properties and strain hardening effects were studied to model the cyclic behavior in the simulations.

Index Properties

Various laboratory and field tests were performed to classify the study soils. The index properties, including the results of compaction testing, are reproduced from Chapter 3 and presented in Table 70.

Table 70. Index Properties of Prototype Test Soils

Sample	LL	PL	PI	G_S	γ_{dmax} in pcf (kN/m^3)	OMC (%)	Classification
Piedmont	44	32	12	2.69	115.7 (18.2)	14.7	A-6(5)
Coastal Plain	20	16	4	2.63	121.6 (19.1)	10.9	A-4
Select Fill Soil	-	-	-	2.64	105 (16.5)	-	A-1-b

Shear Strength Parameters

Several triaxial tests were performed by the NCDOT, and the results were provided to the project team for use in the numerical analyses, as shown in Table 71. Table 72 and Table 73 include the shear strength parameters obtained from the triaxial testing. The 'c' and 'G_S' values in Table 72 are the undrained shear strength and specific gravity, respectively.

Table 71. Typical Effective Angle of Internal Friction and At-Rest Earth Pressure Coefficients for Unbound Granular and Subgrade Material (NCHRP 2004)

Layers	Material Description	ϕ' (deg.)	Ko
Subgrade	Fine sandy silt, nonplastic silt	17 – 19	0.717 – 0.746
	Very stiff and hard residual clay	22 – 26	0.617 – 0.673
	Medium stiff and stiff clay and silty clay	19	0.717
ABC & Sand	Clean gravel, gravel-sand mixtures, and coarse sand	29 – 31	0.548 – 0.575
	Clean fine to medium sand, silty medium to coarse sand, silty or clayey gravel	24 – 29	0.575 – 0.645
	Clean fine sand, silty or clayey fine to medium sand	19 – 24	0.645 – 0.717

Table 72. Results of Triaxial Test for Piedmont Residual Soil (NCDOT)

Sample No.	Classification	LL	PI	ϕ (deg)	c in psf (kPa)	G_S
RT-1 (00)	A-7-5(47)	75	44	18	104.4 (5)	2.70
RT-2 (00)	A-7-6(18)	52	24	15	417.7 (20)	2.84
RT-3 (00)	A-7-5(16)	58	16	16	375.9 (18)	2.76
RT-4 (01)	A-7-6(10)	44	18	26	250.6 (12)	2.74
ST-1 (00)	A-6(5)	39	14	17	313.3 (15)	2.74
ST-2 (00)	A-4(1)	34	5	18	250.6 (12)	2.81
ST-10 (01)	A-7-5(12)	53	13	19	208.9 (10)	2.81
ST-2 (06)	A-7-5(7)	43	11	12	710.1 (34)	2.76

Table 73. Results of Triaxial Tests for Coastal Plain Soil

Sample No.	Soil	c (psi)	ϕ (deg)	ϕ' (deg)	*w* (%)
1	Coastal Plain	2	16.5	33.5	-
2	Mixed Coastal Plain	9.4	20.5	34.5	15.6
3		5.7	19.0	34.5	18.8
4		2	16.5	33.5	20.7

Shear strength parameters also can be estimated by empirical correlations using index properties such as LL (liquide limit) or PI (plasticity index). Figure 108 shows the NCDOT-measured friction angles versus the PI using empirical correlations by Mitchell (1976) and Lambe (1985), although these correlations were developed for mainly clay soils. Figure 108 (a) shows the comparison with the peak friction angle of Mitchell (1976), and Figure 108 (b) shows the comparison with the residual friction angle of Lambe (1985). The relationship used in Figure 108 (a) is presented in Equation (1).

$$\sin\phi_p = 0.8 - 0.094 \cdot \ln(PI) \qquad \textbf{(30)}$$

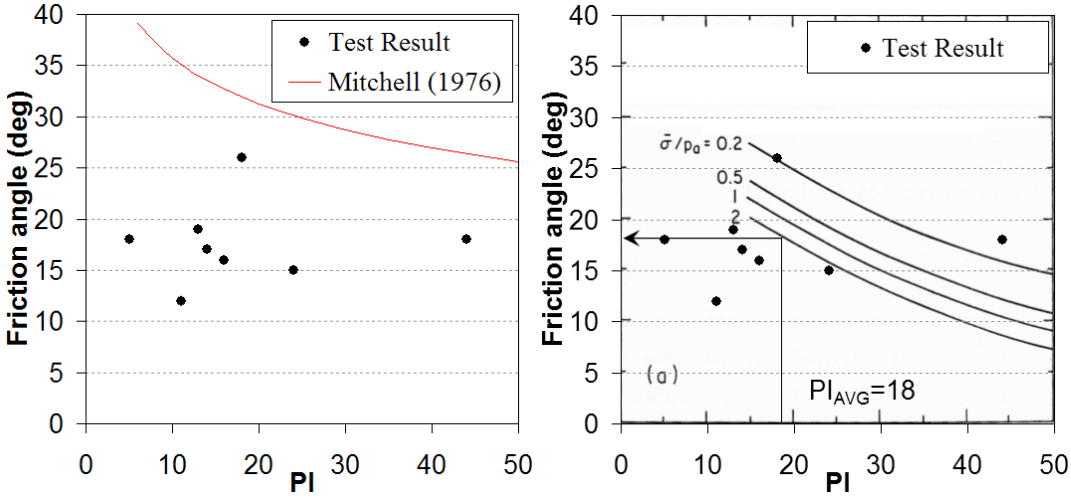

(a) Peak Friction Angle (Mitchell, 1976) (b) Residual Friction Angle (Lambe, 1985)

Figure 108. Friction Angle from Index Properties

If compared with the empirical correlation suggested by Mitchell (1976), the friction angles and PI values from Table 72 and Table 73 plot below the correlation curve, whereas these values are similar to the residual friction angles suggested by Lambe (1985), as shown in Figure 108 where it can be seen that the measured friction angles are within the range of the peak and residual friction angles. In Figure 108 (b), the effective stress normalized by atmospheric pressure (P_a) is assumed to be about 2.0, as this value represents the high end of the measured stress at the interface in the laboratory.

Table 74 presents the basic statistics for the triaxial testing results. The average cohesive strength is 16 kPa, and the average friction angle is 18 degrees. These average values were used in the numerical analysis.

Stiffness Factors

For the subgrade soil and ABC layer, the elastic properties shown in Table 75 serve as a base line reference. The material properties presented in Table 76 and Table 77 have generally been used in the numerical analysis of pavement systems (Huang, 2004). Typical values for the

stiffness moduli reported by Brunton et al. (1992), CROW (1998), and Evdorides and Snaith (1996) are also included.

Table 74. Basic Statistics of Results of Triaxial Tests

Statistics	LL	PI	ϕ (deg)	c in psf (kPa)	G_S
Min	34	5	12.0	104.4 (5.0)	2.70
Max	75	44	26.0	710.1 (34.0)	2.84
Mean (μ)	50	18	17.6	328.9 (15.75)	2.77
Stdev (σ)	12.9	11.8	4.03	182.3 (8.73)	0.046

Table 75. Elastic Moduli and Poisson's Ratio Values Used in Previous Research

Literature	Material	Elastic Modulus (ksi) Range (Typical)	Poisson's Ratio Range (Typical)
Cho (1996)	Subgrade	15	0.4
Blab & Harvey (2002)	ABC	21.8	0.35
Leonard (2002)	Base	72.5	0.5
	Sub-base	29.0	0.5
Shoukry et al. (1999)	Gravel	2.99	0.4
	Sand Soil	11.9	0.3
	Base	34.8	0.4
	Subgrade	9.95	0.45
Davies & Mamlouk (1985)	Base	50 – 200 (100)	0.4
	Sub-base	10 – 40 (20)	0.4
	Subgrade	4 – 16 (8)	0.45
Al-Khoury et al. (2007)	Base	29	0.35
	Subgrade	3.6 – 14.5 (9)	0.35
Kwon et al. (2005)	Base	30	0.4
	Subgrade	4.1	0.45

The elastic modulus values obtained from Huang (2004), Brunton et al. (1992), CROW (1998), and Evdorides & Snaith (1996) (designated as E& S) were selected. The ranges of the elastic modulus values for typical subgrade soil and the ABC are presented in Figure 109. The elastic modulus values for the subgrade soil are obtained from the highest value of the range of medium clay in Table 76, and for the ABC come from Al-Khoury et al. (2007). A summary of the final material properties used in the numerical analysis is presented later in Table 80.

Table 76. Elastic Moduli for Different Materials

Layer	Material	Range (in psi)	Typical(in psi)	Ref.
Subgrade	Stiff clay	7,600 – 17,000	12,000	Huang (2004)
	Medium clay	4,700 – 12,300	8,000	
	Soft clay	1,800 – 7,700	5,000	
	Very soft clay	1,000 – 5,700	3,000	
	Clay subgrade	4400 – 21800	13100	Brunton et al. (1992)
	Clay	2900 –11600	7300	CROW (1998)
	Clay, very soft	300 –2200	1300	Evdorides & Snaith (1996) (E & S)
	Clay, soft	700 –3600	2200	
	Clay, medium	2200 –7300	4800	
ABC	Granular sub-base	7300 – 29000	18200	Brunton et al. (1992)
	Sand and gravel	10200 – 43500	26900	CROW (1998)
	Granular base	7300 – 43500	25400	E & S
Select Fill & Base Sand	Sand	7300 – 43500	25400	CROW (1998)
		4400 – 21800	13100	E & S
Lime	Lime-fly ash materials	500000 – 2500000	1000000	Huang (2004)

Table 77. Poisson's Ratio for Different Materials (Huang, 2004)

Layer	Material	Range (in psi)	Typical(in psi)	Ref.
Subgrade	Stiff clay	0.40 – 0.50	0.45	Huang (2004)
	Clay subgrade	4400 – 21800	0.4	Brunton et al. (1992)
	Clay	-	0.4	CROW (1998)
	Clay, very soft	-	0.5	Evdorides & Snaith (1996)
	Clay, soft	-	0.45	
	Clay, medium	-	0.35	
ABC	Untreated granular materials	0.30 – 0.40	0.35	Huang (2004)
	Granular sub-base	-	0.3	Brunton et al. (1992)
	Granular base	-	0.35	Evdorides & Snaith (1996)
Select Fill & Base Sand	Sand	0.30 – 0.45	0.35	Huang (2004)
		-	0.35	CROW (1998)
		-	0.15	Evdorides & Snaith (1996)
Lime	Lime-stabilized materials	0.10 – 0.25	0.20	Huang (2004)

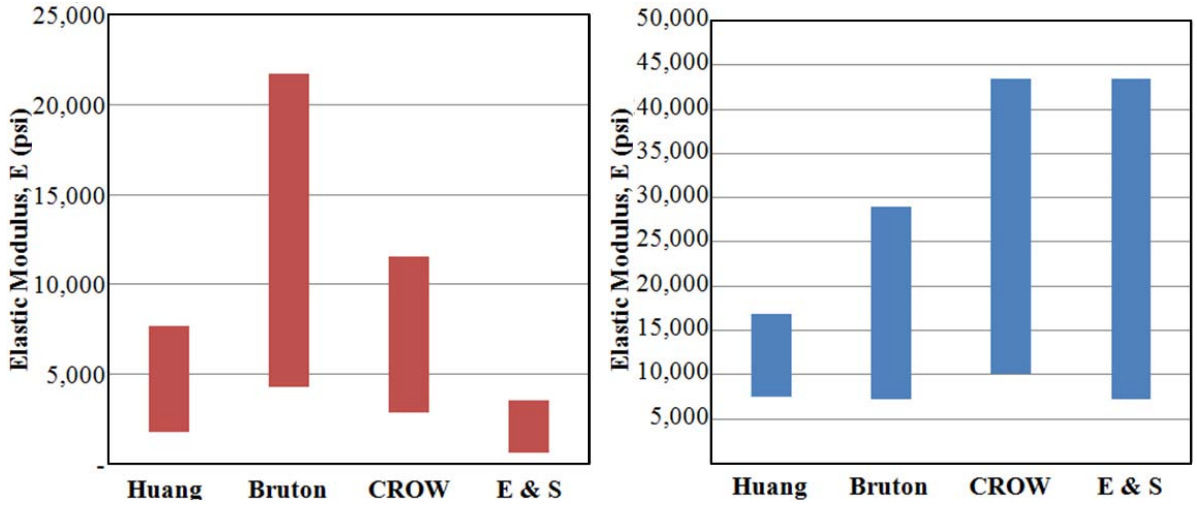

(a) Subgrade Soil Layer (b) ABC Layer

Figure 109. Range of Elastic Modulus Values Obtained From the Literature

Initial and Secant Modulus Values of Subgrade Soil

The initial modulus values for the subgrade soil can be obtained from the stress and strain behavior of samples examined in triaxial testing.

Figure 110 (a) shows stress and strain curves for the U-2524AB (RT-1) sample of Piedmont subgrade soil. The initial modulus values were obtained from the regression scheme suggested by the hyperbolic model (Duncan & Chang, 2000). In addition, the secant modulus at 50% of the failure strain can be estimated. As shown in Figure 110, the estimated modulus values are plotted as a function of confined stress. The range of initial modulus values under the design stress of 70 psi for proof rolling and 80 psi for cyclic traffic loading is estimated to be from 1000 to 1500 psi.

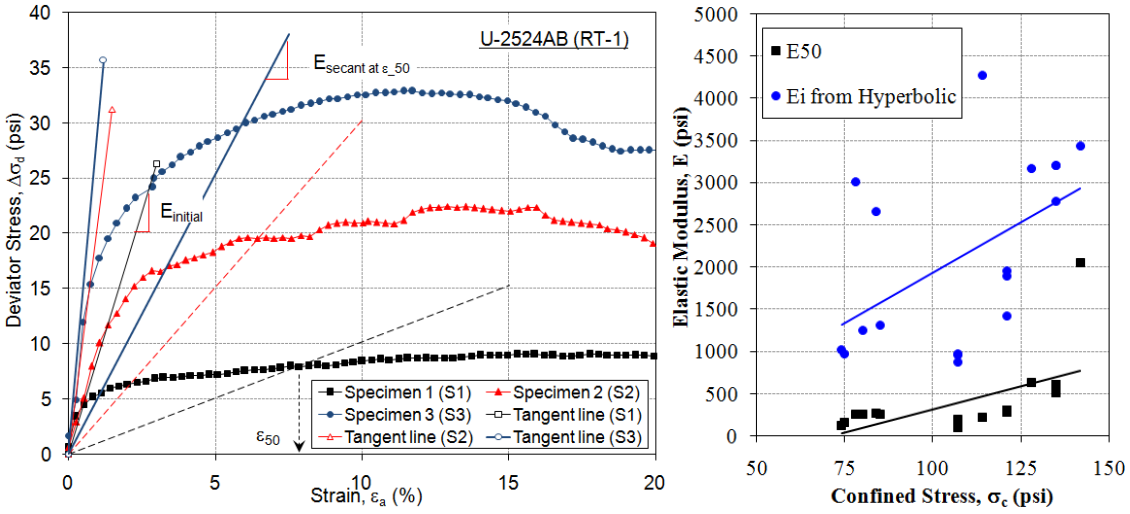

(a) Initial Tangential Modulus and Secant Modulus Values (b) Relation to Confining Stress

Figure 110. Determination of Initial Elastic Modulus Values from Hyperbolic Curves

Inverse Analysis for the Stiffness of the Subgrade Soil Layer

The 21 prototype test cases reported in this study can be categorized into five representative stabilization methods that use: i) select fill material, ii) a thick ABC, iii) geosynthetic reinforcement with high strength geotextile (Mirafi, HP570), iv) geosynthetic reinforcement with high strength geogrid (Tensar, BX1500), and v) lime. Because the degree of compaction and the fabric state of the subgrade soil are different for each stabilization method, the stiffness of the soil matrix in the test pit will vary.

In this analysis, the stiffness and strength of the subgrade soil are postulated to be variable. First, the settlement under static load for each simulation is compared with the test results. The applied static loads range from 10 to 40 psi, such that that the stabilized soil and subgrade soil system can be idealized as elastic. The stiffness factor applied to the elastic modulus can be obtained via backcalculations. Table 78 shows the range of stiffness and strength values.

Table 78. Range of Elastic Moduli Values Used in Backcalculation

Factors	Range	Simulation No.
Elastic Modulus, E (psi)	500 – 2500 psi (100 psi in step)	21
Cohesion, c (psi)	2 – 30 psi (2 psi in step)	15
Friction Angle, ϕ (deg.)	0, 10, 20, and 30 degrees	4

Whereas the material properties obtained from the small-scale tests are representative for the test pit, the condition of the large samples in the test pit is affected by the degree of compaction, moisture content, and the thickness of each soil layer. So, there is a possibility that the material properties obtained from small-scale testing are not significantly different from those of samples in the test pit. Therefore, a wide range of material properties can be considered in order to discern the closest value for representing the deformable behavior of the large-scale test samples using inverse analysis. Subgrade elastic modulus values ranging from 500 to 2,500 psi were applied, and Poisson's ratio was assumed to be 0.4. Four different friction angles also were used.

Because the numerical model is in an elastic state under static loading (maximum load = 40 psi), deformation behavior is not dependent on the strength parameters, but is dependent on the elastic modulus values, as shown in Figure 111. The settlement error is defined as the ratio of the predicted to measured displacement at the center of the loading plate when the applied loading is 40 psi, as presented in Equation (31).

$$Error = \frac{\text{Predicted Displacement}}{\text{Measured Dispalcement}} \qquad \textbf{(31)}$$

Figure 111 (a) shows two different results for the backcalculations: one is the rectangular solid line for the case of cohesion of 2 psi and friction angle of zero degrees (ϕ = 0, c = 2 psi in the legend), and the other is the remainder of the cases with various strength parameters (they overlap due to the same settlement magnitude.) Thus, for cases with a strength parameter greater

than a friction angle of zero and cohesion of 2 psi, the response is dependent only on the stiffness factor. In the case of friction = 0 and cohesion = 2 psi, some plastic deformation is evident, and the results show a different trend for settlement error. However, the subgrade soil used in the prototype tests has a friction angle of approximately 20 degrees and cohesion of 6 psi. Thus, the settlement error curve will represent cases in the 'elastic' state. Figure 111 (b) contains the plots for friction = 20 and cohesion = 6 psi to determine the subgrade elastic modulus. The elastic modulus values presented in Table 79 are the computed values from Figure 111 (b), and in this case, the elastic modulus values of the subgrade obtained from the inverse analysis range from 600 psi to 750 psi.

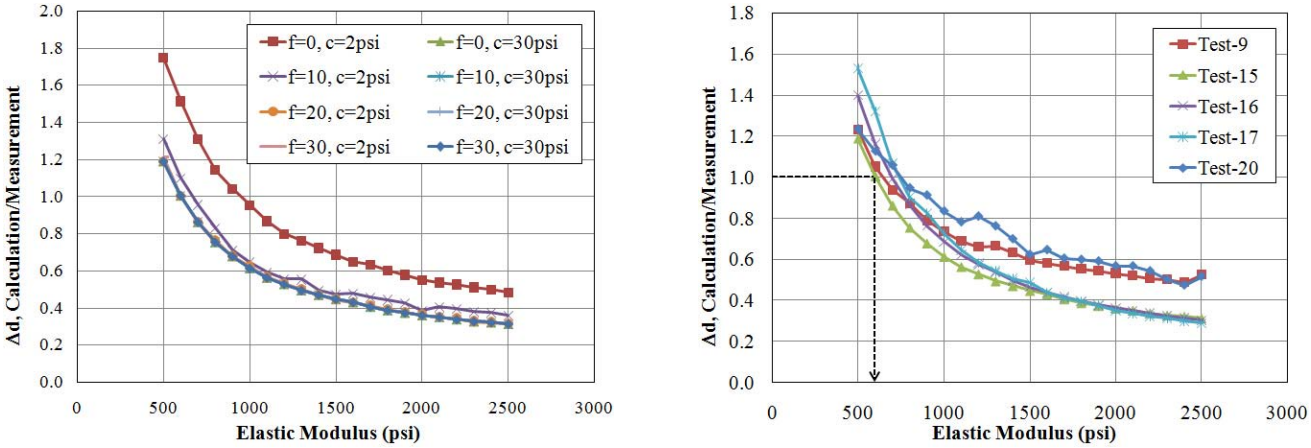

(a) Settlement Error for Test 15 (b) Settlement Error for the Five Tests

Figure 111. Rate of Displacement for Various Elastic Modulus Values

Table 79. Determination of Elastic Modului Values for Subgrade Soil Layer

Item	Test 9	Test 15	Test 16	Test 17	Test 20
Stabilization Method	Select Fill	ABC	HP570	BX1500	LSS
Elastic Moduli (psi)	650	600	700	740	750

A summary of the material properties used in the numerical analysis is presented in Table 80. To cover a wide range of possibilities, the elastic modulus values of the subgrade are assumed to vary between 500 and 1000 psi, which encompasses the range of values compiled from the small-scale laboratory investigation and the inverse analysis.

Interface Properties

Interface elements were used to simulate the interaction between the geosynthetics and the soil medium. Interface material properties include normal stiffness, shear stiffness, and shear strength characteristics, such as cohesion and friction angle. An interface element consists of two springs, a normal spring and a shear spring, with respective spring stiffnesses (K_n, K_{st}). The interface material representation and properties were developed from the suggestions of Clough and Duncan (1969) and Gabr and Hunter (1994) as follows:

$K_n = k_n \gamma_w$ (kPa/m) **(32)**

$K_{st} = k_s \gamma_w (\sigma_n / P_a)^n$ (kPa/m) **(33)**

Table 80. Stiffness and Strength Parameters Used in the Analysis

Material	γ_t, pcf (kN/m^3)	E in psi (kPa)	ν	c, psi (kPa)	ϕ (deg)
ABC	120 (18.9)	10,000 (200,000)	0.15	1~5 (6.9~34.5)	35
Subgrade	114 (17.9)	500 to 1,000 (85,000)	0.35	2~8 (13.8~55.2)	20
Select Fill	107 (16.8)	9,500 (65,500)	0.35	0~1 (0~6.9)	34
LSS	128 (20.1)	18,000 (124,100)	0.2	50 (344.7)	0
Bottom Sand	112 (17.6)	21,000 (144,800)	0.15	0 (0)	38
BX1500	-	20,320 (140,000)	0.2	-	-
HP570	-	12,277 (85,000)	0.2	-	-

where the normal spring coefficient is k_n = 100,000. Based on data from pullout tests, Bauer et al. (1991) and Gabr and Hunter (1994) suggest a shear spring coefficient (k_s) of 4000 for the TN1500 geogrid (which is the same as the UX1500). In this analysis, the shear spring coefficient (k_s) is also assumed to be 4000.

Hardening Effect

A strain hardening/softening model is used to improve the Mohr-Coulomb constitutive law based on a simple linear elastic-perfectly plastic model, because the Mohr-Coulomb law cannot be applied to simulate the hardening or softening of a material characterized by degradation due to repeated plastic deformation. The built-in model provided by the FLAC program is based on the Mohr-Coulomb principle and changes the yield surface in accordance with input strength values (cohesion and friction angle) that are dependent on strain. The strength, cohesion and friction angle were obtained from the stress-strain curves of the triaxial tests, as shown in Figure 112.

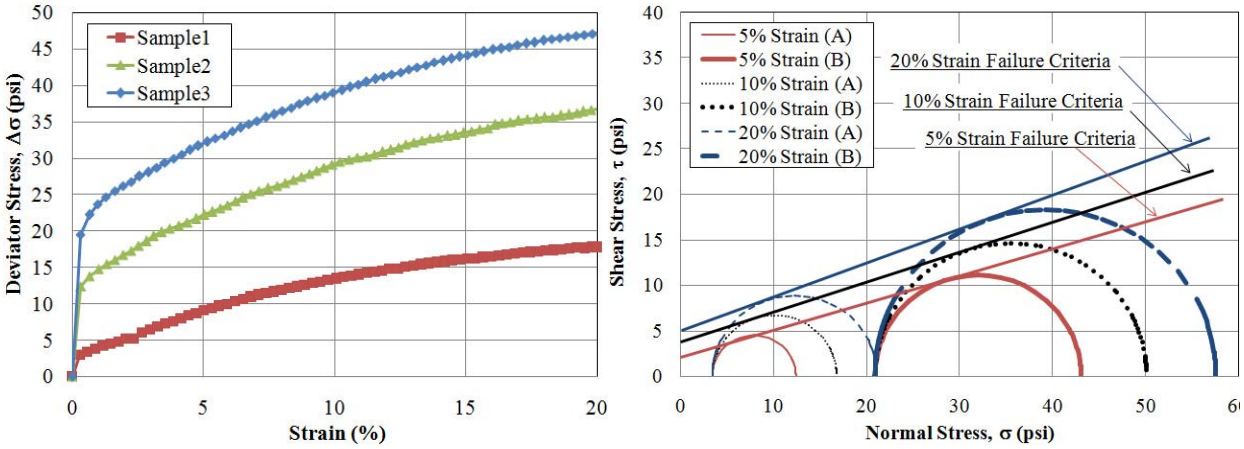

(a) Stress-Strain Curves (b) Estimation of Hardening Effect

Figure 112. Stress-Strain Curves of Typical Triaxial Tests

The strain hardening curves for the subgrade soil and select fill material are presented in Figure 113 (a) and (b), respectively. Because the results of the consolidated undrained (CU) triaxial tests

for the ABC were not available, the hardening curves for the ABC were obtained from unconsolidated undrained (UU) tests described in Cunningham (2009), and calibrated to hyperbolic curves, as shown in Figure 114.

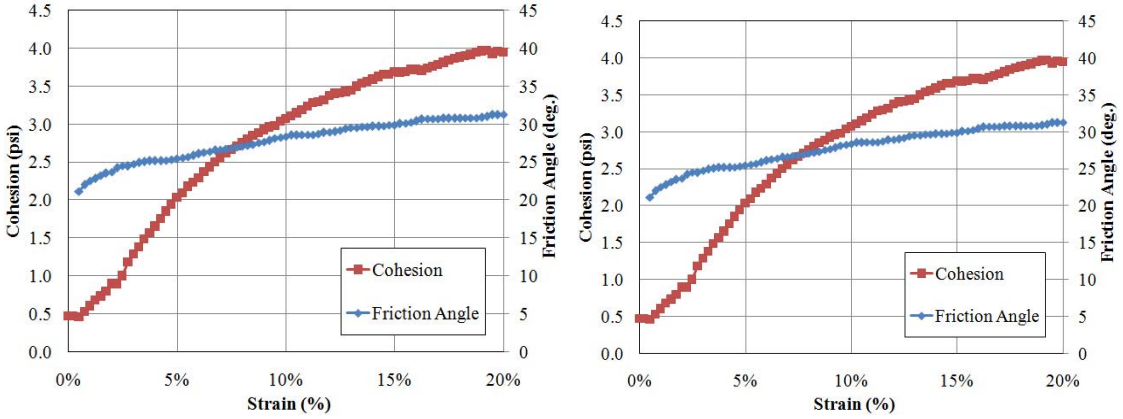

(a) Subgrade Soil (b) Select Fill Material

Figure 113. Strain Hardening Curves for Subgrade and Select Fill Materials

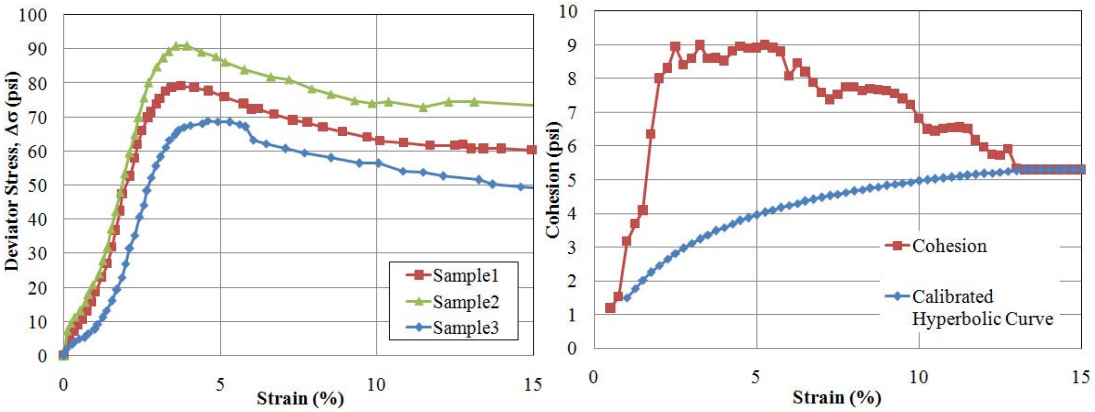

(a) UU Triaxial Testing: ABC (b) Hardening Effect and Calibration

Figure 114. Stress-Strain Relationship with Illustration of Strain Hardening for Aggregate Base Course (after Cunningham, 2009)

Loading Conditions

Three types of loading – static, proof rolling, and cyclic – were used for the large-scale tests. Static loads of 10 to 40 psi in stress increments of 10 psi, and repetitive loading and unloading were applied. Static loads were applied at the beginning of the tests from 10 psi to 40 psi. The loading and unloading were sequentially repeated, as shown in Figure 115. For the dynamic cases of proof rolling and cyclic loading, it was assumed that the loads follow a haversine function with different durations and frequencies, as shown in Figure 116 (a) and (b), respectively, and following the findings reported in Chapter 4.

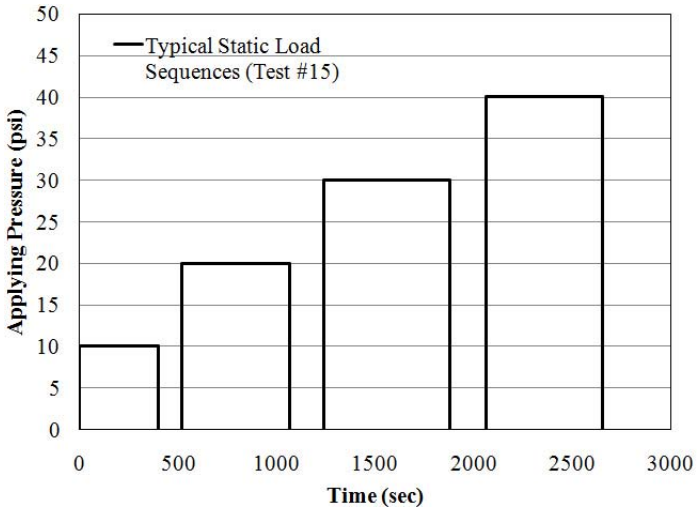

Figure 115. Static Load Sequences

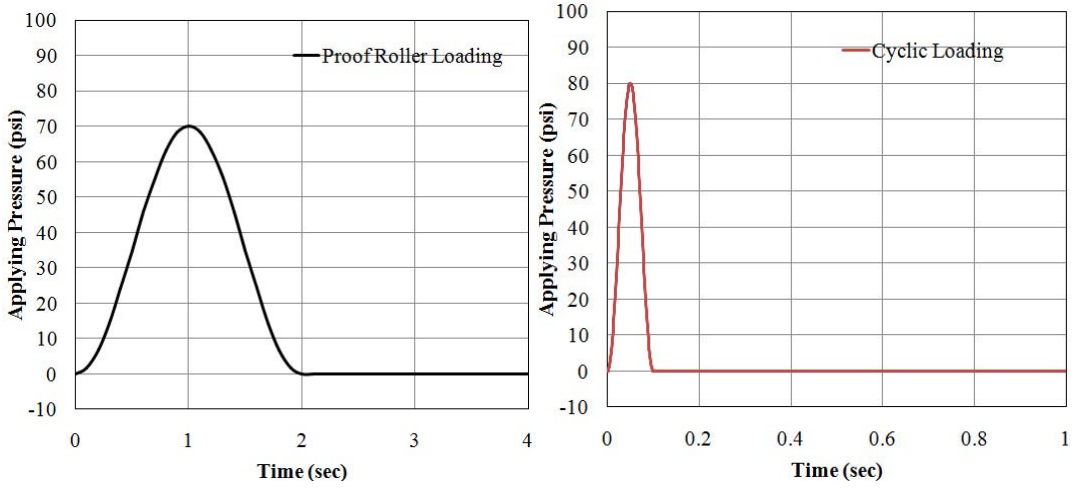

(a) Proof Roller Loading (b) Cyclic Traffic Load

Figure 116. One Cycle of Dynamic Loading

Model Configurations

The model was set in axisymmetrical mode using the finite difference method. The three different loading types of static, proof roller, and cyclic were applied on a plate 1 ft in diameter The computed settlements were compared to the measured values using the results from the various stabilization methods. The results of the numerical simulations are comprised of preliminary analysis, simulation of the test pit, and estimation of the stabilization methods under field conditions. For the preliminary analysis, the modeling method for geosynthetic reinforcement was studied.

Preliminary Analysis: Determination of Elements for Modeling Geosynthetic Material

Geosynthetic material can be simulated using thin solid elements (Han and Gabr, 2002) or structural elements (tensional or flexible beams). FLAC recommends a flexible beam element with a moment of inertia equal to zero as the geosynthetic element (FLAC, 2004). However, because the FLAC program does not provide the structural element in an axisymmetric stress condition, a solid element with interfaces between the geosynthetics and the pavement system is an alternative approach. Thus, the suitability of elements for geosynthetics based on mechanical behavior was studied as part of this research.

As shown in Figure 117, three different models were simulated: i) a solid element without interface elements, ii) a solid element with interface elements, and iii) a flexible beam element with interface elements. In addition, the soil matrix without geosynthetics was simulated as a reference model, and then the settlement at the center of the model was compared with the reinforced cases. The properties used in this phase of modeiling are shown in Table 81.

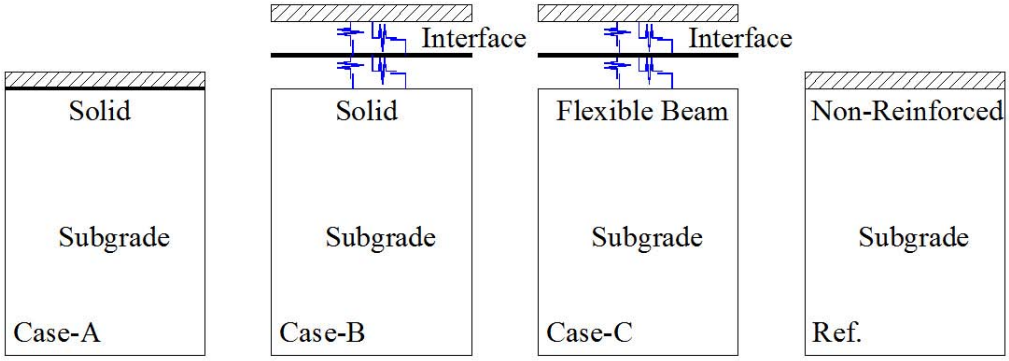

Figure 117. Three Different Models

Table 81. Material Properties for Modeling Geosynthetic and Interface Materials

Materials	Elastic Modulus, psi (kPa)*	Poisson's ratio	Cohesion psi (kPa)	ϕ (deg.)	Thick. (mm)	K_n, $\times 10^8$ lbf/ft^3* ($\times 10^8$kPa/m)	K_s, $\times 10^7$ lbf/ft^3 ($\times 10^6$ kPa/m)
ABC	10,000 (68,948)	0.35	3.0 (20.7)	35	-	-	-
Subgrade	1,000 (6,895)	0.4	2.32 (16.0)	18	-	-	-
Solid Geotextile	20,320 (140,102)	0	-	-	0.2 (5)	-	-
Beam Geotextile	20,320 (140,102)	-	-	-	0.2 (5)	-	-
Interface	-	-	-	-	-	155.5 (24.426)	2.61 (4.1)

* Conversion factors: 1psi = 6.89 kPa; 1 kPa/m=6.36 pcf (lbf/ft^3)

The effect of reinforcements is examined in terms of the thickness (3, 6, 9, 12, 15, 18 inches) of the ABC, as shown in Figure 118. In order to estimate only the effect of reinforcement and eliminate other complicating factors, these simplified models consist of only the ABC and subgrade soil.

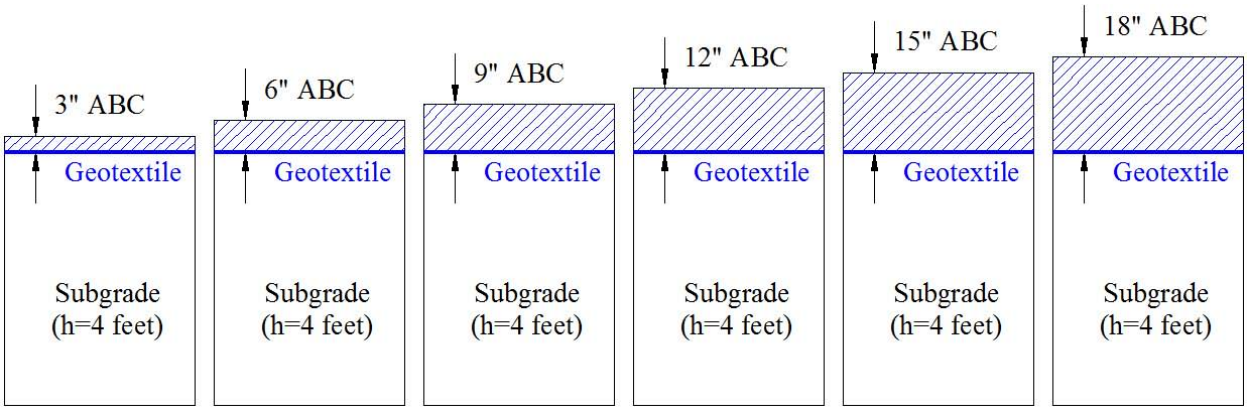

Figure 118. Simulated Models with Various Thicknesses

This analysis includes estimating the bearing capacity and deformable behavior under design stress. The procedure is as follows. First, apply uniform displacement to the model at surface nodes representing loading area and assess pressure corresponding to bearing capacity of the system. Second, for the same model, the settlement is estimated under the the static wheel loading. The bearing capacity and settlement for each reinforcement model and the thickness of the ABC are divided by the same values obtained for the nonreinforced model cases, and are designated as 'ratio of bearing capacity' and 'ratio of displacement', respectively. The ratio of bearing capacity and displacement are presented in terms of the thickness of the ABC, as shown in Figure 119.

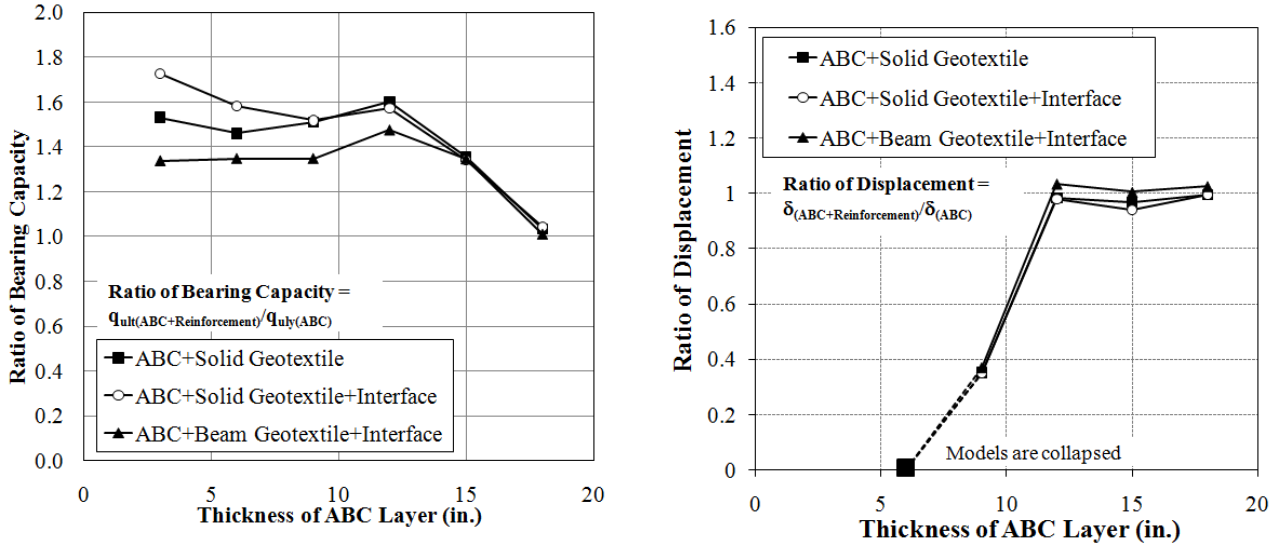

(a) Ratio of Bearing Capacity (b) Ratio of Displacement

Figure 119. Comparison of Three Different Modeling Methods

Figure 119 (a) shows that the bearing capacity from the model with reinforcement elements is approcimately 40% greater than the model without reinforcement elements (i.e., the reference model). For cases with more than 15 inches of base course, however, the bearing capacity ratio is close to the same as for the non-reinforced model. This is due to the thickness of the base course in relation to the size of the loaded area (a ration of 1.5). The effect of reinforcement is shown more clearly in Figure 119 (b). For the 9 inch base course case, the settlement is reduced to 35% of the value of the model without reinforcement. The ratio of displacement for the 3 and 6 inch base course cases are not presented in the Figure 119 (b), as the model collapsed under the applied surface load for these two cases.

From this analysis, it can be estimated that solid elements yield results similar to those of flexible beam elements. In the axisymmetric model, therefore, solid and interface modeling for the geosynthetics will be utilized.

Results of Static Load Correlations

Figure 120 shows the applied stresses and displacements obtained from the numerical simulations compared with the measured responses from the five prototype tests. The second loading of 20 psi is regarded as the first loading to account for any seating errors in the initial 10 psi load steps. The computed initial settlements for test numbers 16, 17, and 20 are close to those of the measured settlements, as shown in
Figure 120 (c), (d), and (e), respectively. For test number 15, the initial settlement of 0.027 inch was computed, and the value for the measurement was 0.079 inch, which is about three times as large. Three reasons may explain the difference between the measured and computed settlements for test number 15 (ABC): over-estimation of the elastic modulus of the base course layer, the degree of compaction on the base course, and the uneven distribution of the elastic modulus in the layer. Of these, the over-estimation of the elastic modulus of the base course layer is the most likely reason, because its value is regarded as a constant in inverse analysis despite the possibility of exhibiting non-linear behavior. However, for most of the prototype tests, it seems that the assumed elastic modulus value of 10,000 psi is appropriate for the ABC layer. The prediction errors for all loading cases are below 0.02 inch, which is about 20% of the measurement, as shown in Figure 120(f), except for test number 15 (ABC). Based on these results, and for the static loading condition, it seems that the modulus values used in the analysis are appropriate.

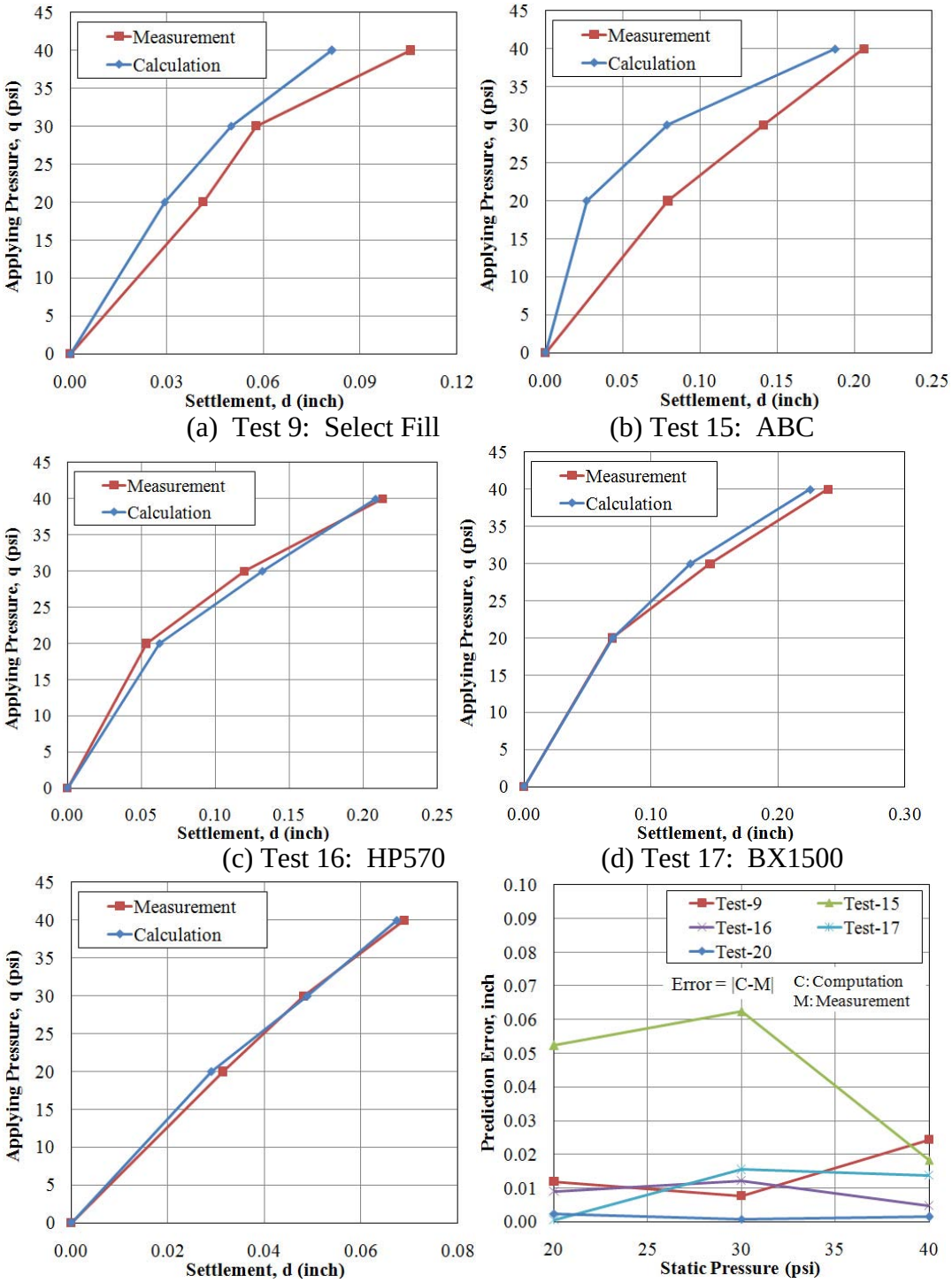

Figure 120. Pressure and Displacement Plots for Large-Scale Tests

Proof Rolling Case

To obtain results for the "proof roller" sequence loading, the settlements at the center were plotted sequentially on the time axis, and compared with the measurements (Figure 121).

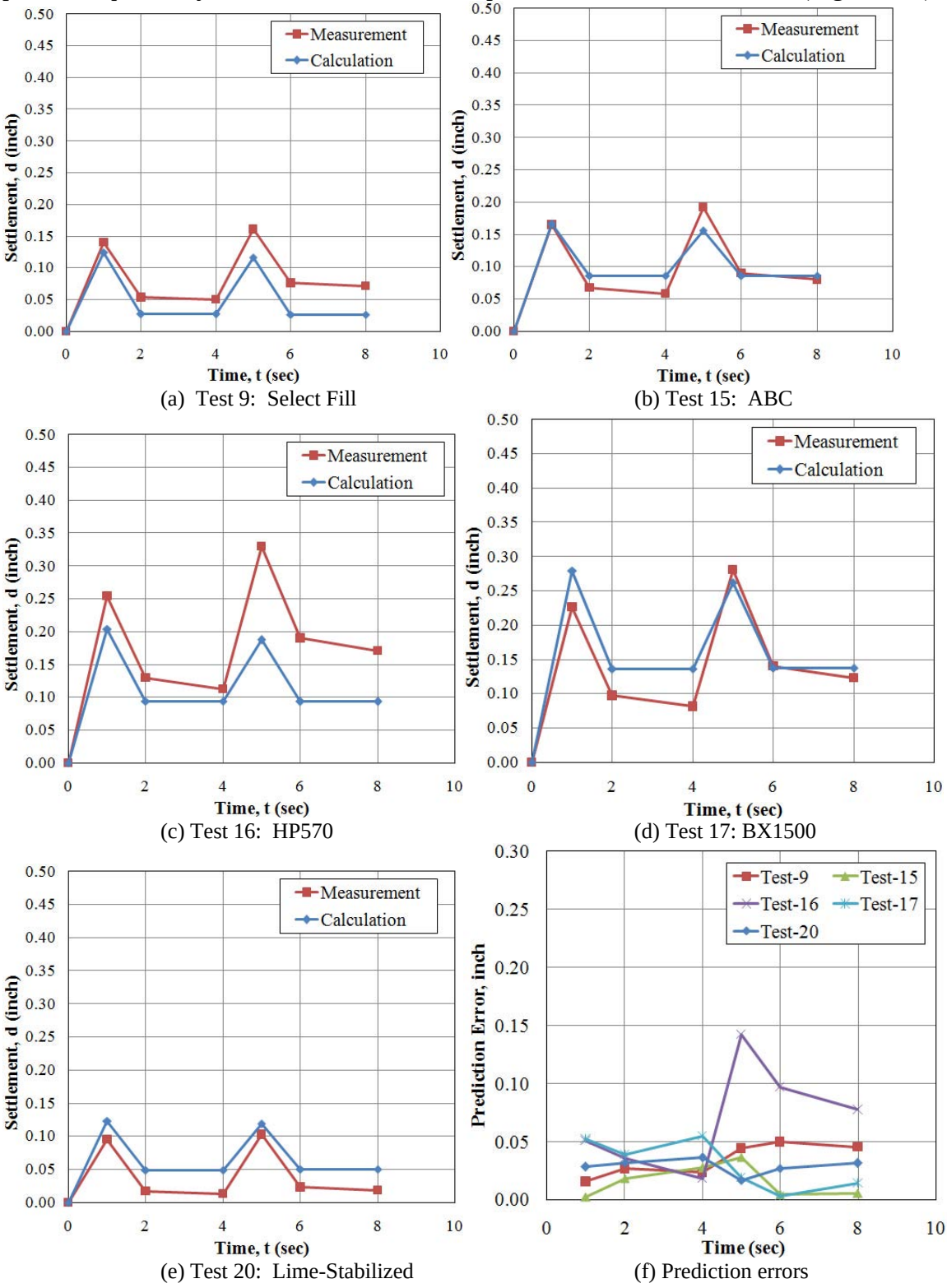

Figure 121. Displacement Results of the Proof Roller Cases

These plots show the difference between the initial settlements and the plastic settlements after unloading for the cyclic loads of two pulses. As shown in Figure 121 (a) to (e), the computed settlements are consistent with the measurements, and especially for test number 15, the initial settlement values are similar the measured values. The differences between the measured and computed values are plotted on the time sequences, as shown in Figure 121 (f). The difference in most of the cases is less than 0.05 inch, except for test number 16.

Cyclic Loading Case

The deformation behavior under repeated cyclic loads is plotted as a function of the number of cycles, as shown in Figure 122. The number of cycles is the same as the loading time because one cycle of loading takes one second, as shown on the loading curve of Figure 116 (b). The differences between the measured and computed settlements at 200 cycles are presented in Figure 123. Figure 122 shows the permanent displacement curves for the five tests with measurements. Results show that the displacement curve for test number 9 is consistent with the measurements.

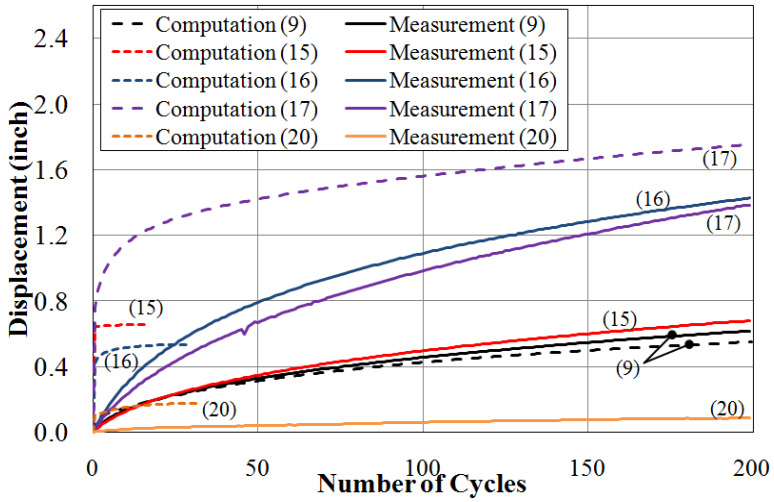

Figure 122. Settlement Development under Cyclic Loading for all Tests

The computations for test numbers 15 and 16, however, yield a maximum limiting settlement within 10 to 30 cycles, and the deformation behavior is different from the measured values. The errors in computed displacement values for test numbers 16 and 20 are 60% and 100%, respectively. The computational error for test number 15 is lowest of all simulations at 3%. However, the error increases after the 200th cycle, because the simulated model is in the elastic state, as shown in Figure 122, but the deformation response is nonlinear as was observed from measuremens even at the initial stage.

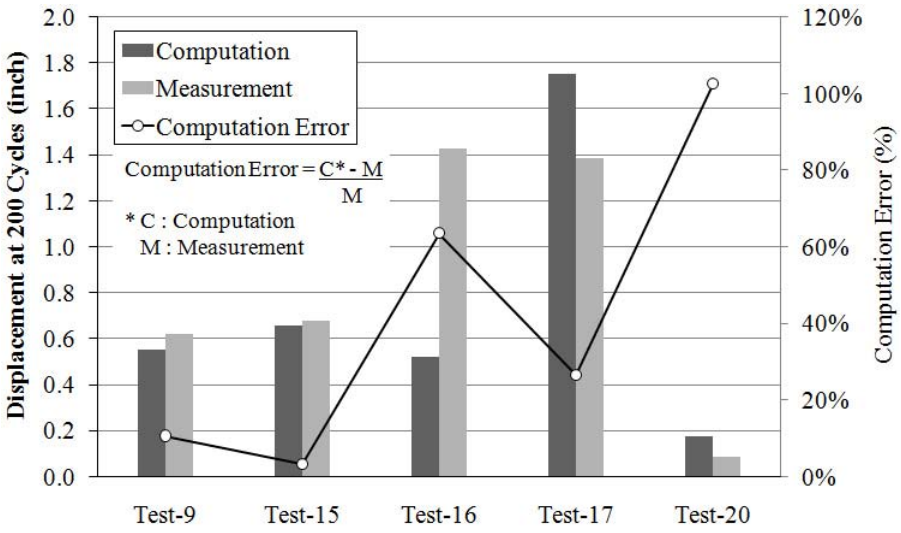

Figure 123. Computed Error for Cyclic Loads

The prediction for over 10,000 cycles can be performed using power function regression. The equation of the power function is presented as follows:

$$S = a\,N^{b} \qquad (34)$$

where S is the settlement in inches, N is the number of cycles, and a and b are the parameters of the power function. The regression lines for the log-log plot of all the settlement curves are shown in Figure 124. The equations for the power function are presented in Table 82.

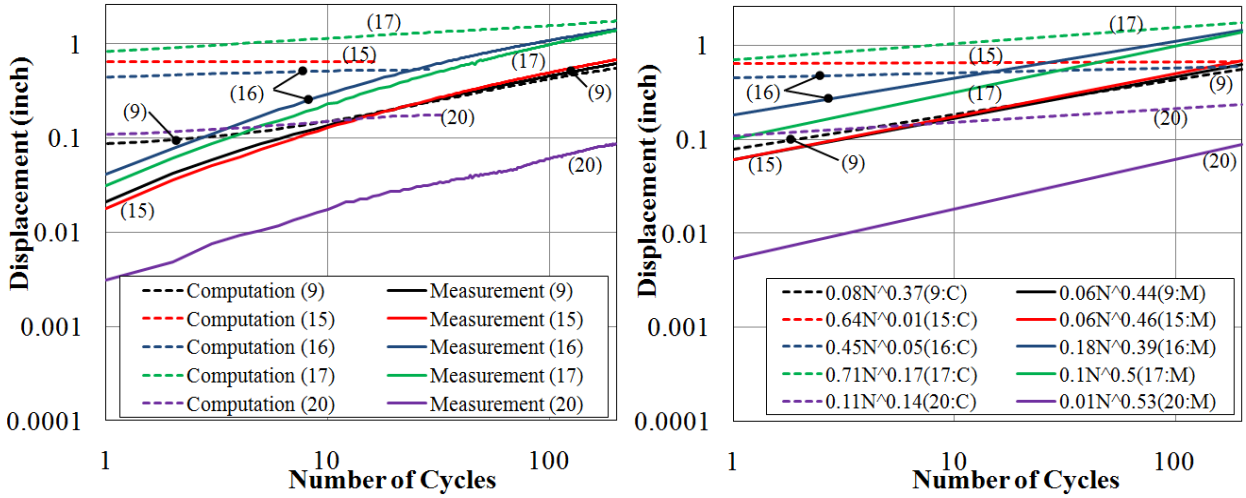

(a) Plot of Settlement Curves (b) Regression Curves by Power Function

Figure 124. Log-Log Plots and Regression Curves of the Power Function

By using the regressive functions, settlements at cycles of 1,000 and 10,000 can be estimated, as presented in Table 83. The errors calculated in the prediction will be used in the analysis of field cases under cyclic loading for subsequent field cases.

Table 82. Parameters of the Regression Curves by Power Functions

Test No.	Computation			Measurement		
	a	*b*	r^2	*a*	*b*	r^2
9	0.078	0.370	0.999	0.061	0.438	0.999
15	0.645	0.006	0.986	0.061	0.457	0.999
16	0.453	0.054	0.966	0.183	0.389	0.999
17	0.706	0.172	0.999	0.101	0.496	0.999
20	0.108	0.145	0.980	0.005	0.527	0.991

Table 83. Predicted Settlement and Estimation by Measured Values

Test No.	Settlement at $1{,}000^{th}$ Cycle			Settlement (in.) at $10{,}000^{th}$ Cycle		
	Prediction	Measurement	Error (%)	Prediction	Measurement	Error (%)
9	1.00	1.16	13.2%	2.35	2.11	11.6%
15	0.67	1.26	46.8%	0.68	2.48	72.6%
16	0.66	2.30	71.5%	0.74	3.54	79.1%
17	2.31	2.74	15.7%	3.43	4.86	29.5%
20	0.29	0.15	101.9%	0.41	0.23	80.4%

CHAPTER 10: UNDERCUT CRITERIA

The stability of subgrade soils has been quantified with the aim of developing undercut design criteria whereby soft soils are assessed for their suitability for excavation and replacement. The possible need to undercut soft soils may be considered during the design stage or in the field during the process of road construction. Therefore, various factors must be considered for the undercut design of subgrade soils and for determining the effectiveness of the stabilization measures; these factors include total and temporary settlement (reflecting rutting and pumping modes) and the appearance of tension cracks after proof rolling. Expedient testing devices, such as the dynamic cone penetrometer (DCP), are sometimes employed to discern the strength profile of the subgrade soil. From an engineering perspective, the ability of the soil to function as a competent subgrade is affected by its stiffness and strength characteristics, the shape, magnitude, and duration of applied loading, and boundary conditions. Accordingly, the undercut design criteria should be considered in light of a combination of these factors in order to assess the stability of a given subgrade soil and to determine whether undercutting the field soils is necessary for the construction of adequate road support.

Work in this chapter describes the development of undercut criteria via extensive numerical modeling. A homogenous soil medium based on continuum mechanics has been developed as a model to represent the subgrade soil. This model was developed using the finite difference platform. Static and proof roller loading modes were applied to the modeled soil medium in the plane strain and axisymmetric modes. During construction, proof roller testing is often used by the NCDOT to determine the field stability of a subgrade soil. Because a proof roller has several wheels per axle, the load applied on a soil medium can be idealized as a plane strain condition, especially when considering the impact of the load on the deep layers of the profile. On the other hand, a typical trailer or construction vehicle can be assumed to be under the axisymmetric loading condition with an impact on the shallow layers of the profile. It is also likely that pumping in the field is associated with a plane strain type of loading that affects the deep layers, and that rutting is associated with plastic deformation within the shallow layers. For both cases, in the numerical model loading is applied as a uniform pressure to represent the tires of a vehicle or proof roller trailer as a flexible load. The dimensions and magnitude of the loading for static analysis were determined using the equivalent contact area and pressure of a single axle with dual tires typical of a semitrailer (Huang, 2004).

After each loading sequence, the settlement under the loaded area and the maximum shear strain at the boundary of the loaded area were calculated. This analysis was performed for a wide range of material strength and stiffness properties for the subgrade soil. The rebounding behavior, referred to as pumping, was also considered in the development of criteria appropriate to both pumping and permanent deformation.

Numerical Modeling

The FLAC computer program version 4.0 (Itasca, 1999) is used in the modeling study. The program is based on the finite difference method (FDM) and provides for plane strain and

axisymmetric stress representations, interface elements to simulate geosynthetic reinforcements, and a variety of soil constitutive laws.

Model Description

The model in the axisymmetric mode was developed with a radius of 3 feet and a height of 4 feet (Figure 125). The mesh consists of 48 horizontal elements and 66 vertical elements. In order to minimize the effects of fixed or rigid boundaries in the model, an analysis of the boundary effects was performed. First, a numerical model height of 10 feet was established and then reduced incrementally to investigate the boundary effects on stresses and displacements. Based on the analysis results, a height of 4 feet was ultimately chosen for the model domain, as discussed in Chapter 4.

The three-dimensional cylindrical shape of the model illustrated in Figure 125 (b) shows the geometrical dimensions and loading area for a 1 foot diameter load contact area. The width of the minimum element, which is placed at the bottom of the loaded area, is 0.5 inches. For the plane strain condition, the numerical mesh is the same as for the axisymmetric case, but the loading is continuous uniform pressure over the 1 foot width.

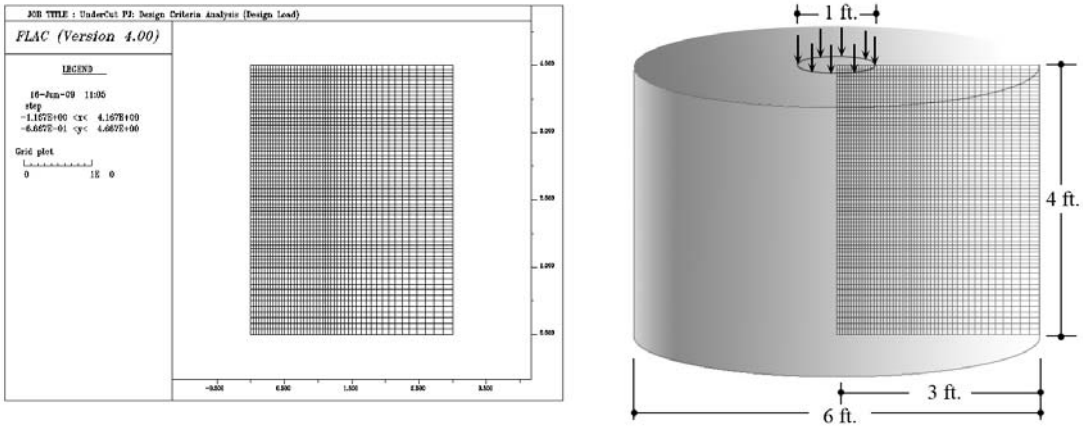

(a) FLAC Mesh (b) Three-Dimensional Shape of Model

Figure 125. Finite Difference Model and Three-Dimensional Shape for Simulated Model

Axisymmetric Model

The axisymmetric stress condition represents stress distributions in cylindrical bodies that are symmetrical about their center, and thus, a cylindrical coordinate system is used in FLAC. The out-of-plane coordinate, i.e., the z direction in this case, is the circumferential coordinate, and the x direction is designated as the radial coordinate, as shown in Figure 126 (a). The attributed stresses in the axisymmetric analysis are presented in Figure 126 (b).

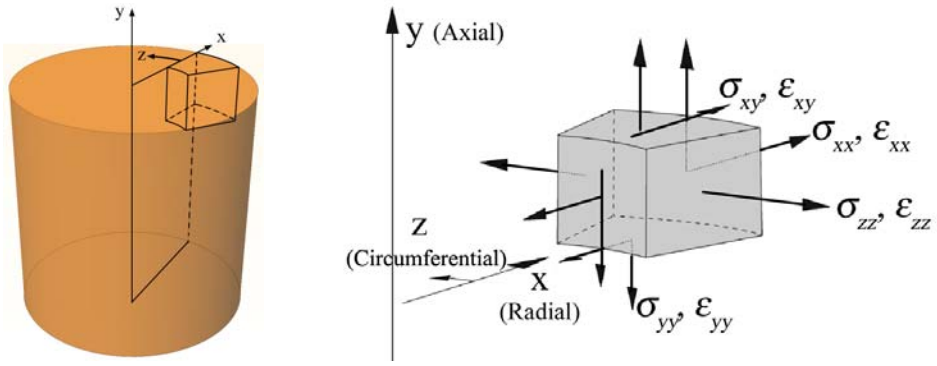

(a) Axisymmetric Condition (b) Stress Condition of Axisymmetric Model

Figure 126. Mechanical Characteristics of Axisymmetric Condition

Constitutive Soil Model

The numerical model was simulated by implementing an elastic-perfectly plastic soil model (the Mohr-Coulomb model). This model requires elastic properties, that is, the elastic modulus and Poisson's ratio, and shear strength parameters, that is, cohesion and the friction angle. Figure 127 shows a general stress-strain relationship of the elastic-perfectly plastic model. The required model properties were obtained from various laboratory and field testing programs, as described in Chapters 3 and 4. For example, the shear strength parameters were obtained from triaxial and DCP testing, and the stiffness parameters were obtained from resilient modulus testing. Reports in the literature concerning shear and stiffness model parameters, and empirical correlations were also used as sources to characterize the model parameters.

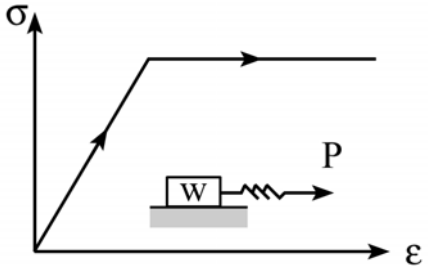

Figure 127. Stress-Strain Relationship of Elastic-Perfectly Plastic Model

Material Properties

As previously mentioned, the material properties required for an elastic-perfectly plastic model are the elastic modulus, Poisson's ratio, cohesive strength, and friction angle. Undercut criteria are developed for subgrade soils with a wide range of strength and stiffness properties. So, in order to focus on the effects of varying strength and stiffness values, the density and Poisson's ratio of the medium were assumed to be constant. Density values were obtained from measurements taken in the test pit (Chapter 5), and Poisson's ratio was estimated from information found in the literature. The range of properties used in the modeling is presented in Table 84. Details of the elastic modulus and strength values are given in 'Simulation Cases' (found in the following section, Simulation Modes) and in Table 85.

Table 84. Material Properties Used in the Design Criteria Analysis

Items	Total Density (slugs/ft^{3*})	Total Unit Weight (lbs/ft^3)	Elastic Moduli (psi)	Poisson's Ratio	Cohesion (psi)	Friction Angle (^{o})
Values	3.997	128.5	500 ~ 30,000	0.4	1.0 ~ 50	0, 10, 20, and 30

* slugs/ft^3 = density unit in English unit system, 1 slug = 1 lbf-s^2/ft (unit required by FLAC).

Simulation Modes

The numerical simulations include the assessment of bearing capacity under axisymmetric static loads by applying increasing uniform displacements under the loaded area. The pressure that corresponds to the bearing capacity failure is estimated through deformation-controlled analysis. Settlement analysis was also performed in axisymmetric and plane strain modes to estimate the deformation behavior under static and proof roller loading. The plane strain mode is assumed to simulate proof roller loading and provide information on potential rutting and excessive pumping. The axisymmetric mode provides a similar type of information but can be used to simulate mainly the effects of construction traffic (or a single wheel) rather than a series of loaded axles that are closely spaced. It is postulated that rutting is associated mainly with plastic shear deformation within the shallow layers, and can be considered as a function of the shear strength parameters. On the other hand, excessive pumping is mainly a function of the stiffness parameters, and is affected by the response of shallow as well as deep layers of the profile.

Simulated Field Loading

Two loading cases were studied. First, a static pressure of 70 psi, assumed to be the maximum proof roller pressure (designated as 'static design load'), was applied. Second, a proof roller load with a duration of two seconds and haversine pulse function shape was also applied, as shown in Figure 128 (a). This loading function is based on measured field responses of construction trucks, as presented in Chapter 4. Figure 128 (b) presents a typical displacement response according to the applied pulse loading.

The numerical analysis for proof roller loading was performed using a dynamic analysis scheme provided by FLAC. The maximum displacement at one-second intervals and the permanent displacement at two-second intervals were estimated from the analysis.

Permanent displacement is caused by the plastic deformation of the subgrade soil under the given loading condition, and resilient displacement is equal to the amount of maximum displacement subtracted from residual displacement.

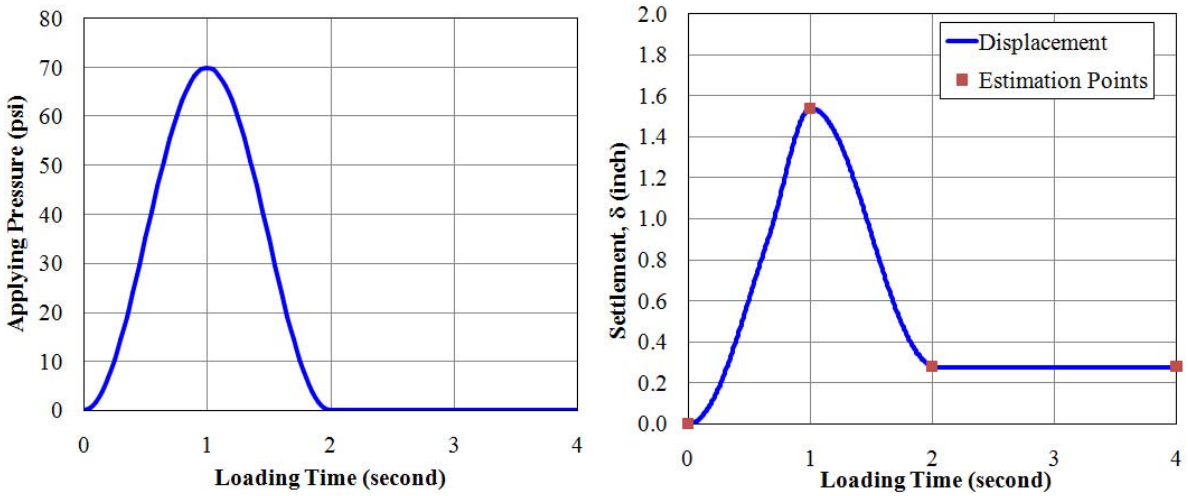

(a) Haversine Load Function of Proof Roller (b) Typical Displacement Plot for Time

Figure 128. Loading Function and Displacement Response

Simulation Cases

The material properties used in the simulations are shown in Table 85. Six elastic modulus values of 0.5, 1.0, 5.0, 10, 20, and 30 ksi, and four friction angles of 0, 10, 20 and 30 degrees were considered with a range of cohesion values, as shown in Table 85. The range of cohesion values were specified after estimating the ultimate bearing capacity. For the case of the soft soils (for example, soil with a cohesion of 10 psi and a friction angle of zero), a numerical solution is not possible because the model collapses and plastic deformation is excessive. Given the range of parameters for each loading condition, 396 total cases for six different elastic moduli were simulated.

Table 85. Number of Cases According to Strength Parameters

Friction Angle (^{o})	Cohesion (psi)	No. of Cases
0	12 to 30, 40, and 50	21
10	6 to 2,0 30, 40, and 50	18
20	4 to 15, 20, 25, 30, and 35	16
30	2 to 10, 15, and 20	11

Proof Roller Loading

A proof roller trailer has several wheels with an external diameter of five to six feet. Typical traffic vehicles considered as design loads have more widely spaced, smaller wheels than a proof roller trailer. For proof roller trailers, the length over the width of the contact area is close to 10 inches, because a contact width is usually less than 10 inches (the contact area is also dependent on the stiffness of the subgrade soil). Accordingly, in addition to axisymmetric mode, the analysis of the proof roller loading has been idealized as a plane strain condition to investigate

the possibility of excessive pumping as the deep layers of the soft subgrade profile are impacted by surface stresses.

Figure 129 (a) shows a picture of a typical proof roller trailer used in field, and the dimensions of a wheel and a footprint of all wheels. In the axisymmetric model, the loading area is equivalently postulated as a circular shape. The deformation and stress increases are therefore less than those obtained from the plane strain condition.

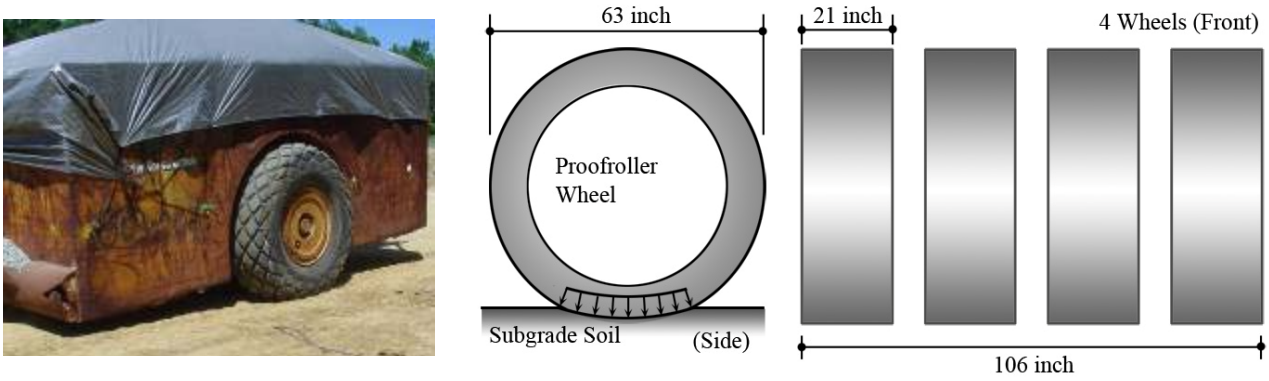

(a) Typical Proof Roller Used by the NCDOT (b) Dimensions of Wheel and Tires

Figure 129. Proof Roller and Dimensions Applied on Subgrade Soil

Flexibility of Loading

The loading used in all the analyses is uniform pressure that simulates pressure from flexible tires of construction vehicles or a proof roller. The difference between rigid and flexible loading conditions was examined by Hambleton and Drescher (2008). A proof roller trailer tire in the field transfers a uniform pressure, causing not only a depression in the subgrade soil but also deformation of the tire itself, as shown in Figure 130 (a). Hambleton and Drescher (2008) assessed the relative deformation between the tire and subgrade using three-dimensional finite element modeling. They denoted the deformed shape of the tire with a flexibility parameter, λ. The relationships of the equivalent wheel diameter, d_e, which represents the radius of part of the deformed tire (as shown in Figure 130 (a)), the applied load (Q) and the flexibility parameter (λ) are expressed by Hambleton and Drescher (2008) as:

$$\mathbf{d_e = d + \lambda Q} \qquad \mathbf{(35)}$$

where d = diameter of the tire used in the analysis.

The flexibility parameters used in the design criteria analysis were estimated for two cohesive strength conditions equal to 2 psi and 20 psi, as shown in Figure 130 (b). The elastic modulus used in the analysis is equal to 2,500 psi, and the friction angle was set to 30 degrees.

For the soft subgrade with c = 2 psi, the flexibility parameter, λ, is 0.0001362 ft/lbf (= 0.0093 m/kN) for 0.5 ft radius of pressure area, as shown in Figure 8 (b). This parameter is similar to the value estimated by Hambleton and Drescher (2008), which is 0.0001449 ft/lbf (= 0.01 m/kN).

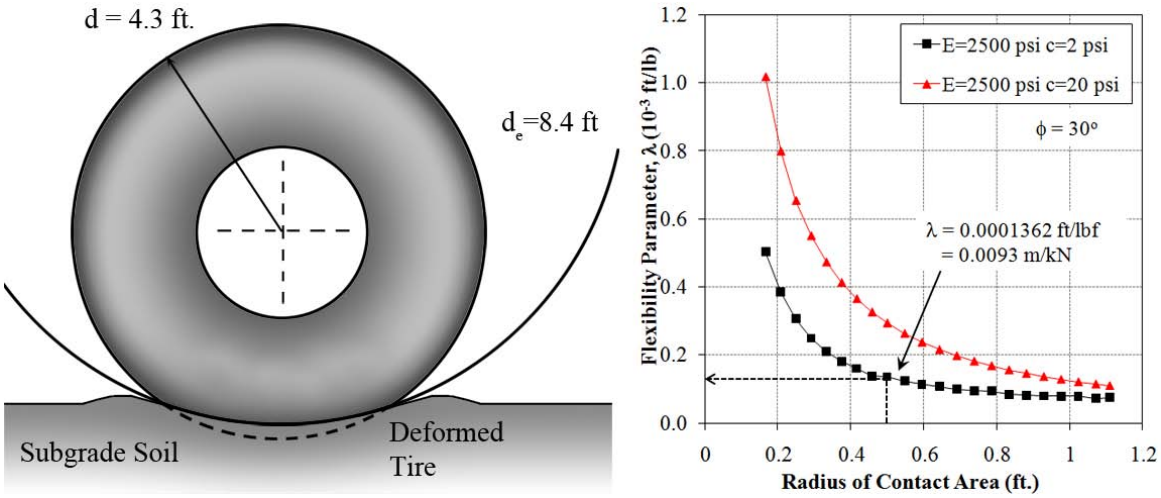

(a) Deformed Wheel Configuration (b) Distribution of Flexibility Parameter, λ

Figure 130. Deformed Wheel Configuration and Flexibility Factor for Different Strengths

Results of Numerical Simulations

Bearing Capacity Analysis

The bearing capacity of the modeled subgrade is estimated by applying a uniform displacement on an area with a 1 foot diameter. Figure 131 (a) shows a failure zone defined displacement vector, indicating an impact zone in a deformation-controlled loading approach. Figure 131 (b) shows the bearing capacity (defined as the point at which a limiting pressure is reached with increasing displacements) for two different strength parameters. For comparison, bearing capacity values obtained using an analytical solution based on Prantdl's wedge theory (Terzaghi and Peck, 1967) are also shown. Because the soil is simulated as an elastic-perfectly plastic medium, the mobilized pressure converges to the bearing capacity value at displacements as large as 6 to 8 inches, as shown in Figure 131 (b). For a subgrade soil with a relatively high strength value (30 psi versus 20 psi, as shown on Figure 4 (b)), the capacity at a settlement of 8 inches trends toward the limit defined by Prantdl's wedge theory.

For the case of a cohesive soil with a friction angle of zero, the ultimate capacity is theoretically equal to 5.14 times the assumed undrained shear strength. For example, a model with a cohesion value of 15 psi has a bearing capacity of 77 psi, which is 5.13 times the undrained shear strength. On the other hand, the case with a cohesion value of 30 psi has a bearing capacity of 144 psi at a displacement of 8 inches, which is 4.8 times that of the undrained shear strength. The ultimate capacity using Prandtl's wedge theory is 154 psi. Thus, the deformation-controlled numerical approach provides a solution that is 94% of the analytical solution. However, because a displacement of 8 inches would be regarded as a failure state for the subgrade soil in the field, the ultimate capacity is obtained conservatively from a numerical solution using this approach.

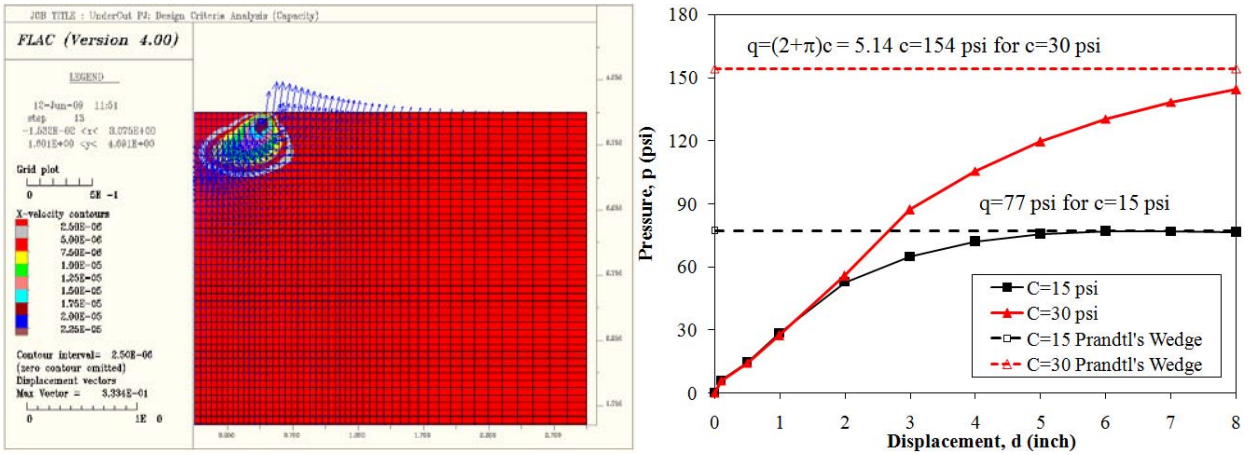

(a) Displacement & X-Velocity Plot of FLAC (b) Bearing Capacity with Prandtl's Wedge

Figure 131. Bearing Capacity Based on Prediction of Prandtl's Wedge Theory Versus Deformation Approach

Typical results of the bearing capacity analysis are presented in Figure 132. The results shown in Figure 132 (a) and (b) are for cohesive soils with assumed elastic modulus values of 1,000 psi and 5,000 psi, respectively. The red dashed lines in Figure 132 (a) and (b) indicate the yielding points at which the curves have converged to limit pressure values defined as the bearing capacity.

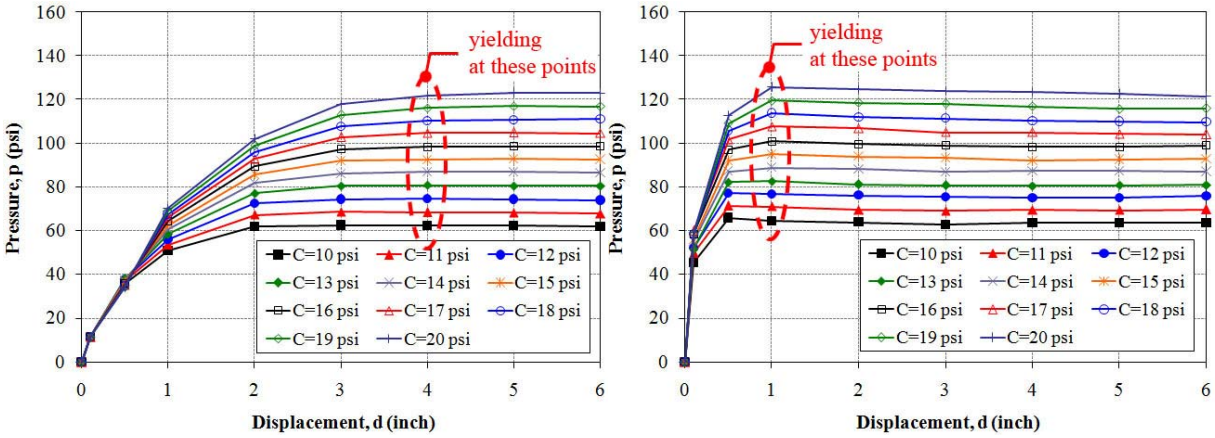

(a) E=1,000 psi (b) E=5,000 psi

Figure 132. Typical Bearing Capacity Plots for Cohesive Soils

For the case of an elastic modulus value of 1,000 psi, the onset of yielding occurred at a displacement of approximately 3 inches (designated as yielding displacement), and for the case of 5,000 psi, the yielding displacement is approximately one inch. However, regardless of the yielding displacement in the charts, two subgrade soils with different stiffness values but the same cohesion values have the same bearing capacity. The bearing resistance beyond the

yielding displacements is dependent on the cohesion of the material, and mainly independent of the stiffness.

For each curve in Figure 132, the bearing capacities were divided by a pressure of 70 psi, which is assumed to be the maximum applied pressure of both static and proof roller loading. A value denoted as the bearing capacity ratio, ξ, and defined by the ratio of the estimated bearing capacity to the field pressure load, is presented as:

$$\xi = \frac{Bearing\ Capacity}{70\,psi} = \frac{q(psi)}{70\ psi} \quad \textbf{(36)}$$

The results of the numerical simulation are classified into three categories: (1) bearing capacity under uniform displacement, (2) deformation behavior under a static pressure of 70 psi, and (3) permanent (rut depth) and maximum displacement (pumping) under proof roller loading. The rutting and pumping simulations were performed for axisymmetric and plane strain modes, respectively, as outlined in Table 86.

Table 86. Classification of Numerical Simulations for Design Criteria

Geometric Condition	Types of Analysis		Estimation Quantities
Axisymmetric	Bearing Capacity		Bearing Capacity Ratio (q_u/70 psi)
	Static		Settlement / Strain
	Proof Rolling	Maximum	Settlement
		Permanent	Settlement
Plane Strain	Bearing Capacity		Bearing Capacity Ratio (q_u/70 psi)
	Static		Settlement / Strain
	Proof Rolling	Maximum	Settlement
		Permanent	Settlement

As mentioned earlier, the plane strain mode can simulate proof roller loading and provide information about potential rutting and excessive pumping. The axisymmetric mode provides similar information but can be used to simulate mainly the effects of construction traffic (or a single wheel) rather than a series of loaded axles that are closely spaced.

Strength and Stability

The definition of unstable subgrade soil strength is discussed in relation to deformable behavior. In evaluating the suitability of soils to provide adequate subgrade support, unstable behavior can be assessed in terms of plastic shear deformation that leads to rutting, or elastic deformation that indicates excessive pumping. Elastic deformation is dependent on the elastic modulus, whereas plastic shear deformation is mainly a function of the shear strength. In performing the numerical analysis, the minimum cohesion values are those required to prevent the model's collapse under applied stress, whereas threshold values are those required for a specific safety level (such as a

factor of safety of two with respect to an applied tire pressure of 70 psi). For example, in the case where the friction angle is zero, the minimum undrained shear strength value of 12 for the axisymmetric condition and 14 psi for the plane strain condition are the lowest values allowable for the model not to collapse. Traylor and Thompson (1977) studied the behavior of construction vehicles on soft subgrades and concluded that undrained shear strength values of 13.5 to 16.8 psi are required to minimize sinking into subgrade soil. Recently, Hambleton and Drescher (2008) presented penetration depth and strength charts obtained from analytical solutions that address rutting issues in the field. A cohesion value of 17.4 psi was used in the Hambleton and Drescher (2008) solution for model integrity. The minimum cohesion and threshold values for the two different behaviors are presented in Table 87.

Table 87. Minimum Cohesion Threshold Values (assuming bearing capacity ratio = 2)

No.	Geometry	Chart Types	Friction (deg.)	Cohesion (psi)	
				Minimum	Threshold
1	Axi-Symmetric	Displacement (Maximum)	0	12	30
2			10	7	20
3			20	4	15
4			30	2	10
5		Rut Depth (Residual)	0	12	22
6			10	7	17
7			20	4	12
8			30	2	10
9	Plane Strain	Pumping (Maximum)	0	14	24
10			10	9	16
11			20	5	13
12			30	3	10
13		Rut Depth (Residual)	0	14	24
14			10	9	19
15			20	5	15
16			30	3	10

Axisymmetric Loading Condition

Bearing Capacity

Bearing capacity plots for four friction angles and an elastic modulus value of 5,000 psi are presented in Figure 133 (a) to (d). Figure 133 shows that the bearing capacity increases in accordance with the shear strength of the subgrade soil. For example, the bearing capacity for c = 10 psi and $\phi = 0$ degrees is approximately 60 psi, whereas the capacity for c = 20 psi is 120 psi using E = 5,000 psi, as shown by ‘A’ and ‘B’ in Figure 133 (a).

The capacity ratios (defined as bearing capacity normalized with respect to tire pressure of 70 psi) are plotted versus cohesion in Figure 134. The capacity ratios correlate linearly with the strength values for the elastic modulus values used in this study, except for the cases where the elastic modulus values are 500 and 1,000 psi.

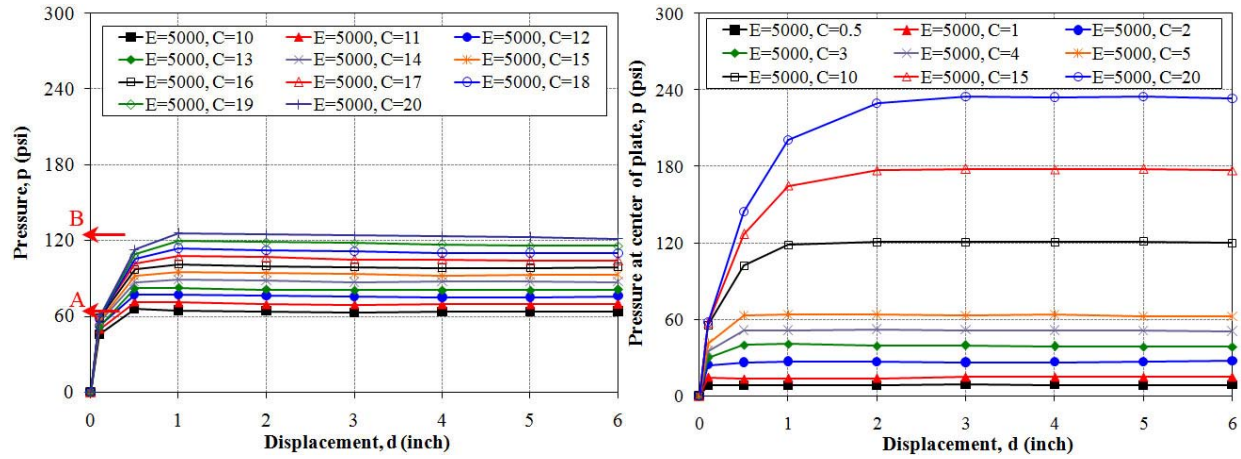

(a) ϕ = 0 degrees (b) ϕ = 10 degrees

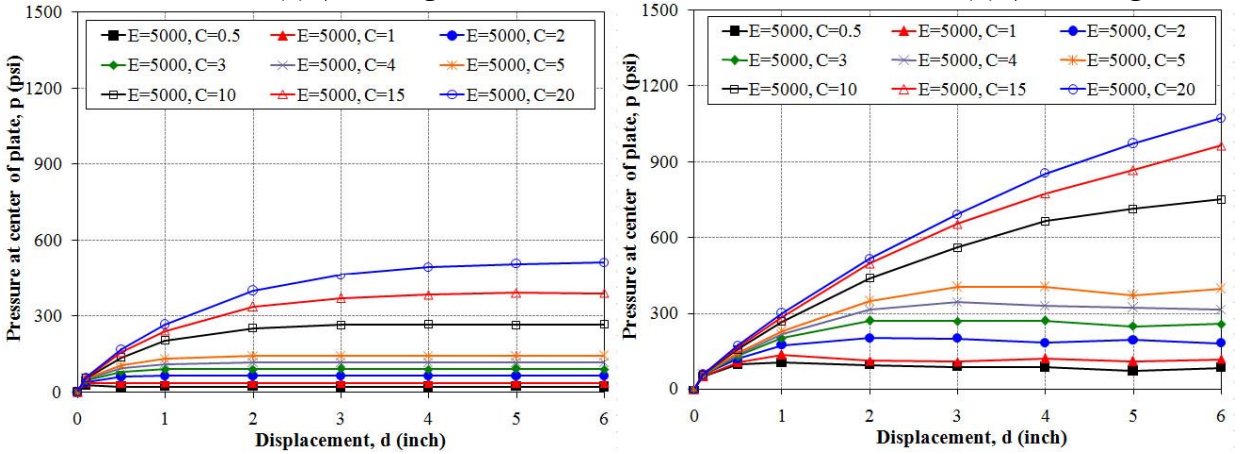

(c) ϕ = 20 degrees (d) ϕ = 30 degrees

Figure 133. Bearing Capacity Plots for E = 5,000 psi Cases

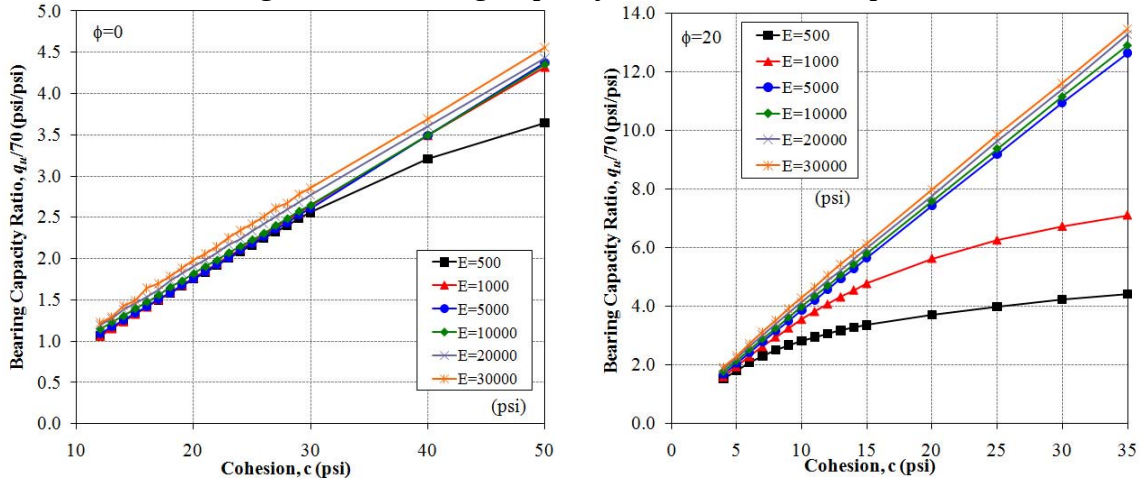

(a) ϕ = 0 degrees (b) ϕ = 20 degrees

Figure 134. Capacity Ratios According to Elastic Modulus Values

These cases of high cohesion and low modulus values yield a nonlinear variation of the capacity factor with increasing cohesion. This phenomenon is due to the fact that the deformation threshold of 6 to 8 inches was reached prior to the complete failure of the subgrade in terms of

shear zones under the applied stress. For example, an undrained shear strength of 50 psi and an elastic modulus of 500 psi for cohesive soils give the ratio of stiffness to strength as 10 (usually, E_u/S_u is within 150 to 300). Accordingly, excessive deformation due to low stiffness induces a local plastic deformation around the loading plate, and the rate of increase in the bearing capacity ratios decreases as the strength increases, as shown in Figure 134 (b).

Design Criteria Based on Maximum Shear Strain

The first method explored in this study for assessing the suitability of a subgrade for a roadway application is to estimate the maximum shear strain under the design load. The maximum shear strain is correlated with tension cracking that occurs at the boundary of the loading zone. Figure 135 shows the maximum shear strain for a wide range of cohesion values for two cases of friction angle, i.e., 0 and 20 degrees.

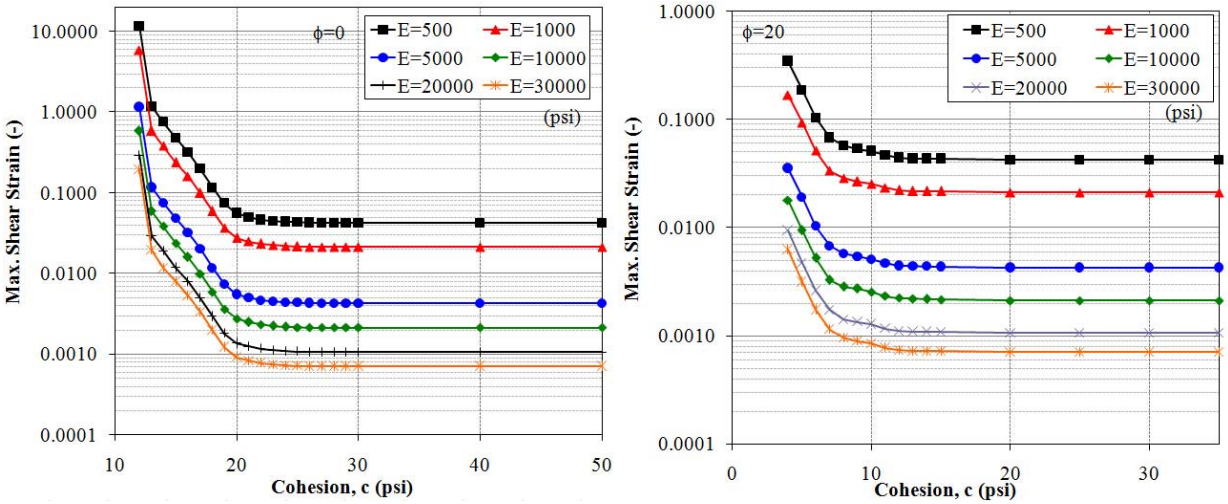

(a) ϕ = 0 degrees (b) ϕ = 20 degrees

Figure 135. Design Criteria Chart Based on Maximum Shear Strain at Boundary of Loading Plate

The horizontal trend observed in the right half of the graphs in Figure 135 indicates that the subgrade soil behaves elastically and that settlement is independent of the strength parameters. The nonlinear portion on the left side of the graphs indicates that the subgrade soil is in a plastic state. The models with lower strength parameters (far left side of the curves) collapsed under the design and/or proof roller loading. This behavior (presented in terms of the magnitudes of shear strain) confirms the notion that rutting is mainly a function of the shear strength, whereas excessive pumping is a function of the soil stiffness. This distinction can explain, for example, a proof roller on a relatively thin lime-stabilized soil layer over soft subgrade where pumping is observed but with minimum rutting.

Undercut Criteria: Axisymmetric Condition

Figure 136 (a) to (d) present the undercut design criteria chart for friction angles 0, 10, 20, and 30 degrees, respectively. These charts are for static loading. Results for friction angles between those values can be obtained via interpolation.

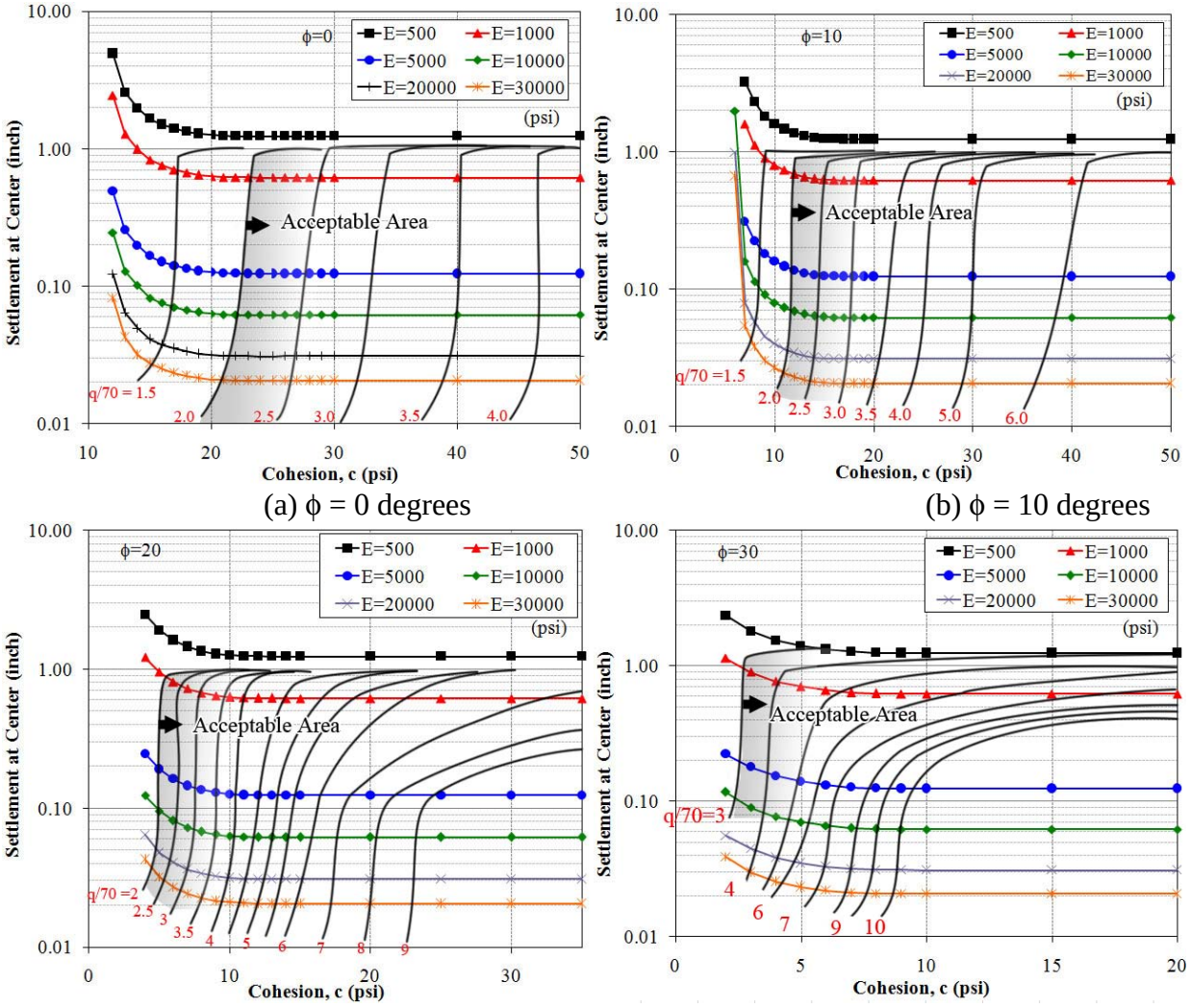

(a) ϕ = 0 degrees (b) ϕ = 10 degrees

(c) ϕ = 20 degrees (d) ϕ = 30 degrees

Figure 136. Design Criteria Charts for Axisymmetric Load Condition

An acceptable rut is defined as less than 1.0 inch displacement, and the acceptable capacity factor is set to 2.0. These values can change according to NCDOT practice or the desired level of conservatism. The acceptance areas are indicated in Figure 136 (a) to (d). If these criteria (capacity factor = 2.0 and less than 1 inch settlement) are applied to the soils modeled in Figure 136 (b) to (d), the acceptance lines are located partially in the zone of plastic deformation, which means that some plastic displacement is acceptable for those frictional soils. As shown in the undercut design charts, the settlement curve for soils with an elastic modulus of 500 psi is always outside of the acceptable one-inch displacement zone, implying that the elastic modulus value of the stabilized soil should be higher than 500 psi.

Undercut Design Criteria: Proof Roller Loading

Figure 137 (a) and (b) show the maximum settlement estimated at the peak of the load pulse and the permanent settlement that corresponds to the plastic deformation after the applied load has passed, respectively.

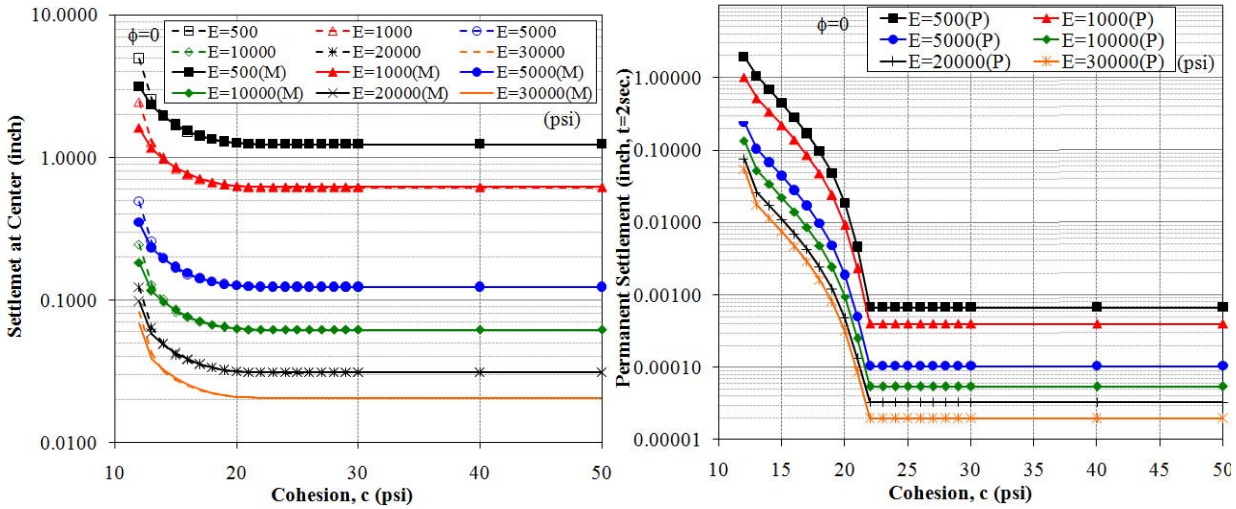

(a) Maximum Settlement (Pumping) (b) Permanent Settlement (Rut Depth)

Figure 137. Design Charts for Proof Roller Loading

The difference between the maximum and permanent displacements is regarded as a value directly related to pumping behavior during proof roller testing. As shown in Figure 137 (a), the maximum settlement design charts are similar to the static load cases, but with a minor difference in plastic areas. In Figure 137 (a), the results from the static load cases are plotted using dashed lines. It seems that the similarity of maximum displacement to static loads is caused by the low frequency (0.5 Hz) of the proof roller load. Such a loading frequency is not sufficient to cause a significant difference due to dynamic effects. Therefore, the design chart for the maximum displacement of the proof roller load can be replaced by that for the static load cases.

Figure 138 (a) to (d) present the design charts for permanent displacement with proof roller loading, separated into four charts according to the value of the friction angle (as was done for the static load cases). In this case, permanent displacement values are below the 1.0 inch settlement. Accordingly, acceptance lines are not related to the amount of settlement, but are dependent on the capacity of the subgrade soil for soils with friction angles of 0 and 10 degrees, as shown in Figure 138 (a) and (b).

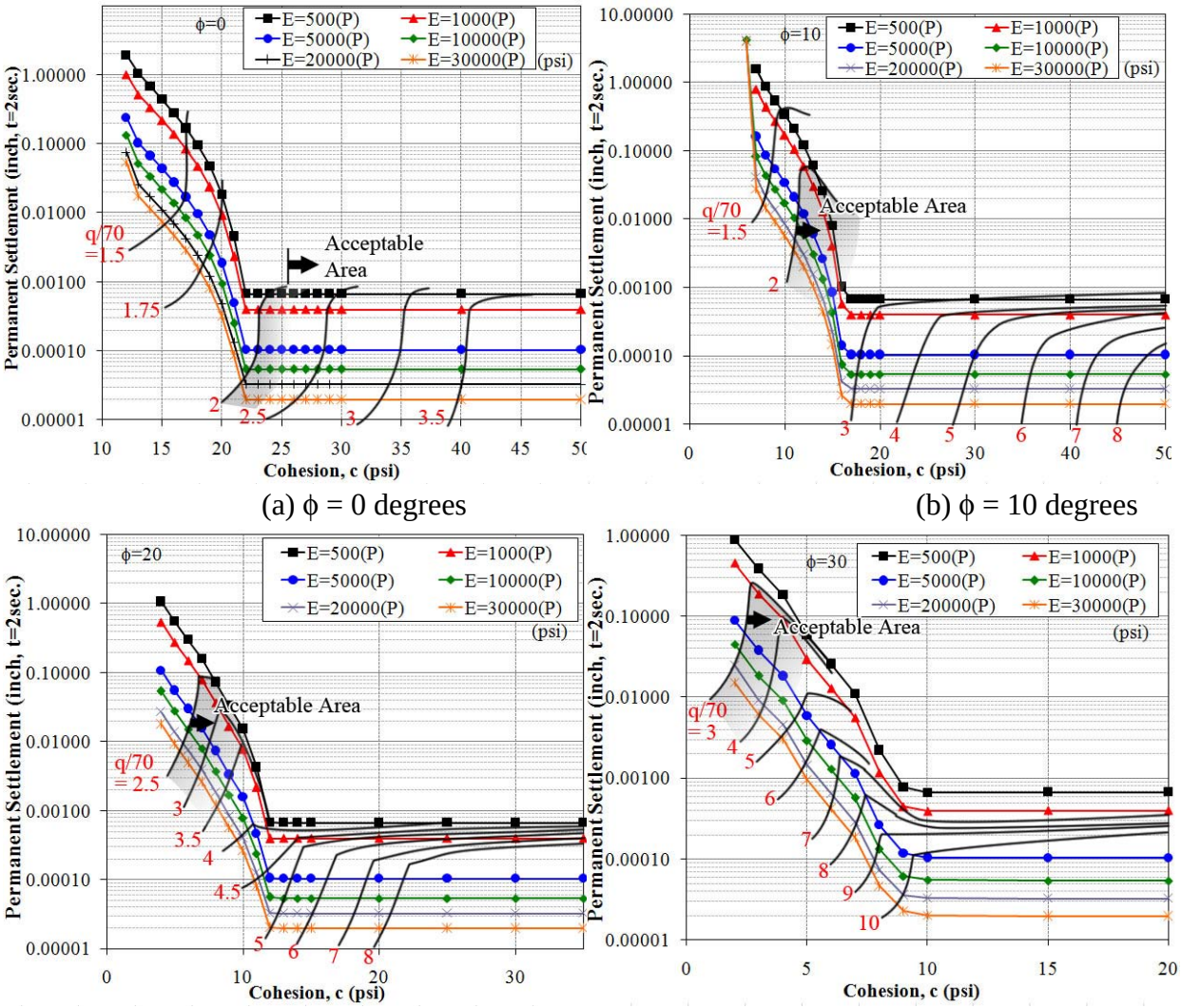

(a) ϕ = 0 degrees (b) ϕ = 10 degrees

(c) ϕ = 20 degrees (d) ϕ = 30 degrees (note axis scales)

Figure 138. Design Charts for Permanent Settlement of Proof Rolling Test

When the cases with friction angles of 20 and 30 degrees are considered, the permanent settlement over 0.1 inch can be regarded as excessive plastic deformation and in the failure state, based on correlations with data from the field modeling and observations from the laboratory studies.

Plane Strain Condition

In parallel to the cases that assume the axisymmetric condition, bearing capacity and deformation analyses under static and proof roller loading were performed assuming a plane strain condition. Because most proof roller trailers used in the field cannot be regarded as a single-axle vehicle, it seems reasonable that the required design values are based on the plane strain condition. A plane strain loading imact a larger depth of the profile and it is the deeper weak layers that may lead to "pumping" observation of the proof roller. At similar deformation levels, the results for bearing capacity are lower than those for the axisymmetric condition, so consequentially, the shear

strength values needed to obtain the same displacement are higher than those obtained for the plain strain case.

Bearing Capacity

Bearing capacity plots for the four friction angles and elastic modulus of 5,000 psi are presented in Figure 139 (a) to (d).

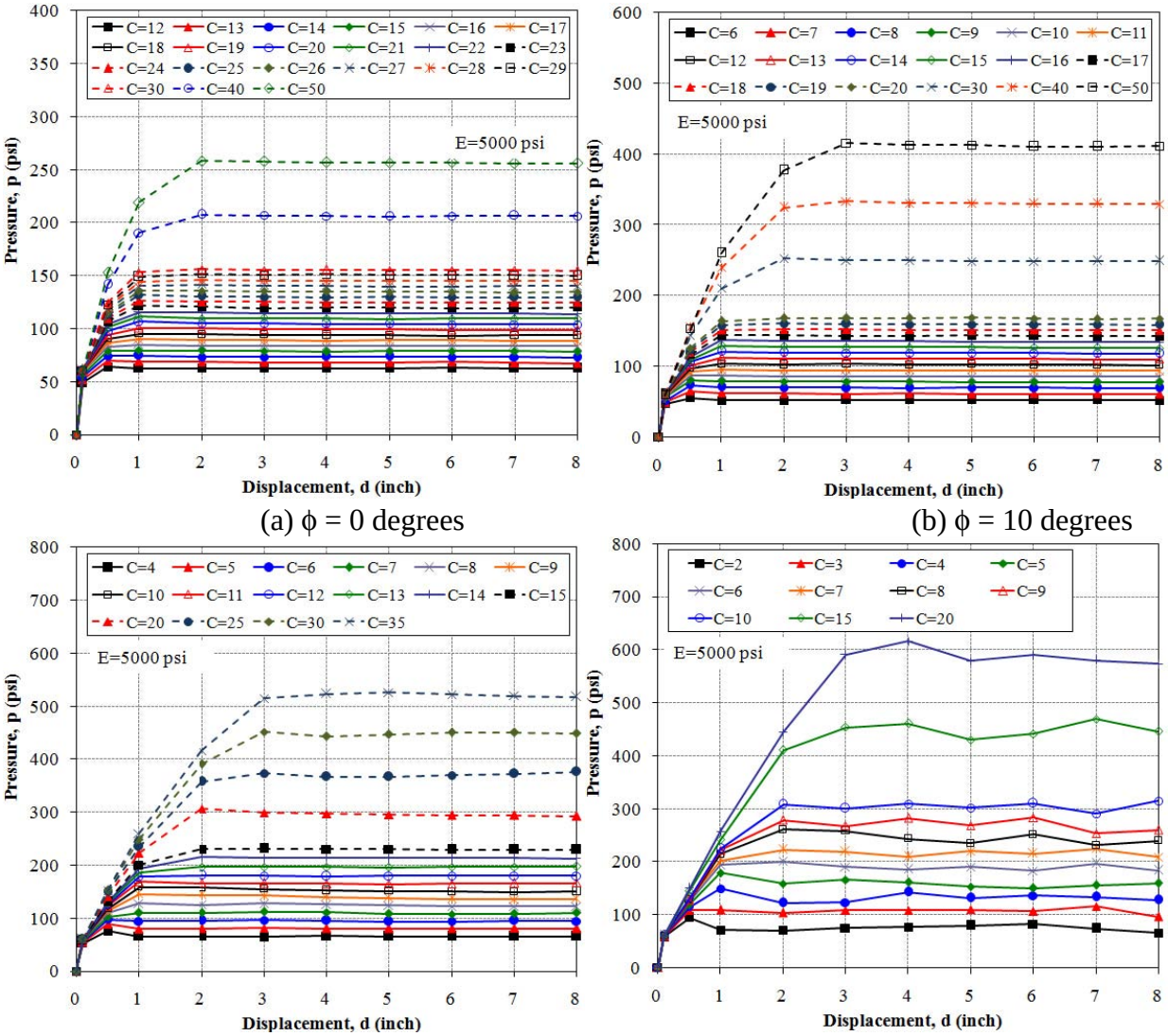

(a) ϕ = 0 degrees (b) ϕ = 10 degrees

(c) ϕ = 20 degrees (d) ϕ = 30 degrees

Figure 139. Bearing Capacity Plots for E = 5,000 psi Cases

The capacity factors are plotted versus cohesion values using various elastic modulus values, as shown in Figure 140 for friction angles of 0 and 20 degrees, respectively. Compared with the same plots in an axisymmetric condition, the capacity factors (0.5 Hz) range from 0.8 to 3.6 for a friction angle of zero, and from 1.0 to 8.0 for a friction angle of 20 degrees. These results are 60 to 80% less than those computed assuming the axisymmetric condition. The results show that if

the capacity safety factor of 2.0 or higher is set as the acceptance criterion, an undrained shear strength value over 30 psi is required. As mentioned earlier, the specification of the capacity safety factor is at the discretion of NCDOT engineers. .

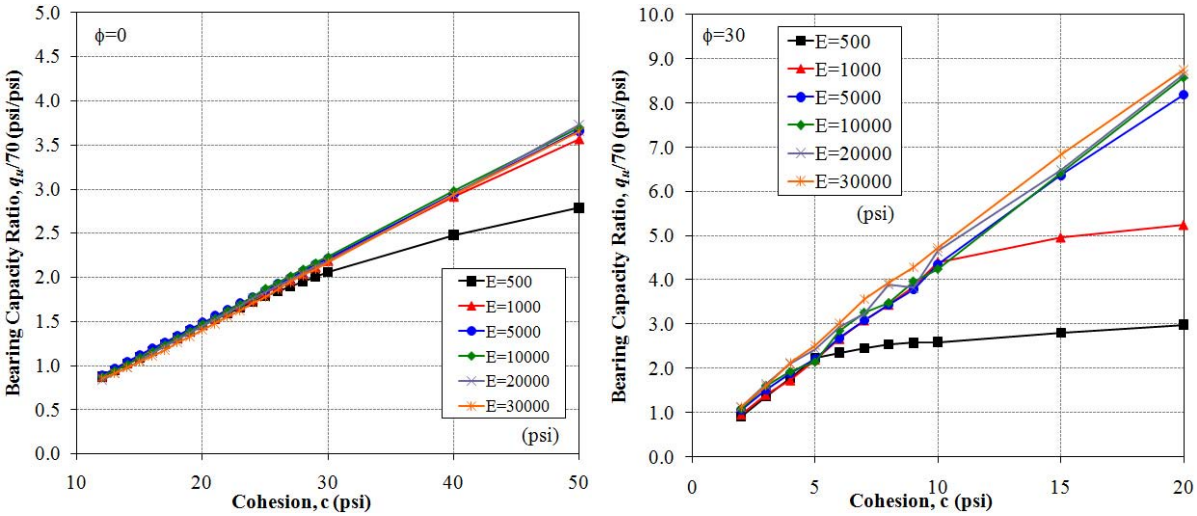

(a) ϕ = 0 degrees (b) ϕ = 20 degrees

Figure 140. Capacity Factors According to Elastic Modulus

Undercut Criteria: Static Loading

Undercut criteria charts based on displacement plots are presented in Figure 141 (a) to (d) for friction angles of 0, 10, 20, and 30 degrees, respectively. The acceptable deformation is defined as 1.0 inch, and the acceptable capacity factor is set to 2.0, but can be changed at the discretion of NCDOT engineers. The acceptable areas, where undercutting is not recommended, are presented in Figure 141 (a) to (d). Whereas the cases with elastic modulus values equal to 1000 psi are in the acceptable area for the axisymmetric condition, assuming plane strain condition for the same cases yields a deformation close to the 1.0 inch displacement limit, or at times outside the acceptable area. This finding highlights the difference between the axisymmetric and plane strain conditions, and perhaps highlights one of the reasons as to why proof rolling approach has been providubg acceptable results in the field.

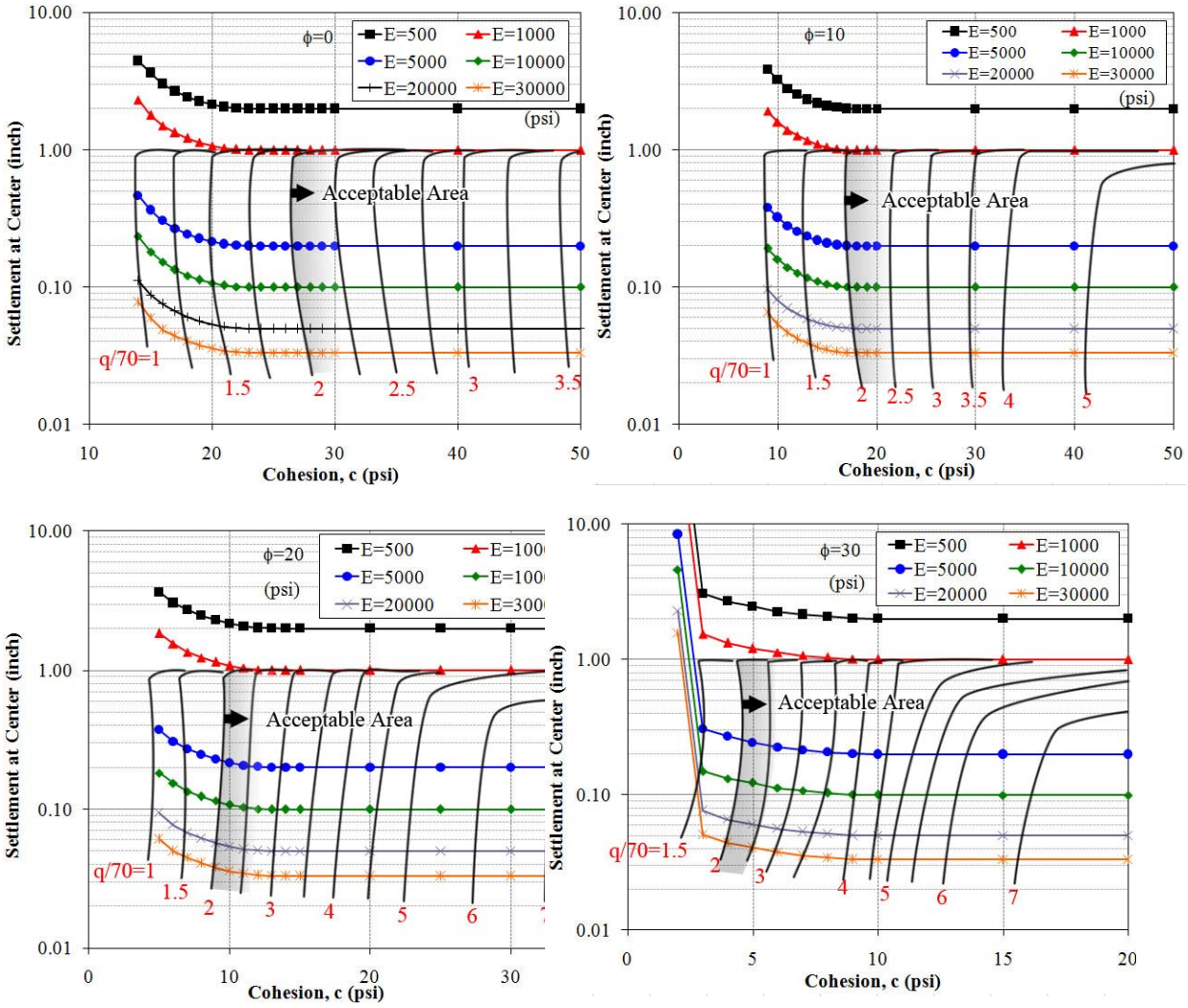

(a) ϕ = 0 degrees (b) ϕ = 10 degrees

(c) ϕ = 20 degrees (d) ϕ = 30 degrees

Figure 141. Design Criteria Charts for the Plane Strain Load Condition

Undercut Criteria: Pulse Loading

The deformation plots for proof roller loading consist of maximum and permanent displacements, as shown in Figure 142 (a) and (b), respectively.

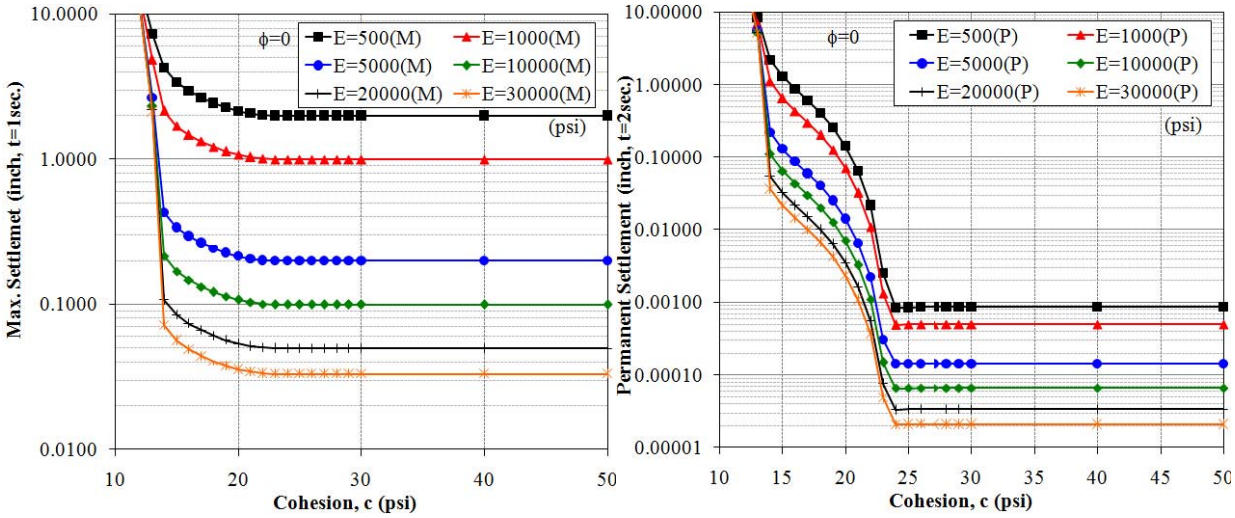

(a) Maximum Settlement (Pumping) (b) Permanent Settlement (Rut Depth)

Figure 142. Design Charts for Proof Roller Loading for the Plane Strain Condition

Figure 143 shows the maximum and permanent settlement curves on the same plot where the differences indicate the resilient displacement. When compared to the axisymmetric condition (Figure 14), it can be seen that the maximum settlements increase, whereas the permanent settlements decrease or stay nearly the same. The difference between the two values, however, indicates pumping in the field.

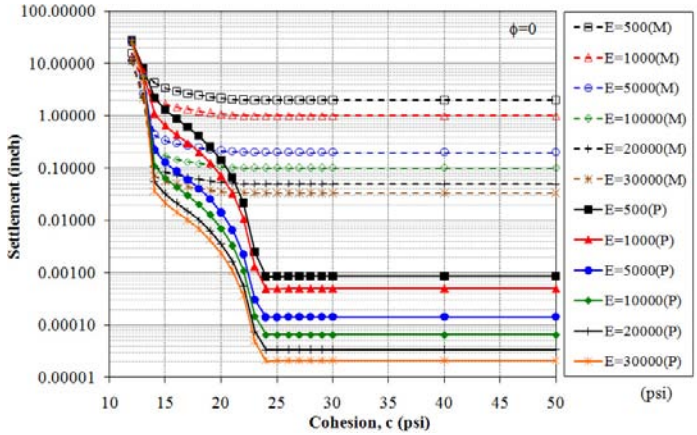

Figure 143. Maximum and Permanent Settlement Curves for Proof Roller Loading

Within the elastic response range of the response, where the deformation is mainly a function of soil stiffness, the permanent deformation is relatively small, on the order of 0.0001 inch. Figure 20 shows the difference between the maximum and permanent deformation for both axisymmetric and plane strain modes of loading. For example, the maximum settlement for the case of the elastic modulus of 1000 psi and under the plane strain condition is 1.0 inch within the elastic state (the part of the curve where the computed settlement is independent of the shear strength), and the value for the axisymmetric condition is 0.62 inch. On the other hand, the permanent settlement for the plane strain condition is 4.0×10^{-4} inch, and the value for the axisymmetric condition is 5.0×10^{-4} inch. As mentioned earlier, the difference between maximum and permanent displacements is indicative of pumping behavior.

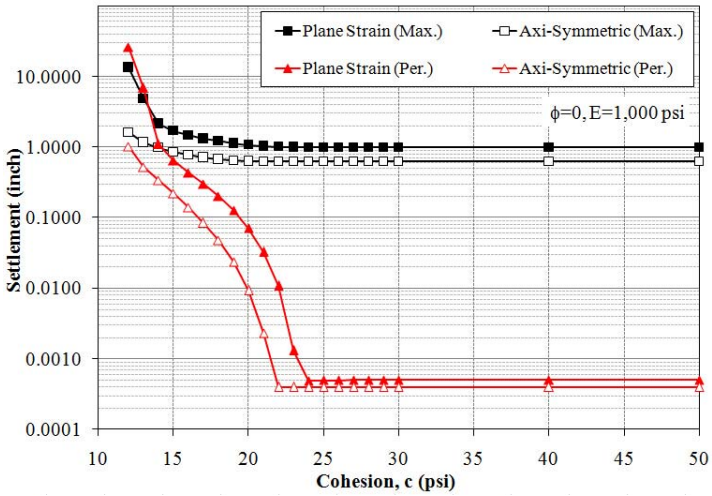

Figure 144. Comparison of Maximum and Permanent Displacement for Axisymmetric and Plane Strain Conditions

Bearing Capacity by Limit Equilibrium

The bearing capacities obtained from the numerical approach are compared with general approaches by Terzaghi or the Vesic method. These general approaches are independent of stiffness factors, and the ultimate capacities for a wide range of strength factors are estimated.

Table 88 presents the results, assuming a cohesion value of 15 psi. Figure 145 shows the bearing capacity ratios (which is the ratio of bearing capacity normalized with respect to a tire pressure of 70 psi) for the two cases of friction angles of zero and 20 degrees, and assuming the axisymmetric (Figure 145a) and plane strain (Figure 145b) conditions.

Table 88. Estimation of Ultimate Bearing Capacity by Terzaghi and Vesic Methods (c = 15 psi)

Mechanical Condition	ϕ (deg)	Terzaghi				Vesic			
		Nc	Nq	Nγ	q_{ult} (psi)	Nc	Nq	Nγ	q_{ult} (psi)
Axisymmetric	0	5.7	1.0	0.0	111.2	5.1	1.0	0.0	92.1
	10	9.6	2.7	1.0	190.6	8.3	2.5	1.2	166.2
	20	17.7	7.4	4.4	359.1	14.8	6.4	5.4	335.8
	30	37.2	22.5	20.1	789.3	30.1	18.4	22.4	800.1
Plane Strain	0	5.7	1.0	0.0	85.5	5.1	1.0	0.0	77.1
	10	9.6	2.7	1.0	149.6	8.3	2.5	1.2	131.7
	20	17.7	7.4	4.4	289.0	14.8	6.4	5.4	251.4
	30	37.2	22.5	20.1	665.2	30.1	18.4	22.4	572.1

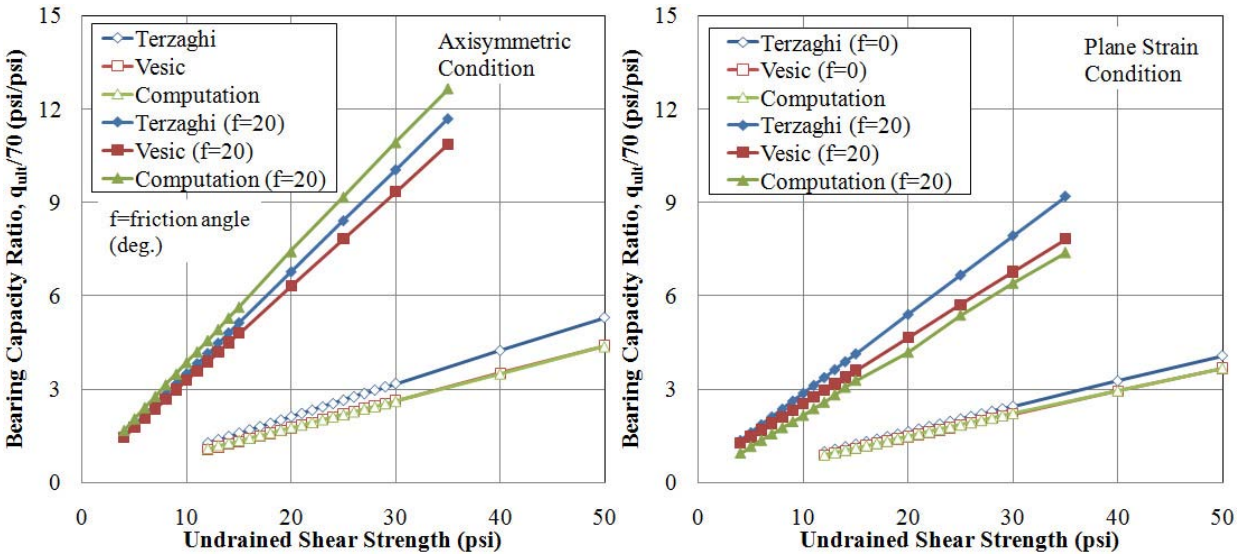

(a) Axisymmetric Condition (b) Plane Strain Condition

Figure 145. Comparison of Bearing Capacity Using General Approaches

As shown in Figure 145, the bearing capacities obtained from numerical simulations are consistent with those obtained using the well-documented general approaches. For the cases of cohesive soil (friction angle = 0), the undrained shear strengths vary from 12 to 50 psi, and the corresponding bearing capacities values obtained by the Vesic method vary from 74 to 307 psi for the axisymmetric condition and from 62 to 257 psi for the plane strain condition, respectively. The corresponding bearing capacity ratios vary from 1.0 to 4.4 for the axisymmetric condition, and from 0.9 to 3.7 for the plane strain condition. For the case of cohesive soils with a friction angle of zero, the Vesic solution is nearly the same as the FLAC numerical solution (99 to 101% agreement). The elastic modulus value of the numerical solution used in this comparison is 5,000 psi. For the different elastic modulus values used in the analysis, the rate of agreement is within 95%.

Application of Undercut Criteria

Laboratory Testing

Undercut criteria were applied to discern the suitability of the subgrade soil and stabilization measures used during large-scale testing. The predicted settlements obtained from these criteria were compared with the measurements. The results of the consolidated undrained (CU) triaxial tests for the coastal plain mixed soil were used to obtain the stiffness and strength parameters. Table 89 shows the strength and stiffness parameters obtained from the results of CU triaxial testing at strains of 1 % and 5%. Table 89 also presents the settlements for three coastal plain mixed soils. The subgrade soil was tested in the test pit under static (maximum pressure of 40 psi) and proof roller-simulated loading, and the maximum settlement after proof rolling was measured as 1.776 inches. The subgrade soil tested in the test pit is also the soil with the water content of 18.8 %, according to the measurements presented in Chapter 3.

In Figure 146, the hollow symbols represent the stability of each subgrade soil. Based on the acceptance line in the chart, the soils with water contents of 18.8% and 20.7% do not satisfy the criteria, and will show both rutting in terms of shear failure and excessive displacement. The subgrade at 15.6% moisture content seems to plot in a zone on the chart that indicates the unlikely occurrence of significant shear failure, but excessive displacement and pumping. The results of five large-scale tests on stabilized subgrade soils are presented in the same chart. The settlement magnitudes plotted for the five stabilization measures are those obtained after rutting was repaired and the second cycle of simulated proof roller loading was applied. The deformation magnitudes, which were also measured at the maximum load of the proof roller loading, are within 0.1 to 0.26 inch. In this case, the five stabilization approaches rendered the construction on the soft subgrade acceptable.

Table 89. Results of CU Triaxial Testing for Mixed Coastal Plain Subgrade Soil

Terms		*w* = 15.6 %	*w* = 18.8%	*w* = 20.7%
Elastic Modulus (secant; psi)	ε =1%	2,349	2,379	2,104
	ε =5%	797	**639**	539
Cohesion (psi)		9.4	**5.7**	2
Friction Angle (°)		20.5	**19**	16.5
Predicted Settlement (in.)		0.91	**1.36**	9.11

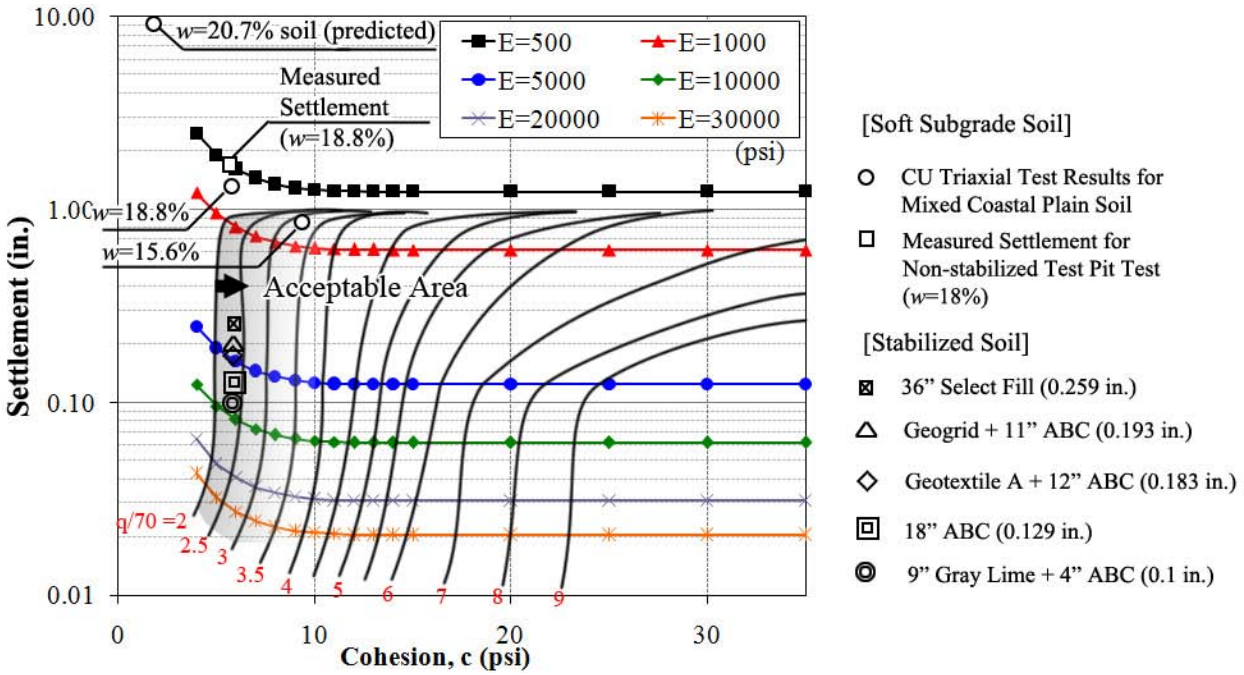

Figure 146. Application of Undercut Criteria for the Subgrade Soil and Stabilization Measures Used in Large-Scale Testing

Application to Field Data

The application of the proposed undercut criteria is demonstrated in field cases where Dynamic Cone Penetration Index (DCPI) values are available. The DCPI values were obtained from the field measurements presented in Chapter 4 and are summarized in Table 6. The DCPI values were obtained during field work in the city of High Point (located mostly in Guilford County) and Wake County sites that include both soft and stiff subgrade locations.

In order to apply DCPI values to the undercut criteria, undrained shear strength and elastic modulus values were estimated using correlations presented in Chapter 4. The wave equation model results were used to obtain the undrained shear strength values from the DCPI. In the case of the elastic modulus, the resilient modulus values and DCPI correlations (Mohammed et al., 2007) presented in Figures 4 to 8 were used. As shown in Table 90, the estimated ratios of undrained shear strength and elastic modulus values (E_u/S_u) vary from 80 to 150.

Table 90. DCPI Values and Correlated Parameters: Demonstration of Undercut Criteria Using Field Data

Site	Soil	Term	DCPI	Elastic Modulus, E			Cohesion, c	
			(mm/blow)	(MPa)	(psi)	E_u/S_u	(kPa)	(psi)
High Point	Stiff	H1	13.6	104.8	15203	148	707.9	102.6
	Soft	H2	40.6	17.6	2551	104	169.6	24.6
Wake	Stiff	W1	27	30.0	4353	122	246.6	35.8
	Soft	W2	53	10.9	1575	82	132.9	19.3

The maximum settlement, factor of safety, and ultimately whether or not undercutting is required can be estimated using these values. The charts used in this example are for maximum settlement under axisymmetric and plane strain conditions for the case of a friction angle of zero, as presented in Figure 136 (a) and Figure 141 (a), respectively. The field data, as plotted on the undercut criteria charts, are presented in Figure 147.

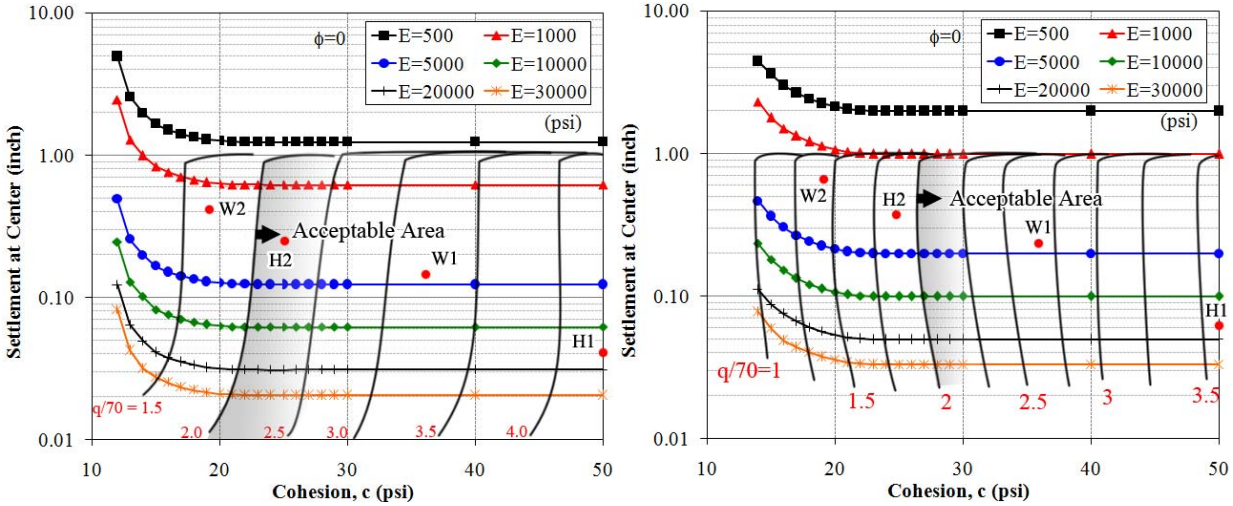

(a) Axisymmetric Condition (b) Plane Strain Condition

Figure 147. Samples Located in Design Chart

The field data for the soft subgrade cases, designated as H2 and W2, did not pass the proposed undercut criteria for the plane strain mode. For the the axisymmetric mode, as shown in Figure 147 (a), H2 is plotted within the acceptable margin, which may indicate a level of rutting to be expected on soils with profiles similar to H2 (which is a soft subgrade soil with a California bearing ratio (CBR) of less than 8%).

Summary

Undercut design criteria have been developed using numerical analysis for static and proof roller loading. Two modes of modeling were considered, plane strain and axisymmetric conditions. The plane strain mode is assumed to simulate proof roller loading and provide information about potential rutting and excessive pumping. The axisymmetric mode provides a similar type of information, but can be used to simulate the effects of construction traffic (or a single wheel) rather than a series of axle loads that are closely spaced. When considering the subgrade to be used for roadway construction support, two failure mechanisms that may occur during proof rolling must be avoided: excessive rutting and pumping. It is postulated that rutting is associated mainly with plastic shear deformation within the shallow layers and can be considered as a function of the shear strength parameters. On the other hand, excessive pumping is mainly a function of stiffness parameters, and is affected by the response of shallow as well as deep layers of the profile. It is possible to have pumping without rutting. An example that illustrates such an occurrence is the case of a relatively thin chemically-stabilized subgrade layer over a deep layer of soft soils. The shear strength of the top layer may be high enough to prevent plastic shear failure, yet the soil mass that is affected by the surface stresses can have a low stiffness value that leads to excessive pumping.

Results of the numerical analysis were used to establish undercut criteria for both axisymmetric and plane strain modes. The bearing capacity and deformation of the modeled cases were estimated for a wide range of stiffness and strength parameters. The strength and elastic parameters can be obtained from DCPI values in the field and triaxial and resilient modulus testing in the laboratory. The proposed undercut design criteria are based on the suitability of bearing capacity ratios to minimize the potential for rutting, and the definition of a limit displacement value to minimize the potential for excessive pumping. The proposed criteria determined from this study and presented in this report are 2.0 for the bearing capacity ratio and 1.0 inch settlement for pumping, but these criteria may be changed at the discretion of NCDOT engineers. The proposed undercut criteria were validated through data from laboratory and field testing. The validation results show that the proposed criteria are reasonable and provide an indication of the suitability of subgrade soils for the support of roadways.

CHAPTER 11: SIMULATION OF FIELD CASES

The estimation of the response of field sections using construction sequences and geometrical characteristics is important in understanding the effectiveness of the stabilization measures included in this study. Thus, this study recognizes that the stress state in the subgrade soil layer is affected by construction sequences and geometric conditions as well as the strength of the materials. Work in this chapter explores the response of subgrade soil for four field configurations subjected to proof rolling and construction traffic loading. The four field cases are taken from three projects related to undercutting. The model considers five stabilization methods included in this study. Input properties for the four field models are estimated from small- and large-scale testing, as previously described.

Study Cases

Based on information provided by the NCDOT, Case 1 of the study cases represents the at-grade road widening of an existing roadway by adding a fill section where the embankment is less than four feet high. Case 2 represents the construction of a new alignment in a fill situation where the thickness of the fill is typically less than six feet. Case 3 represents a new alignment in a cut situation; typically in such a case, 3 feet of undercut is implemented in areas where the subgrade fails proof rolling. Case 4 represents the widening of a highway median.

In all four cases, the thickness of the soft subgrade layer is assumed to be approximately 7 feet to provide an adequate depth for estimating the stress distribution without being affected by boundary effects. Construction traffic is considered to be one of the loading conditions. Prior to the construction of the embankment or the addition of fill, static, proof roller, and cyclic construction loads are applied on the surface of the subgrade soil for both stabilized and unstabilized cases. After the construction of the embankment or addition of fill for Cases 1 and 2, static and proof rolling loads are applied. Cases 3 and 4 do not have additional construction stages beyond preparation of the subgrade. For all cases, the response of the unstabilized subgrade is computed and used for reference. Information regarding the configuration of each field case and the reference project are presented in Table 91.

Table 91. Typical Sections of Field Cases

Cases	Category	Project	Station No.
Case-1	Widening: Existing Road (<4 ft.)	R-2510A NBL	224+50
Case-2	New Alignment: Fill (< 6 ft.)	R-2510A NBL	57+50
Case-3	New Alignment: Cut	U-2524AB	54+20
Case-4	Widening: Median	I-4744	-

The modeled sections of Cases 1 and 2 were obtained from project R-2510A and are presented graphically in Figure 148 (a) and (b). Project R-2510A NBL consists of numerous undercut sections; some relate to widening the existing roadway, and others relate to new alignment fill. The section selected for numerical analysis is constructed with a slight geometry simplification from the real section, as shown in Figure 148. A fill section was selected for Case 2 modeling, as shown in Figure 148 (b). The height of the embankment is approximately 4.6 feet at the center for both Cases 1 and 2.

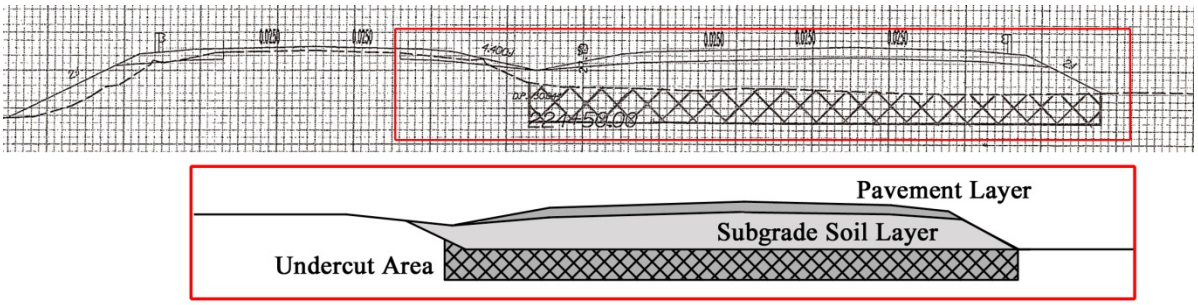

(a) Case 1 (R-2510A NBL: 224+50)

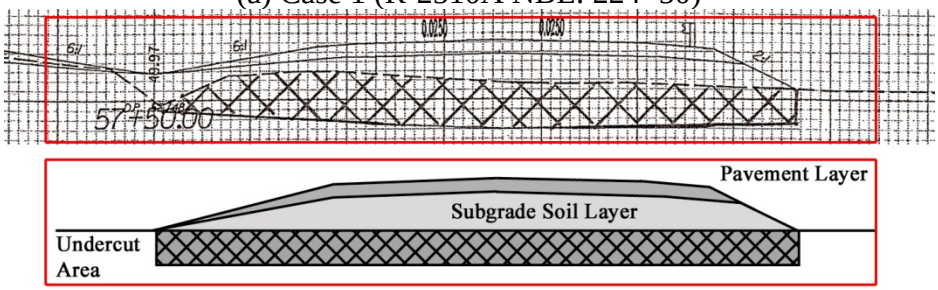

(b) Case 2 (R-2510A NBL: 57+50)

Figure 148. Project Section and Corresponding Idealization for Numerical Model: Cases 1 and 2

Figure 149 and Figure 150 show the numerical discretization of the domain and the mesh layers for Case 1 and Case 2, respectively. For Case 1, the existing embankment section with the subgrade layer is simulated as an initial condition, as shown in Figure 149. The road widening fill is then constructed in layers. The thickness of each lift is assumed to be 1.1 feet, and 4 layers are simulated. It is assumed also that the left boundary of the initial ground and the right boundary of the embankment fill are five to six times the height of the embankment. The depth of the undercut section is simulated as 4 feet due to the thickness of the soft soil. Simulated static, proof roller, and dynamic loading are applied in two construction stages, before and after embankment construction.

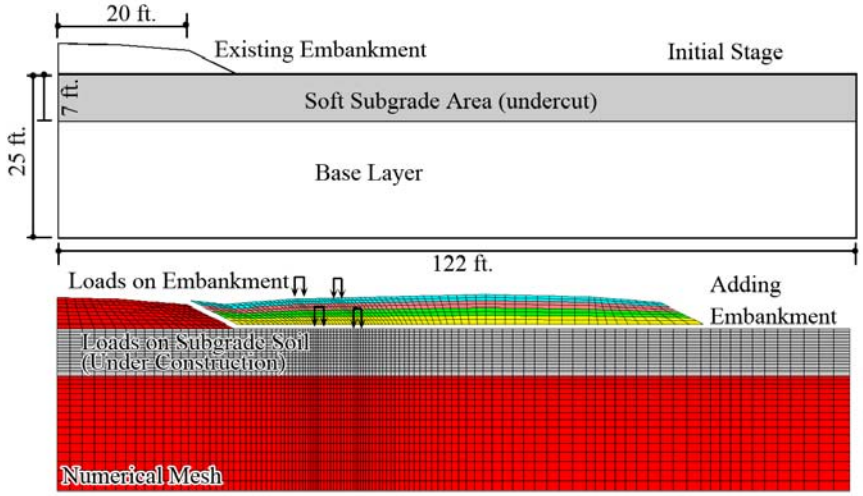

Figure 149. Dimensions, Construction Sequences, and Numerical Mesh: Case 1

The numerical model of Case 2 is considered as a symmetrical section, as shown in Figure 150. Both the right margin and the height of the model are 25 feet, which is 6 times the embankment height at the center.

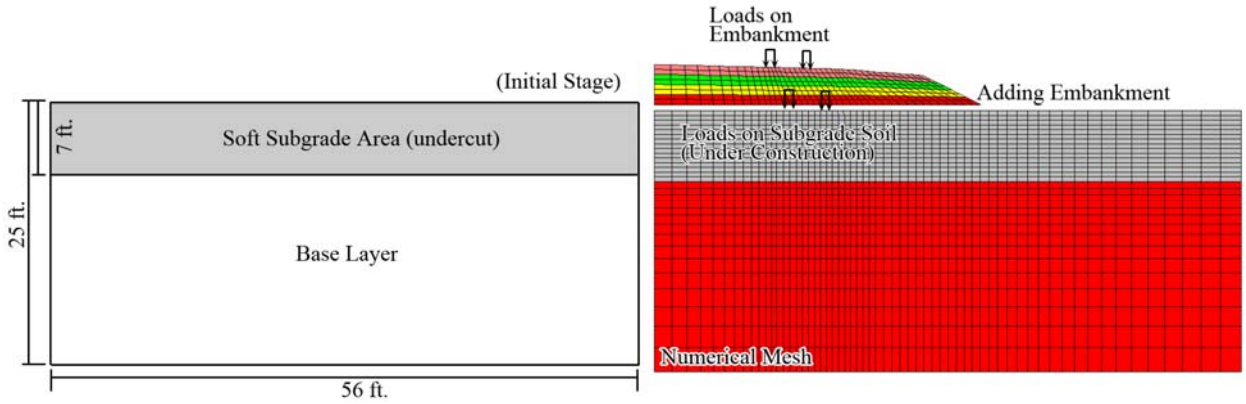

Figure 150. Dimensions, Construction Sequences, and Numerical Mesh: Case 2

Case 2 represents the construction of a new alignment in a fill situation. The numerical model mesh and construction sequence are almost the same as for Case 1, with one difference being the absence of an existing embankment. The initial state in the model is assumed prior to constructing the embankment, and then, the embankment is constructed in lifts to a height of 4.0 feet. The thickness of each lift is approximately 1.0 foot, and the depth of the undercut layer is 3.5 feet. After the construction of the embankment, two pressure areas, 1.0 foot wide and 6.0 feet apart, are modeled, as shown in Figure 150 .

Case 3 represents a new alignment in a cut situation. A typical section for numerical simulation was taken from project U-2524AB, as shown in Figure 151 (a). Before applying the surface stresses, excavation is simulated through four stages, as shown as the ‘excavation area’ in Figure 151 (b). The surface stresses are applied on the left lane of the section, as shown in Figure 151 (c), because the settlement of the subgrade soil might also be affected by the loading due to the cut slope on the right side of the model.

Case 4 represents a project in which a highway median is widened. The section for numerical simulation comes from the plans for NCDOT project I-4744. The controlling condition of this section is that the existing road must remain in operation while construction proceeds. The section for Case 4 does not have additional construction layers, such as cut or back fill. An idealized section is shown in Figure 152 (a), and the numerical model mesh is shown in Figure 5 (b).

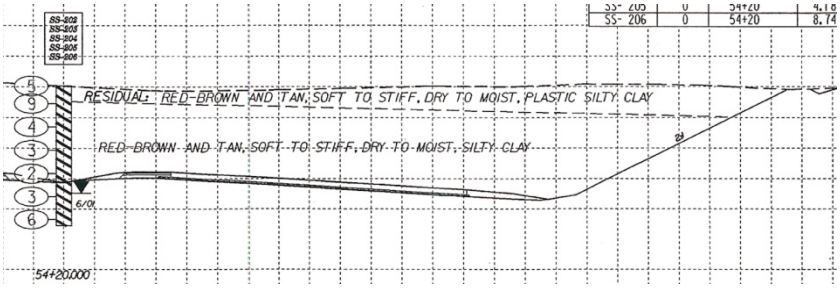

(a) Section of U-2524AB (STA. 19+20)

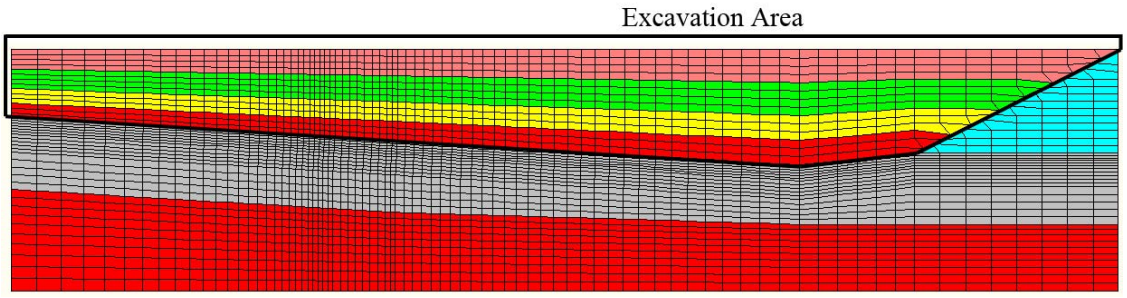

(b) Numerical Model Mesh for Simulation of Excavation Area

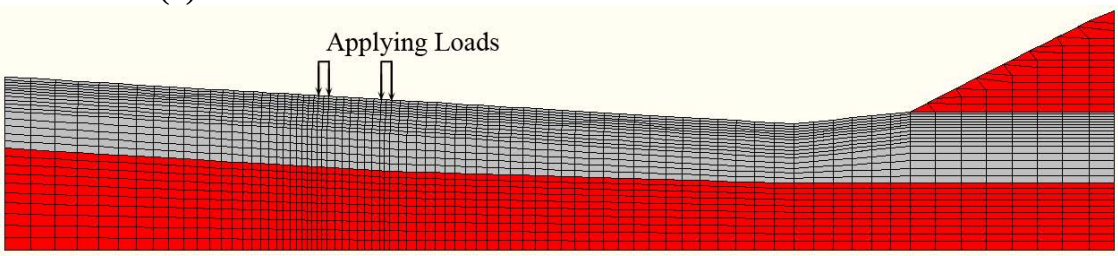

(c) Numerical Model Mesh after Excavation and Loading

Figure 151. Modeled Sections for Case 3

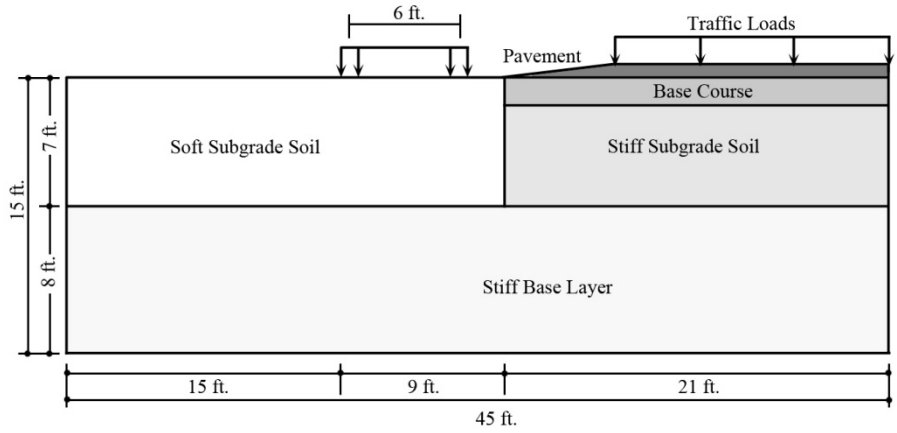

(a) Dimensions for Numerical Simulation of Case 4

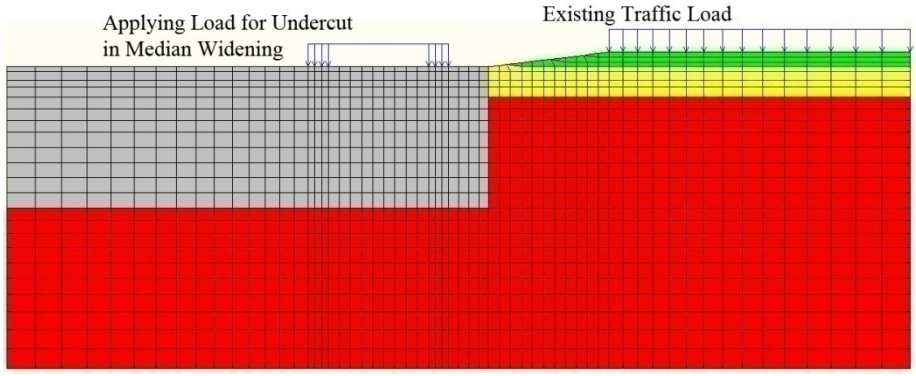

(b) Numerical Model Mesh of Case 4

Figure 152. Numerical Mesh for Case 4 Section

Stabilization Measures

Analysis was performed using the profile configuration of Case 1 for five stabilization cases: the use of select fill, an aggregate base course (ABC), a geotextile-ABC layer, a geogrid-ABC layer, or a lime-stabilized soil layer. Figure 153 schematically shows each construction sequence and an "evaluation point" at which the displacement is tracked for demonstrating comparative performance. The area of the soft subgrade, shown in gray in Figure 153, is to be replaced by one of the five stabilization measures, as shown in Figure 154 (b) through (f). Similar to the scheme employed for the development of undercut criteria, a displacement controlled loading is applied by inducing displacement at a uniform velocity to nodes that represent a loaded area. The mobilized force at key nodes is then estimated and plotted versus the displacement to establish rutting levels.

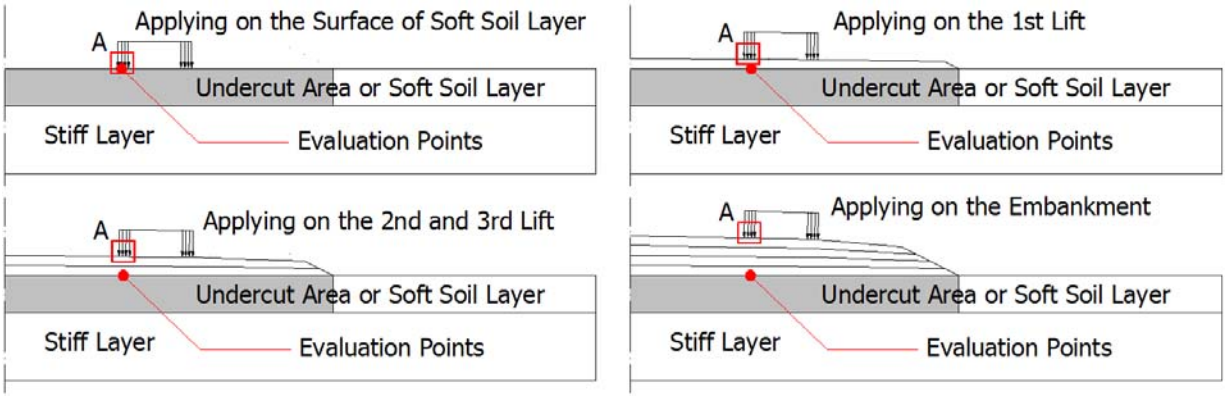

Figure 153. Simulated Models According to Construction Sequence

Input Material Properties

Similar to the discussion regarding model calibration, the model layers (consisting of an embankment, soft soil, and stabilizing layers) were simulated based on an elastic-perfectly plastic constitutive law. Input parameters for the field case models are presented in Table 92.

Table 92. Computed Stabilization Factors for onditions Modeled in Case 1

Material	γ_t, pcf (kN/m^3)	E in psi (kPa)	ν	c, psi (kPa)	ϕ (deg)	ϕ_{max} (deg)
Stiff Layer (Base)	135.7 (21.3)	29,000 (200,000)	0.15	100 (689)	35	-
Soft Subgrade Soil	128.6 (20.2)	1,000 (6,895)	0.4	5 (34)	20	31
Embankment	128.6 (20.2)	15,000 (103,400)	0.35	5 (34)	35	-
Selected Fill Material	107.4 (16.9)	10,000 (69,000)	0.35	2 (14)	35	42
Aggregate Base Course	135.7 (21.3)	10,000 (69,000)	0.35	4.5 (31)	35	-
Lime-Stabilized Soil	127.7 (20.1)	18,000 (124,100)	0.2	50 (340)	30	45
Pavement (Case 4)	143.5 (22.6)	300,000 (2,070,000)	0.15	100 (689)	30	-
Stiff Subgrade (Case 4)	128.6 (20.2)	5,000 (34,500)	0.35	20 (138)	30	-

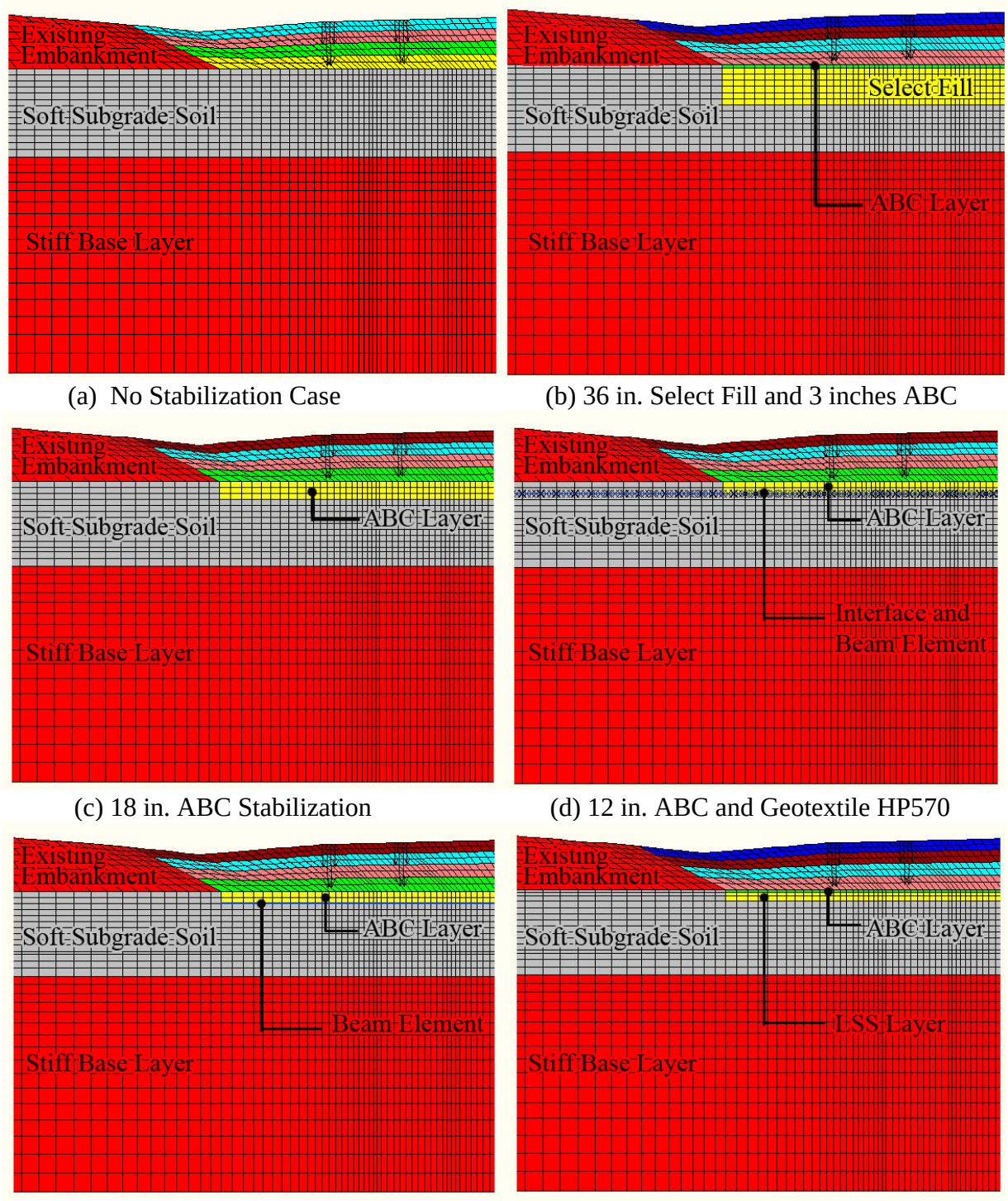

(a) No Stabilization Case (b) 36 in. Select Fill and 3 inches ABC

(c) 18 in. ABC Stabilization (d) 12 in. ABC and Geotextile HP570

(e) 12 in. ABC and Geogrid BX1500 (f) 3 in. ABC and 8 inch Lime Stabilization

Figure 154. Modeling of Stabilization Options for Case 1

For the stiff base soil layer underneath the subgrade soil, the elastic modulus value is assumed as 29 ksi, and the cohesive strength and friction angle values are assumed to be 60 kPa and 35 degrees, respectively, as shown in Table 92. The elastic modulus value of the soft soil layer is assumed based on the recommendation of Huang (2004). The pavement and stiff subgrade soil

material properties presented in Table 92 are used only for the Case 4 model. The values designated ϕ_{max} represent the strength with strain hardening. The strain hardening effect is used in this case due to the accumulated shear deformation associated with cyclic loading.

Equivalent Loading Condition

The loading conditions are static, proof roller, and cyclic loading. The load pulse for proof roller and cyclic loading is the same as used previously during prototype experimental testing. The field loading configuration was implemented assuming the plane strain condition. Loading in the plane strain mode means a continuous loading in a "third dimension" on an indicated two-dimensional cross-section, whereas loading in the axisymmetric mode means the width of the applied stress is the diameter of the loaded area. At a shallow depth, the pressure applied on the subgrade soil underneath the tire contact area is close to the axisymmetric condition. To approximate such a loading condition in plane strain mode, an equivalent pressure corresponding to the same displacement level obtained under the axisymmetric condition is used in the plane strain analysis. The ratio of the mobilized pressure in plane strain mode to that under an axisymmetric condition for the same displacement is shown in Figure 155 as a function of the modulus (E).

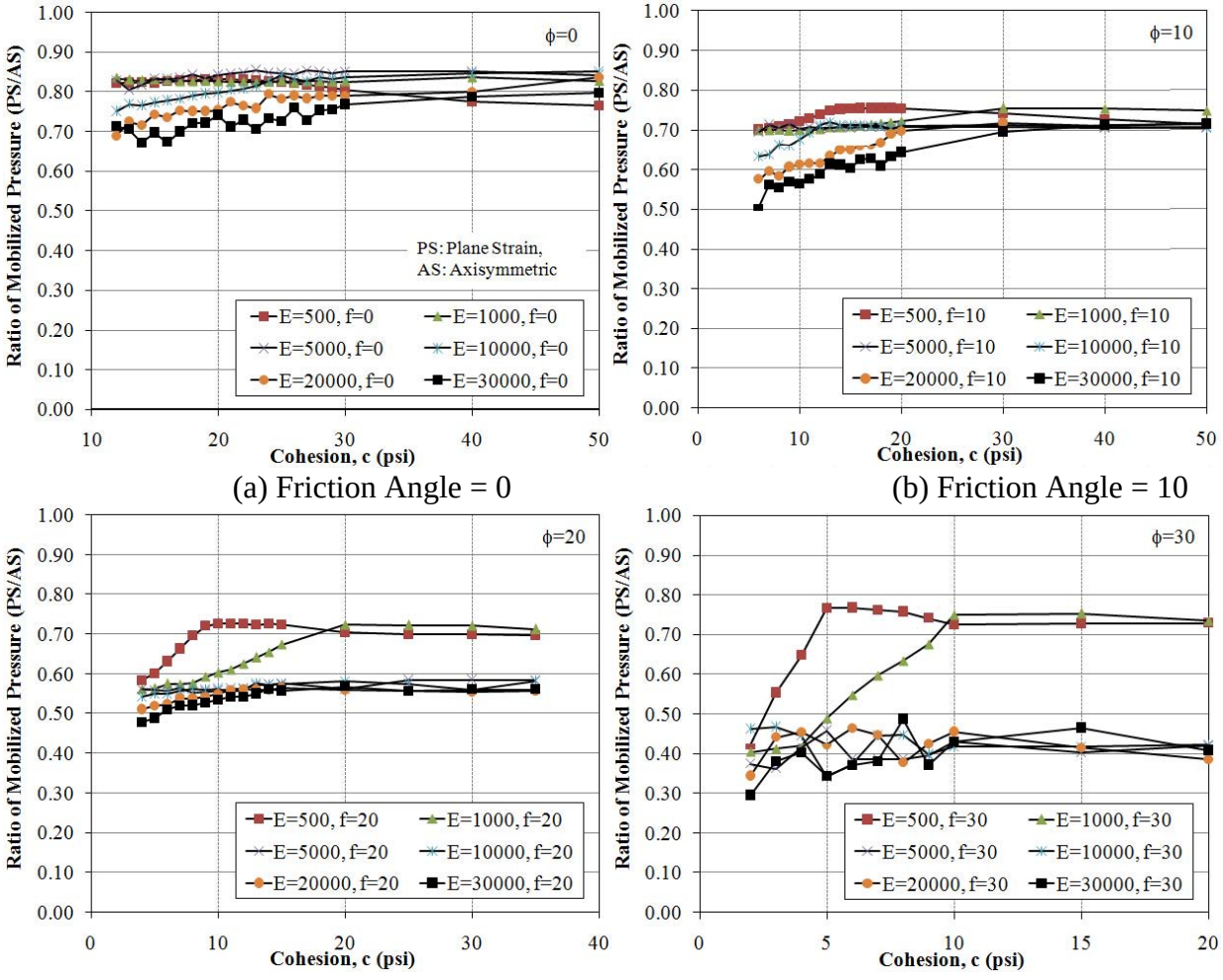

(a) Friction Angle = 0 (b) Friction Angle = 10

(c) Friction Angle = 20 (d) Friction Angle = 30

Figure 155. Ratio of Mobilized Pressures Assuming Axisymmetric Versus Plane Strain Conditions at a Uniform Displacement

The ratios of the pressures in the two different analysis modes vary from 0.4 to 0.9, depending on the shear strength and modulus parameters. The ratio for the equivalent pressure used in this study is approximately 0.85, on average, considering the case of a friction angle of zero, as shown in Figure 8 (a). This case is used because it represents soft subgrade soil. Accordingly, an equivalent pressure of 60 psi is applied in plane strain mode for static loading (to represent 70 psi in axisymmetric mode), and 70 psi for cyclic traffic loading (to represent 80 psi in axisymmetric mode.) For proof roller loading, a maximum pressure of 70 psi is applied in plane strain mode, because the wheel configuration of a proof roller can be regarded as being in the plane strain mode of loading.

Results of Numerical Simulation

Bearing Capacities

The capacity of the subgrade with and without stabilization is estimated by applying uniform displacement to node locations that represent the contact width of the tires. As shown in Figure 156, the computed stress mobilized within the loading area by uniform displacement is in close agreement with the capacity calculated by Prandtl's wedge solution, as given by Terzaghi and Peck (1967). Figure 156 (a) shows a comparison of the computed bearing capacity using both approaches. Figure 156 (b) shows the magnified mesh plot of the bearing capacity analysis for Case 1 and shows the soil mass that is affected by the loading scheme.

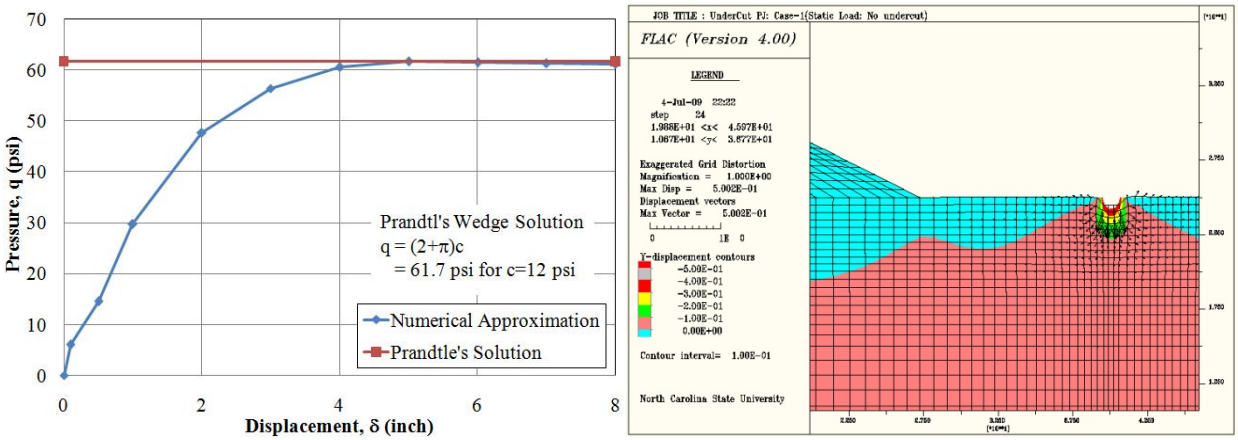

(a) Comparison with Prandtl's Solution (b) Displacement Plot with Magnified Mesh

Figure 156. Bearing Capacity Analysis

Figure 157 shows the mobilized pressure for the various stabilization methods, including the non-stabilized case. The converging pressure values on the graphs indicate the bearing capacity of the profile, or magnitude of pressure, that may cause rutting. A bearing capacity of 90 psi for Case 4 is the lowest value for all the field conditions. This result should be viewed in conjunction with the fact that Case 4 represents a median already under traffic loading and near the location of additional stress over soft subgrade. The bearing capacity of Case 1 is approximately 105 psi, and for Case 2 is 110 psi for the unstabilized condition.

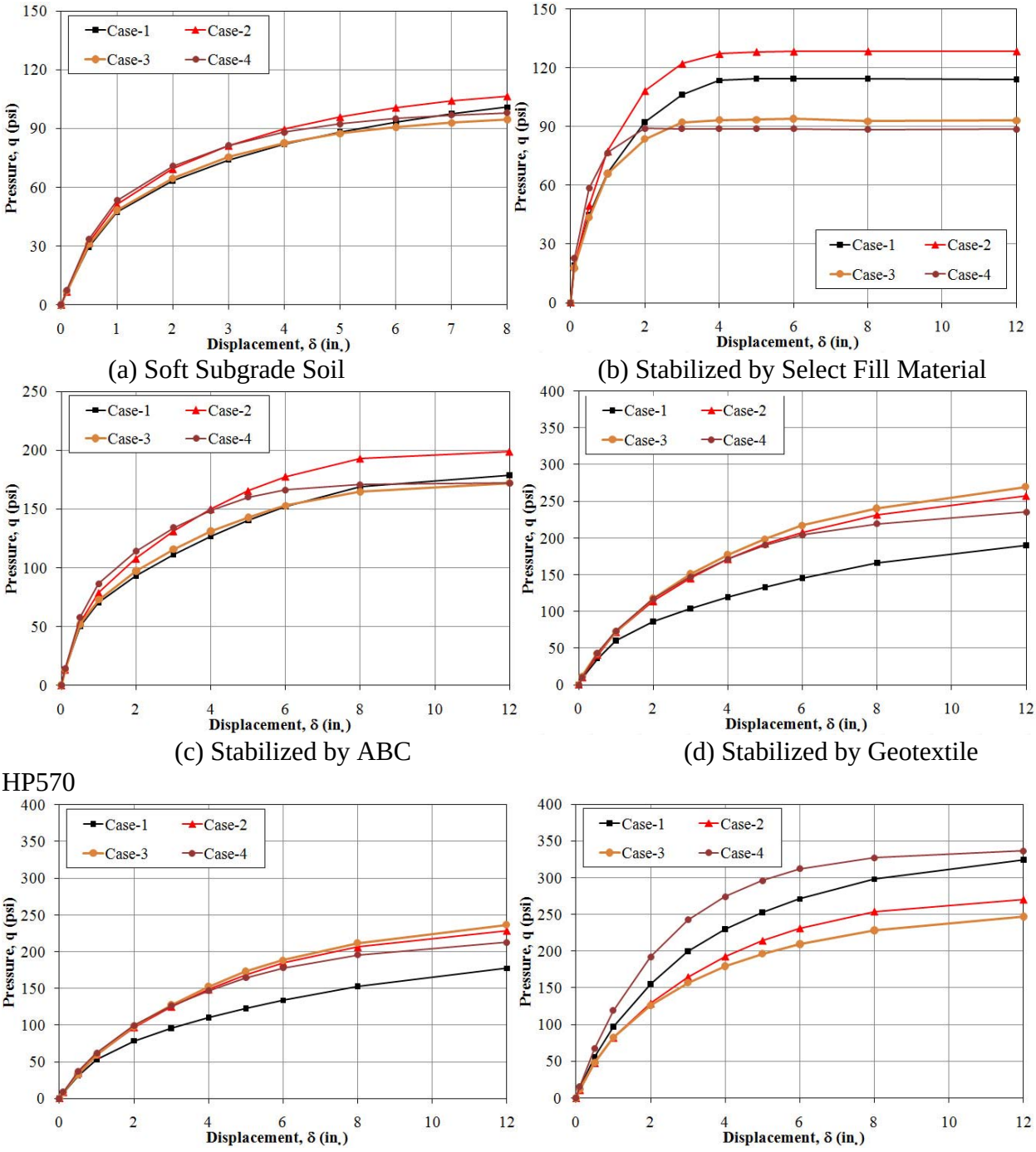

(a) Soft Subgrade Soil

(b) Stabilized by Select Fill Material

(c) Stabilized by ABC HP570

(d) Stabilized by Geotextile

(e) Stabilized by Geogrid BX1500

(f) Stabilized by Lime

Figure 157. Displacement and Mobilized Pressure Curves

As stabilization measures are implemented, an increase in the bearing capacities is estimated. The highest bearing capacities are for the profile with lime stabilization and range from 250 psi for Case 3 to approximately 340 psi for Case 4. With the introduction of the non-symmetrical loading of Case 4, a moment is introduced into the system that leads to the generation of non-uniform stress. The introduction of soil elements with significant cohesion (such as lime-

stabilized soil) provides the ability to lessen the stress that is transferred to the soft subgrade layer, which results, therefore, to the high bearing resistance observed in the simulations.

Deformation Response: Static Loading

Deformation responses for the four case studies with the various stabilization measures are shown in Figure 158 (a) to (d). For all the field cases, the settlements of the non-stabilized subgrade are over one inch. Results suggest that for Case 1 the use of lime-stabilized soil, an ABC, and select fill as stabilization measures lead to satisfactory performance, if the 1 inch criterion is applied. Using the same criterion for Cases 2, 3 and 4, the use of lime-stabilized soil, an ABC, and HP 570 seems to provide acceptable performance

.

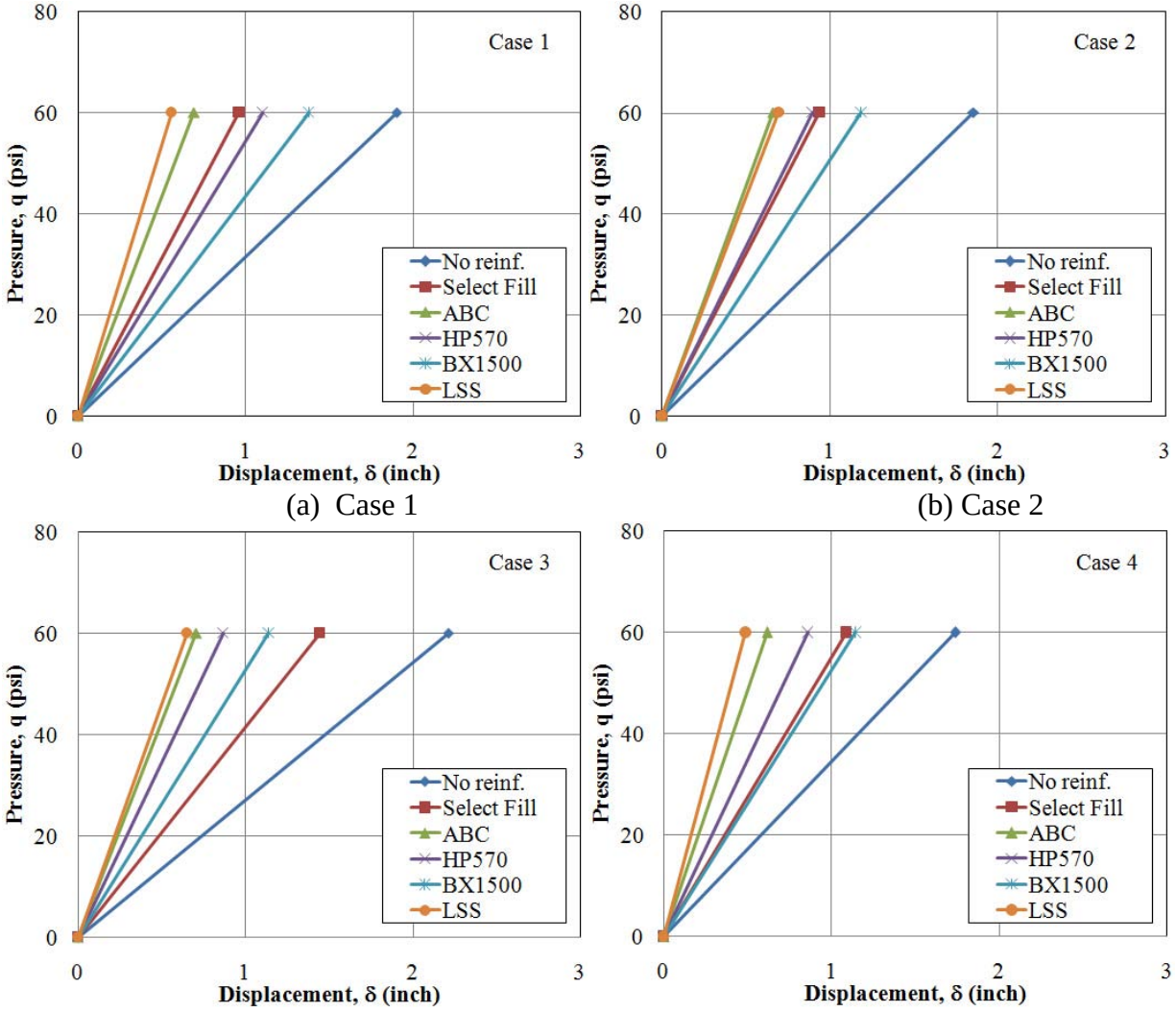

(a) Case 1 (b) Case 2

(c) Case 3 (d) Case 4

Figure 158. Pressure Versus Displacement Plots

In general, when lime stabilization is used, deformation is reduced by approximately 30% of the value estimated for the non-stabilized case, as shown in Figure 159. For the cases stabilized

using a geogrid (BX1500), the settlements for the four field cases range from 1.1 to 1.4 inches. These results are dependent, however, on the choice of the interface element properties that are used in the numerical simulations. This finding is the subject of current research that investigates the possible inclusion of geosynthetics in the mechanistic-empirical approach for pavement design, so the results of the numerical analysis should be viewed in conjunction with the assumed properties of the interface elements.

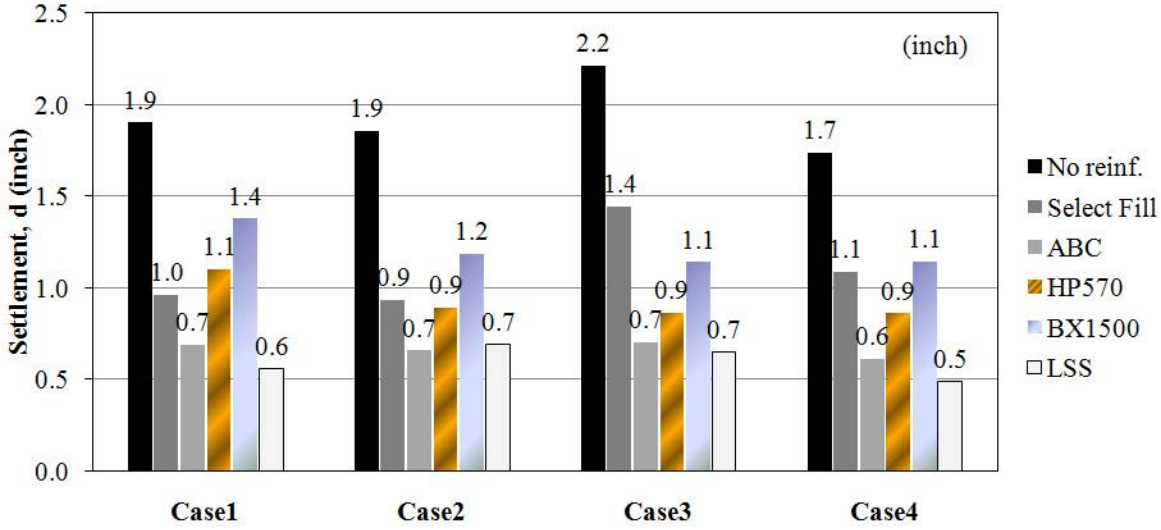

Figure 159. Settlements for Each Stabilization Method for All Field Conditions

Data presented in Figure 159 also show that settlement magnitudes are reduced with the introduction of stabilization measures. As a means of providing comparative performance information, the effectiveness of the stabilization measures is estimated by the ratio of displacement of the stabilized to the non-stabilized response, as shown in Figure 160. It seems that lime stabilization and the use of an ABC are the most effective stabilization measures for the four field cases.

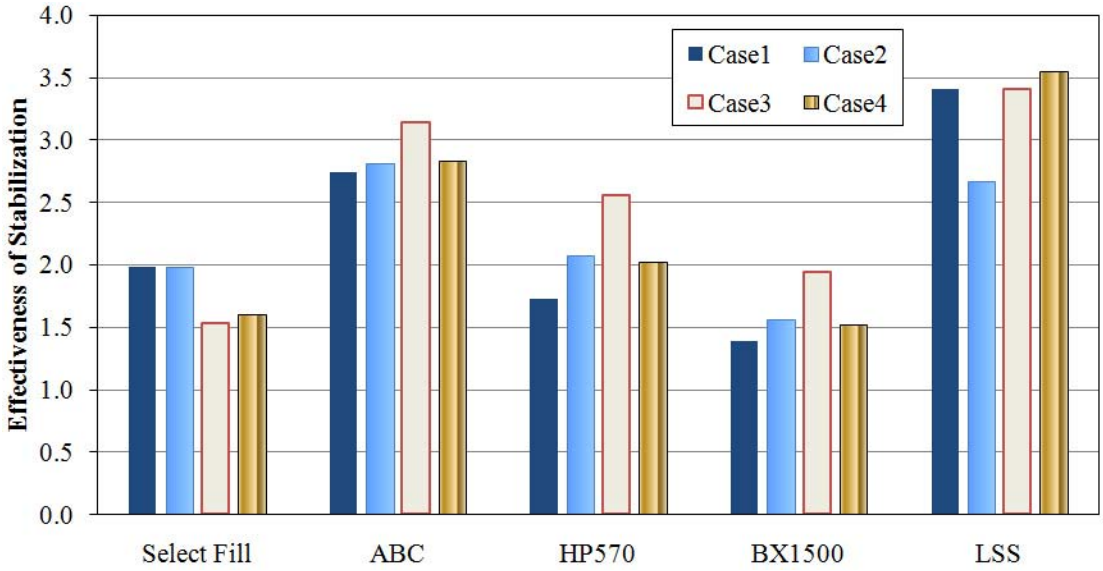

Figure 160. Effectiveness of the Stabilization Methods

Deformation Response: Proof Roller Loading

Figure 161 (a) to (d) shows two cycles of simulated proof roller loadings and the sequential settlement magnitudes plotted with time for Cases 1 to 4, respectively. Similar to the analysis using the static loading condition, the settlement magnitudes under proof roller loading are dependent on the strength and modulus of the subgrade soil. The unstabilized subgrade soil for the four field case configurations yields a deformation range from 2.2 to 4.0 inches. In comparing maximum and minimum deformation as indicators for potential pumping, the difference between the two modes exceeds 1 inch for the unstabilized subgrade but is generally on the order of 1 inch or less for the five stabilization measures. In Case 3, which models the cut section with fill placed over four simulated lifts, the "Select Fill" stabilization approach shown in Figure 161 (c) indicates the greatest potential for the most pumping. This result is perhaps due to the assumed properties of the select fill where its cohesion is less than half of the value assumed for the ABC layer.

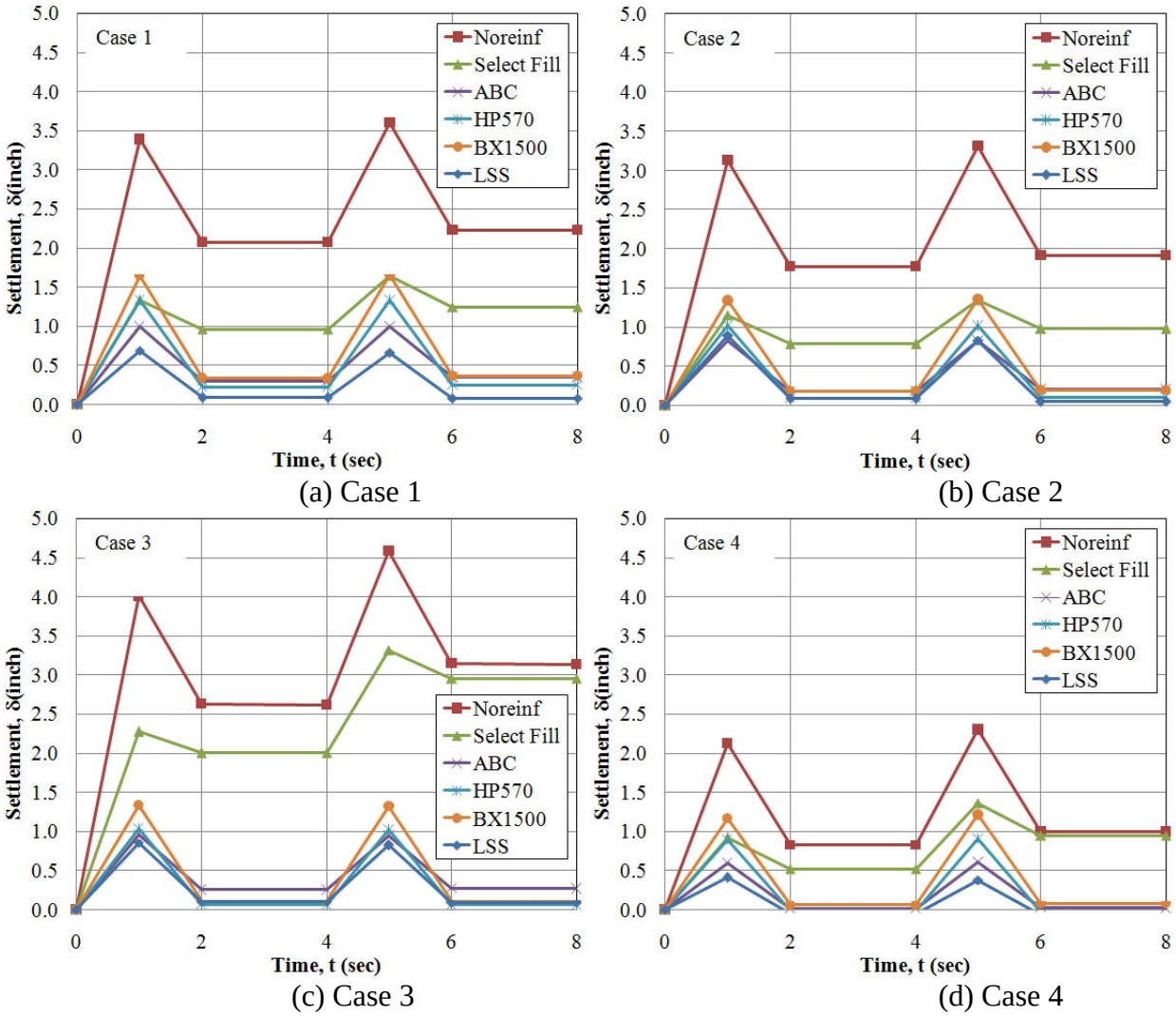

(a) Case 1 (b) Case 2

(c) Case 3 (d) Case 4

Figure 161. Settlement with Time at the Center of Proof Roller Loading Pulse

Permanent settlement is an indicator of whether the subgrade or stabilized subgrade soil is in the failure state as well as an indicator of the potential for rutting and pumping. As shown in Figure 162, the permanent settlement of the non-stabilized subgrade soil is in the range of 2.0 to 2.5 inches for Cases 1, 2 and 3. Based on these results, it seems that other than the select fill stabilization approach for Case 3, the stabilization methods are generally suitable for the four cases.

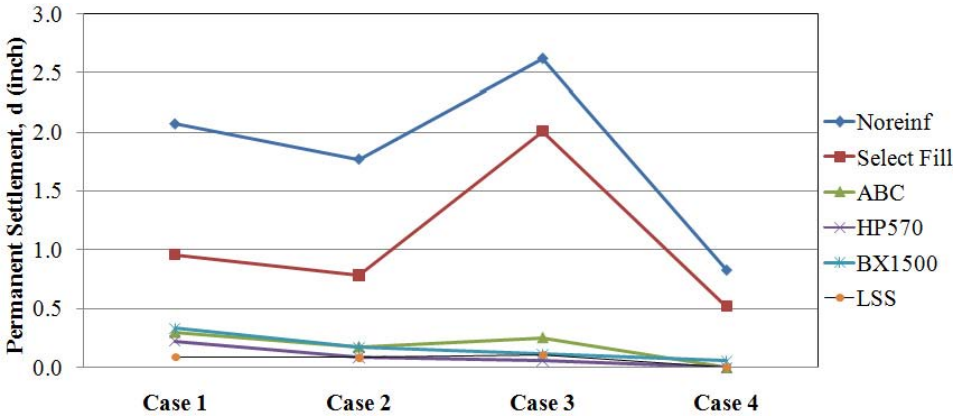

Figure 162. Permanent Settlements for Proof Roller Loading

Figure 163 shows the first maximum settlements using the various stabilization measures. The responses are shown for two cycle loadings and according to stabilization method. In terms of pumping, some of the cases show a maximum settlement of less than 1.0 inch when lime-stabilized soil and ABC measures are used. The responses of the four cases for the remaining stabilization measures exceed the 1-inch limit, which may indicate excessive pumping in the field.

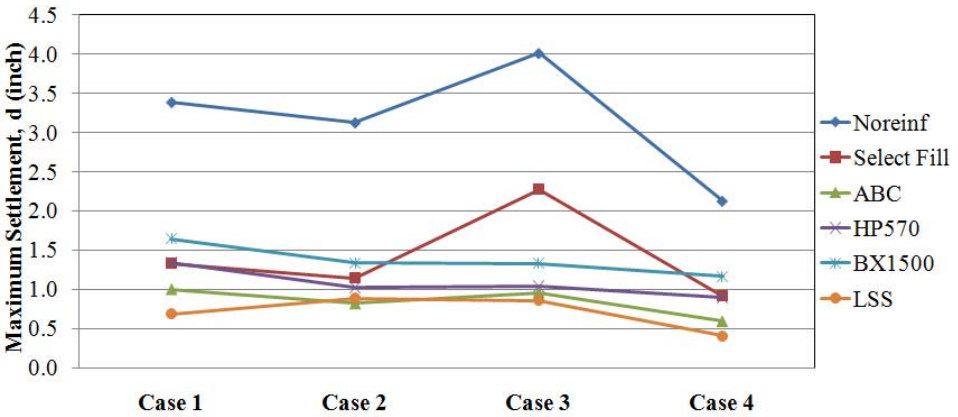

Figure 163. Maximum Displacements for Proof Roller Loading

Deformation Response: Cyclic Loading

The results for the cyclic loading cases are presented in Figure 164 (a) to (d) for field Cases 1 to 4, respectively. As previously mentioned, cyclic loading is applied after construction of the subgrade that consists of the various stabilization measures. As shown in Figure 164, the

permanent settlement for non-stabilized subgrade soil for all the field conditions converges to 5 to 7 inches after the 20th cycle. This result indicates the unsuitability of the soft subgrade to support construction traffic. On the other hand, all the stabilization approaches improve the subgrade soil response and reduce the settlement magnitude under cyclic loading. The analysis was terminated when plastic deformation no longer accumulated with an increase in the number of cycles. Therefore, the settlement curves for some cases are not plotted in Figure 164.

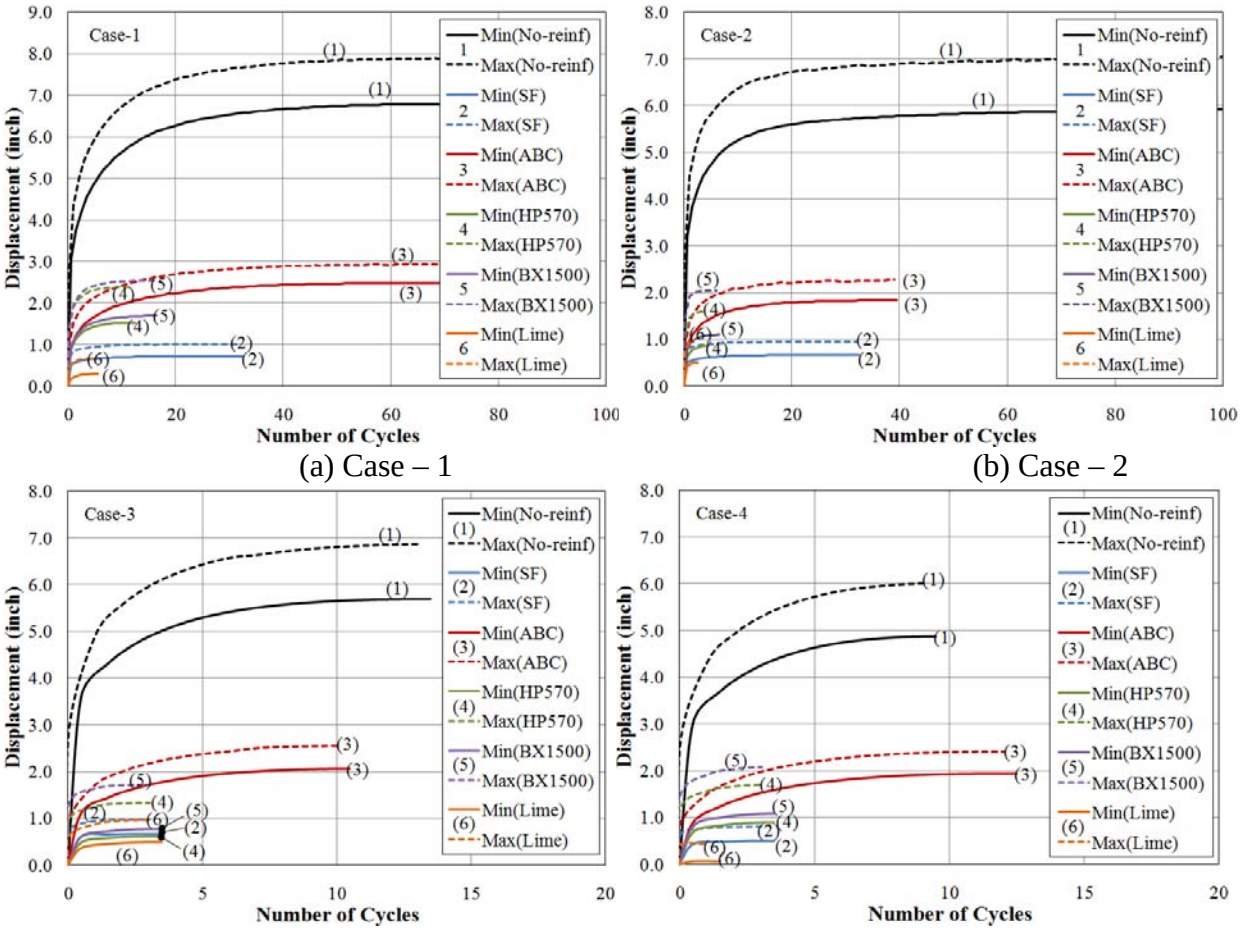

(a) Case – 1 (b) Case – 2

(c) Case – 3 (d) Case – 4

Figure 164. Displacement Plots for Field Conditions under Cyclic Loading

Figure 165 provides a summary of converged settlement magnitudes under maximum cyclic loading for the four field cases. It can be seen that stabilization by lime and select fill material yields the lowest displacements. For all the field conditions, settlement measurements obtained from these two methods are less than one inch, whereas with the other stabilization measures, settlement accumulates from 1.3 to 2.9 inches.

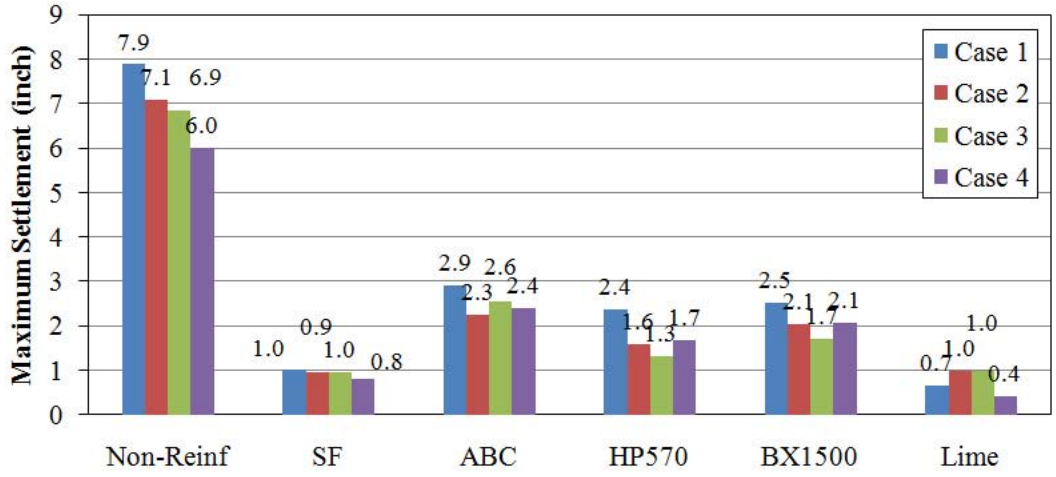

Figure 165. Maximum Settlement of Each Case According to Stabilization Method

The maximum settlement magnitudes for the four cases that use select fill as the stabilization measure are comparable to the values obtained using lime as the stabilization approach. This finding is explained by employing the friction angle for the select fill with strain hardening such that the friction angle of the select fill material is initially about 25 degrees and increases to 35 degrees at the yield, and then reaches 40 degrees at the strain of 10 %. As the strength of the select fill layer increases, the response of the layer tends to be in the elastic range, and therefore, the response becomes similar to that of the lime-stabilized layer at a steady state in cyclic load cases.

The percentage of settlement using select fill as the stabilization approach is 15 % of the settlement magnitude, as estimated for the case of unstabilized subgrade. Depending on the field case, this reduction in percentage using lime stabilization is in the range of 7.5 to 15%. The lime stabilization method seems to be the most effective for field Cases 1 and 4.

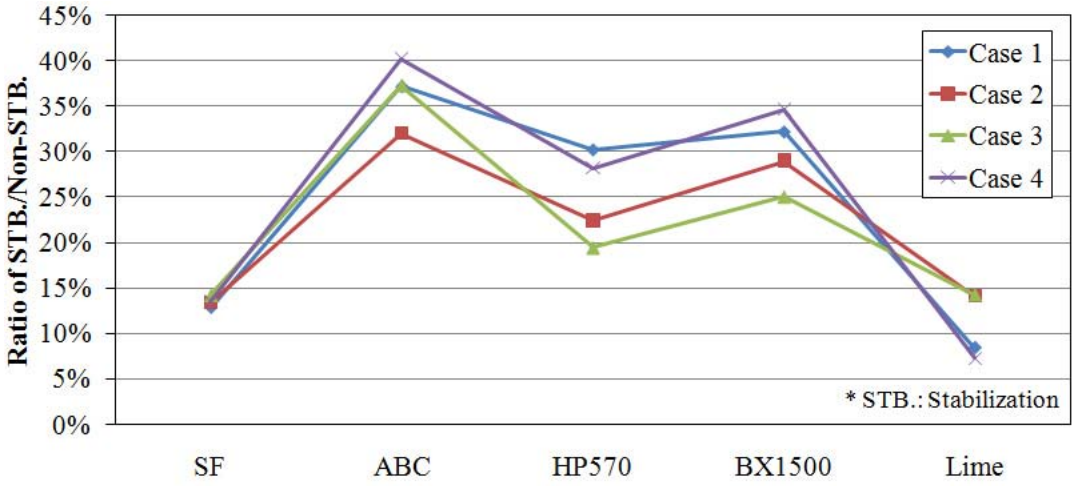

Figure 166. Effectiveness of Stabilization Method by Estimating the Ratio of Settlement Magnitudes

These two cases, i.e., 1 and 4, have asymmetrical geometric configuration that leads to non-uniform stress in the system. A stiff element, such as a lime-stabilized layer with relatively high cohesion and tensile strength, albeit small in magnitude, provides resistance to the non-uniform stress applied to the section. This phenomenon is illustrated in Figure 167 where the computed displacement and displacement vectors for the case with lime stabilization are nearly one order of magnitude less than for the case with geotextile stabilization.

For comparison, the response of a flexible stabilization system that incorporates geotextile is shown in Figure 168 (a) to (d). In this case, the axial strain of the interface elements (representing geosynthetics) for the four field cases is shown. It can be seen that the highest magnitudes of axial strain are estimated for Case 1 and Case 4 where the field geometry and sequence of construction lead to non-symmetrical configurations.

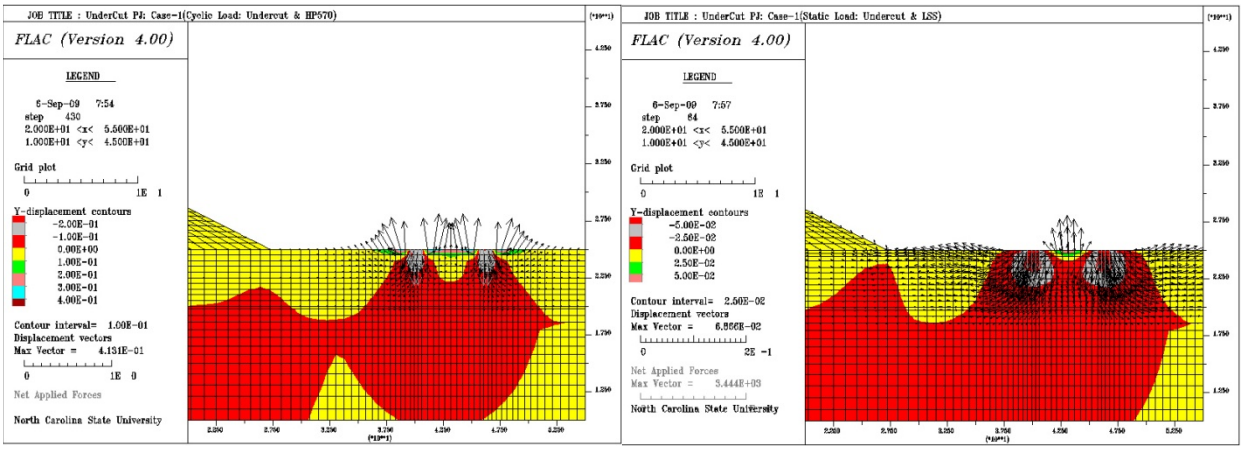

(a) Case-1 Stabilization by Geotextile (HP570) (b) Case-1 Stabilization by Lime Amendment

Figure 167. Vertical Displacement Contours and Vectors: Case 1

Aspects of Response

The construction of an embankment or adding fill in lifts in order to achieve the final grade for placement of a pavement layer may have an impact on the response of the stabilized section. As such, and from a long-term perspective, the extent to which a given stabilization measure affects the magnitude of stresses imposed on the soft subgrade layer may change, and therefore, the magnitude of deformation may change also. Case 1 represents widening a road section, and Case 2 is a typical fill section in a new alignment. Both cases serve to illustrate this possible circumstance. A stress magnitude of 60 psi, regarded as an equivalent load using the maximum pressure of the proof roller, is applied to the lane closest to the existing embankment in Case 1 and close to the slope of the fill section for Case 2, as presented earlier in Figure 149 and Figure 150.

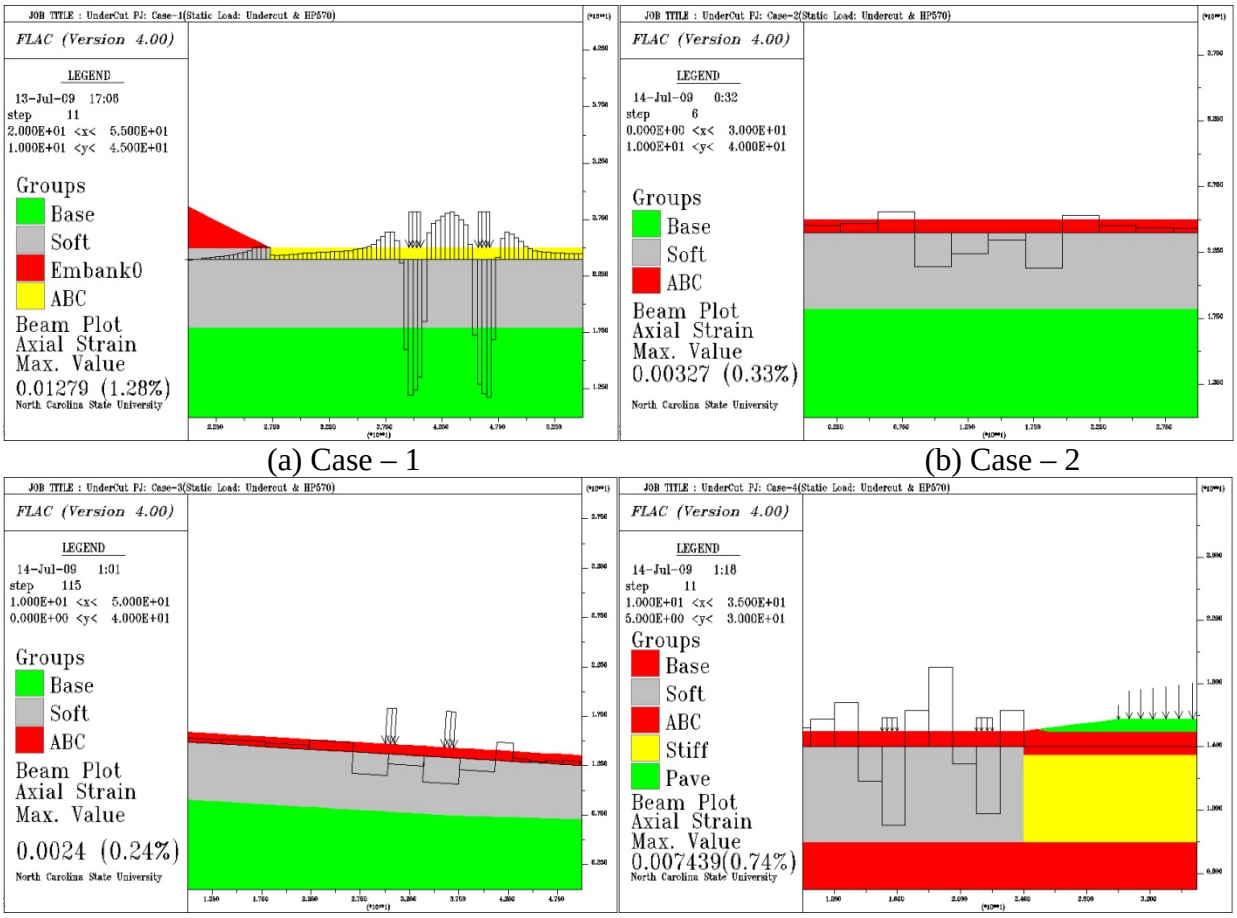

(a) Case – 1 (b) Case – 2

(c) Case – 3 (d) Case – 4

Figure 168. Strain Distribution of Geotextile (HP570) Stabilized Cases

Figure 169 shows the vertical displacement distribution in terms of depth. Two scenarios are compared: loading applied to the subgrade, and then loading applied to the completed embankment. The displacement estimated after applying the load to the subgrade is set to zero prior to the embankment loading. The vertical displacement profile is shown in Figure 169 for Case 1 before and after the addition of the embankment fill. A zero depth indicates the top surface after the embankment fill is added (in four lifts).

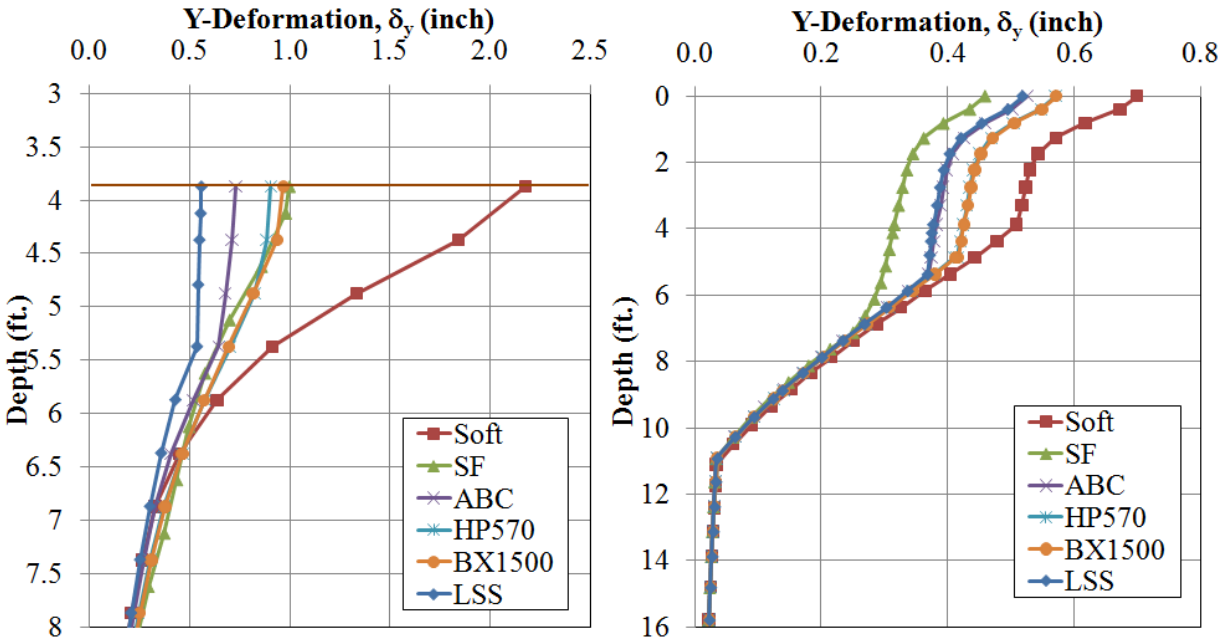

(a) Before Adding Fill (b) After Adding Fill

Figure 169. Y-Direction Displacement Profiles for Each Stabilization Method for Case 1

Results indicate that before adding fill (stage 0) the trend of displacement for each stabilization method is similar to that observed from the test pit experimental results. The displacement level of the unstabilized soft subgrade soil yields approximately 2.2 inches versus approximately 0.6 inch for the case with lime stabilization. The stabilization with 3 feet of select fill yields approximately 1.0 inch. However, as the widening embankment fill is added, the thickness of the stabilization layer becomes an important factor with regard to additional surface displacement. As shown in Figure 169 (b), the least 'additional' settlement magnitude profile is obtained for the case with select fill as the stabilization measure. This additional settlement magnitude is obtained by adding the fourth embankment lift and then 60 psi of pressure on the surface. The additional settlement magnitude can be considered to reflect additional deformation under construction traffic for the top pavement surface.

The reason for this behavior is that, within a similar profile, a greater depth of the soft subgrade profile is replaced with select fill as the stabilization measure. The select fill has a higher modulus value and higher strength properties than the soft subgrade soils. As shown in Figure 170, the stress increase with depth is relatively similar for all the stabilization measures at a depth of 7 feet. The depth of 7 feet in the case where select fill is used corresponds to a thickness of 4 feet for the road widening embankment and a depth of 3 feet of select fill with engineered strength and modulus properties. A relatively low stress increase is applied to the soft subgrade, which leads, therefore, to a lower additional settlement magnitude. It should be noted that the stress increase with depth noted in Figure 170 is due to having two adjacent loaded areas on the surface of the embankment, as shown in Figure 149.

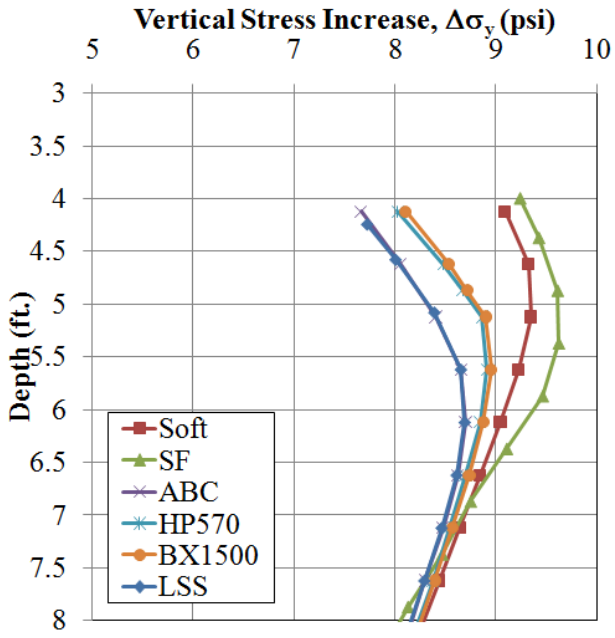

Figure 170. Stress Increase with Depth for Various Stabilization Measures (Case 1): Loading Imposed by the Fourth Lift and 60 psi Surface Pressure

The discussion can be formalized by introducing a factor obtained by multiplying an elastic modulus and a thickness of the stabilized layer that represents an overall stiffness factor of the subgrade layer. The factor is designated as a stabilization factor, η, as:

Stabilization factor (lb/in), $\eta = E_i \cdot h_i$ = elastic modulus (E) × thickness (h) **(37)**

The stabilization factors for Case 1 are presented in Table 93 for each stabilization measure. As shown in Table 93, the highest η value is for the case of select fill stabilization, which reflects the trend observed from the additional settlement values shown in Figure 169(b).

Table 93. Computed Stabilization Factors for Conditions Modeled in Case 1

Methods	E_0*	E_1	E_2	Case 1					
				h_0	h_1	h_2	η	$\Delta\delta_{stage\ 0}$	$\Delta\delta_{stage\ 4}$
NS**	1	1	0	7.23	0	0	86,760	2.20	0.51
SF	1	10	10	3.8	3	0.25	435,600	1.00	0.32
ABC	1	10	0	5.55	1.5	0	246,600	0.73	0.38
HP570	1	10	0	6.05	1	0	192,600	0.91	0.42
BX1500	1	10	0	6.05	1	0	192,600	0.97	0.43
LSS	1	18	10	6.13	0.67	0.25	248,280	0.56	0.38

* E_0, E_1, & E_2: elastic modulus (ksi in unit); h_0, h_1, & h_2: thickness (feet) of the base layer of the soft subgrade, stabilization measure, and a confining layer (such as ABC on the top of select fill), respectively;
η: stabilization factor (lb/in); δ: settlement at the final stage of adding fill (inch)
** NS: non-stabilized; SF: select fill; ABC: aggregate base course; HP570: geotextile (HP570) and ABC; BX1500: geogrid (BX1500) and ABC; LSS: lime-stabilized soil cases

Figure 171 shows the displacement before the construction of the widening embankment, the additional displacement with the construction of the fourth lift, and the application of 60 psi of surface pressure, as a function of stabilization. It is not surprising that the displacement magnitude generally decreases with increasing η values. However, the R-square values indicate that the correlation of displacement level to stabilization factor is 0.92 after the placement of the embankment, but is 0.29 for stage 0 prior to the construction of the embankment. It may be concluded then that the surface settlement is affected more by the reduction of the stress level imposed on the unstabilized subgrade than by the strength of the stabilization layer. Therefore, it is important to consider not only the modulus or strength of the stabilization layer, but also its stiffness, as manifested by the modulus value and thickness. Based on the results of these analyses, this consideration is applicable when the soft subgrade is at a depth equal to or exceeding four times the width of the loaded area.

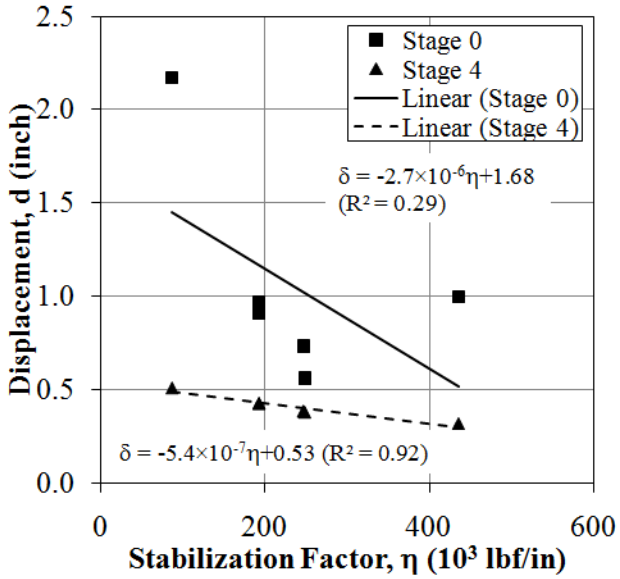

Figure 171. Relationship of Stabilization Factor with Settlement: Case 1

Summary

Four field case studies involving undercut in a soft subgrade profile were studied using numerical analysis. The soft subgrade was stabilized using five representative stabilization methods that were tested as part of the large-scale experimental program. The numerical approach was implemented using the computer program, FLAC, and employed an elastic-perfectly plastic constitutive soil model. Case 1 represents the at-grade road widening of an existing roadway by adding a fill section. Case 2 represents the construction of a new alignment in a fill situation where the thickness of the fill is typically less than six feet. Case 3 represents a new alignment in a cut situation; typically, 3 feet of undercut is implemented in areas where the subgrade fails proof rolling. Case 4 represents the widening of a highway median.

Rutting and pumping were studied during various stages of construction. Three loading configurations were simulated in plane strain mode: i) static under 60 psi pressure, ii) proof rolling under 70 psi pressure, and iii) cyclic, representing construction traffic under 60 psi

pressure. A strain-hardening model was used to estimate deformation behavior under cyclic loading. Based on the analysis results, the following conclusions can be drawn:

1. The five stabilization measures provide adequate response in terms of less rutting and pumping as compared to cases of an unstabilized subgrade profile.
2. In terms of the response of the stabilized subgrade, the lime stabilization approach provides the least potential for rutting and pumping. However, as the widening embankment fill is added, the thickness of the stabilization layer becomes an important factor with regard to additional surface displacement. The least 'additional' settlement magnitude profile is obtained for the case that uses select fill as the stabilization measure. A reason for this behavior is that within a similar profile, a greater depth of the soft subgrade profile has been replaced with the use of select fill as the stabilization measure, which leads to a relatively low stress increase applied to the soft subgrade and, therefore, a lower additional settlement magnitude.
3. Results also indicate the effects of non-symmetrical geometry and/or load configuration (such as loading near the existing embankment slope) on the response of the stabilized subgrade. With the introduction of non-uniform stress, the stiffer the stabilization measure, the less potential for rutting and pumping is indicated from the modeling results. This result is exemplified in the case of the response under proof roller loading, where use of select fill shows a greater deformation response than in the other four stabilization measures.
4. For the response under cyclic loading, a simulation based on the elastic-perfectly plastic model is shown to yield continuously increasing stresses, thus leading to failure of the model. Accordingly, strain hardening, as obtained from triaxial testing, is used in this phase of modeling. As the strength increases due to strain hardening, the response may become elastic with no accumulation of plastic deformation with loading cycles.
5. To improve the modeling of the response under cyclic loading, a model that incorporates strain hardening for all of the study soil types is needed. The incorporation of strain hardening is important in discerning the response of the stabilized grade under cyclic loading. This topic is recommended for further research.
6. A stabilization factor, termed "η", is introduced to aid in comparing the effectiveness of the various stabilization measures in cases where the soft subgrade is at a depth equal to or exceeding four times the width of the loaded area. The η factor is the product of the modulus value and the thickness of the stabilization layer and can be viewed as analogous to the "EI" or stiffness parameter commonly used for beams. Following this approach, select fill is found to be the stabilization measure that provides the least rutting and pumping response.

CHAPTER 12: COST ANALYSIS

The large scale prototype test results were analyzed to determine the relative cost to displacement for each of the 22 tests. In this chapter, unit costs are derived from bid averages and supplier reported costs, while subgrade stiffness (DCP), displacements, and required volume of undercut material are estimated from Chapter 5 and Chapter 6, respectively.

Performance-Cost Analysis: Average Unit Costs

Several sources were consulted for typical material unit costs. Table 94 presents the unit costs obtained from the North Carolina DOT bid averages of 2008 statewide projects (NCDOT, 2008b). The 'Lime Treated Subgrade' item is the cost of LSS layer construction, while 'Lime' is the cost of the raw lime material. 'Select Granular Material' is synonymous with select fill.

Table 94. Unit Costs from NCDOT 2008 Statewide Project Bid Averages

Item	Avg. Cost ($)	Units
Undercut Excavation	$10.04	/yd^3
Select Granular Material	$24.59	/yd^3
Aggregate Base Course	$24.12	/ton
Lime Treated Subgrade	$2.54	/yd^3
Lime	$195.36	/ton

The items with per ton units had to be converted into per square foot units using unit weight values from quality control testing. With an average dry unit weight of 128 pcf, the ABC converted to $41.84 per cubic yard. For lime, the price equated to $8.53 per cubic yard assuming an application rate of 3% by unit weight of the average subgrade dry unit weight of 108.5 pcf. All costs per cubic yard were multiplied by the stabilization layer depth (in yards) to obtain a per square yard application cost. The amount of undercut excavation for each test section depended on the stabilization layer depth. All tests with granular layers required the same depth of undercut. In other words, if 14 inches of ABC was placed, then 14 inches of subgrade was removed through undercut to have the same final subgrade surface elevation. However, tests with LSS only assumed that the depth of ABC placed on top of it was undercut since LSS is produced by in-place mixing without subgrade removal. Geosynthetic manufacturers were contacted for average unit costs, which are summarized below in Table 95 (Dull, 2009; Close, 2009). The values used for later calculations were those for large-volume state projects. All reported costs through personal communication are listed for reference.

Table 95. Geosynthetic Unit Costs Provided by Manufacturers

Geosynthetic	Avg. Cost ($/yd^2)
Geotextile A – Large Volume	$5.67
Geotextile B – Large Volume	$4.67
Geogrid A – Large Volume	$3.04
Geogrid A – Small Volume	$4.50
Geogrid B – Large Volume	$1.28
Geogrid B – Small Volume	$2.25

Stabilization Method Cost Calculation

Based on the given unit costs, the cost per square yard of each stabilization type was calculated for initial loading cycling. The unit costs for each test are presented in Table 96. The unit costs were then multiplied by the incremental surface deformations between the cycle intervals as a normalization approach, therefore producing final units in inch-dollars per square yard. This information is presented, Table 96, Table 97, and Table 98 for cycle intervals of 0 and 200, 200 and 1000, and 1000 and 10,000, respectively. The data in these tables are sorted by lowest to highest (good to poor) performance-cost. Values calculated with extrapolated displacements are noted with an asterisk.

A qualitative performance chart including cost factor is illustrated in Figure 172. Tests with both low displacement and cost would produce a small number and represent good performance-cost. The opposite is true for poor performance-cost. Moderate performance-cost stabilization methods may be viable if the project can afford initially high construction costs (bottom right zone) or if the subgrade is going to be repaired before final paving (upper left zone). The values for which a test has either good, moderate, or poor performance-cost depends on the situation.

Table 96. Stabilization Method Cost per Square Yard for Cyclic 1

Test Configuration (Test No.)	Unit Cost ($/yd^2)
16" ABC (2)	$23.06
20" ABC (3)	$28.82
16" ABC with Geogrid B (4)	$24.34
14" ABC (5)	$20.18
19" ABC with Geotextile A (6)	$33.05
17" Select Fill/3" ABC with Geotextile A (8)	$26.35
36" Select Fill/3" ABC (9)	$38.95
25" Select Fill/3" ABC with Geotextile B (10)	$33.04
14" Select Fill/3" ABC with Geotextile A (11)	$23.46
20" ABC with Geotextile B (13)	$33.49
13" ABC with Geotextile B (14)	$23.40
18" ABC (15)	$25.94
13" ABC with Geotextile A (16)	$24.40
11" ABC with Geogrid A (17)	$18.89
12" ABC with Geotextile A (18)	$22.96
12" LSS/5" ABC (19)	$12.59
9" LSS/4" ABC (20)	$10.44
9" Gray LSS/4" ABC (21)	$10.44

Table 97. Sorted Cyclic 1 Performance-Cost between 0 and 200 Cycles

Test Configuration (Test No.)	Perf.-Cost (in-$/yd^2)
9" LSS/4" ABC (20)	0.90
9" Gray LSS/4" ABC (21)	2.72
12" LSS/5" ABC (19)	3.44
20" ABC (3)	10.02
25" Select Fill/3" ABC with Geotextile B (10)	12.49
19" ABC with Geotextile A (6)	13.00
16" ABC (2)	13.70
20" ABC with Geotextile B (13)	16.83
16" ABC with Geogrid B (4)	16.87
18" ABC (15)	17.57
17" Select Fill/3" ABC with Geotextile A (8)	21.18
14" ABC (5)	22.57
36" Select Fill/3" ABC (9)	24.06
13" ABC with Geotextile B (14)	24.61
11" ABC with Geogrid A (17)	26.16
14" Select Fill/3" ABC with Geotextile A (11)	29.60
13" ABC with Geotextile A (16)	34.81
12" ABC with Geotextile A (18)	38.68

Table 98. Sorted Cyclic 1 Performance-Cost between 200 and 1,000 Cycles

Test Configuration (Test No.)	Perf.-Cost (in-$/yd^2)
9" LSS/4" ABC (20)	0.62
9" Gray LSS/4" ABC (21)	2.63
12" LSS/5" ABC (19)	3.15
20" ABC (3)	9.91
19" ABC with Geotextile A (6)	12.34
16" ABC (2)	14.12
18" ABC (15)	15.11
25" Select Fill/3" ABC with Geotextile B (10)	16.62
16" ABC with Geogrid B (4)	18.61
14" ABC (5)	19.34
20" ABC with Geotextile B (13)	19.93
36" Select Fill/3" ABC (9)	20.96
13" ABC with Geotextile A (16)	21.22
13" ABC with Geotextile B (14)	23.74
11" ABC with Geogrid A (17)	25.55
17" Select Fill/3" ABC with Geotextile A (8)	26.77
14" Select Fill/3" ABC with Geotextile A (11)	35.35
12" ABC with Geotextile A (18)	37.07

Table 99. Sorted Cyclic 1 Performance-Cost between 1,000 and 10,000 Cycles

Test Configuration (Test No.)	Perf.-Cost (in-$/yd^2)
9" LSS/4" ABC (20)	0.86
9" Gray LSS/4" ABC (21)	3.79
12" LSS/5" ABC (19)	8.73
20" ABC (3)	24.38
16" ABC (2)	26.49
14" ABC (5)	28.71*
13" ABC with Geotextile A (16)	30.35
18" ABC (15)	31.55
16" ABC with Geogrid B (4)	31.72
19" ABC with Geotextile A (6)	33.01
36" Select Fill/3" ABC (9)	37.09
11" ABC with Geogrid A (17)	40.20
20" ABC with Geotextile B (13)	42.32
25" Select Fill/3" ABC with Geotextile B (10)	46.33
12" ABC with Geotextile A (18)	55.13
13" ABC with Geotextile B (14)	65.81
17" Select Fill/3" ABC with Geotextile A (8)	89.76*
14" Select Fill/3" ABC with Geotextile A (11)	133.74*

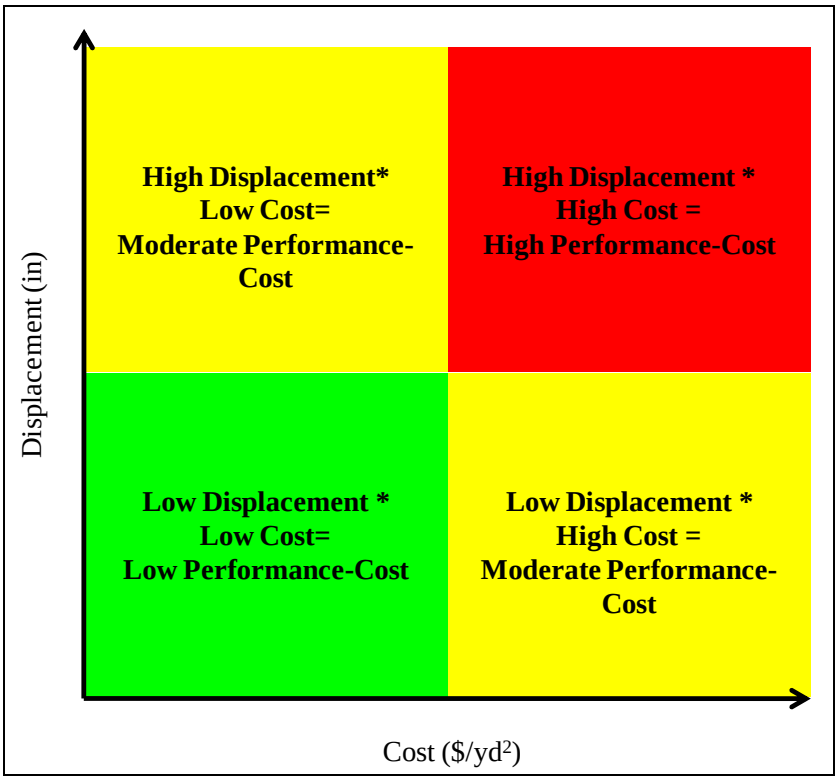

Figure 172. Performance-Cost Visualization Graph

In summary, the performance-cost analysis compared how much "bang for the buck" each stabilization method provided. These analyses do not however consider the expedience of

construction time, which in many cases may be an overriding factor in the decision making process. The following conclusions can be made about performance-cost during initial cycles:

- Subgrades with LSS were the most economical alternatives because of low initial construction cost as well as low surface deformation.
- Thick (between 16 and 20 inches) unreinforced ABC stabilization was also economical. Although the ABC underwent some initial displacement likely due to compaction, the layer thickness allowed vertical stresses to be reduced at the soft subgrade level to reduce subsequent surface deformations.
- Geotextile A and B inclusion with "thick" ABC layer stabilization had moderate performance-cost, but higher initial cost and higher displacements over initial cycles hurt performance-cost during most initial loading intervals.
- Even though geosynthetic-reinforced tests with less ABC (around 12 inches) required less undercut and material placement, performance-cost was hurt by high deformations. A few of these sections showed increased performance-cost at higher intervals after mobilization.
- The select fill was less expensive than ABC per cubic yard, but because the sections underwent punching shear failure at low cycles, the sections had poor performance-cost over all intervals.
- Deep undercut (greater than 24 inches) and backfill with select fill had high construction cost. However, the sections did not undergo punching shear failure of the load plate through the ABC layer because of less vertical stress increase in the soft unstabilized subgrade. Subsequently, the deep undercut sections had better performance-cost than most thin reinforced ABC tests over initial cycle intervals.

Notes on Performance-Cost Analysis

The major findings drawn from the performance-cost analysis should be viewed in light of the following factors:

1. Although LSS was the most economical undercut subgrade stabilization method of new roadway construction, it may not be appropriate for "remedial undercut", or repair of an already paved roadway or previously stabilized subgrade that has experienced failure. Associated mellowing and curing times may significantly prolong roadway reopening. Unreinforced or reinforced granular material stabilization is much quicker to construct.
2. Early tests (up to test number 7) had less remolded subgrade and may have had less resulting surface deformation. Thus, the inch-dollar per square yard value may have been higher than previously reported. A possible approach to account for strength variation is to normalize the performance-cost values by the average Coastal Plain subgrade DCPI which provides an indication of shear strength. This is presented in Table 100 to Table 102. In general the results are similar to those in Table 99 and Table 100, but earlier tests may drop one or two spots in the order of performance due to the additional stiffness benefit of the less remolded subgrade placed early in the protocol.

Table 100. Performance-Cost between 0 and 200 Cycles Considering Subgrade Stiffness

Test Configuration (Test No.)	Perf.-Cost (in-$/yd^2-DCPI)
9" LSS/4" ABC (20)	0.009
9" Gray LSS/4" ABC (21)	0.028
12" LSS/5" ABC (19)	0.034
25" Select Fill/3" ABC with Geotextile B (10)	0.122
20" ABC (3)	0.125
19" ABC with Geotextile A (6)	0.129
20" ABC with Geotextile B (13)	0.146
18" ABC (15)	0.154
16" ABC (2)	0.157
16" ABC with Geogrid B (4)	0.165
17" Select Fill/3" ABC with Geotextile A (8)	0.181
36" Select Fill/3" ABC (9)	0.218
13" ABC with Geotextile B (14)	0.227
11" ABC with Geogrid A (17)	0.234
14" ABC (5)	0.249
14" Select Fill/3" ABC with Geotextile A (11)	0.268
13" ABC with Geotextile A (16)	0.303
12" ABC with Geotextile A (18)	0.351

Table 101. Performance-Cost between 200 and 1,000 Cycles Considering Subgrade Stiffness

Test Configuration (Test No.)	Perf.-Cost (in-$/yd^2-DCPI)
9" LSS/4" ABC (20)	0.006
9" Gray LSS/4" ABC (21)	0.027
12" LSS/5" ABC (19)	0.031
19" ABC with Geotextile A (6)	0.122
20" ABC (3)	0.123
18" ABC (15)	0.133
16" ABC (2)	0.161
25" Select Fill/3"ABC with Geotextile B (10)	0.162
20" ABC with Geotextile B (13)	0.173
16" ABC with Geogrid B (4)	0.182
13" ABC with Geotextile A (16)	0.185
36" Select Fill/3" ABC (9)	0.190
14" ABC (5)	0.213
13" ABC with Geotextile B (14)	0.219
11" ABC with Geogrid A (17)	0.228
17" Select Fill/3" ABC with Geotextile A (8)	0.229
14" Select Fill/3" ABC with Geotextile A (11)	0.320
12" ABC with Geotextile A (18)	0.337

Table 102. Performance-Cost between 1,000 and 10,000 Cycles Considering Subgrade Stiffness

Test Configuration (Test No.)	Perf.-Cost (in-$/yd^2-DCPI)
9" LSS/4" ABC (20)	0.009
9" Gray LSS/4" ABC (21)	0.039
12" LSS/5" ABC (19)	0.085
13" ABC with Geotextile A (16)	0.264
18" ABC (15)	0.277
16" ABC (2)	0.303
20" ABC (3)	0.303
16" ABC with Geogrid B (4)	0.310
14" ABC (5)	0.317
19" ABC with Geotextile A (6)	0.328
36" Select Fill/3" ABC (9)	0.336
11" ABC with Geogrid A (17)	0.359
20" ABC with Geotextile B (13)	0.368
25" Select Fill/3" ABC with Geotextile B (10)	0.453
12" ABC with Geotextile A (18)	0.501
13" ABC with Geotextile B (14)	0.607
17" Select Fill/3" ABC with Geotextile A (8)	0.767
14" Select Fill/3" ABC with Geotextile A (11)	1.211

CHAPTER 13: SUMMARY AND CONCLUSIONS

Work in this report has focused on the development of systematic criteria for discerning the need for undercutting and stabilization of soft subgrade soil and the comparative performance of the various stabilization measures. *Undercut* refers to the removal and replacement of soft soils during roadway construction or reconstruction of new pavement sections. The NCDOT typically identifies sections for undercutting during the design phase and based on the strength and plasticity of *in situ* soils, or when proof roller testing shows excessive rutting or pumping. Currently, proof roller testing involves pulling a 50-ton trailer with tires inflated to between 68 and 72 psi on several axles over compacted, prepared subgrade at a speed of 2.5 to 3.5 mph. This proof roller testing also identifies any observed rutting and pumping. Similarly, DCP testing by the NCDOT has shown that a DCP index of approximately 38 mm/blow (1.5 inches/blow) or greater indicates that undercutting is likely to be required.

The main objectives of this research were to develop a systematic approach for determining whether or not undercutting is necessary and to investigate the adequacy of stabilization measures typically employed if undercutting is deemed necessary. To that end, this research project has sought to:

i. Establish undercut design criteria based on the strength and modulus data obtained for the subgrade soils. The undercut criteria are based on meeting a limit state of 1 inch for both pumping and rutting, but with the additional requirement that the bearing resistance of the subgrade is at least two times the applied tire pressure to minimize the potential for rutting.

ii. Explore the use of the DCP to provide data for the undercut criteria on the basis of modulus and strength values. A new procedure for analyzing DCP data using wave mechanics has been established and presented. The advantage of using the DCP data is the ability to determine the need for undercutting according to depth by applying the proposed undercut criteria incrementally.

iii. Provide guidelines for specifying a stabilization measure to achieve adequate subgrade support. Five stabilization measures have been investigated via 22 large-scale laboratory tests. These measures include the use of select fill, an ABC, geogrids with ABC, geotextiles with ABC, and lime stabilization. The performance of each stabilization measure was investigated in the laboratory and through numerical analyses.

iv. Demonstrate the applicability of the proposed measures in field configurations, including cut and fill situations. Four field cases were idealized from actual project sections. The field cases incorporating the stabilization measures were modeled numerically, and observations were made regarding the subgrade response under static, proof roller, and cyclic loading.

v. Perform a comparative cost analysis to illustrate the relative cost of each stabilization measure in relation to measured performance. The cost analyses were performed with results presented in a normalized form in an attempt to account for variables such as the strength of the stabilization measure and subgrade.

This research work encompassed small-scale and large-scale laboratory testing, limited field testing using the DCP, and numerical analyses and modeling. The laboratory testing proceeded along two tracks. The material characterization testing program was performed for soil samples obtained from the piedmont and coastal plain regions of North Carolina, as well as for sandy select fill, ABC, and lime-stabilized coastal plain soils. This materials characterization testing included the following: grain size distribution, Atterberg limits, standard Proctor, resilient modulus, consolidated undrained triaxial compression, California bearing ratio (CBR), unconfined compression strength, and permeability tests. The small-scale testing results were used to define key parameters for prototype large-scale testing as well as for the numerical modeling of performance behavior as observed during the large-scale testing.

The field testing included DCP tests and the monitoring of proof rolling equipment parameters. DCP data were collected for three sites and were compared to the 'rule of thumb' undercut criteria described above. At these sites, the 38 mm/blow DCP index criterion generally proved to be a reasonable predictor of whether that site's inspector deemed the proof roller tests either passed or failed. Wave equation analysis of the DCP results showed that the correlated shape of the DCP index versus the CBR or shear strength curves can be recreated using basic principles and with proper calibration of the damping parameter. The field work also was used to confirm the load pulse imposed by a given construction traffic vehicle and a proof roller.

The large-scale laboratory testing included twenty-two tests that simulated undercut roadway sections built in a 6 foot wide by 9 foot long by 7 foot deep concrete test pit. Different stabilization configurations were constructed over a soft coastal plain subgrade typically undercut in North Carolina. The subgrade was placed at a low CBR of approximately 2.0% and stabilized with granular layers, granular layers reinforced with geosynthetics, and lime-stabilized soil. The granular layers were comprised of an ABC, sandy select fill, or select fill with a thin ABC surface layer. The geosynthetics included a stiff woven reinforcement geotextile (Geotextile A), a less stiff woven separation-only geotextile (Geotextile B), and two biaxial polypropylene geogrids (Geogrid A and B). Quality control was performed every one to two feet using a nuclear density gauge, sand cone, and the DCP. Eight earth pressure cells were embedded within the subgrade to measure the horizontal and vertical stresses at specific locations. A 12-inch diameter plate was placed on the surface, and proof roller and cyclic loadings were simulated using half-sine wave-pulsed pressures of 70 psi and 80 psi of 2-second and 0.1-second durations, respectively.

Displacement versus time plots for the five stabilization measures were compared to the numerical output from FLAC for model calibration. A numerical study was then performed to develop the design undercut criteria in terms of rutting and pumping. The undrained shear strength and elastic modulus values estimated by the DCP were used to discern the potential need for undercutting based on satisfying limit-state displacement and bearing resistance criteria.

The proposed criteria have been validated using data obtained from the large-scale laboratory tests as well as from the field tests.

These models were then incorporated into a range of field geometries to determine the efficacy of the stabilization solutions in a field situation. Four field case studies involving undercutting in soft subgrade profiles have been examined using numerical analysis. The soft subgrade was stabilized using five representative stabilization methods that were tested during the large-scale experimental program. The numerical approach was implemented using the computer program FLAC and utilizing an elastic-perfectly plastic constitutive soil model. Case 1 represents the at-grade road widening of an existing roadway by adding a fill section where the embankment is less than four feet high. Case 2 represents the construction of a new alignment in a fill situation where the thickness of the fill is typically less than six feet. Case 3 represents a new alignment in a cut situation; typically in such a case, 3 feet of undercut is implemented in areas where the subgrade fails proof rolling. Case 4 represents the widening of a highway median. Finally, the relative economics of the stabilization methods were calculated using the displacement results of the large-scale tests and the bid averages collated by the NCDOT.

Based on the work conducted in this study, the following conclusions and observations are advanced:

1. The literature surveyed indicates a significant body of work for all five subgrade stabilization measures considered in this study. Considerable and ongoing efforts have been undertaken to standardize and generalize design methodologies for geosynthetic-reinforced roadways that do not require a specific manufacturer's product or a significant pre-design phase laboratory study of the interaction between *in situ* soil properties and selected geosynthetics. To this end, the quantification of the benefits of geosynthetics via laboratory box-type tests and full-scale field demonstrations has been undertaken by many researchers, with a wide range of results and conclusions. However, direct performance comparisons between the use of lime or cement stabilization and reinforcement of the subgrade with geosynthetics have not been widely reported in the literature.

2. As a quality control and design tool, the DCP has long been regarded by researchers as a fast instrument to use to test various points along a roadway. DCP testing traditionally has relied on statistical correlations of the DCP index to a range of stiffness or compaction parameters. The literature, however, contains little information about the mechanical behavior of the DCP in terms of its interaction with the soil as the DCP moves through the soil, and contains no clear guidance as to the use of the DCP in discerning the need for undercutting.

3. The literature contains a number of numerical approaches for modeling layered pavement systems. Typically, axisymmetric models are applied, with a circular footing used to model the wheel load application. Other approaches use axisymmetric plane strain or full 3-dimensional models.

Materials Characterization Testing

4. The characterization of the four different types of soils examined in this study shows that the low plasticity clay obtained from the coastal plain region typically would be selected for undercutting in high moisture situations. The soil selected for the large-scale testing is classified as A-6 (6) according to the AASHTO system, and approximately 56% of this soil passes the No. 200 sieve. The value of the plasticity index (PI) is 16%, and the maximum dry unit weight is 113.2 pcf at an optimum moisture content of 15.3%. A CBR of 2% was measured at a water content of approximately 19%. The resilient modulus value was approximately 4930 psi at 2 psi confining pressure and 5.4 psi deviatoric stress.

Field Measurements:

5. The field measurements generally confirmed the traffic pulse durations using the speed and measurement depth suggested by Barksdale (1971). The measured pulse magnitudes determined by the field measurements were scattered, but the maximum values were very close to the monitored tire pressure of the pan scraper or proof roller trailer.

6. Through field testing, statistical correlations, and wave equation analysis, the DCP is shown to yield relatively consistent results in predicting whether undercutting will be necessary. The NCDOT's current DCP index cut-off of 38 mm/blow is generally supported by the field observations, and yields a required CBR of greater than between 5 to 8, depending on the correlation or wave equation result used. The correlated resilient modulus values were estimated at confining pressures of 13.8 kPa (2 psi) with a cyclic deviator stress of 37.2 kPa (5.4 psi). At a DCP index cut-off of 38 mm/blow, the predicted resilient modulus values ranged between 25 and 50 MPa, although scatter in the DCP index and resilient modulus data for the studies surveyed made a precise determination difficult.

Large-Scale Testing:

7. The quality control tests, which consisted of readings from a nuclear moisture-density gauge, sand cone, rubber balloon, and DCP, revealed that reuse of coastal plain subgrade soil results in a high dry unit weight and DCP index at a given water content. This finding is likely due to increased efficiency of the particle arrangement over several iterations of tilling and compacting. The subgrade exhibited more consistent values after the seventh test and for the remainder of the tests. Laboratory testing to quantify changes in shear strength is in progress at the time of this writing. Because most unreinforced ABC tests had been conducted prior to the seventh test, making comparisons for geosynthetic-reinforced and lime-stabilized sections was difficult.

8. Samples in tests that used lime-stabilized subgrade displaced the least amount over initial and post-rut repair cycles. When increasing the lime-stabilized subgrade unconfined compressive strength, the loading resulted in less surface deformation, even when less ABC was placed above the subgrade. A higher unconfined compressive strength was achieved through both greater compactive efforts and longer mellowing time, which allowed for more flocculation of the lime/subgrade mixture and reduced the water content closer to optimum.

9. Thin ABC surface layers over select fill significantly decrease surface displacement by reducing heave that is seen only when select fill is cyclically loaded. This stabilization measure was configured as such based on the recommendation of the NCDOT based on standard field practice.

10. Tests with deep select fill stabilization and thin ABC surface layers resulted in lower surface displacement than thinner ABC-only stabilization tests. Deep stabilization resulted in less subgrade surface deformation and an increase in vertical stress. The inclusion of Geotextile B in the deep select fill tests did not significantly reduce the surface deformation, because the fabric was far enough from the load plate to have little effect.

11. Tests with less select fill and thin ABC layers reinforced with Geotextile A or B exhibited greater displacment than similar ABC sections. The load plate punched through the thin ABC layer at low cycles followed by lateral densification of the select fill without mobilizing the strength of the geotextile. The select fill test sections showed improvement over the secondary cycles only because the repaired ABC layer did not allow for punching through as easily.

12. Tests with Geotextile A had the least displacement when compared to similar unreinforced ABC tests. This geotextile had the highest tensile strength of the four geosynthetics tested and also provided layer separation. The Geotextile A reinforcement of the ABC with depth that is approximately equal to the load plate diameter exhibited high displacements during initial cycles. However, these high initial displacements provided enough mobilization and tension such that loading after rut repair resulted in very little displacement.

13. Geotextile A (strength = 70 kN/m) yielded half the displacement (~0.5 in.) of either Geogrid A (30 kN/m) or Geotextile B (36 kN/m) in sections with approximately equivalent ABC thicknesses and subgrade strength values. The performance benefits of sections reinforced with Geotextile B versus unreinforced ABC layers are minimal. The fabric likely does not have enough tensile strength to reinforce the stabilization layer.

14. Geogrid A placed below thin ABC layers showed less surface displacement than the less stiff Geogrid B with more ABC. Geogrid A resisted downward movement better after some initial layer compaction and mobilization. Similar to the geotextiles, geogrid reinforcement benefits are more apparent when placed at depths similar to the load plate diameter.

15. As generally observed by other researchers, geosynthetic reinforcement shows the most improvement when placed at a depth approximately equal to the load plate diameter from the surface. At this depth, the reinforcement undergoes more mobilization and potentially intercepts shear failure surfaces.

16. None of the four geosynthetics dramatically increased the initial density of the granular stabilization materials. This result may be due to the small laboratory compaction

equipment used in the testing. Larger field compaction equipment may have been able to mobilize the reinforcement more, but the soft underlying subgrade soil might still prevent this mobilization from occurring.

17. The excavation of tested sections revealed that Geotextiles A and B were stained with pumped subgrade fines. Neither fabric met the filter criteria for the coastal plain subgrade, but because the openings are large, excess pore water pressure generated during loading may have dissipated upward into the granular layers if clogging did not occur.

Undercut Criteria:

18. The undercut design criteria encompass two modes of loading: axisymmetric and plane strain. The plane strain mode is assumed to simulate proof roller loading and provide information on potential rutting and excessive pumping. The axisymmetric mode provides similar information, but is thought to simulate mainly the effects of construction traffic (or a single wheel) rather than a series of loads that are closely spaced on an axle.

19. It is postulated that rutting is associated mainly with plastic shear deformation within the shallow layers, and thus can be considered as a function of the shear strength parameters. Excessive pumping is mainly a function of the stiffness parameters and is affected by the response of shallow as well as deep layers of the profile.

20. It is possible to have pumping without rutting. An example is the case of a relatively thin chemically-stabilized subgrade layer over a deep layer of soft soils. The shear strength of the top layer may be high enough to prevent plastic shear failure, yet the soil mass affected by the surface stress has a low stiffness that leads to excessive pumping.

21. The proposed undercut design criteria are based on the ability of the bearing capacity ratio to minimize the potential for rutting, and are based also on the definition of a limit displacement value to minimize the potential for excessive pumping. The proposed criteria used in this report are 2.0 for the bearing capacity ratio and 1.0 inch settlement for pumping, but these criteria can be changed at the discretion of NCDOT engineers. The validation results show that the proposed criteria are reasonable and provide an indication of the extent to which specific subgrade soils are suitable for the support of roadways.

Simulated Field Sections:

22. For the four field cases, the five stabilization measures provide an adequate response in terms of less rutting and pumping as compared to the case of the unstabilized subgrade profile.

23. In terms of the response of the stabilized subgrade, the lime stabilization approach provides the least potential for rutting and pumping. However, as the widening embankment fill is added, the thickness of the stabilization layer becomes an important factor with regard to additional surface displacements. The least ‘additional’ settlement magnitude profile is obtained for the case that uses select fill as the stabilization measure.

24. A reason for this behavior is the fact that within a similar profile, a larger depth of the soft subgrade profile has been replaced with the use of the select fill as a stabilization measure, which leads to a relatively low stress increase applied to the soft subgrade and, therefore, a lower additional settlement magnitude.

25. Results also indicate the effect of non-symmetrical geometry and/or load configuration (such as loading near an existing embankment slope) on the response of the stabilized subgrade. With the introduction of non-uniform stress, the stiffer the stabilization measure, the less potential for rutting and pumping is indicated from the modeling results. This occurrence is the case for proof roller loading, where the select fill showed a higher deformation response than the other four stabilization measures.

26. For the response under cyclic loading, a simulation based on the elastic-perfectly plastic model yielded continuously increasing displacements leading to failure of the model. Accordingly, strain hardening data obtained from triaxial testing was used in this phase of modeling. As the strength increases with strain hardening, the response may become elastic with no accumulation of plastic deformation with load cycles.
27. For improved modeling of the response under cyclic loading, a model that incorporates strain hardening for all of the soil types in the study is needed. The incorporation of strain hardening is important in discerning the response of the stabilized grade under cyclic loading. This topic is recommended for further research.

28. A stabilization factor, termed "η", is introduced to aid in comparing the effectiveness of the various stabilization measures in cases where the soft subgrade is at a depth equal to or exceeding four times the width of the loaded area. The η factor is the product of the modulus value and the thickness of the stabilization layer and can be viewed as analogous to the "EI" or stiffness parameter commonly used for beams. Following this approach, select fill was indicated as the stabilization measure that has the potential to provide the least rutting and pumping response.

Cost Analyses

29. Subgrades with lime-stabilized soil are most economical to use during the initial and post-rut repair loadings because of their low construction costs and negligible surface displacements. However, lime-stabilized soil may not be appropriate for time-sensitive situations, such as 'remedial' undercutting or repair of failed subgrades beneath existing paved roads.

30. Thick (between 16 and 20 inches) unreinforced ABC stabilization also proved to be economical during the initial cycles prior to rut repair. Although the ABC underwent some initial displacement likely due to compaction, the layer thickness allowed vertical stresses to be reduced at the soft subgrade level to reduce subsequent surface deformations. However, during secondary cycles, its cost performance was hurt by continued displacements.

31. The inclusion of Geotextiles A and B with a thick ABC (around 18 inches) shows a moderately good cost performance, but the high initial costs and high displacements during the initial cycles hurt cost performance during most initial loading intervals.

32. Even though geosynthetic-reinforced subgrades with an ABC of around 12 inches provide low construction costs, their cost performance was hurt by high displacements during initial cycles. The Geotextile A test results showed better cost performance during the later cycles and all post-rut repair cycles because the mobilized fabric resisted secondary cyclic displacements.

33. Shallow select fill stabilization provides lower unit costs than similar ABC sections, but because the sections undergo punching shear failure and high surface displacement during initial cycles, the shallow select fill test results showed poor cost performance. The high costs of deep rut repair also hurt cost performance during secondary cycles.

34. Deep select fill stabilization (greater than 24 inches) provides the highest initial construction costs per square yard. However, the sections showed relatively small displacements during initial cycles that produce better cost performance results than thin ABC tests with geosynthetic reinforcement. During secondary cycles, the deep undercut test results indicated worse cost performance than the thin ABC layer tests reinforced with Geotextile A, and exhibited a comparable cost performance to thin ABC tests using the other three geosynthetics.

35. After the initial rut depth was filled in, and the simulation of the subgrade in preparation of the installation of top pavement layers, again the lime-stabilized soil was the most economical choice of stabilization measures because of its low initial construction costs and negligible surface deformation. Stabilization using a thin (around 12 inches) ABC layer reinforced with Geotextile A was also cost effective. The fabric helps to prevent layer mixing, and the high tensile strength of the geotextile, once mobilized, reduces secondary cyclic deformation. Geotextile B and Geogrid A reinforcement of ABC layers is less cost effective because neither geosynthetic has the high tensile strength of Geotextile A to resist long-term displacement.

36. Test results for thin select fill stabilization and geosynthetic reinforcement indicate high initial rutting, increasing the unit cost for secondary cycles because of the need for rut repair. Deep undercuts (greater than 24 inches) and backfill with select fill is a moderately economical alternative. However, unlike during the initial cycles, deep stabilization did not outperform thin ABC layers reinforced with Geotextile A. Thick (between 16 and 20 inches) unreinforced ABC stabilization was moderately economical during low cycle intervals.

The findings and conclusions of this research program are based on laboratory testing and numerical modeling. Several aspects of the recommendations require validation based on field data and monitoring. These aspects include the proposed undercut criteria in conjunction with the proposed DCP index approach, the performance of the five stabilization measures, and the performance cost comparison.

REFERENCES

AASHTO Guide for Design of Pavement Structures, (1993)

AASHTO (2001). "Geosynthetic Reinforcement of the Aggregate Base Course for Flexible Pavement Structures." AASHTO Provisional Standards, PP 46-01, American Association of State Highway and Transportation Officials, Washington, D.C.

Abu-Farsakh, M.Y., Alshibli, K., Nazzal, M., and Seyman, E., 2004, "Assessment of In-situ Test Technology for Construction Control of Base Courses and Embankments". Louisiana Transportation Research Center (LRTC) Project No. 02-1GT, Louisiana Department of Transportation and Development, May 2004, 143 Pages.

Alexander, L. G. (1977). "Discussions to some results concerning displacement and stresses in a non-homogeneous elastic half-space." Geotechnique, 27(2), 253–254.

Al-Khoury, R., Scarpas,A., Kasbergen,C., and Blaauwendraad,J. (2007). "Nonhomogeneous Spectral Element for Wave Motion in Multilayer Systems," International Journal of Geomechanics, Vol. 7, No. 5, pp. 362-370.

Al-Qadi, I. L. and Appea, A. K. (2003). "Eight-Year Field Performance of Secondary Road Incorporating Geosynthetics at Subgrade-Base Interface." *Transportation Research Record*, n 1849. 212-220.

Aufmuth, R.E. Strength and Durability of Stabilized Layers under Existing Pavements. Construction Engineering Research Laboratory Report M-4, 1970.

Awojobi, A. O. (1975). "The settlement of a foundation on Gibson soil of the second kind." Geotechnique, 25(2), 221–228.

Ayres, M. (1997). "Development of a Rational Probabilistic Approach for Flexible Pavement Analysis." D.Phil. dissertation, University of Maryland, College Park, MD.

Barksdale, R.G. (1971). "Compressive Stress Pulse Times in Flexible Pavements for Use in Dynamic Testing." *Highway Research Record 345.* Highway Research Board. 32-44.

Bauer, G.E., and Abd El Halim, A.O., 1987, "The Performance of Geogrid Reinforced Road Bases". *Construction & Building Materials*, Vol. 1, No. 2, June 1987, Pages 71-75.

Bender, D.A., and Barenberg, E.J., 1978, "Design and Behavior of Soil-Fabric-Aggregate Systems". *Transportation Research Record No. 671*, Transportation Research Board, Washington, D.C., Pages 64-75.

Berg, R. R., Christopher, B. R., and Perkins, S. (2000). "Geosynthetic Reinforcement of the Aggregate Base/Subbase Courses of Pavement Structures." Geosynthetics Materials Association. Roseville, Minnesota. http://www.gmanow.com/pdf/WPIIFINALGMA.pdf

Biczysko, S.J. Long-Term Performance of Lime Stabilized Road Subgrade. In Lime Stabilization. Thomas Telford Publisher, London, 1996, pp. 62-71.

Blab, R., and Harvey, J.T. (2002). "Modeling Measured 3D Tire Contact Stresses in a Viscoelastic FE Pavement Model," Int. J. Geomech., 2(3), pp. 271-290

Booker, J. R., Balaam, N. P., and Davis, E. H. (1985). "The behavior of an elastic non-homogeneous half-space. Part II—Circular and strip footings." Int. J. Numer. Analyt. Meth. Geomech., 9(4), 369–381.

Boussinesq, J. (1885). "*Application des Potentiels a l'etude de l'equilibre et du Mouvement des Solids Elastiques*." Gauthier-Villars, Paris.

Brill, D.R., and Parsons, I.D. (2001). "Three-Dimensional Finite Element Analysis in Airport Pavement Design," Int. J. Geomech., 1(3), pp. 273-290.

Brill, D.R., Hayhoe, G.F., and Lee, X. (1997). "Three-dimensional finite element modeling of rigid pavement structures, Aircraft/Pavement Technology: In the Midst of Change, Hermann, F.V., Ed." Proc., ASCE Airfield Pavement Conf., Seattle, WA, pp. 151–165.

Brown, P. T., and Gibson, R. E. (1972). "Surface settlement of a deep elastic stratum whose modulus increases linearly with depth." Can. Geotech. J., 9(4), 467–476.

Burmister, D. M. (1945). "The general theory of stress and displacements in layered soil systems. I." J. Appl. Phys., 16(2), 89–94.

Bruton, J.M., Armitage, R.J., and Brown, S.F. (1992) "Seven Years Experience of Pavement Evaluation," 7th International Conference on Asphalt Pavements, Volume 3, pp. 17-30.

Carrier, W. D., III, and Christian, J. T. (1973a). "Analysis of an inhomogeneous elastic half-space." J. Soil Mech. Found. Div., 99(3), 301–306.

Carrier, W. D., III, and Christian, J. T. (1973b). "Rigid circular plate resting on a non-homogeneous elastic half-space." Geotechnique, 23(1), 67–84.

Caterpillar (2008). "631G WHEEL TRACTOR SCRAPER"
http://www.cat.com/cda/layout?m=111776&x=7&f=151786

Chai, G., and Roslie, N., 1998, "The Structural Response and Behavior Prediction of Subgrade Soils using Falling Weight Deflectometer in Pavement Construction". *Third International Conference on Road and Airfield Pavement Technology*, April 1998.

Chen, D.H., Zaman, M., Laguros, J., and Soltani, A. (1995). "Assessment of computer programs for analysis of flexible pavement structures," Transportation Research Record 1482, TRB, National Research Council, Washington, DC, pp. 123–133.

Chen, D-H., Lin, D-F., Liau, P-H., and Bilyeu, J., 2005, "A Correlation Between Dynamic Cone Penetrometer Values and Pavement Layer Moduli." *Geotechnical Testing Journal*, Vol. 28, No. 1, January 2005, Pages 42-49.

Chen, T-C., Chen, R-H., and Lin, S-S. (2000). "Nonlinear homogenized model applicable to reinforced soil analysis," Geotextiles and Geomembranes, Vol. 18, No. 6, pp. 349-366.

Cho, Y.H., McCullough, B. F., and Weissmann, J. (1996). "Considerations on finite-element method application in pavement structural analysis." *Transp.Res.Rec.*, (1539), 96-101.

Christensen, A.P. Cement Modification of Clay Soils. Research and Development Bulletin RD002.01S, Portland Cement Association, Skokie, I11, 1969.

Christopher, B.R., and Lacina, B., 2008, "Roadway Subgrade Stabilization Study". *Proceedings*, First Pan American Geosynthetics Conference & Exhibition, March 2-5, 2008, Cancun, Mexico, Pages 1013-1021.

Chua, K.M, 1988, "Determination of CBR and Elastic Modulus of Soils Using a Portable Pavement Dynamic Cone Penetrometer." *Proceedings of the First International Symposium on Penetration*, Pages 407-414.

Chuaprasert, M. F., and Kassir, M. K. (1974). "Displacements and stresses in nonhomogeneous solid." J. Eng. Mech. Div., Am. Soc. Civ. Eng., 100(5), 861–872.

Coonse, J., 1999, "Estimating California Bearing Ratio for Cohesive Piedmont Residual Soil Using the Scala Dynamic Cone Penetrometer". Master's Thesis (MSCE), North Carolina State University, Raleigh, NC.

CROW. (1998). "Deflection profile; not a pitfall anymore, record 17, Ede, the Netherlands.

CRREL (2004). "Base-Course Reinforcement: Proposed FHWA Pooled Fund Study." http://www.crrel.usace.army.mil/pavement_geosynthetics/br_reinforcement.htm

Cuelho, E. and Perkins, S. (2009). "Field Investigation of Geosynthetics Used for Subgrade Stabilization." Western Transportation Research Institute. FHWA Report No. FHWA/MT-09-003/8193. Accessed March 2010.
http://www.westerntransportationinstitute.org/research/4w2005.aspx

Cunningham, C.N. (2009). "Mechanical Response of Crushed Stone Mixtures", Master Thesis, North Carolina State University, Raleigh, North Carolina.

Davids, W. (1998) "EverFE: A Rigid Pavement 3D Analysis Tool." 1998 Annual Meeting of the Transportation Research Board, Washington, DC, January.

Davids, W.G. (2001). “3D Finite Element Study on Load Transfer at Doweled Joints in Flat and Curled Rigid Pavements,” Int. J. Geomech., 1(3), pp. 309-323.

Davies, T. G., and Mamlouk, M. S. (1985). “Theoretical Response of Multilayer Pavement Systems to Dynamic Nondestructive Testing,” Transportation Research Record, 1985, pp. 1-7.

Dempsey, B. J. and M. R.Thompson. Durability Properties of Lime-Soil Mixtures. In Highway Research Record 235, HRB, National Research Council, Washington, D.C., 1968, pp. 61-75.

Desai, C. S. (2007). "Unified DSC constitutive model for pavement materials with numerical implementation." *International Journal of Geomechanics*, 7(2), 83-101.

Doherty, J. P., and Deeks, A. J. (2003a). “Elastic response of circular footings embedded in a non-homogeneous half-space.” Geotechnique, 53(8), 703–714.

Doherty, J. P., and Deeks, A. J. (2003b). “Scaled boundary finite-element analysis of a non-homogeneous axisymmetric domain subjected to general loading.” Int. J. Numer. Analyt. Meth. Geomech., 27(10), 813–835.

Doherty, J. P., and Deeks, A. J. (2003c). “Scaled boundary finite-element analysis of a non-homogeneous elastic half-space.” Int. J. Numer. Methods Eng., 57(7), 955–973.

Dong., Q., Matsui, K., and Yamamoto, K. (2001). “Time Domain Backcalculation of Pavement Structure Material Properties Using 3D FEM with Ritz Vectors,” Int. J. Geomech., Volume 1, Issue 3, pp. 325-336.

Douglas, R.A., and Valsangkar, A.J., 1992, “Unpaved Geosynthetic-Build Resource Access Roads: Stiffness Rather than Rut Depth as the Key Design Criterion”. *Geotextiles and Geomembranes*, Vol. 11, Pages 45-59.

Eades, J. L., and R. E. Grim. A Quick Test to Determine Lime Requirement for Lime Stabilization. In Highway Research Record 139, Highway Research Board, National Research Council, Washington, D.C., 1966, pp. 61-72.

Erkens, S.M.J.G., Liu, X., and Scarpas, A. (2002). “3D Finite Element Model for Asphalt Concrete Response Simulation,” Int. J. Geomech., 2(3), pp. 305-330.

Ese, Dag, Myre, Jostein, Noss, Per Magne, and Vaernes, Einar, 1994, “The Use of Dynamic Cone Penetrometer (DCP) for Road Strengthening Design in Norway”. *Proceedings of the International Conference on Bearing Capacity of Roads and Airfields*, Pages 3-22.

Evans, P. Lime Stabilization of Black Clay Soils in Queensland Australia. In Proceedings, National Lime Association Convention, San Diego, California, 1998.

Evdorides, H.T., and Snaith, M.S. (1996), "A Knowledge-Based Analysis Process for Road Pavement Condition Assessment," Proceedings, Transport, The Institution of Civil Engineers, 117, Aug., United Kingdom, pp 202-210.

Gabr, M.A. (2001). ''Cyclic Plate Loading Tests on Geogrid Reinforced Roads.'' *Research Rep. to Tensar Earth Technologies, Inc.*, NC State Univ.

Gabr, M.A., and Hart, J.H., 2000, "Elastic Modulus of Geogrid-Reinforced Sand Using Plate Load Tests". *Geotechnical Testing Journal*, GTJODJ, Vol. 23, No. 2, June 2000, Pages 215-220.

Gabr, M.A., Coonse, J., and Lambe, P.C., 2001, "A Potential Model for Compaction Evaluation of Piedmont Soils Using Dynamic Cone Penetrometer (DCP)." *Geotechnical Testing Journal*, Vol. 24, No. 3, September 2001, Pages 308-313.

Gabr, M.A., Dodson, R., and Collin, J.G., 1998, "A Study of Stress Distribution in Geogrid-Reinforced Sand". *Geotechnical Special Publication (GSP) No. 76: Geosynthetics in Foundation Reinforcement and Erosion Control Systems*, Pages 62-76.

Gabr, M.A., Hopkins, K., Coonse, J., and Hearne, T., 2000, "DCP Criteria for Performance Evaluation of Pavement Layers." *Journal of Performance and Constructed Facilities*, ASCE, Vol. 14, No. 4, November 2000, Pages 141-148.

Gibson, R. E. (1967). "Some results concerning displacements and stresses in a non-homogeneous elastic half-space." Geotechnique, 17(1), 58–67.

Gibson, R. E. (1974). "The analytical method in soil mechanics." Geotechnique, 24(2), 115–140.

Gibson, R. E., and Sills, G. C. (1969). "On the loaded elastic half-space with a depth varying Poisson's ratio." Z. Angew. Math. Phys., 20(5), 691–695.

Giroud, J. P. and Han, J. (2006). Closure to "Design Method for Geogrid-Reinforced Unpaved Roads. I: Development of Design Method" J. Geotech. and Geoenvir. Engrg. **132**, 549

Giroud, J.P. and Han, J. (2004a). "Design Method for Geogrid-Reinforced Unpaved Roads –Part I: Theoretical Development." ASCE *Journal of Geotechnical and Geoenvironmental Engineering*, 130(8), 776-786.

Giroud, J.P. and Han, J. (2004b). "Design Method for Geogrid-Reinforced Unpaved Roads –Part II: Calibration And Verification." ASCE *Journal of Geotechnical and Geoenvironmental Engineering*, 130(8), 787-797.

Giroud, J.P. and Noiray, L. (1981). "Geotextiles-Reinforced Unpaved Road Design." ASCE, *Journal of Geotechnical Engineering*, 107(9), 1233-1253.

Gunaratne M., Sanders, O. III. (1996). "Response of a Layered Elastic Medium to a Moving Strip Load," Int. J. Num. Anal. in Geomech., Vol.20, Issue 3 , Pages 191 – 208.

Hambleton, J.P, and Drescher, A., (2008). "Development of Improved Test Rolling Methods for Roadway Embankment Construction," Report No. MN/RC 2008-08, Minnesota Department of Transportation.

Hammons, M. (1998). "Validation of Three-Dimensional Finite Element Modeling Technique for Jointed Concrete Pavements." 1998 Annual Meeting of the Transportation Research Board, Washington, DC.

Haque, M. E., Zaman, M., and Soltani A. A. (1998). "Cracking Characteristics of Model Continuously Reinforced Concrete Pavements," Transportation Research Record, Volume 1629, pp. 90-98.

Harison, J.A., 1987, "Correlation Between California Bearing Ratio and Dynamic Cone Penetrometer Strength Measurement of Soils". *Proceedings of the Institution of Civil Engineers*, London, Part 2, Volume 83, December 1987, Pages 833-844.

Hassan, A.B., 1996, "The Effects of Material Parameters on Dynamic Cone Penetrometer Results for Fine-Grained Soils and Granular Materials". PhD Dissertation, Oklahoma State University, December 1996.

Hemsley, J. A. (1998). Elastic analysis of raft foundations, Thomas Telford, London.
Herath, A., Mohammad, L.N., Gaspard, K., Gudishala, R. , and Abu-Farsakh, M.Y. , 2005, "The Use of Dynamic Cone Penetrometer to Predict Resilient Modulus of Subgrade Soils." *Geotechnical Special Publication No. 130: Advances in Pavement Engineering*, *Geo-Frontiers 2005*, pages 17-32.

Heukelom, W., and Klomp, A.J.G., 1962, "Dynamic Testing as Means of Controlling Pavements During and After Construction". *Proceedings of the 1st International Conference on Structural Design of Asphalt Pavement*, University of Michigan, Ann Arbor, MI.

Hibbitt, Karlsson, and Sorensen, Inc. (1998). "ABAQUS/Standard User's Manual (Version 5.8)," Hibbitt, Karlsson, and Sorensen, Inc., Pawtucket, RI.

Holtz, R.D., Christopher, B. R., and Berg, R. R. (1998). "Geosynthetic Design and Construction Guidelines." Publication No. FHWA HI-95-038. Federal Highway Administration, Washington, D.C. 459 pages.

Huang, Y. H. (1973). "Stresses and strains in viscoelastic multilayer systems subjected to moving loads." Highway Research Record. 457, Highway Research Board, National Research Council, Washington, D.C., 60–71.

Huang, Y.H. (2004). "Pavement Analysis and Design 2nd Edition," Prentice-Hall, Englewood Cliffs, NJ.

Ioannides, A. M., and Donnelly, J. P. (1988). "Three-dimensional analysis of slab on stress-dependent foundation." *Transp.Res.Rec.*, (1196), 72-84.

Jarzebowski A, and Maciejewski J. (1998) “Localisation effects in a compaction process under the rigid rolling cylinder.” In: Proceedings of the Fourth International Workshop, Localisation and bifurcation theory for soils and rocks, Gifu, Japan,, Balkema. p. 107–16

Jarzebowski A, Maciejewski J, Szyba D, Trcampczynski W. (1995). “The optimization of tool shapes and trajectories in heavy machines.” In: Proc. XII ISARC Symposium ’’Automation and Robotics in Construction’’, Warsaw, Poland, 1995. p. 159–66.

Jianzhou, C., Hossain, M., and LaTorella, T.M., 1999, “Use of Falling Weight Deflectometer and Dynamic Cone Penetrometer in Pavement Evaluation”. *Transportation Research Record*, n 1655, Transportation Research Board, Washington, D.C., p 145-151.

Kennedy, T.W., R. Smith, R. J. Holmgreen Jr., and M. Tahmoressi. An Evaluation of Lime Cement Stabilization. In Transportation Research Record 1119, TRB, National Research Council, Washington, D.C., 1987, pp. 11-25.

Kim, W.H., Edil, T.B., Benson, C.H., and Tanyu, B.F., 2006, “Deflection of Prototype Geosynthetic-Reinforced Working Platforms over Soft Subgrade”. *Transportation Research Record No. 1975*, Transportation Research Board, Washington, D.C., Pages 137-145.

Kleyn, E.G., 1975, “The Use of the Dynamic Cone Penetrometer (DCP)”. Report No. 2/74, Transvaal Roads Department, South Africa.

Kleyn, E.G., and Savage, P.F., 1982, “The Application of the Pavement DCP to Determine the Bearing Properties and Performance of Road Pavements”. *International Symposium on Bearing Capacity of Roads and Airfields*, Trondheim, Norway, June 1982.

Kreider, C. (2009). Personal e-mail communication with transmitted data.

Lai, J.S., and Robnett, Q.L., 1981, “Design and Use of Geotextiles in Road Construction”. *Proceedings of the Third Conference of the Road Engineering Association of Asia & Australia*, Vol. 1; April 20-24, 1981, Taipei, Taiwan, Pages 699-718.

Lai, J.S., and Robnett, Q.L., 1982, “Fabric-Reinforced Aggregate Roads-Overview”. *Transportation Research Record No. 875*, Transportation Research Board, Washington, D.C., Pages 42-50.

Leng, J. and Gabr, M.A. (2002). “Characteristics of Geogrid-Reinforced Aggregate under Cyclic Load,” *Journal of Transportation Research Board*, No. 1786, November, National Research Council, Washington, D.C. 29-35.

Leng, J. and Gabr, M.A. (2005). “Numerical Analysis of Stress-Deformation Response in Reinforced Unpaved Road Sections” *Geosynthetics International*, v 12, n 2. 111-119.

Léonard, D., Vanelstraete, A., and Parewyck, S. (2002). "Structural Design of Flexible Pavements Using Steel Netting as Base Reinforcement," Int. J. Geomech., 2(3), pp. 291-303

Oklahoma State (1980). "Lime Treated Subgrade Soils: An Evaluation." Final Report of Oklahoma State Study No.74-03-I, Oklahoma Department of Transportation, Oklahoma City, Okla., pp. 1-83.

Little, D.N. Evaluation of Structural Properties of Lime Stabilized Soils and Aggregates, Volume 1: Summary of Findings. Report prepared for National Lime Association, 1999.

Little, D.N., T. Scullion, P.V. Kota, and J. Bhuiyan. Guidelines for Mixture Design and Thickness Design for Stabilized Bases and Subgrades. Report 1287-3F, Texas Transportation Institute, 1995.

Livneh, M., 2000, "Friction Correction Equation for the Dynamic Cone Penetrometer in Subsoil Strength Testing". *Transportation Research Record*, n 1714, Transportation Research Board, Washington, D.C., Pages 89-97.

Livneh, M., Ishai, I., and Livneh, N.A., 1992, "Automated DCP Device Versus Manual DCP Device". *Road and Transport Research*, Vol. 1, No. 4.

Livneh, M., Ishai, I., and Livneh, N.A., 1995, "Effect of Vertical Confinement on Dynamic Cone Penetrometer Strength Values in Pavement and Subgrade Evaluations". *Transportation Research Record*, n 1473, Transportation Research Board, Washington, D.C., Pages 1-8.

Maciejewski J and Jarzebowski A. (2004). "Experimental analysis of soil deformation below a rolling rigid cylinder," Journal of Terramechanics, Volume 41, Issue 4, October, pp. 223-241

Masad, E., and Scarpas, A. (2007). "Towards a Mechanistic Approach for the Analysis and Design of Asphalt Pavements." International Journal of Geomechanics, Vol. 7, No. 2, American Society of Civil Engineering, Editorial, pp.81-82.

McAllister, L. D., and T. M. Petry. (1991). Physical Property Changes in a Lime-Treated Expansive Clay Caused by Leaching. In Transportation Research Record 1295, TRB, National Research Council, Washington, D.C., pp. 37-44.

Meier, R.W., and Baladi, G.Y. (1988). "Cone Index Based Estimates of Soil Strength: Theory and User's Guide for Computer Code CIBESS". *Technical Report No. SL-88-11*, United States Army Corps of Engineers (USACE) Waterways Experiment Station, Vicksburg, MS, March 1988.

Mitchell, J. K. Practical Problems from Surprising Soil Behavior. Journal of Geotechnical Engineering, ASCE, 1986, pp. 259-289.

Molenaar, A. A. A. (2005). "*Lecture Notes* CT4850, *Road Materials* Part I. Cohesive and Non - Cohesive Soils and ...", *33-34*

NCDOT (2006). "Standard specifications for Roads and Structures." http://www.ncdot.org/doh/preconstruct/ps/specifications/english/2006.html

NCHRP (2004). "Guide for Mechanistic-Empirical Design of Pavement Structures: Part 2 – Design Inputs." ARA, Inc., ERES Consultants Division, Champaign, Illinois.

Neubauer, C.H., and M. R. Thomson. Stability Properties of Uncured Lime-Treated Fine Grained Soils. In Highway Research Record 381, HRB, National Research Council, Washington, D.C., 1972, pp. 20-26.

Oner, M. (1990). "Vertical and horizontal deformation of an inhomogeneous elastic half-space." Int. J. Numer. Analyt. Meth. Geomech., 14(9), 613–629.

Pavement Condition Survey Manual, 1998, North Carolina Department of Transportation (NCDOT), Raleigh, NC.

Perkins, S.W. and Edens, M.Q. (2003) "Finite Element and Distress Models for Geosynthetic-Reinforced Pavements", *International Journal of Pavement Engineering* 3(4), 239–250.

Perkins, S.W., 1999, "Mechanical Response of Geosynthetic-Reinforced Flexible Pavements". *Geosynthetics International*, Vol. 6, No. 5, Pages 347-382.

Perkins, S.W., Bowders, J.J., Christopher, B.R., and Berg, R.R. (2005a). "Advances in Geosynthetic Reinforcement in Pavement Systems." *Proceedings of the ASC GeoInstitute GeoFrontiers Conference.*

Perkins, S.W., Christopher, B.R., Eiksund, G.R., Schwartz, C.S., and Svano, G. (2005b). "Modeling Effects of Reinforcement on Lateral Confinement of Roadway Aggregate." *Geotechnical Special Publication*, n 130-142, *Geo-Frontiers 2005*, 283-296.

Petry, T., and S. K. Wohlgemuth. The effects of Pulverization on the Strength and Durability of Highly Active Clay Soil Stabilized with Lime and Portland Cement. In Transportation Research Record 1190, TRB, National Research Council, Washington, D.C., 1988, pp.38-45.

Ping, W.V., and Yang, Z., 1998, "Experimental Verification of Resilient Deformation for Granular Subgrades". *Transportation Research Record No. 1639*, Transportation Research Board, Washington, D.C., Pages 12-22.

Popov, G. I. (1962). "The contact problem of the theory of elasticity for the case of a circular area of contact." J. Appl. Math. Mech., 26(1), 207–225.

Popov, G. I. (1973). "Axisymmetric contact problem for an elastic inhomogeneous half-space in the presence of cohesion." J. Appl. Math. Mech., 37(6), 1052–1059.

Powell, W.D., Potter, J.F., Mayhew, H.C., and Nunn, M.E., 1984, "The Structural Design of Bituminous Roads". *Transport and Road Research Laboratory* (TRRL) Report LR 1132, Crowthorne, United Kingdom.

Rahim A.M. (2005) "Subgrade soil index properties to estimate resilient modulus for pavement design" International Journal of Pavement Engineering, Vol. 6(3), 163-169

Rahim, A.M., and George, K.P. , 2002, "Automated Dynamic Cone Penetrometer for Subgrade Resilient Modulus Characterization." *Transportation Research Record*, n 1806, Transportation Research Board, Washington, D.C., Pages 70-77.

Rajapakse, R. K. N. D., and Selvadurai, A. P. S. (1989). "Torsion of foundations embedded in a non-homogeneous soil with a weathered crust." Geotechnique, 39(3), 485–496.

Rajapakse, R. K. N. D., and Selvadurai, A. P. S. (1991). "Response of circular footings and anchor plates in non-homogeneous elastic soils." Int. J. Numer. Analyt. Meth. Geomech., 15(7), 457–470.

Roberts, J. D. Performance of Cement-Modified Soils: A Follow-Up Report. In Transportation Research Record 1089, TRB, National Research Council, Washington D.C., 1986, pp. 81-86.

Rostovtsev, N. A. (1961). "An integral equation encountered in the problem of a rigid foundation bearing on nonhomogeneous soil." J. Appl. Math. Mech., 25(1), 238–246.

Scala, A.J., 1956, "Simple Methods of Flexible Pavement Design Using Cone Penetrometer". *New Zealand Engineering*, Vol. 11, No. 2, February 15, 1956.

Schwartz, C.W. (2002). "Effect of Stress-Dependent Base Layer on the Superposition of Flexible Pavement Solutions," Int. J. Geomech., 2(3), pp. 331-352.

Selvadurai, A. P. S. (1996). "The settlement of a rigid circular foundation resting on a half-space exhibiting a near surface elastic nonhomogeneity." Int. J. Numer. Analyt. Meth. Geomech., 20(5), 351–364.

Smith, R.B., and Pratt, D.N., (1983), "Field Study of In-Situ California Bearing Ratio and Dynamic Cone Penetrometer Testing for Road Subgrade Investigations". *Australian Road Research*, Vol. 13, No. 4, December, pages 285-294.

Steward, J. Williamson, R. and Mohney, J. (1977). "Guidelines for Use of Fabrics in Construction and Maintenance of Low-Volume Roads." USDA, Forest Service, Portland, OR. Also reprinted as Report No. FHWA-TS-78-205.

Sun, L., Hopkins, T.C., and Beckham, T. (2006). "Load reduction by geofoam for culvert extension: Numerical analysis," GeoCongress 2006: Geotechnical Engineering in the Information Technology Age, Vol. 2006, p. 221.

Ter-Mkrtich'ian, L. N. (1961). "Some problems in the theory of elasticity of nonhomogeneous elastic media." J. Appl. Math. Mech., 25(6), 1667–1675.

Tingle, J.S. and Webster, S.L. (2003). "Review of Corps of Engineers Design of Geosynthetic Reinforced Unpaved Roads." Presentation and CD-Rom Publication at the TRB 82nd Annual Meeting, Washington, DC, 24 p.

Tingle, J.S., and Jersey, S.R., 2005, "Cyclic Plate Load Testing of Geosynthetic-Reinforced Unbound Aggregate Roads". *Transportation Research Record No. 1936,* Transportation Research Board, Washington, D.C., Pages 60-69.

Tompson, M.R. Engineering Properties of Lime-Soil Mixtures. Journal of Materials, ASTM, Vol. 4, 1969.

Thompson, M.R. and Robnett, Q.L., (1976). "Resilient Properties of Subgrade Soils, Final Report-Data Summary", Transportation Engineering Series 14, Illinois Cooperative Highway Research and Transportation Program Series 160

Van Vuuren, D.J., 1969, "Rapid Determination of CBR With the Portable Dynamic Cone Penetrometer". *The Rhodesign Engineer,* Paper No. 105, September 1969.

Vischer, W. (2003). "Low-Volume Road Flexible Pavement Design with Geogrid-Reinforced Base." Transportation Research Record No. 1819, Volume 1, Eighth International Conference on Low-Volume Roads, 247-254.

Wainaina, N. (2006). "Geotechnical Problems and Practical Solutions." Presentation, NCDOT Construction Engineers Conference.
http://www.ncdot.org/doh/Operations/dp_chief_eng/constructionunit/CEC2006/pdfs/H1.pdf

Wallace, K.B., and Sapkota, B.K. (1994). "Modelling the response of pavements to subgrade volume change ," Proceedings - Conference of the Australian Road Research Board, Vol. 17, No. 2, Pavement Design & Performance Quality in Road Construction, pp. 199-210.

Wang, C., Pan, E., Tzeng, C., Han, F., and Liao, J. (2006). "Displacements and stresses due to a uniform vertical circular load in an inhomogeneous cross-anisotropic half-space." *International Journal of Geomechanics,* 6(1), 1-10.

Watn, A., Gudmund, E., Jenner, C. and Rathmayer, H. (2005). "Geosynthetic Reinforcement for Pavement Systems: European Perspectives." *Proceedings of the ASCE/GeoInstitute GeoFrontiers Conference.*

Watts, G. R. A., Blackman, D. I., and Jenner, C. G. (2004). "The performance of reinforced unpaved sub-bases subjected to trafficking." Flos, Brau, Nussbaumer, and Laackmann _eds._ *Proc., EUROGEO 3 Third European Geosynthetics Conference,* German Geotechnical Society and Zentrum Geotechnik, 261–26

Wu, S., and Sargand, S., 2007, “Use of Dynamic Cone Penetrometer in Subgrade and Base Acceptance”. Final Technical Report, Ohio Department of Transportation (ODOT) State Job Number 14817(0), 124 p.

Yankelevsky, D.Z., and Adin, M.A., 1980, “A Simplified Analytical Method for Soil Penetration Analysis”. *International Journal for Numerical and Analytical Methods in Geomechanics*, Vol. 4, No. 3, July-Sept 1980, Pages 233-254.

Yen, S., and Lee, Y. (2007). "Parameter identification and analysis of a slab track system using 3D ABAQUS program." *J.Transp.Eng.*, 133(5), 288-297.

You, Z., Xia, Y., Hu, C., and Wang, B. (2001) “Finite Element Analysis of Concrete Pavements Over Culverts,” Int. J. Geomech., Volume 1, Issue 3, pp. 337-350.

Yue, Z. Q., Yin, J. H., and Zhang, S. Y. (1999). “Computation of point load solutions for geo-materials exhibiting elastic non-homogeneity with depth.” Comput. Geotech., 25(2), 75–105.

Zaghloul, S.M., and White, T.D. (1993). “Use of a Three-Dimensional, Dynamic Finite Element Program for Analysis of Flexible Pavement,” In Transportation Research Record 1388, TRB, National Research Council, Washington, D.C., 1993, 60-69.

APPENDICIES
(ALL APPENDICIES ARE INCLUDED ON THE ELECTRONIC CD ONLY)

Appenix A: Reults of Material Characterization from Small Scale Testing

Appendix B: Moisture and Density Data for the Large Scale Test Samples

Appendix C: Complete Measure Results of the Test Sections Including Static and Cyclic Responses